

**SYNTHETIC AND MECHANISTIC STUDIES OF SMALL-MOLECULE ACTIVATION
AT LOW-VALENT IRON, COBALT, AND IRIIDIUM CENTERS**

Thesis by
Matthew Thomas Whited

*In Partial Fulfillment of the Requirements
for the Degree of
Doctor of Philosophy*

California Institute of Technology
Pasadena, California
2009

(Defended April 17, 2009)

© 2009

Matthew Thomas Whited

All Rights Reserved

Acknowledgments

It is a very strange feeling to be condensing 4+ years of one's life into a single thesis, but fortunately it provides the happy occasion to recollect those who have been instrumental in helping to bring these 4+ years of work to fruition. Without hesitation, my first acknowledgment must go to Bob Grubbs, who has now served as my advisor for the past two or so years and, fortunately, as a friend for longer than that. He has been nothing but supportive since I first approached him about joining the lab, and I especially appreciate his approach of letting me take my ideas and run with them, irrespective of how crazy or unrelated to traditional Grubbs lab projects they were. It has also been a phenomenal experience working for someone who has so much perspective on the development of a field, and some of my most enjoyable and enlightening graduate school experiences have come from simply discussing random details about the history of organometallic chemistry (sometimes while climbing or hiking). More than anything, however, I appreciate Bob's example that having an exciting scientific career can (and should) come as a complement to a really fulfilling personal life, not as an alternative to it.

I also need to recognize and acknowledge Jonas Peters, who served as my advisor for the first half of my graduate career. I came into his lab with very little experience or knowledge of inorganic chemistry, and the environment in the Peters lab was one that helped (i.e., forced) me to make tremendous strides in a very short time. Without his guidance, I certainly would not have been able to move to an organic chemistry lab and carry out the projects that fill many of the pages of this thesis. Anyone who is familiar with Peters group chemistry will certainly see his stamp on the work I have undertaken in the Grubbs lab, and that should be taken as something of a tribute in itself.

One of the biggest advantages to being at a place as small and tight-knit as Caltech is that the community extends beyond individual labs. As a result, several other faculty deserve

recognition for their advice and assistance. Jackie Barton, Dennis Dougherty, and Theo Agapie, who have served on my committee, have been excellent sounding boards for my ideas (both chemistry- and career-related). I have been fortunate that they were not hesitant to give me criticism when I needed it, and thus I know I can trust that their praise is deserved. I have also had a considerable amount of interaction with John Bercaw, Harry Gray, and Jay Labinger through the BP MC² collaboration, and their feedback has been invaluable, even if it is a bit intimidating for me to get up in front of Bob, John, Harry, and Jay to talk about organometallic chemistry. Finally, Brian Stoltz has been a helpful and approachable, if underutilized, resource when it came to working through tough spots in ligand synthesis or looking for practical applications of new organic transformations.

Aside from my advisors, there have been many individuals who played direct roles in the development of the chemistry described herein. Larry Henling, who manages the day-to-day operations of the X-ray crystallography facility, has probably spent nearly as much time interacting with me as my advisors have, and the number of crystal structures in this thesis (40 at last count) should be some indication of the debt of gratitude I owe him. Larry has always been eager to teach me whatever he can about crystallography and has been extremely patient when I did not catch on as fast as I would have liked. I am also grateful to Mike Day and Dick Marsh, who have at various times helped me with all kinds of crystallography issues. Rick Gerhart has ended up being more important to my work than I would have liked since he usually ends up fixing the glassware that I break, but he really is exceptional and has always been extremely friendly and helpful. Also, Dan Nieman deserves recognition for teaching me nearly everything I know about plumbing and being instrumental in the “great glove box move” toward the end of our laboratory renovations, which cost me about four weeks worth of work but would have taken much more without his tireless assistance.

Before mentioning specific individuals, I want to extend thanks to all of those with whom I have overlapped in the Peters and Grubbs groups since I could not possibly name everyone who has helped at some point. In the Peters lab, Ted Betley, Steve Brown, Seth Harkins, and Connie Lu were my examples when I first joined. They had all seen the lab start from the ground up and provided a fantastic sense of perspective, and I ended up seeking their advice and assistance on many occasions. I overlapped with Chris Thomas for a bit longer, and I am grateful that I did, as she became a good friend and did a wonderful job of taking the lead in lab after we graduated the large class above her. Neal Mankad joined at the same time I did and contributed in important ways to the chemistry described in chapter 3, and I benefited a great deal from his insight and advice. Eric Rivard, as postdoc in the Peters lab, should be acknowledged for beginning some of the chemistry described in chapter 2. I also shared a glove box with Bruce MacKay and Alex Miller, who have both helped me in various ways. Bruce was integral in helping me learn the ropes of working in an inorganic lab and always went out of his way to assist me. Alex has been a good friend and resource both during and after our time in the Peters lab, and it is always great to be able to bounce ideas off of him.

In the Grubbs group, I should start with my thanks to Patricio Romero, who helped provide some inspiration and early ideas for my iridium project (chapters 4–7) that really took off in the Grubbs group. In him, I found a kindred organometallic soul who was able to help me a lot since we think about science in similar ways. My inclusion in the “fifth year brain trust” with John Matson and Kevin Kuhn has been a real privilege and honor, albeit one we bestowed on ourselves. It has been fantastic to have trusted co-workers who bring such different perspectives to the table, and my science has been enhanced as a result. Ian Stewart has been a valuable resource as I have sought to set a course for my chemistry, and he assisted with the DFT calculations that are presented in Chapter 5. I will also briefly thank A. J. Boydston and Keith

Keitz, who in addition to the people named above, have helped review various papers and research proposals for me. Although I hesitate to stray from science too much, I should also give a shout out to John, Kevin, Ian, and more recently Paul and Keith as the core group of Ath-goers through the past year, carrying on a long and illustrious Grubbs group tradition that I hope will continue after we are all gone.

I also greatly appreciate the interaction we have had with our collaborators. In particular, Professor Brian Yates and Nigel Brookes (University of Tasmania) have been instrumental in helping us understand many of the factors controlling the carbene generation and subsequent reactivity discussed in chapters 4 and 5, and I have enjoyed interacting with them. Additionally, Professor Oleg Ozerov and Yanjun Zhu (Texas A&M) have been very helpful when it came to discussing the nuances of pincer iridium chemistry and contributed some of the cyclic ether C–H activation results that are discussed in chapter 4.

Aside from my immediate colleagues, I am grateful to Alon Gorodetsky for his input and advice on research ideas that were removed from my field, and to Paul Oblad, who contributed to some of the work described in chapter 3. Also, while not wishing to acknowledge every individual who has influenced my choice of vocation, I do want give special thanks to Ron Hicks, my high school chemistry teacher who helped confirm my passion for the field, and Rodger Nutt, who steered me against all odds in the direction of inorganic chemistry, for which I am most grateful.

Lastly, I am incredibly thankful for my family: Jim, Janet, Ben, Rob, and my wife Charlotte. While not directly contributing to the ideas and experiments described herein, they have been a continuing source of love and support for me and have found the best possible balance of encouraging me and giving me a hard time when necessary. I am without a doubt a better scientist and person because of them.

Abstract

The preparation of transition-metal systems for catalytic multielectron transformations of small molecules remains a significant challenge for synthetic chemists. The realization of new transformations often depends critically on the design of frameworks capable of stabilizing unusual oxidation states and molecular geometries, providing a frontier molecular-orbital landscape that is well suited to interact with the molecules of interest. This thesis has sought to address two particularly noteworthy challenges in the field of small-molecule activation, dinitrogen reduction and C–H bond functionalization, through judicious ligand choice and design.

Chapters 2 and 3 describe the syntheses of new tri- and tetradentate hybrid ligands incorporating a single X-type donor (amido or silyl) and multiple phosphine donors designed to stabilize low oxidation states at iron and cobalt and support dinitrogen reduction and other multielectron redox transformations. While the amidophosphine ligands do allow access to unusual monovalent iron and cobalt complexes, the isolation of dinitrogen adducts supported by these ligands remains elusive and the weakness of the silicon–nitrogen bond makes the complexes prone to decomposition. In contrast, the tris(phosphino)silyl ligands presented in Chapter 3 afford straightforward access to the first terminally bonded dinitrogen complexes of monovalent iron, and the structure of these and related complexes are described along with preliminary experiments showing that protonolysis of the iron(I)–dinitrogen complexes produces hydrazine in reasonable stoichiometric yields.

Chapters 4 through 7 address the functionalization of ether and amine C–H bonds by a double C–H activation route. Chapter 4 describes the investigation of reactivity of low-valent, pincer-supported iridium species with a variety of ethers, leading to a number of selective C–H,

C–C, and C–O bond cleavage events, affording in several cases iridium carbene complexes by double C–H activation and loss of dihydrogen.

Chapter 5 presents an exploration of the electronic structure of the unusual square-planar iridium(I) alkoxy-carbenes and their nucleophilic activation of several heterocumulene substrates, leading to multiple-bond metathesis events promoted by metal- rather than ligand-initiated reactivity. Chapter 6 describes the discovery of new atom and group transfer reactions from diazo reagents to the alkoxy-carbenes and the implementation of these reactions in an unprecedented catalytic cycle for C=E bond formation by multiple C–H activations.

Chapter 7 explores the related reactivity of a low-valent pincer iridium complex with methyl amines and the reactivity of the resulting iridium(III) dihydrido aminocarbenes, which is shown to diverge substantially from that observed for the iridium(I) carbene species.

Table of Contents

Acknowledgments	iii
Abstract	vii
Table of Contents	ix
List of Figures	xi
List of Tables	xiii
List of Schemes	xiv
Chapter 1. Introduction	1
<i>Introduction</i>	2
<i>Dinitrogen Reduction: Insights and Challenges</i>	2
Background.....	2
Reduction of Dinitrogen at Iron Centers	5
<i>C–H Functionalization and Metal Carbene Reactivity</i>	6
Background.....	6
Carbene Generation by Multiple C–H Activations	7
Late-Metal Carbenes and the Continuum of M=C Reactivity	10
References and Notes.....	14
Chapter 2. Iron and Cobalt Complexes Supported by Tripodal Amidophosphine	
Hybrid Ligands	17
<i>Introduction</i>	18
<i>Results and Discussion</i>	20
Synthesis and Metalation of Amidophosphine Ligands	20
Reactivity of [SiNP _x]-Supported Iron and Cobalt Complexes	30
<i>Conclusions</i>	41
<i>Acknowledgment</i>	42
<i>Experimental Section</i>	43
<i>References and Notes</i>	61
Chapter 3. Dinitrogen Complexes Supported by Tris(phosphino)silyl Ligands	64
<i>Introduction</i>	65
<i>Results and Discussion</i>	66
Synthesis and Characterization of H[SiP ^{iPr} ₃]	66
Synthesis and Characterization of Di- and Trivalent [SiP ^{iPr} ₃]M Complexes	68
Electrochemical Characterization of Divalent Iron and Cobalt Complexes.....	73
Chemical Reduction to Generate Monovalent [SiP ^{iPr} ₃]M(N ₂) (M = Fe, Co, Ir)	77
Protonolysis of [SiP ^R ₃]Fe(N ₂) Complexes	85
<i>Conclusions</i>	87
<i>Acknowledgment</i>	87
<i>Experimental Section</i>	88
<i>References and Notes</i>	104

Chapter 4. C–H, C–O, and C–C Bond Activation at Pincer-Supported Iridium Frameworks	107
<i>Introduction</i>	108
<i>Results and Discussion</i>	110
Preparation of Anthraphos Ligands.....	110
Preparation of Iridium Precursors.....	111
Dehydrogenation of <i>tert</i> -Butyl Methyl Ether	114
Mechanism of MTBE Decarbonylation.....	120
Reaction of (PNP)Ir with Other Linear and Cyclic Ethers	124
Probing the Mechanism of Carbene Formation.....	138
<i>Conclusions</i>	142
<i>Acknowledgment</i>	144
<i>Experimental Section</i>	145
<i>References and Notes</i>	165
Chapter 5. A Distinct Class of M=C Bond Reactivity: Elucidation of Heterocumulene	
Activation by a Nucleophilic-at-Metal Iridium(I) Carbene	170
<i>Introduction</i>	171
<i>Results and Discussion</i>	173
Oxygen-Atom Transfer from CO ₂ to a Fischer Carbene at (PNP)Ir.....	173
Elucidation of Heterocumulene Activation at a (PNP)Ir Fischer Carbene	177
Computational Examination of (PNP)Ir–L Complexes.....	185
<i>Conclusions</i>	187
<i>Acknowledgment</i>	189
<i>Experimental Section</i>	189
<i>References and Notes</i>	202
Chapter 6. Catalytic Oxidation of Methyl Ethers by a Double C–H Activation-Group	
Transfer Process	206
<i>Introduction</i>	207
<i>Results and Discussion</i>	208
Stoichiometric Atom and Group Transfer from Diazo Reagents.....	208
Catalytic Oxidation of Methyl Ethers by a Double C–H Activation-Group	
Transfer Process.....	212
<i>Conclusions</i>	214
<i>Acknowledgment</i>	214
<i>Experimental Section</i>	215
<i>References and Notes</i>	222
Chapter 7. Synthesis and Reactivity of Iridium(III) Dihydrido Aminocarbenes	224
<i>Introduction</i>	225
<i>Results and Discussion</i>	226
Synthesis of Iridium(III) Dihydrido Aminocarbenes.....	226
Reactivity of Iridium(III) Dihydrido Aminocarbenes.....	229
<i>Conclusions</i>	232
<i>Acknowledgment</i>	233
<i>Experimental Section</i>	233
<i>References and Notes</i>	240

List of Figures

Chapter 1.

Figure 1.1. Possible interactions of metal carbenes with nucleophilic and electrophilic reagents	12
---	----

Chapter 2.

Figure 2.1. Displacement ellipsoid (35%) representation of $[\text{Si}^{\text{NP}_3}]\text{FeCl}$ (2.6)	22
Figure 2.2. UV-vis spectrum of $[\text{Si}^{\text{NP}_3}]\text{FeCl}$ (2.6) at various temperatures.....	23
Figure 2.3. Solid-state magnetic susceptibility of $[\text{Si}^{\text{NP}_3}]\text{FeCl}$ (2.6)	24
Figure 2.4. Cyclic voltammetry of $[\text{Si}^{\text{NP}_3}]\text{FeCl}$ (2.6)	24
Figure 2.5. Displacement ellipsoid (35%) representation of $[\text{Si}^{\text{NP}^{\text{Pr}}_3}]\text{FeCl}$ (2.8).....	25
Figure 2.6. Displacement ellipsoid (35%) representation and space-filling model of $[\text{Si}^{\text{NP}_3}]\text{CoI}$ (2.10).....	27
Figure 2.7. Displacement ellipsoid (35%) representations of $[\text{Si}^{\text{NP}_2}]\text{FeCl}$ (2.11) and $[\text{Si}^{\text{NP}_2}]\text{CoI}$ (2.13) and a space-filling representation of $[\text{Si}^{\text{NP}_2}]\text{FeCl}$ (2.11)	28
Figure 2.8. Cyclic voltammetry of $[\text{Si}^{\text{NP}_2}]\text{FeCl}$ (2.11) and $[\text{Si}^{\text{NP}_2}]\text{CoCl}$ (2.12)	29
Figure 2.9. Single-crystal X-ray structure of $[\text{Si}^{\text{NP}_3}]\text{Co}$ (2.14)	31
Figure 2.10. Molecular representations of dimeric siloxide complex (2.16)	33
Figure 2.11. Displacement ellipsoid (35%) representation of imido complex 2.18	35
Figure 2.12. Displacement ellipsoid (35%) representations of $[\text{Si}^{\text{NP}_2}]\text{Fe}(\text{Np})$ (2.19) and $[\text{Si}^{\text{NP}_2}]\text{Fe}(\text{NPh}_2)$ (2.20).....	37
Figure 2.13. Displacement ellipsoid (35%) representation of the dimeric bis(μ -phosphido) product from Na/Hg amalgam reduction of complex (2.21)	39
Figure 2.14. Displacement ellipsoid (35%) representation of $[\text{Si}^{\text{NP}_2}]\text{Fe}(\text{PMe}_3)$ (2.24)	40

Chapter 3.

Figure 3.1. Neutral and anionic tetradentate ligands related to the chemistry described herein	66
Figure 3.2. Displacement ellipsoid (35%) representations of $[\text{SiP}^{\text{Pr}}_3]\text{CoCl}$ (3.2) and $[\text{SiP}^{\text{Pr}}_3]\text{NiCl}$ (3.3)	68
Figure 3.3. Displacement ellipsoid (35%) representation of $[\text{SiP}^{\text{Pr}}_3]\text{Ir}(\text{H})(\text{Cl})$ (3.4) with inset of IR stretch and ^1H NMR signal for the Ir–H.....	70
Figure 3.4. Displacement ellipsoid (35%) representation of $[\text{SiP}^{\text{Pr}}_3]\text{FeCl}$ (3.6)	72
Figure 3.5. Space-filling models of $[\text{PhBP}^{\text{Pr}}_3]\text{FeCl}$ and $[\text{SiP}^{\text{Pr}}_3]\text{FeCl}$ (3.6)	73
Figure 3.6. Cyclic voltammograms of $[\text{SiP}^{\text{Pr}}_3]\text{FeCl}$ (3.6) under N_2 , $[\text{SiP}^{\text{Pr}}_3]\text{FeCl}$ (3.6) under Ar, and $[\text{SiP}^{\text{Ph}}_3]\text{FeCl}$ (3.8) under N_2	75
Figure 3.7. Cyclic voltammograms of $[\text{SiP}^{\text{Pr}}_3]\text{CoCl}$ (3.2) and $[\text{SiP}^{\text{Ph}}_3]\text{CoCl}$ (3.9) under N_2	76
Figure 3.8. Cyclic voltammogram of $[\text{SiP}^{\text{Pr}}_3]\text{NiCl}$ (3.3) under N_2	77
Figure 3.9. Displacement ellipsoid (35%) representation of $[\text{SiP}^{\text{Pr}}_3]\text{Fe}(\text{N}_2)$ (3.10).....	78
Figure 3.10. Cyclic voltammograms of $[\text{SiP}^{\text{Ph}}_3]\text{Fe}(\text{N}_2)$ (3.11) and $[\text{SiP}^{\text{Pr}}_3]\text{Fe}(\text{N}_2)$ (3.10).....	79
Figure 3.11. Displacement ellipsoid (35%) representation of $[\text{SiP}^{\text{Pr}}_3]\text{Co}(\text{N}_2)$ (3.13)	80
Figure 3.12. Displacement ellipsoid (35%) representation of $[\text{SiP}^{\text{Pr}}_3]\text{Ir}(\text{N}_2)$ (3.15)	81

Figure 3.13. Displacement ellipsoid (35%) representations of $[\text{SiP}^{i\text{Pr}}_3]\text{Co}(\text{CO})$ (3.16) and $\{[\text{SiP}^{i\text{Pr}}_3]\text{Co}(\text{OTf})\}\{\text{OTf}\}$ (3.17)	84
Figure 3.14. Displacement ellipsoid (35%) representation of $[\text{SiP}^{\text{Ph}}_3]\text{Fe}(\text{OTf})$ (3.18)	85
Chapter 4.	
Figure 4.1. Pincer-type ligands used in this study	110
Figure 4.2. Displacement ellipsoid (35%) representation of $(^{i\text{Pr}}\text{Anthraphos})\text{Ir}(\text{CH}_3)(\text{I})$ (4.6) ..	114
Figure 4.3. Structural representation of <i>trans</i> - $(^{i\text{Pr}}\text{Anthraphos})\text{Ir}(\text{H})_2(\text{CO})$ (4.7)	116
Figure 4.4. Displacement ellipsoid (35%) representation of $(\text{PNP})\text{Ir}=\text{C}(\text{H})\text{O}^t\text{Bu}$ (4.9)	118
Figure 4.5. Displacement ellipsoid (35%) representation of <i>trans</i> - $(\text{PNP})\text{Ir}(\text{H})_2(\text{CO})$ (4.10) ...	119
Figure 4.6. Predicted ground-state molecular-orbital diagram for $(\text{PNP})\text{Ir}=\text{C}(\text{H})\text{O}^t\text{Bu}$ (4.9). 122	
Figure 4.7. Structural representation of $(\text{PNP})\text{Ir}=\text{CO}(\text{CH}_2)_3$ (4.15)	129
Figure 4.8. Displacement ellipsoid (35%) representation of ethyl vinyl ether adduct 4.16 .	131
Figure 4.9. Structure representation of $(\text{PNP})\text{Ir}(\text{Ph})(\text{CO})(\text{H})$ (4.18)	134
Chapter 5.	
Figure 5.1. Possible modes of reactivity of metal carbenes with nucleophiles and electrophiles	172
Figure 5.2. Displacement ellipsoid (35%) representation of $(\text{PNP})\text{Ir}-\text{CO}$ (5.3)	174
Figure 5.3. Plot of k_{obs} versus concentration of CO_2 for the reaction of 5.2 with CO_2 at $-20\text{ }^\circ\text{C}$	176
Figure 5.4. Displacement ellipsoid (35%) representation of $(\text{PNP})\text{Ir}(\text{C}_2\text{S}_4)(\text{CHO}^t\text{Bu})$ (5.4)	179
Figure 5.5. Displacement ellipsoid (35%) representation of $(\text{PNP})\text{Ir}-\text{CS}$ (5.5)	180
Figure 5.6. Displacement ellipsoid (35%) representation of $(\text{PNP})\text{Ir}-\text{CNPh}$ (5.6)	182
Figure 5.7. Displacement ellipsoid (35%) representation of complex 5.8	184
Figure 5.8. Common bonding motifs for isothiocyanate dimers	184
Figure 5.9. Molecular surfaces of frontier orbitals calculated for $(\text{PNP})\text{Ir}=\text{C}(\text{H})\text{O}^t\text{Bu}$ (5.2) ...	185
Figure 5.10. Frontier molecular orbitals for $(\text{PNP})\text{Ir}=\text{C}(\text{H})\text{O}^t\text{Bu}$ (5.2)	196
Figure 5.11. Frontier molecular orbitals for $(\text{PNP})\text{Ir}-\text{CO}$ (5.3)	197
Figure 5.12. Frontier molecular orbitals for $(\text{PNP})\text{Ir}-\text{CS}$ (5.5)	198
Figure 5.13. Frontier molecular orbitals for $(\text{PNP})\text{Ir}-\text{CNPh}$ (5.6)	199
Chapter 6.	
Figure 6.1. Displacement ellipsoid (35%) representation of $(\text{PNP})\text{Ir}-\text{N}_2$ (6.3)	210
Chapter 7.	
Figure 7.1. Displacement ellipsoid (35%) representation of aminocarbene 7.2_{anti}	228
Figure 7.2. Displacement ellipsoid (35%) representation of complex 7.4	230
Figure 7.3. Displacement ellipsoid representation of complex 7.6	231

List of Tables

Chapter 2.

Table 2.1. Comparison of N–Fe bond lengths in tetrahedral Fe(II) amido complexes	38
Table 2.2. X-ray crystallographic data for Chapter 2	57

Chapter 3.

Table 3.1. Representative dinitrogen stretching frequencies for complexes of Fe, Co, and Ir	82
Table 3.2. Summary of protonolytic hydrazine formation experiments for $[\text{SiP}^{\text{R}}_3]\text{Fe}(\text{N}_2)$	86
Table 3.3. X-ray crystallographic data for Chapter 3	100

Chapter 4.

Table 4.1. X-ray crystallographic data for Chapter 4	162
---	-----

Chapter 5.

Table 5.1. Energies of Ir(d_{z^2}) orbitals for (PNP)Ir–L molecules	187
Table 5.2. X-ray crystallographic data for Chapter 5	200

Chapter 6.

Table 6.1. Iridium-catalyzed oxidation of methyl ethers to formimidates	213
Table 6.2. X-ray crystallographic data for Chapter 6	221

Chapter 7.

Table 7.1. X-ray crystallographic data for Chapter 7	239
---	-----

List of Schemes

Chapter 1.

Scheme 1.1. Cummins' cleavage of dinitrogen at tris(anilido)molybdenum(III) centers	4
Scheme 1.2. Chatt-type cycle for nitrogen fixation at a monovalent iron center	5
Scheme 1.3. Alkane C–H activation at Cp*-supported iridium(I)	7
Scheme 1.4. A typical transfer dehydrogenation reaction	8
Scheme 1.5. Different products obtained by α - versus β -elimination from a metal alkyl.....	8
Scheme 1.6. Shaw's chelate-assisted formation of an iridium carbene	9
Scheme 1.7. Generation of a cyclic carbene at Tp*-supported iridium(III)	10
Scheme 1.8. Reversible α -hydrogen migration at Bergman's iridium(III) carbene.....	11

Chapter 2.

Scheme 2.1. Synthesis of Li[^{Si} NP ₃] Ligand	21
Scheme 2.2. Synthesis of Li[^{Si} NP ₂] Ligand	21
Scheme 2.3. Synthesis of Li[^{Si} NP ^{iPr} ₃] ligand and metalation at iron.	25
Scheme 2.4. Reaction of [^{Si} NP ₃]Co (2.14) with CO ₂	34
Scheme 2.5. Formation of cationic cobalt imide 2.18 by Si–N bond cleavage	34
Scheme 2.6. Representative ligand metathesis reactions at [^{Si} NP ₂]FeCl (2.11).....	36

Chapter 3.

Scheme 3.1. Synthesis and displacement ellipsoid representation of H[SiP ^{iPr} ₃] (3.1)	67
Scheme 3.2. Metalation of H[SiP ^{iPr} ₃]ligand by chelate-assisted Si–H oxidative addition	69
Scheme 3.3. Metalation of H[SiP ^{iPr} ₃] ligand at iron and displacement ellipsoid representation of (H[SiP ^{iPr} ₃])FeCl ₂ (3.5).....	71
Scheme 3.4. Generation of [SiP ^{iPr} ₃]M(N ₂) complexes from corresponding di- and trivalent metal halides (M = Fe, Co, Ir)	81
Scheme 3.5. Dinitrogen release from complex 3.13 upon displacement or chemical oxidation	83

Chapter 4.

Scheme 4.1. Accepted mechanism for alkane dehydrogenation at pincer-supported iridium	109
Scheme 4.2. Formation of heteroatom-substituted carbenes by double C–H activation	109
Scheme 4.3. Preparation of ^{iPr} Anthrphos ligand 4.2	111
Scheme 4.4. Metalation of pincer ligands and precursor syntheses	112
Scheme 4.5. Synthesis and derivatization of (^{iPr} Anthrphos)Ir(N ₂) (4.5)	113
Scheme 4.6. Decarbonylation of MTBE at (^{iPr} Anthrphos)Ir to give <i>trans</i> -dihydrido carbonyl complex 4.7	115
Scheme 4.7. Formation and decarbonylative decomposition of (PNP)Ir=C(H)O ^t Bu (4.9)	117
Scheme 4.8. Proposed mechanism for decarbonylation of MTBE by (pincer)Ir frameworks	120
Scheme 4.9. Reaction of (PNP)IrH ₂ (4.8) with excess carbon monoxide	123
Scheme 4.10. An alternative mechanism for carbene decarbonylation by generation of an alkoxy carbene	123

Scheme 4.11. Dehydrogenation of diethyl ether at (tmeda)Pt to afford vinyl ether and carbene adducts.....	125
Scheme 4.12. Formation of carbenes from methyl ethers at (PNP)Ir	127
Scheme 4.13. C–H activation of dioxane at (PNP)Ir	133
Scheme 4.14. Proposed mechanisms of benzyl methyl ether decarbonylation at (PNP)Ir ..	136
Scheme 4.15. Possible mechanism for decarbonylation of 1,3,5-trioxane at (PNP)Ir	138
Scheme 4.16. Proposed mechanism of formation for carbene 4.15	139
Scheme 4.17. Proposed mechanisms of formation for carbene 4.9 and trapped intermediate 4.19-CO	141
Scheme 4.18. Possible isomers of the elemental content [(PNP)Ir + ether] ([Ir] = (PNP)Ir) .	143
Chapter 5.	
Scheme 5.1. Generation of an iridium carbene by double C–H activation of MTBE.	171
Scheme 5.2. Proposed mechanism of CO ₂ decarbonylation by carbene 5.2	175
Scheme 5.3. Acceptorless dehydrogenative oxidation of MTBE to <i>tert</i> -butyl formate via oxygen-atom transfer from CO ₂	177
Scheme 5.4. Reaction of carbene 5.2 with carbon disulfide.....	179
Scheme 5.5. Reaction of carbene 5.2 with phenyl isothiocyanate	182
Scheme 5.6. Nucleophilic reactivity of (PNP)Ir–CNPh (5.6)	184
Scheme 5.7. Contrasting carbon dioxide reactivity of a high-valent alkylidene and nucleophilic-at-metal carbene 5.2	188
Chapter 6.	
Scheme 6.1. Proposed cycle for MTBE oxidation.....	209
Scheme 6.2. Proposed mechanism of nitrene-group transfer from RN ₃ to carbene 6.1	210
Scheme 6.3. Stepwise oxidation of MTBE via double C–H activation to generate carbene 6.1	212
Chapter 7.	
Scheme 7.1. Dehydrogenation of <i>tert</i> -butyl methyl ether at (PNP)Ir generates an Ir(I) carbene.	226
Scheme 7.2. Dehydrogenation of TMEDA at (PNP)Ir yields two isomeric aminocarbenes. .	227
Scheme 7.3. Reaction of aminocarbene 7.2 with PMe ₃ and CO (R = (CH ₂) ₂ NMe ₂).....	230

Chapter 1

Introduction

The text in this chapter is reproduced in part with permission from:

Whited, M. T.; Grubbs, R. H. *Acc. Chem. Res.*, submitted.

Unpublished material copyright 2009 American Chemical Society

Introduction

The use of low-valent transition metals to transform the strongest bonds of small molecules has become a hallmark of modern inorganic chemistry. Inspired by Nature's ability to perform such intriguing transformations as dinitrogen reduction, the water-gas shift reaction, and selective alkane oxidation under ambient conditions, scientists have sought to make these and other reactions into accessible tools for the synthetic chemist by taming the transition metals through deliberate ligand design.

This introduction seeks to provide background on two key challenges in the field of small-molecule activation that are addressed in this thesis: dinitrogen reduction and C–H bond functionalization. The topic of dinitrogen reduction will be presented from a biologically relevant and biomimetic context and will focus on the use of iron-based systems to accomplish this task. The topic of C–H functionalization will especially focus on the strategy of utilizing multiple C–H activations to generate metal carbenes for further elaboration, and as a result the reactivity of metal carbene complexes will also be briefly examined.

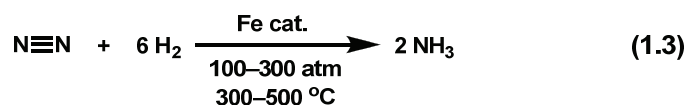
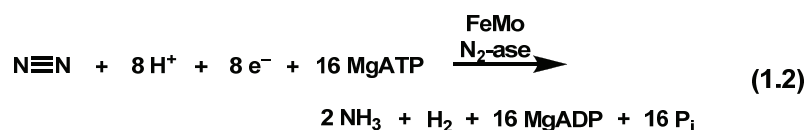
Dinitrogen Reduction: Insights and Challenges

Background

The use of transition-metal catalysts to effect the reduction of dinitrogen to ammonia has long been an important goal for inorganic chemists (eq 1.1).¹ The standard free-energy change, ΔG° , for the gas-phase reaction in eq 1.1 is -7.7 kcal/mol at 298 K and 1 atm.² Thus, transition-metal catalysis should offer the possibility of selective N_2 reduction under ambient conditions.



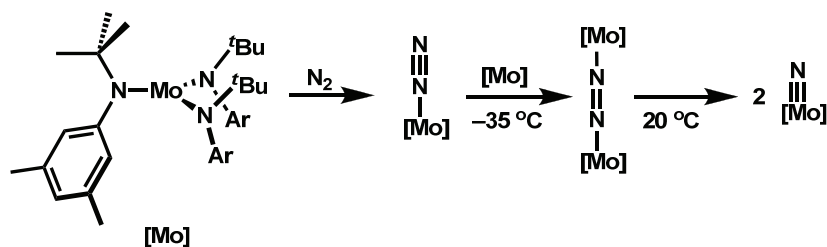
Nature provides much of the inspiration for this goal, since the nitrogenase enzymes are well known to effect the conversion of atmospheric nitrogen to ammonia under physiological conditions (eq 1.2), a process that is essential for providing much of the bioavailable nitrogen required for sustaining life on earth.^{2,3} Alternatively, the Haber-Bosch process effects the same outcome by somewhat different means, utilizing high temperatures and pressures to convert dinitrogen to ammonia over heterogeneous catalysts (eq 1.3).⁴



The common element of both catalytic transformations is the frequent use of iron. Although the most familiar version of the nitrogenase enzyme contains a molybdenum site in the cofactor (FeMo-N₂ase), iron is the only element that is common to all versions of the nitrogenase enzymes.⁵ As shown above (eq 1.3), iron is also used as a solid catalyst for the Haber-Bosch process. The iron centers certainly play different roles in these markedly divergent approaches to nitrogen fixation, but the presence of iron as a common thread that links the two processes has encouraged chemists to search for ways to emulate the biological system through deliberate ligand design. In this context, the chemistry of dinitrogen coordination and functionalization at iron centers is surprisingly underdeveloped.

The coordination chemistry of dinitrogen is vast, and even a cursory review of the relevant literature is beyond the scope of this introduction. However, two salient examples of N₂ reduction at molybdenum have been particularly important in motivating the work described in this thesis and warrant some examination. The first example of a well-defined scission of the

N≡N bond came from the laboratory of Cummins, who reported that certain three-coordinate tris(anilido)molybdenum(III) complexes were competent to generate the corresponding tris(anilido)molybdenum(VI) nitrides from dinitrogen via a bimetallic cleavage mechanism, as shown in Scheme 1.1.⁶



Scheme 1.1. Cummins' cleavage of dinitrogen at tris(anilido)molybdenum(III) centers.

More recently, Schrock has expanded on these results, showing that Mo(III) centers supported by a related bulky triamidoamine ligand can serve as catalysts for dinitrogen fixation under mild conditions upon addition of proton and electron equivalents.⁷ A key to the realization of this chemistry was the design of molybdenum systems capable of supporting terminal adducts of dinitrogen without dimerization,⁸ an observation has motivated the work described in chapter 3 of this thesis. The Schrock system represents a variation on the Chatt cycle, formulated in the early days of nitrogen-fixation research, which outlines a mechanism for reduction of dinitrogen to ammonia at molybdenum(0) centers,⁹ proving that a commercially viable process for homogeneous reduction of N₂ may be feasible.

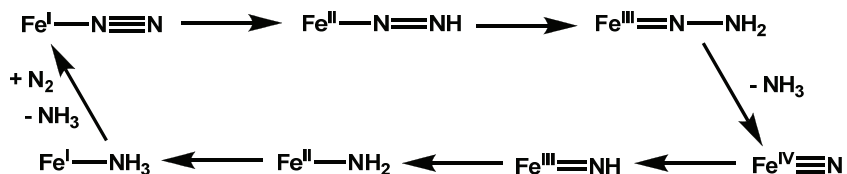
These findings highlight several keys to the discovery of methods for N₂ fixation. First and most obviously, the requirements for coordination of N₂ at transition metals must be understood and exploited. Second, fine control over the environment of the metal center and binding pocket must be achieved in order to prevent undesirable side reactions. Finally, to be able to fix N₂ in a catalytic fashion, the metal centers utilized must be able to access a large range of oxidation states in order to support this six-electron process. It has been our goal to

extend to iron many of the principles and findings previously demonstrated at molybdenum and other early-metal centers.

Reduction of Dinitrogen at Iron Centers

Before 2003, the great majority of dinitrogen research utilizing iron focused on iron(0) since low-valent, electron-rich metals can often accommodate the weakly π -acidic N_2 ligand in a vacant coordination site. Polyphosphine-supported iron(0) centers were shown to bind N_2 readily,¹⁰ and in some cases low yields of ammonia and/or hydrazine could be obtained by protonolysis of these complexes.^{10a,c} However, catalytic N_2 fixation was not demonstrated and, in contrast with the molybdenum systems, very few relevant intermediates could be prepared due to the reluctance of iron to accommodate π -basic nitrogenous ligands.

More recently, the Peters and Holland research groups have shown that low-coordinate iron(I) sites can accommodate dinitrogen ligands and, in some cases, these same platforms can exhibit the necessary redox flexibility to facilitate multielectron small-molecule reductions.¹¹ Inspired by these results and relevant studies on the biological systems, we have recently targeted a scheme akin to the Chatt cycle in which a monovalent iron center binds N_2 and mediates its reduction via proton/electron equivalents (Scheme 1.2).¹²



Scheme 1.2. Chatt-type cycle for nitrogen fixation at a monovalent iron center.

In this context, multidentate, monoanionic ligands are particularly attractive since they allow such a cycle to proceed at neutral iron centers. As mentioned above, Peters and Holland have recently shown that certain monoanionic ligands can support iron(I)- N_2 adducts, but in all

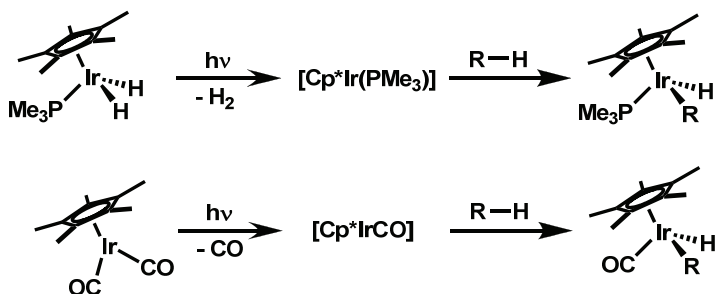
cases these complexes have contained bridging N_2 units.^{11d,f} This characteristic is certainly at least partially responsible for the observation that, in contrast to many terminal N_2 adducts of iron(0) and iron(II), such bridging $Fe^I-N_2-Fe^I$ complexes do not afford ammonia or hydrazine upon protonolysis.^{11d} Unfortunately, all attempts to retrofit the tris(phosphino)borate ligands of Peters in order to prevent dimerization have failed to allow access to such terminal N_2 adducts of iron(I).

Thus, if the desired Fe^I-N_2 complexes, which serve as a starting point for the hypothetical N_2 reduction cycle depicted in Scheme 1.2, are to be accessed, unique ligand architectures will be needed. It is with this observation in mind that we have targeted two families of monoanionic polyphosphine ligands containing a single X-type donor that binds directly to the metal center, rendering them distinct from the formally zwitterionic tris(phosphino)borate metal complexes pioneered by Peters and co-workers. Chapters 2 and 3 of this thesis describe the synthesis and fundamental coordination chemistry of new amidophosphine and silylphosphine ligands and efforts toward the realization of a Chatt-type cycle for dinitrogen fixation at iron centers supported by these scaffolds.

C–H Functionalization and Metal Carbene Reactivity

Background

Like dinitrogen reduction, the activation and functionalization of typically inert carbon–hydrogen bonds has occupied a central role in inorganic and organometallic chemistry for many years. Pioneering studies by Bergman¹³ and Graham¹⁴ showed that isolable iridium complexes could cleave C–H bonds in a well-defined and predictable way (Scheme 1.3).



Scheme 1.3. Alkane C–H activation at Cp^{*}-supported iridium(I).

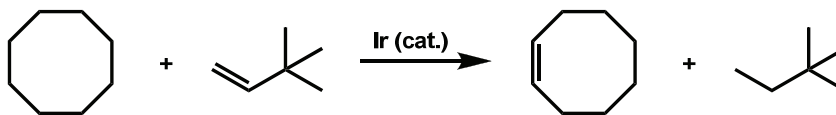
Since these initial reports, myriad transition-metal complexes have been reported that are capable of cleaving C–H bonds by such diverse methods as oxidative addition, σ -bond metathesis, electrophilic activation, 1,2-addition, and radical pathways.¹⁵ Some progress has been made toward the development of new catalytic oxidative C–H functionalization methods.¹⁶ However, the general application of such methods in organic synthesis still remains a somewhat elusive goal for organometallic chemists.

Carbene Generation by Multiple C–H Activations

Most schemes for C_{sp}³–H functionalization involve an initial C–H cleavage step, leading to the formation of a singly bonded M–C_{sp}³ species that may be further elaborated. However, in addition to the difficulty associated with achieving catalytic turnover, this approach limits the kinds of products that may be formed to those generated by functionalizing a metal–carbon single bond. As a result, there are few successful examples of catalytic C_{sp}³–H functionalization at transition-metal centers.

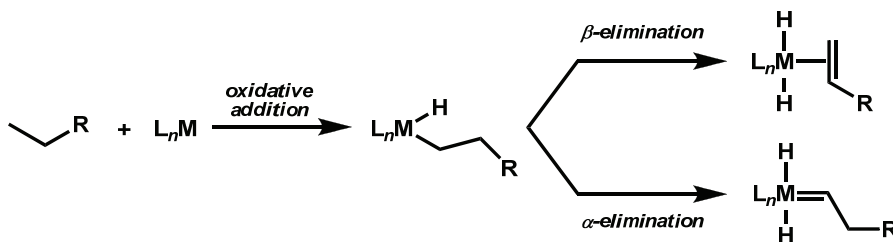
One approach to functionalizing the intermediate M–C_{sp}³ complexes is to utilize a second C–H cleavage event, often a β -hydrogen elimination to generate alkene. This method was first introduced by Crabtree¹⁷ and has seen major improvements in scope and efficiency with the advent of pincer-type ligands.¹⁸ Nevertheless, the most common schemes employ

olefins as terminal oxidants, so their utility is somewhat hampered by the fact that one olefin is simply being traded for another (Scheme 1.4).



Scheme 1.4. A typical transfer dehydrogenation reaction.

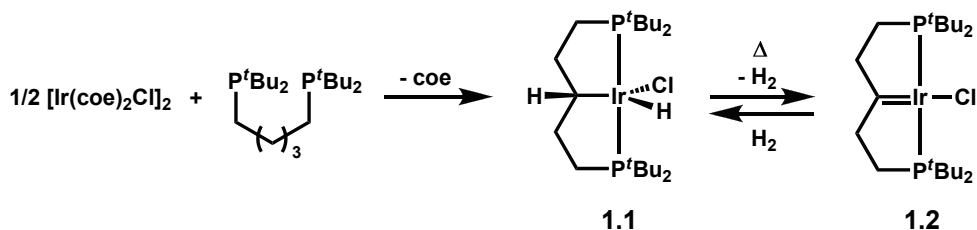
One might easily envision, however, that the second C–H cleavage is not required to be a β -elimination. Instead, if α -hydrogen migration ensues, a metal–carbene complex (an isomer of the metal-bound olefin) will be formed (Scheme 1.5). Generation of an $M=C_{sp^2}$ species by such a route could offer new possibilities for catalytic C–H functionalization, particularly in light of the rich reactivity previously demonstrated for metal-bound carbenes.¹⁹ We were intrigued by this possibility since, at the outset of our work, there were few examples of well-defined reactivity for any $M=C_{sp^2}$ complexes generated by multiple C–H activations.²⁰



Scheme 1.5. Different products obtained by α - versus β -elimination from a metal alkyl.

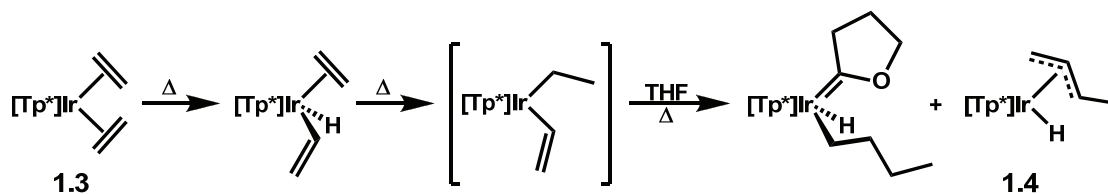
The first indication that late metals may be capable of generating carbenes by α,α -dehydrogenation came from the laboratory of Shaw, who reported that a pincer iridium complex (**1.1**), formed from reaction of an iridium(I) synthon with 1,5-bis(di-*tert*-butylphosphino)pentane, would release hydrogen upon sublimation to afford the pincer-type carbene complex **1.2** (Scheme 1.6).²¹ This reaction is certainly helped by the chelate assistance of the strong phosphine donors, preorganizing the system and stabilizing the carbene that is

ultimately formed, but the report was very important in showing that α,α -dehydrogenation and loss of H_2 to afford a stable metal carbene can be a favorable process at late metals. In fact, it was this finding that inspired much of the work we have undertaken at pincer-supported iridium centers.



Scheme 1.6. Shaw's chelate-assisted formation of an iridium carbene (coe = cyclooctene).²¹

Several other examples of chelate-assisted carbene formation via multiple C–H activations have been reported,²² but the catalytic potential of this route is generally limited because the chelate assistance not only favors carbene formation but also prevents functionalization and release since the carbene must be linked to at least one strong donor that can be difficult to labilize. Thus, Carmona's 1992 report of selective double C–H activation of cyclic ethers to generate the corresponding Fischer-type carbenes was a major advance for this field.²³ The $[Tp^*]Ir(C_2H_4)_2$ complex (**1.3**) was shown to form heteroatom-substituted carbenes from tetrahydrofuran, 2-methyltetrahydrofuran, 1,3-dioxolane, and 1,4-dioxane (Scheme 1.7, $Tp^* = HB(3,5-Me_2-pz)_3^-$). For this system, competitive degradation to an allyl hydride (**1.4**) was inevitably observed, accounting for between 20% and 60% of the iridium-containing product. Clearly a quantitative method would be needed in order to implement this process in any catalytic cycle.



Scheme 1.7. Generation of a cyclic carbene at Tp*-supported iridium(III).²³

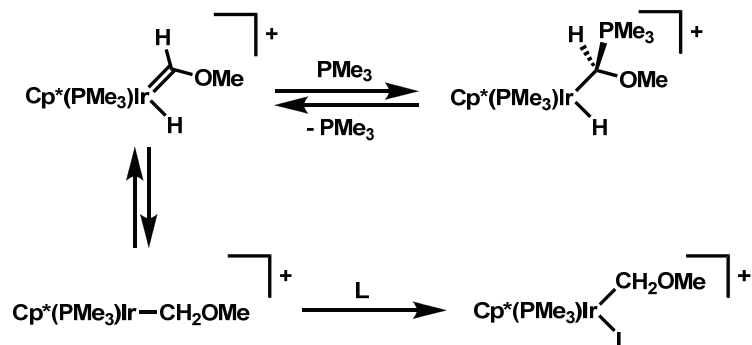
Shortly after Carmona's seminal discovery, Taube reported that reduction of Os^{III}(NH₃)₄(CF₃SO₃)₃ with Zn/Hg amalgam in THF affords an octahedral osmium(II) product with carbene and dihydrogen ligands.²⁴ This system also generates carbenes by double C–H activation of 1,4-dioxane and tetrahydropyran. Unlike [Tp*]Ir(C₂H₄)₂ (**1.3**), Taube's system forms the carbene in good yield (>80%) and the reaction completes in less than 1 h at ambient temperature.

In the years following Taube's paper, the generation of carbenes by double C–H activation was shown to be a more general phenomenon, and Bergman (Ir),²⁰ Bercaw (Pt),²⁵ Caulton (Ru, Os),²⁶ and Crabtree (Ir)²⁷ all published examples of systems capable of forming heteroatom-substituted carbenes by multiple C–H cleavage events. Carmona also reported variants of the original [Tp*]Ir(C₂H₄)₂ system that could generate heteroatom-substituted carbenes cleanly from a large number of ethers and amines.²⁸

Late-Metal Carbenes and the Continuum of M=C Reactivity

Although there are now several systems that can generate late-metal carbenes through a multiple C–H activation process, the reactivity of the resulting carbenes has not been thoroughly investigated. One case for which reactivity has been reported is Bergman's methoxycarbene, Cp*(PMe₃)Ir=C(H)OCH₃ (**1.5**), for which reactivity appears to be dominated by

reversible iridium-to-carbene hydride migration (Scheme 1.8).²⁰ Thus, the reactive species for the Bergman system is typically not an iridium carbene but an iridium alkyl.²⁹



Scheme 1.8. Reversible α -hydrogen migration at Bergman's iridium(III) carbene.

However, late transition metals such as the ones shown to form carbenes by multiple C–H activations are well known to form coordinatively unsaturated complexes, the most prevalent of which is the square-planar, d^8 configuration.³⁰ For such complexes, metal-initiated reactivity must be considered since an electrophilic or, more plausibly, nucleophilic metal center might dominate reactivity pathways. This principle is beautifully exemplified in the formation of 1:1 adducts between Vaska's complex, which acts as a transition-metal Lewis base, and trifluoroborane, a typical strong Lewis acid.³¹ Thus, it is reasonable to expect that a square-planar iridium(I)–carbene complex, if it can be isolated, will react in a similar fashion and to provide products derived from metal-initiated nucleophilic reactivity. Here an analogy can be made to the carbenes of coordinatively unsaturated, high-valent early metals, where the electrophilic metal center can play an important role in directing reaction pathways.

This formulation differs in important ways from the archetypal descriptions of Shrock- and Fischer-type carbenes, which are typically assumed to react in either a nucleophilic or electrophilic fashion at C_α .³² However, the description fits nicely into a continuum for metal carbene reactivity originally proposed by Roper more than 20 years ago, where the interactions

of metal carbenes with nucleophiles and electrophiles fall into four limiting categories that may be metal or carbene initiated (Figure 1.1).³³

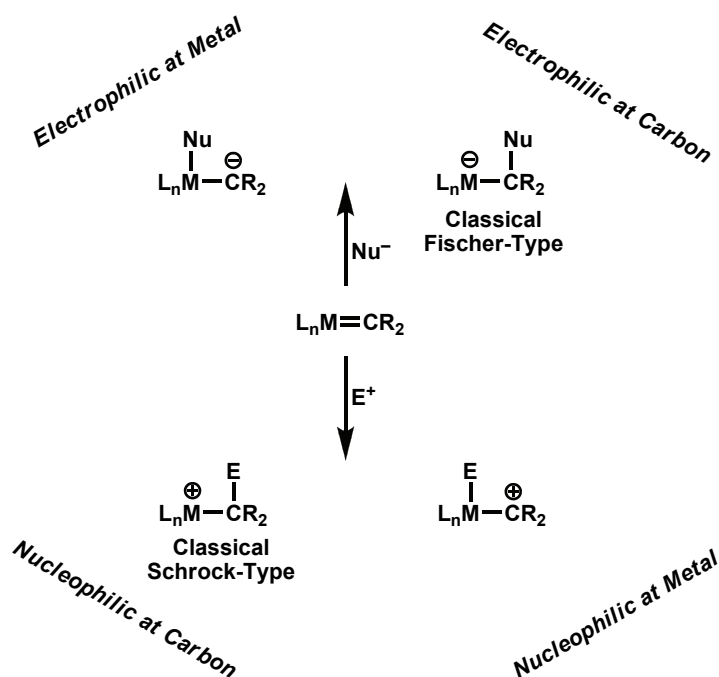


Figure 1.1. Possible interactions of metal carbenes with nucleophilic and electrophilic reagents.³³

Classical Fischer-type reactivity (top right in Figure 1.1) is often observed for heteroatom-substituted carbenes attached to early metals with electron-withdrawing co-ligands, and has been exploited frequently to exchange substituents on Fischer-type complexes.³⁴ Nucleophilic reactivity at C_{α} (bottom left in Figure 1.1) is most frequently observed for Schrock-type alkylidenes, for instance in the coordination of trimethylaluminum to a well-characterized tantalum(V) methylidene.³⁵ However, nucleophilic reactivity at C_{α} has also been reported for heteroatom-substituted carbenes ligated to sufficiently reduced metal centers.³⁶ Electrophilic reactivity at the metal center is also common for high-valent alkylidenes, as demonstrated in the trapping of a titanium(IV) methylidene with phosphine ligands.³⁷

Clearly these designations are not absolute, with many complexes showing ambiphilic reactivity depending on reaction conditions. Additionally, cooperative substrate activation across metal–carbon multiple bonds, which falls somewhere between the top and bottom hemispheres of Figure 1.1, is clearly important in several processes such as the Wittig-type olefination of amides and esters by Tebbe’s reagent, which does not occur with simple phosphorus ylides.³⁸

Nonetheless, this description of potential modes for metal carbene reactivity provides an important framework for understanding the electronic descriptions and reaction profiles for late-metal carbenes. It is with these findings as a backdrop that Chapters 4 and 7 present a thorough study of the C–H activation of a variety of ethers and amines, affording in some cases the desired square-planar iridium(I) carbenes as products. Additionally, in Chapters 5 and 6, the reactivity of such species is examined and shown to diverge in important ways from classical Fischer- or Schrock-type systems, and it is shown that the description of Roper provides a useful framework for understanding the unprecedented reaction pathways that are observed for several of the carbenes generated in such a fashion.

References and Notes

- (1) (a) Gambarotta, S. *J. Organomet. Chem.* **1995**, *500*, 117. (b) Hidai, M. *M. Y. Chem. Rev.* **1995**, *95*, 1115. (c) Fryzuk, M. D.; Johnson, S. A. *Coord. Chem. Rev.* **2000**, *200–202*, 379.
- (2) Howard, J. B.; Rees, D. C. *Chem. Rev.* **1996**, *96*, 2965.
- (3) Burgess, B. K.; Lowe, D. J. *Chem. Rev.* **1996**, *96*, 2983.
- (4) (a) Ertl, G. In *Catalytic Ammonia Synthesis*; Jennings, J. R., Ed.; Plenum Press: New York, 1991. (b) Appl, M. *Ammonia*; Wiley-VCH: Weinheim, 1999. (c) Greenwood, N. N.; Earnshaw, A. *Chemistry of the Elements*, 2nd ed.; Butterworth-Heinemann: Oxford, 1997.
- (5) MacKay, B. A.; Fryzuk, M. D. *Chem. Rev.* **2004**, *104*, 385.
- (6) (a) Laplaza, C. E.; Cummins, C. C. *Science* **1995**, *268*, 861. (b) Laplaza, C. E.; Johnson, M. J. A.; Peters, J. C.; Odom, A. L.; Kim, E.; Cummins, C. C.; George, G. N.; Pickering, I. J. *J. Am. Chem. Soc.* **1996**, *118*, 8623.
- (7) (a) Yandulov, D. V.; Schrock, R. R. *Science* **2003**, *301*, 76. (b) Yandulov, D. V.; Schrock, R. R. **2002**, *124*, 6252.
- (8) Schrock, R. R. *Acc. Chem. Res.* **2005**, *38*, 955.
- (9) (a) Chatt, J.; Dilworth, J. R.; Richards, R. L. *Chem. Rev.* **1978**, *78*, 589. (b) Pickett, C. J. *J. Biol. Inorg. Chem.* **1996**, *1*, 601.
- (10) (a) Leigh, G. J. *Acc. Chem. Res.* **1992**, *25*, 177. (b) Komiyama, S.; Akita, M.; Yoza, A.; Kasuga, N.; Fukuoka, A.; Kai, Y. *J. Chem. Soc., Chem. Commun.* **1993**, 787. (c) George, T. A.; Rose, D. J.; Chang, Y. D.; Chen, Q.; Zubieta, J. *Inorg. Chem.* **1995**, *34*, 1295.
- (11) (a) Brown, S. D.; Betley, T. A.; Peters, J. C. *J. Am. Chem. Soc.* **2003**, *125*, 322. (b) Brown, S. D.; Peters, J. C. *J. Am. Chem. Soc.* **2005**, *127*, 1913. (c) Brown, S. D.; Mehn, M. P.; Peters, J. C. *J. Am. Chem. Soc.* **2005**, *127*, 13146. (d) Betley, T. A.; Peters, J. C. *J. Am. Chem. Soc.* **2003**, *125*, 10782. (e) Betley, T. A.; Peters, J. C. *J. Am. Chem. Soc.* **2004**, *126*, 6252. (f) Smith, J. M.; Lachicotte, R. J.; Pittard, K. A.; Cundari, T. R.; Lukat-Rodgers, G.; Rodgers, K. R.; Holland, P. L. *J. Am. Chem. Soc.* **2001**, *123*, 9222. (g) Holland, P. L. *Can. J. Chem.* **2005**, *83*, 296. (h) Smith, J. M.; Sadique, A. R.; Cundari, T. R.; Rodgers, K. R.; Lukat-Rodgers, G.; Lachicotte, R. J.; Flaschenriem, C. J.; Vela, J.; Holland, P. L. *J. Am. Chem. Soc.* **2006**, *128*, 756. (i) Hendrich, M. P.; Gunderson, W.; Behan, R. K.; Green, M. T.; Mehn, M. P.; Betley, T. A.; Lu, C. C.; Peters, J. C. *Proc. Natl. Acad. Sci. U.S.A.* **2006**, *103*, 17107.
- (12) MacBeth, C. E.; Harkins, S. B.; Peters, J. C. *Can. J. Chem.* **2005**, *83*, 332.
- (13) (a) Janowicz, A. H.; Bergman, R. G. *J. Am. Chem. Soc.* **1982**, *104*, 352. (b) Janowicz, A. H.; Bergman, R. G. *J. Am. Chem. Soc.* **1983**, *105*, 3929.

- (14) Hoyano, J. K.; McMaster, A. D.; Graham, W. A. G. *J. Am. Chem. Soc.* **1983**, *105*, 7190.
- (15) (a) Labinger, J. A.; Bercaw, J. E. *Nature*, **2002**, *417*, 507. (b) Periana, R. A.; Bhalla, G.; Tenn, W. J.; Young, K. J. H.; Liu, X. Y.; Mironov, O.; Jones, C. J.; Ziatdinov, V. R. *J. Mol. Catal. A: Chem.* **2004**, *220*, 7.
- (16) For leading references, see: Dick, A. R.; Sanford, M. S. *Tetrahedron* **2006**, *62*, 2439.
- (17) Crabtree, R. H.; Mihelcic, J. M.; Quirk, J. M. *J. Am. Chem. Soc.* **1979**, *101*, 7738.
- (18) (a) Jensen, C. M. *Chem. Commun.* **1999**, *24*, 2443. (b) Liu, F.; Pak, E. B.; Singh, B.; Jensen, C. M.; Goldman, A. S. *J. Am. Chem. Soc.* **1999**, *121*, 4086. (c) Gupta, M.; Hagen, C.; Flesher, R. J.; Kaska, W. C.; Jensen, C. M. *Chem. Commun.* **1996**, *17*, 2083. (d) Göttker-Schnetmann, I.; White, P.; Brookhart, M. *J. Am. Chem. Soc.* **2004**, *126*, 1804.
- (19) (a) Doyle, M. P. *Chem. Rev.* **1986**, *86*, 919. (b) Doyle, M. P.; Forbes, D. C. *Chem. Rev.* **1998**, *98*, 911. (c) *Handbook of Metathesis*; Grubbs, R. H., Ed.; Wiley-VCH: Weinheim, Germany, 2003.
- (20) Luecke, H. F.; Arndtsen, B. A.; Burger, P.; Bergman, R. G. *J. Am. Chem. Soc.* **1996**, *118*, 2517.
- (21) Empsall, H. D.; Hyde, E. M.; Markham, R.; McDonald, W. S.; Norton, M. C.; Shaw, B. L.; Weeks, B. *J. Chem. Soc., Chem. Commun.* **1977**, 589.
- (22) For another early example, see Werner, H.; Weber, B.; Nürnberg, O.; Wolf, J. *Angew. Chem., Int. Ed.* **1992**, *31*, 1025.
- (23) Boutry, O.; Gutiérrez, E.; Monge, A.; Nicasio, M. C.; Pérez, P. J.; Carmona, E. *J. Am. Chem. Soc.* **1992**, *114*, 7288.
- (24) Li, Z.-W.; Taube, H. *J. Am. Chem. Soc.* **1994**, *116*, 11584.
- (25) Holtcamp, M. W.; Labinger, J. A.; Bercaw, J. E. *J. Am. Chem. Soc.* **1997**, *119*, 848.
- (26) Coalter, J. N.; Ferrando, G.; Caulton, K. G. *New J. Chem.* **2000**, *24*, 835.
- (27) Lee, D.-H.; Chen, J.; Faller, J. W.; Crabtree, R. H. *J. Chem. Soc., Chem. Commun.* **2001**, 213.
- (28) Carmona, E.; Paneque, M.; Santos, L. L.; Salazar, V. *Coord. Chem. Rev.* **2005**, *249*, 1729.
- (29) Carmona and co-workers have also reported metal–carbene complexes for which 1,2-hydride migration is facile: Paneque, M.; Poveda, M. L.; Santos, L. L.; Salazar, V.; Carmona, E. *Chem. Commun.* **2004**, 1838.

- (30) Collman, J. P.; Hegedus, L. S.; Norton, J. R.; Finke, R. G. *Principles and Applications of Organotransition Metal Chemistry*; University Science Books: Mill Valley, CA, 1987.
- (31) Scott, R. N.; Shriver, D. F.; Vaska, L. *J. Am. Chem. Soc.* **1968**, *90*, 1079.
- (32) Nugent, W. A.; Mayer, J. M. *Metal-Ligand Multiple Bonds*; Wiley: New York, 1988.
- (33) Gallop, M. A.; Roper, W. R. *Adv. Organomet. Chem.* **1986**, *25*, 121.
- (34) Casey, C. P.; Burkhardt, T. J. *J. Am. Chem. Soc.* **1973**, *95*, 5833.
- (35) Schrock, R. R.; Sharp, P. R. *J. Am. Chem. Soc.* **1978**, *100*, 2389.
- (36) Lee, S.; Cooper, N. J. *J. Am. Chem. Soc.* **1990**, *112*, 9419.
- (37) Meinhardt, J. D.; Anslyn, E. V.; Grubbs, R. H. *Organometallics* **1989**, *8*, 583.
- (38) Brown-Wensley, K. A.; Buchwald, S. L.; Cannizzo, L.; Clawson, L.; Ho, S.; Meinhardt, D.; Stille, J. R.; Straus, D.; Grubbs, R. H. *Pure Appl. Chem.* **1983**, *55*, 1733.

Chapter 2

Iron and Cobalt Complexes Supported by Tripodal Amidophosphine Hybrid Ligands

The text in this chapter is reproduced in part with permission from:

Whited, M. T.; Rivard, E.; Peters, J. C. *Chem. Commun.* **2006**, 1613–1615.

Copyright 2006 Royal Society of Chemistry

Introduction

Rational ligand design has figured prominently in the discovery of metal complexes with novel properties, allowing the synthesis of structural mimics of biological systems and complexes capable of activating small molecules.¹ Changes in ligand scaffolds can be utilized to tune the reactivity of a metal and elicit new properties both by the choice of donors and the geometry conferred about the metal center. Even within a given framework, changes in donor substituents can have a marked effect on reactivity, both by changing the electronic character of the complex and providing protective steric bulk about the metal center.^{2,3} Thus, there is a continuing demand for new, well-defined, versatile ligands whose preparations are highly modular.⁴

Within our research group, much effort has been focused on the development of monoanionic polyphosphine ligand scaffolds that can educe new reactivity from iron and cobalt toward many substrates and stabilize a range of oxidation states. Specifically, formally zwitterionic complexes of iron and cobalt with tris(phosphino)borate ligands have shown a propensity to form multiply bonded metal–ligand moieties,^{3,5} and cobalt complexes with [PhBP₃] ([PhBP₃] = [PhB(CH₂PPh₂)₃][−]) have revealed a number of unexpected electronic properties due to the strong field and unusual distorted-tetrahedral geometry conferred by the ligand.⁶ In this context, we were eager to consider analogues of the (phosphino)borates in which the negative charge would be carried by an X-type donor ligand rather than the borate backbone.

Particularly interesting to us were the mixed amide-phosphine hybrid ligands first developed by Fryzuk and co-workers (see Chart 2.1 for representative examples).⁷ As Fryzuk has noted, these scaffolds combine “hard” amido and “soft” phosphine donors, allowing them to bind many transition metals, stabilize a variety of oxidation states, and induce interesting transformations.⁸ Several properties of these hybrid ligands were appealing to us. First, the

uninegative charge would be borne by an amide donor rather than a borate unit separated spatially and electronically from the metal center. We also anticipated that amidophosphines would be electron-releasing, like their poly(phosphino)borate analogues, but with the distinction that the lone pair of the amido substituent would be available for π -donation. Such ligands should likewise support low- and mid-valent group transfer reactions, though it is likely that the potential for π -donation from the amide will alter the reactivity of other multiply bonded ligands. While the chemistry of iron and cobalt amidophosphine complexes is very limited in scope,^{9,10} these general types of hybrid ligands have been used successfully on second- and third-row late transition metals.¹¹

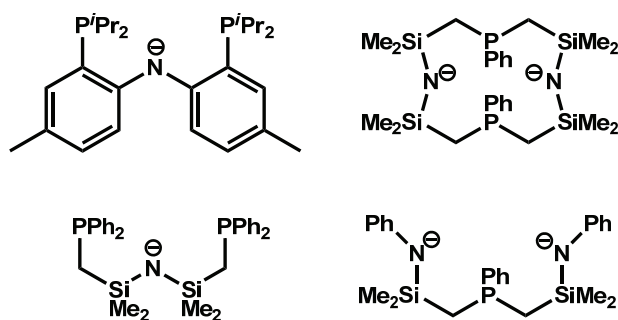


Chart 2.1. Representative amidophosphine hybrid ligands.

Accordingly, synthetic protocols have been developed for the preparation of two new amidophosphine ligands, depicted in Chart 2.2. Each of the ligands is monoanionic, bearing the negative charge on the amide unit, and they are related in that each is designed to bind in a well-defined manner, leaving a protected reactive pocket on the transition-metal center. However, differences in donor sets and geometric requirements are expected to elicit distinct reactivity for each.

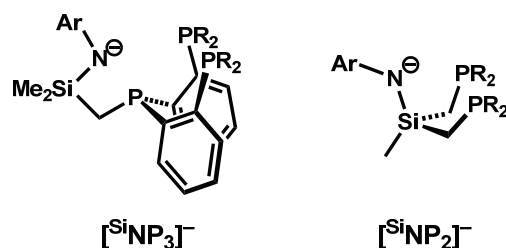


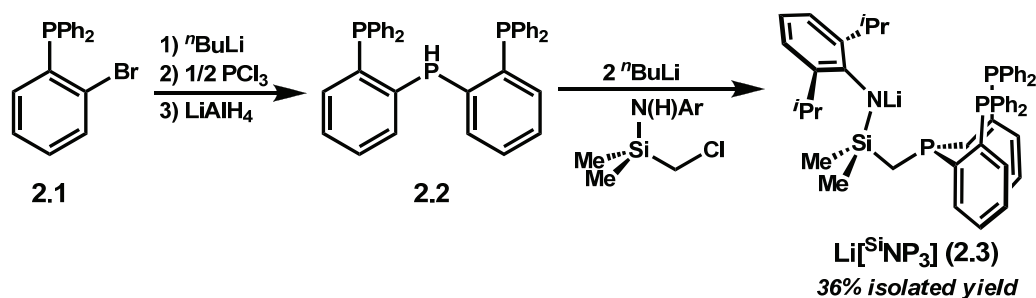
Chart 2.2. Amidophosphine ligands used in this study.

Results and Discussion

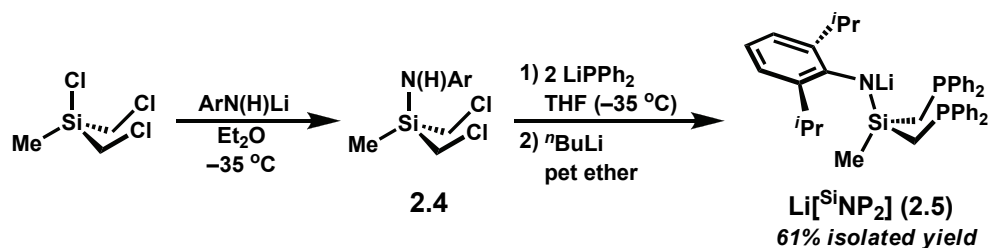
Synthesis and Metalation of Amidophosphine Ligands

Ligand Design. In devising ways to implement amidophosphine (NP_x) ligand motifs in the chemistry of iron and cobalt, we were particularly interested in ligands that would bind in a tripodal manner. In view of the classical NP₃⁻ and PP₃⁻-supported chemistry of iron and cobalt^{12,13} and recent results from our laboratory exposing new reactivity with facially coordinating tridentate ligands,^{3,5,14} it seemed likely that tripodal amide-based ligands might also reveal a distinct set of reactivity.

Using methods developed by Fryzuk and others for the synthesis of classical “PNP” ligands,^{7a} we have prepared two new hybrid ligands (Chart 2.2). Each contains a single arylamido donor and either two or three phosphines. $[\text{SiNP}_3]^-$ was designed as a monoanionic relative of Sacconi’s tris(phosphino)amine ligands,¹³ whereas $[\text{SiNP}_2]^-$ bears more similarity to facially coordinating polyphosphine ligands of Huttner¹⁰ and the tris(phosphino)borates explored by Peters and others.¹⁵



Scheme 2.1. Synthesis of $\text{Li}[\text{SiNP}_3]$ Ligand (Ar = 2,6-diisopropylphenyl).



Scheme 2.2. Synthesis of $\text{Li}[\text{SiNP}_2]$ Ligand (Ar = 2,6-diisopropylphenyl).

Syntheses of the ligands are straightforward and modular (Schemes 2.1 and 2.2). $[\text{SiNP}_3]$ is made from an *ortho*-brominated triarylphosphine (**2.1**), which is lithiated *in situ* and quenched with 0.5 equivalents of PCl_3 to generate a bis(2-phosphinophenyl)chlorophosphine that is subsequently reduced with LiAlH_4 to afford the bis(2-phosphinophenyl)phosphine **2.2**. The phosphine will react with a (chloromethyl)aminosilane in the presence of *n*-butyllithium (2 equiv) to give $\text{Li}[\text{SiNP}_3]$ (**2.3**). $\text{Li}[\text{SiNP}_2]$ is prepared in a similar fashion: nucleophilic attack of diphenylphosphide on a bis(chloromethyl)methylaminosilane (**2.4**) generates a bis(phosphino)silylamine, which is deprotonated *in situ* to yield $\text{Li}[\text{SiNP}_2]$ (**2.5**) as a white solid.

Metalation and Fundamental Properties of $[\text{SiNP}_3]$. Reaction of $\text{Li}[\text{SiNP}_3]$ (**2.3**) with FeCl_2 in THF afforded $[\text{SiNP}_3]\text{FeCl}$ (**2.6**) as a brown powder in 64% isolated yield. We were surprised to find that the complex possessed a high-spin electronic configuration ($\mu_{\text{eff}} = 4.6 \mu_{\text{B}}$ by Evans' method),¹⁶ rather than the intermediate $S = 1$ state predicted for a five-coordinate Fe(II) complex. The high-

spin formulation was consistent with the presence of highly shifted peaks in the ^1H NMR spectrum, from δ 50.8 ppm to -49.1 ppm. In order to obtain a solid-state molecular structure, compound **2.6** was crystallized as light-yellow plates by vapor diffusion of petroleum ether into a concentrated benzene solution. XRD analysis showed a pseudotetrahedral complex with one unbound phosphine arm (Figure 2.1).

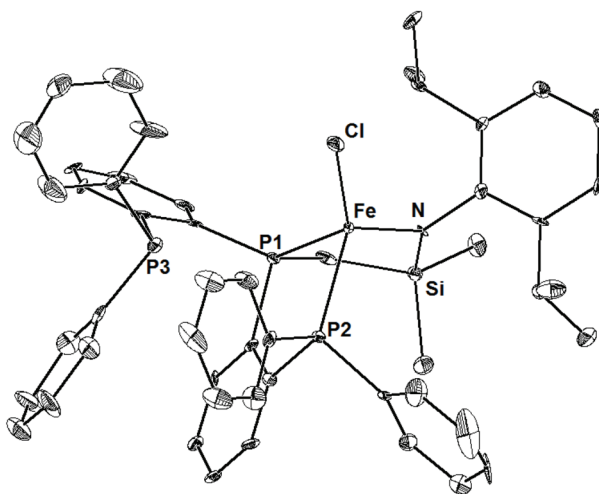


Figure 2.1. Displacement ellipsoid (35%) representation of $[\text{SiNP}_3]\text{FeCl}$ (**2.6**). Two essentially identical molecules were present in the asymmetric unit of **2.6**, and one is depicted with hydrogen atoms and solvent molecules omitted for clarity. Selected bond lengths (\AA) and angles ($^\circ$): Fe–N, 1.933(9); Fe–P1, 2.420(3); Fe–P2, 2.480(3); Fe–P3, 3.954(6); Fe–Cl, 2.242(3); N–Fe–P1, 91.0(3); N–Fe–P2, 113.8(3); P1–Fe–P2, 84.1(1); N–Fe–Cl, 121.8(3); P1–Fe–Cl, 125.9(1); P2–Fe–Cl, 113.3(1).

However, we also noticed that at low temperatures, solutions of complex **2.6** exhibited a dramatic change in color from yellow to red, indicating a possible spin-state transition. A solution magnetic susceptibility measurement confirmed that, at low temperature, the $S = 1$ state was predominantly populated ($\mu_{\text{eff}} = 3.3 \mu_{\text{B}}$ at -66 $^\circ\text{C}$), suggesting that the ligand may have adopted the desired tetradentate binding mode to give a trigonal-bipyramidal Fe(II) complex. We also examined the low-temperature solution behavior of **2.6** by UV-vis spectroscopy and noted that two bands corresponding to the new species grew into the spectrum at 770 nm ($740 \text{ M}^{-1} \text{ cm}^{-1}$) and 540 nm ($1400 \text{ M}^{-1} \text{ cm}^{-1}$) upon cooling to -80 $^\circ\text{C}$. In Figure 2.2, a UV-vis spectrum is

depicted in which **2.6** has been examined at 4 different temperatures, showing that the relative population of the red $S = 1$ species decreases during warming. Finally, the solid-state magnetic properties of **2.6** were examined by SQUID magnetometry, and these showed that $[\text{SiNP}_3]\text{FeCl}$ (**2.6**) is rigorously high spin ($\mu_{\text{eff(avg)}} = 4.9 \mu_{\text{B}}$, 50–300K) in the solid state, where the dangling arm would not be expected to bind (Figure 2.3). Taken collectively, these data confirm that the binding mode for $[\text{SiNP}_3]$ with Fe(II) is not dictated by sterics, but by the relative preference of the metal center to populate particular spin states in the presence of a potential phosphine donor. This finding is not surprising when compared to related reports by Macbeth et al. that neutral Sacconi-type $[\text{NP}_3]$ ligands show a tendency to dissociate a donor in order to accommodate higher spin states.¹⁷

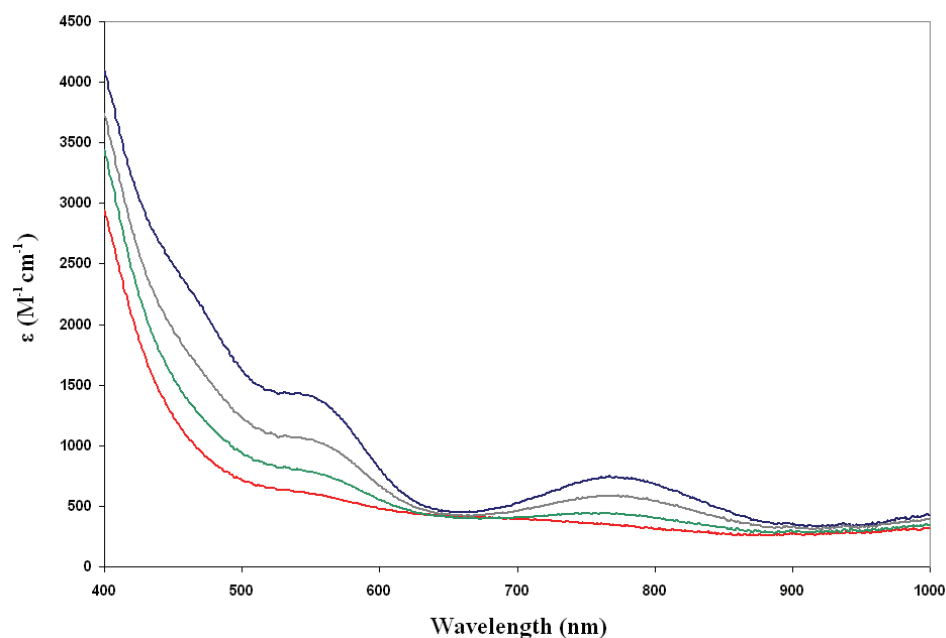


Figure 2.2. UV-vis spectrum of $[\text{SiNP}_3]\text{FeCl}$ (**2.6**) at various temperatures (blue = -80 °C; red = 25 °C; gray and green lines traces are intermediate spectra obtained during warming of the sample).

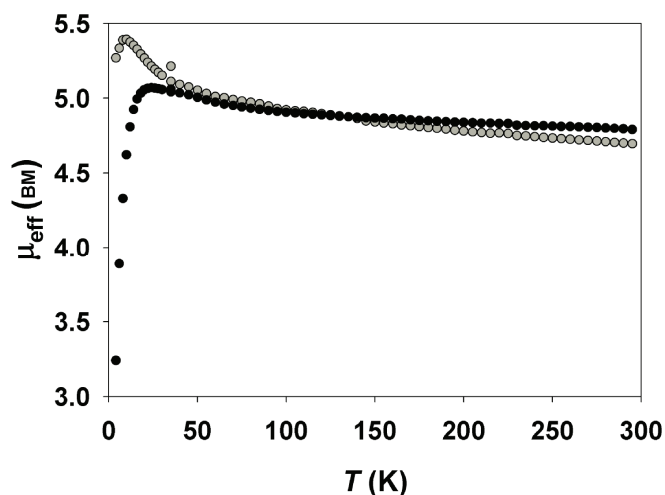


Figure 2.3. Solid-state magnetic susceptibility of $[\text{SiNP}_3]\text{FeCl}$ (**2.6**) (gray = 0.5 T; black = 5.0 T).

Electrochemical analysis of **2.6** revealed a reversible $\text{Fe}^{\text{III/II}}$ couple centered at -0.40 V versus Fc/Fc^+ , as well as irreversible waves at -2.0 and -2.5 V. A small wave grew in at -1.0 V that appeared to be associated with the irreversible reduction event at -2.0 V (Figure 2.4). Chloride loss likely occurs upon reduction, forming a new species that is oxidized at -1.0 V. In light of the behavior observed for a related cobalt(II) species (*vide infra*), it is likely that this new species is a “naked” tetracoordinate “ $[\text{SiNP}_3]\text{Fe}$ ” species, but further synthetic studies will be required to elucidate the exact nature of this complex.

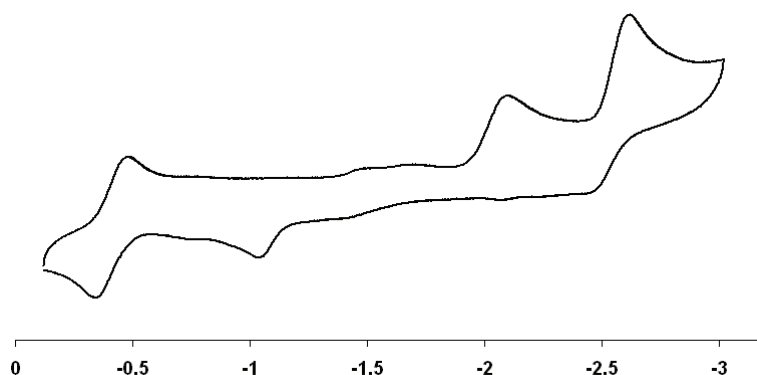
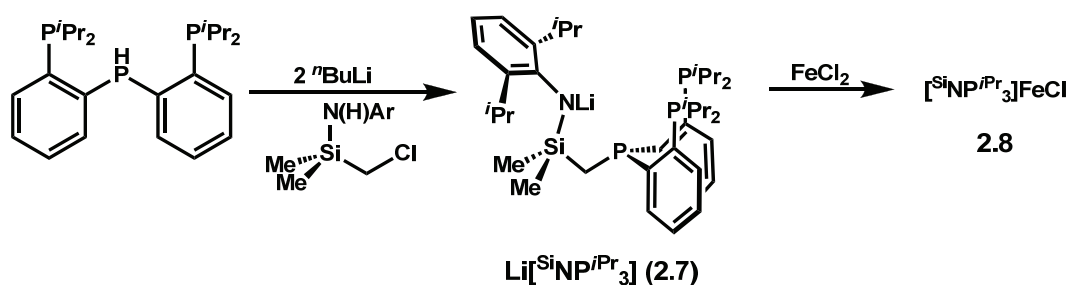


Figure 2.4. Cyclic voltammogram of $[\text{SiNP}_3]\text{FeCl}$ (**2.6**) under N_2 in 0.35 M $[\text{TBA}][\text{PF}_6]/\text{THF}$, scan rate = 250 mV/s, V versus Fc/Fc^+ .

In order to probe whether incorporation of stronger isopropylphosphine donors would allow observation of a five-coordinate Fe(II) species as the ground state at room temperature, an analogous $\text{Li}[\text{SiNP}^i\text{Pr}_3]$ ligand (**2.7**) was prepared from the known compound bis(2-(diisopropylphosphino)phenyl)phosphine¹⁸ by the same method as phenyl-substituted ligand **2.4**, and $[\text{SiNP}^i\text{Pr}_3]\text{FeCl}$ (**2.8**) was synthesized by reaction of the lithium amide with FeCl_2 (Scheme 2.3). Although iron complex **2.8** was not fully characterized, XRD analysis confirmed a binding mode similar to that observed for complex **2.6**, with two bound and one free phosphine donor (Figure 2.5).



Scheme 2.3. Synthesis of $\text{Li}[\text{SiNP}^i\text{Pr}_3]$ ligand and metalation at iron.

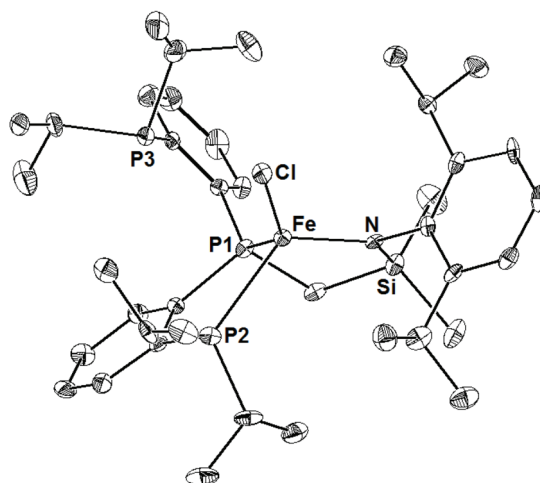


Figure 2.5. Displacement ellipsoid (35%) representation of $[\text{SiNP}^i\text{Pr}_3]\text{FeCl}$ (**2.8**). Selected bond lengths (\AA) and angles ($^\circ$): Fe–N, 1.944(4); Fe–P1, 2.417(2); Fe–P2, 2.505(2); Fe–P3, 3.730(2); Fe–Cl, 2.250(2); N–Fe–P1, 92.6(1); N–Fe–P2, 124.3(1); P1–Fe–P2, 80.66(6); N–Fe–Cl, 115.2(1); P1–Fe–Cl, 137.45(7); P2–Fe–Cl, 105.44(6).

Since these frameworks proved reluctant to bind iron(II) in a tetradentate manner, further studies focused on divalent ions that would more readily adopt a five-coordinate, trigonal-bipyramidal geometry. Thus, to structurally establish that [^{Si}NP₃] ligand could assume the more desirable tetradentate binding mode, we examined its coordination to Co(II). Brick-red [^{Si}NP₂]CoCl (**2.9**) and [^{Si}NP₂]CoI (**2.10**) were prepared metathetically by the reaction between Li[^{Si}NP₃] and CoCl₂ or CoI₂, respectively. Compound **2.9** features a low-spin Co(II) center ($\mu_{\text{eff}} = 1.9 \mu_{\text{B}}$). Maroon crystals of **2.9** and **2.10** were grown by vapor diffusion of petroleum ether into a concentrated benzene solution, and a structural representation of iodide **2.10** is depicted in Figure 2.6. The X-ray crystal structure of **2.10** reveals a trigonal-bipyramidal Co(II) center in which the halide ligand occupies an apical position. The metal–phosphine distances are shorter than those found in iron(II) complex **2.6**, consistent with the low-spin configuration, and the axial Co–P1 bond is ca. 0.1 Å shorter than the equatorial Co–P2 and Co–P3 bonds. The amide, P2, and P3 ligands lie in a plane that contains the cobalt center, but the P1–Co–I axis is slightly bent (P1–Co–I = 172°) due to the iodide ligand being positioned away from the amide donor.

A space-filling model of **2.10** (Figure 2.6) reveals an iodide ligand that is nestled within a binding pocket comprised of the phosphine phenyl substituents and a rotated diisopropylphenyl group. Canting of the 2,6-diisopropylanilide donor minimizes steric interactions between the isopropyl groups and the phenylphosphine substituents and also tilts the lone pair of the amido ligand out of the equatorial plane. The cyclic voltammetry of **2.9** resembles that of **2.6**, featuring a reversible Co^{III/II} couple at –0.43 V and an irreversible cathodic peak at –2.1 V. Once again, a new and irreversible anodic peak grows at –1.0 V that appears to be associated with the reduction event at –2.1 V. As with **2.6**, this new species is most likely generated by expulsion of a chloride ligand upon reduction.

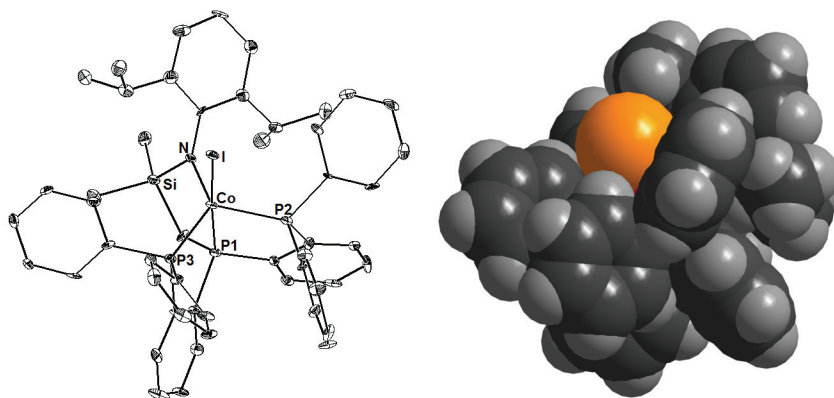


Figure 2.6. Displacement ellipsoid (35%) representation (left) and space-filling model (right) of $[\text{SiNP}_3]\text{CoI}$ (**2.10**). Selected bond lengths (Å) and angles ($^\circ$): Co–N, 1.990(6); Co–P1, 2.139(2); Co–P2, 2.260(2); Co–P3, 2.250(2); Co–I, 2.642(1); N–Co–P1, 86.5(2); N–Co–P2, 121.8(2); N–Co–P3, 129.4(2); N–Co–I, 101.5(2); P1–Co–P2, 85.81(8); P1–Co–P3, 86.78(8); P1–Co–I, 171.93(7); P2–Co–P3, 107.57(8); P2–Co–I, 89.24(6); P3–Co–I, 88.66(6).

Metalation and Fundamental Properties of $[\text{SiNP}_2]$. Unlike $[\text{SiNP}_3]$, the $[\text{SiNP}_2]$ ligand is geometrically predisposed to tridentate, facial coordination.¹⁹ This feature distinguishes it from other Fryzuk-type amidophosphine ligands, for which meridional chelation dominates.^{9a,b} $\text{Li}[\text{SiNP}_2]$ (**2.5**) and FeCl_2 react to generate $[\text{SiNP}_2]\text{FeCl}$ (**2.11**) cleanly in 83% isolated yield. Likewise, $[\text{SiNP}_2]\text{CoCl}$ (**2.12**) and $[\text{SiNP}_2]\text{CoI}$ (**2.13**) can be obtained using CoCl_2 and CoI_2 , respectively. Complex **2.11** is high spin ($\mu_{\text{eff}} = 4.8 \mu_{\text{B}}$), consistent with the expected tetrahedral Fe(II) structure.

XRD analysis of single crystals of **2.11** and **2.13** confirmed the tripodal binding mode of the $[\text{SiNP}_2]$ ligand (Figure 2.7). Interestingly, the N–Fe–P and P–Fe–P angles in both **2.11** and **2.13** are much closer to 90° than we had anticipated, providing structures distinct from those of typical tetrahedra. In this regard, the $[\text{SiNP}_2]$ donors are better described as occupying three corners of an octahedron, in a manner analogous to several tripodal borate ligands such as $[\text{Tp}]$,²⁰ $[\text{PhTt}^{\text{R}}]$,²¹ and $[\text{PhBP}_3]$.⁶ The propensity of $[\text{SiNP}_2]$ to enforce such a distorted-tetrahedral

geometry likely stems from the tight chelate that results from having both phosphine arms branch from a common silyl linker. As expected, a space-filling model of **2.11** (Figure 2.7c) reveals significantly less steric protection about the halide binding site in comparison to **2.10**. Additionally, it is interesting to note that for both **2.11** and **2.13**, the 2,6-diisopropylanilide donor lies perpendicular to the M–Cl vector rather than canted as in **2.10**, likely because the environment is less sterically demanding. Compared with the structurally related $[\text{PhBP}_3]\text{FeCl}$ and $[\text{PhBP}^{i\text{Pr}}_3]\text{FeCl}$ complexes, **2.11** exhibits a slightly elongated Fe–Cl bond (2.24 versus 2.20 Å for $[\text{PhBP}_3]\text{FeCl}^{5\text{b}}$ and 2.22 Å for $[\text{PhBP}^{i\text{Pr}}_3]\text{FeCl}^{15\text{c}}$). Given the gross structural similarities among these complexes, we attribute this lengthening to the greater electron density at iron due to the presence of a π -basic amido donor.

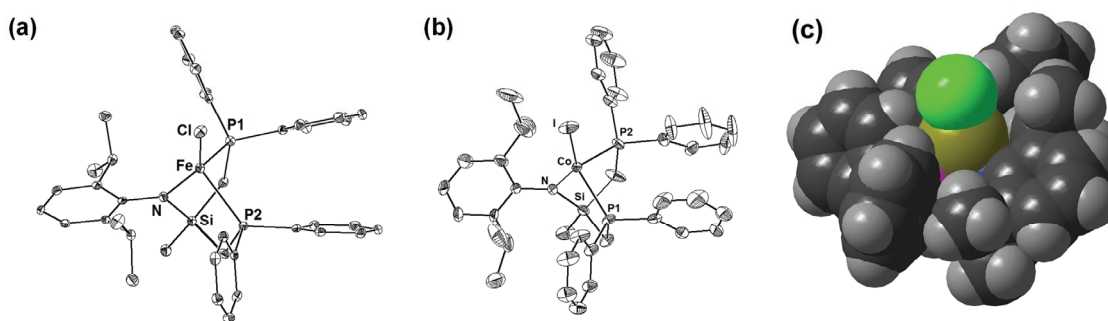


Figure 2.7. Structural representations of (a) $[\text{SiNP}_2]\text{FeCl}$ (**2.11**) and (b) $[\text{SiNP}_2]\text{CoI}$ (**2.13**) with displacement ellipsoids at 35% probability, and (c) a space-filling representation of $[\text{SiNP}_2]\text{FeCl}$ (**2.11**). Selected bond lengths (Å) and angles (°) for **2.11**: Fe–N, 1.953(2); Fe–P1, 2.4180(8); Fe–P2, 2.4903(8); Fe–Cl, 2.2418(8); N–Fe–P1, 89.76(5); N–Fe–P2, 90.91(6); N–Fe–Cl, 140.03(6); P1–Fe–P2, 94.98(3); P1–Fe–Cl, 118.30(3); P2–Fe–Cl, 112.48(3). For **2.13**: Co–N, 1.910(3); Co–P1, 2.3849(9); Co–P2, 2.3731(8); Co–I, 2.5258(5); N–Co–P1, 89.78(8); N–Co–P2, 90.29(9); N–Co–I, 143.57(8); P1–Co–P2, 93.44(3); P1–Co–I, 115.61(3); P2–Co–I, 112.33(3).

Given this binding geometry and the additional presence of the arylamido donor ligand, we had expected that cobalt complexes **2.12** and **2.13** might adopt low-spin configurations, akin to certain $[\text{PhBP}_3]\text{Co}^{\text{II}}\text{--X}$ systems we have previously described.⁶ However, both **2.12** and **2.13** are high spin. These assignments are consistent with their room-temperature Evans method determinations ($\mu_{\text{eff}} = 3.7 \mu_{\text{B}}$ for **2.12**, $4.0 \mu_{\text{B}}$ for **2.13**) and the elongated Co–P and Co–I bond

distances revealed by the 100 K X-ray structure of **2.13**. In a comparative context, these data continue to underscore how unusual the electronic properties of the [PhBP₃] ligand are compared with structurally related tripodal ligands.

Complexes **2.11** and **2.12** were also examined by cyclic voltammetry (Figure 2.8). The CV of **2.11** shows no reversible redox events. An irreversible reduction peak beginning at -2.1 V is evident, as is an oxidative wave at $+0.24$ V. A smaller reduction wave centered at -0.63 V grows in as a result of scanning through the oxidation process at $+0.24$ V. The CV data for **2.12** show a quasi-reversible wave centered at -0.17 V, corresponding to a $\text{Co}^{\text{III/II}}$ oxidation event. Additionally, there is an irreversible reduction wave at -1.4 V and a smaller irreversible oxidative wave at -0.40 V. The putative Co^{II} reduction event occurs at a potential ca. 0.7 V more positive for compound **2.12** compared with **2.9**.

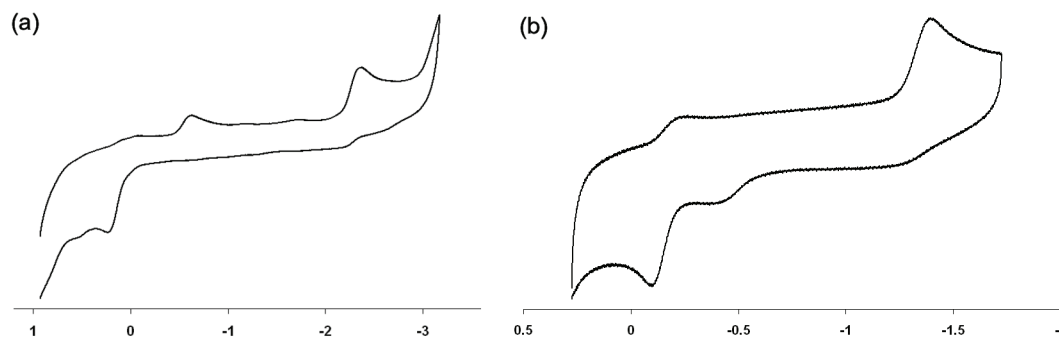


Figure 2.8. Cyclic voltammetry of (a) $[\text{SiNP}_2]\text{FeCl}$ (**2.11**) under N_2 in 0.35 M $[\text{TBA}][\text{PF}_6]/\text{THF}$, scan rate = 250 mV/s, and (b) $[\text{SiNP}_2]\text{CoCl}$ (**2.12**) under N_2 in 0.35 M $[\text{TBA}][\text{PF}_6]/\text{THF}$, scan rate = 250 mV/s, V versus Fc/Fc^+ .

Reactivity of [^{Si}NP_x]-Supported Iron and Cobalt Complexes

Reactivity of [^{Si}NP₃]M–Cl Complexes: Chemical Reduction. The fact that formation of a new species was observed electrochemically for [^{Si}NP₃]FeCl (**2.6**) and [^{Si}NP₃]CoCl (**2.9**) upon reduction and expulsion of halide indicated to us that both compounds might evince N₂ uptake upon reduction. Since the [^{Si}NP₃] scaffold was designed as an anionic relative of Sacconi's tris(phosphino)amine ligand, which supports N₂ coordination at iron and cobalt, early studies of the reactivity of **2.6** and **2.9** have focused on their reduction chemistry.

Reduction of **2.6** was attempted both with Mg⁰ powder and Na/Hg amalgam. Although IR spectroscopy indicated possible N₂ uptake upon reduction with Mg⁰, NMR spectroscopy (³¹P) revealed the presence of two diamagnetic ligand-containing products. Successive crystallizations did not aid in the isolation of one of the products, and a number of different conditions for the reduction did not result in a cleaner reaction. Similarly, Na/Hg amalgam reduction of **2.6** was seen to form a single paramagnetic product by NMR (¹H), but free ligand and degradation products were also evident.

In an attempt to clarify the reduction chemistry of [^{Si}NP₃] complexes, similar reactions were pursued with [^{Si}NP₃]CoCl (**2.9**). Clean reduction of **2.9** was realized with Na/Hg amalgam (1 equiv). However, in contrast to our expectations, the resulting Co(I) product was paramagnetic ($\mu_{\text{eff}} = 2.7 \mu_{\text{B}}$, $S = 1$) and exhibited no N₂ stretch in its infrared spectrum. Instead, XRD analysis revealed that one-electron reduction had effected expulsion of the chloride ion without subsequent uptake of solvent or dinitrogen to serve as an apical L-type donor ligand, cleanly generating a trigonal-pyramidal [^{Si}NP₃]Co (**2.14**) (eq 2.1). Interestingly, the overall structure is quite close to those of halide complexes **2.9** and **2.10** (with the exception of the missing apical ligand), and the core bond lengths are essentially unchanged (Figure 2.9). This overall geometry, while quite unusual for Co(I), is not unprecedented.²² Sacconi reported a similar complex with

his tris(phosphino)amine (NP₃) ligand,²³ and more recently, Meyer and co-workers have reported a related compound supported by a tris(carbene) amine ligand that serves as a useful precursor to an isolable Co(III) imide.²⁴ However, in neither of these cases was the complex supported by a monoanionic ligand, which may have a marked effect on reactivity. Borovik and co-workers also reported an isoelectronic nickel(II) complex.²⁵ Taken together, these findings also suggest that the iron(I) complex formed upon reduction of **2.6** is probably [^{Si}NP₃]Fe, though further studies will be necessary to confirm the identity of this species.

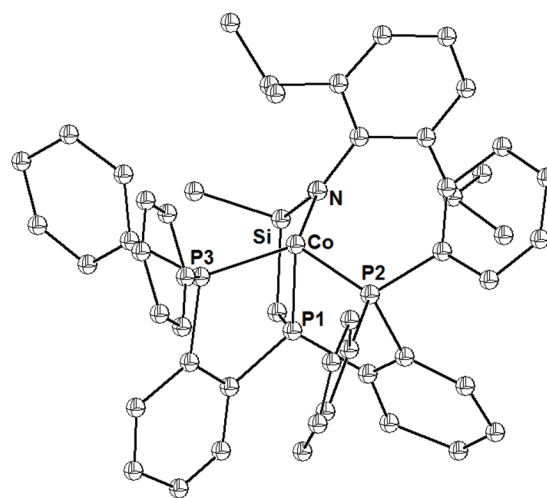
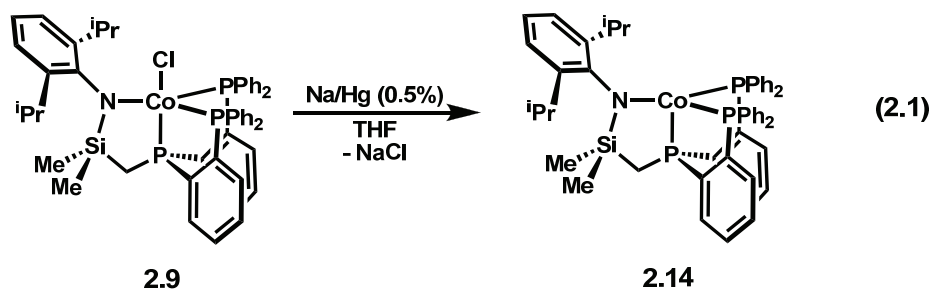
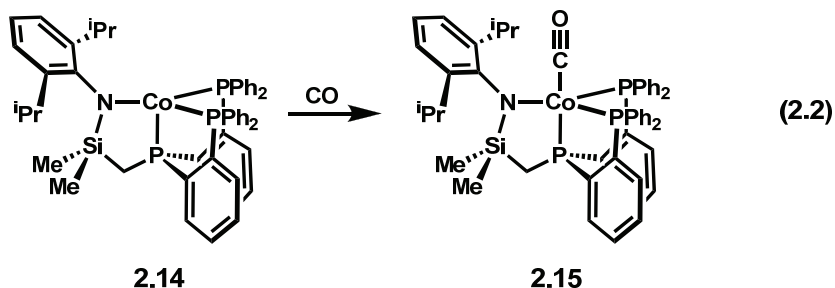


Figure 2.9. Single-crystal X-ray structure of [^{Si}NP₃]Co (**2.14**) (isotropic representation). Selected bond lengths (Å) and angles (°): Co–N, 1.98(1); Co–P1, 2.153(4); Co–P2, 2.208(4); Co–P3, 2.226(5); N–Co–P1, 90.4(3); N–Co–P2, 121.7(3); N–Co–P3, 132.4(3); P1–Co–P2, 87.0(2); P1–Co–P3, 86.7(2); P2–Co–P3, 105.6(2).

Reactivity of $[\text{SiNP}_3]\text{Co}$. The presence of a vacant reactive site in **2.14** suggests that this complex may serve as a platform for a number of group transfer and small-molecule activation reactions. Accordingly, we focused on the fundamental reactivity of this complex upon exposure to a number of small molecules or oxidation.

Although **2.14** was not observed to react with atmospheric dinitrogen, facile reaction with the isoelectronic carbon monoxide was realized. In the presence of excess CO, both mono- and dicarbonyl complexes were observed by infrared spectroscopy and ^{31}P NMR. However, exposure of **2.14** to a single equivalent of CO allowed clean generation of $[\text{SiNP}_3]\text{Co-CO}$ (**2.15**, eq 2.2), which was identified by a prominent infrared absorption associated with the carbonyl ligand stretch ($\nu_{\text{CO}} = 1932 \text{ cm}^{-1}$). Unlike **2.14**, carbonyl complex **2.15** is diamagnetic, as expected for a five-coordinate Co(I) complex supported by a strong-field ligand set.



Somewhat unexpected behavior was observed upon exposure of $[\text{SiNP}_3]\text{Co}$ (**2.14**) to excess carbon dioxide. A single paramagnetic product was observed by NMR spectroscopy as well as diamagnetic side products, and IR spectroscopy revealed an intense stretch at 2291 cm^{-1} . The high energy of the C=O stretch suggested the presence of a cumulene, leading us initially to suspect an end-on CO_2 unit supported by $[\text{SiNP}_3]\text{Co}$.²⁶ When the reaction was monitored by infrared spectroscopy, a strong IR absorption was also observed at 1661 cm^{-1} , likely representing an intermediate species. Ultimately, some light was shed on the reaction by obtaining a single-crystal X-ray structure of the cobalt-containing product **2.16** (Figure 2.10). The

structure revealed replacement of the NAr unit with an oxygen atom to give siloxide dimer **2.16**, indicating that 2,6-diisopropylphenyl isocyanate had been lost as an organic by-product and was responsible for the intense, high-energy IR absorption, which matched that recorded for an authentic sample of 2,6-diisopropylphenyl isocyanate.²⁷

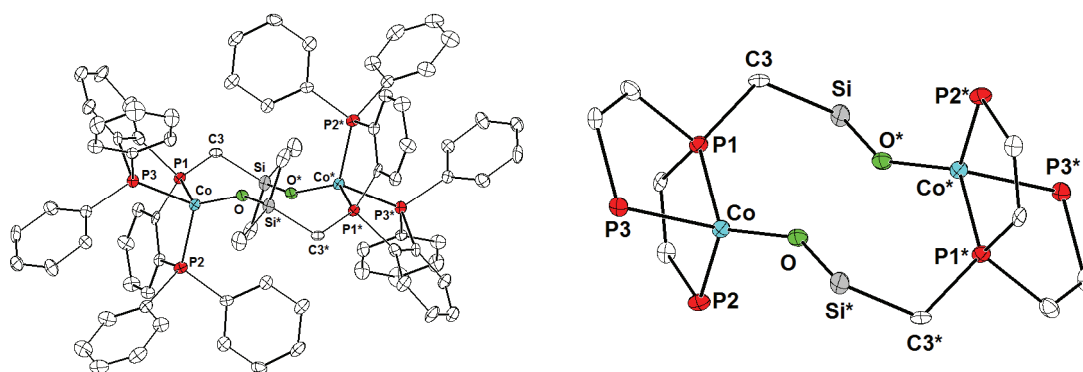
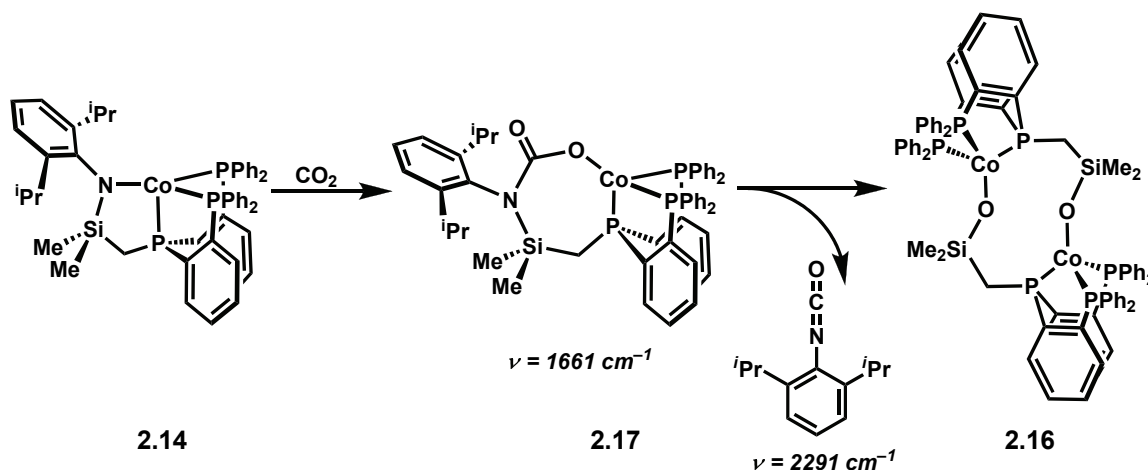


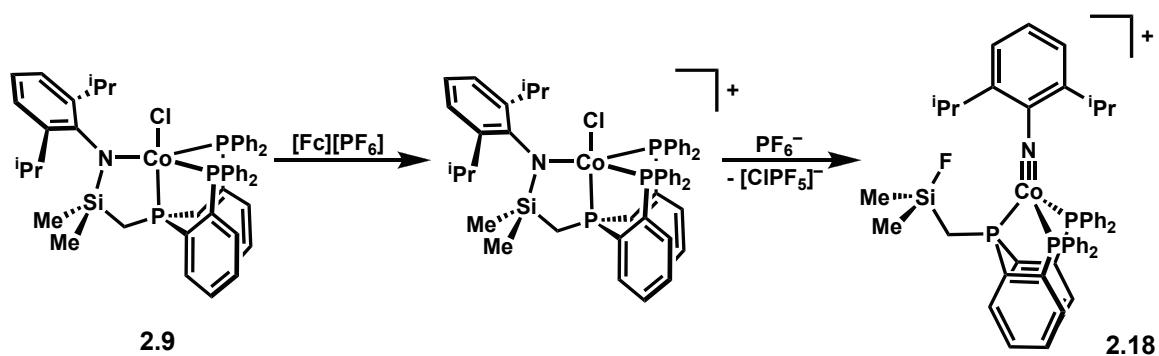
Figure 2.10. Molecular representation of dimeric siloxide complex **2.16** with ellipsoids at 35% probability (left) and the core of the complex (right). Selected bond lengths (Å) and angles (°): Co–O, 1.839(3); Co–P1, 2.196(2); Co–P2, 2.215(2); Co–P3, 2.220(2); O–Co–P1, 126.9(1); O–Co–P2, 122.3(1); O–Co–P3, 119.1(1); P1–Co–P2, 88.07(7); P1–Co–P3, 86.70(6); P2–Co–P3, 105.40(6).

We propose that this deoxygenation proceeds by initial insertion of CO₂ into the cobalt–amide bond to form the cobaltacarbamate **2.17**, which is associated with the intense infrared absorption at 1661 cm⁻¹. This complex decomposes by loss of isocyanate to form a monomeric cobalt siloxide, which undergoes rapid dimerization to afford **2.16** (Scheme 2.4). This behavior also highlights the inherent instability of the Si–N linkage of these types of ligands, a feature that has been noted by Schrock,²⁸ Fryzuk,²⁹ and Caulton.^{9c,30}



Scheme 2.4. Reaction of $[\text{SiNP}_3]\text{Co}$ (**2.14**) with CO_2 .

The instability of the Si–N linkage in the $[\text{SiNP}_3]$ ligands was also demonstrated upon oxidation of $[\text{SiNP}_3]\text{CoCl}$ (**2.7**) with ferricenium hexafluorophosphate (1.1 equiv). In this case, the reaction proceeds quite cleanly (as judged by NMR spectroscopy) to afford the unusual cationic cobalt(III) imido complex **2.18** (Scheme 2.5), for which a molecular representation is provided in Figure 2.11. The short Co–N bond (1.641 Å) is consistent with a cobalt–nitrogen triple bond, and the geometry is quite similar to those previously reported for pseudo-tetrahedral cobalt(III) imides.^{5a,14a}



Scheme 2.5. Formation of cationic cobalt imide **2.18** by Si–N bond cleavage.

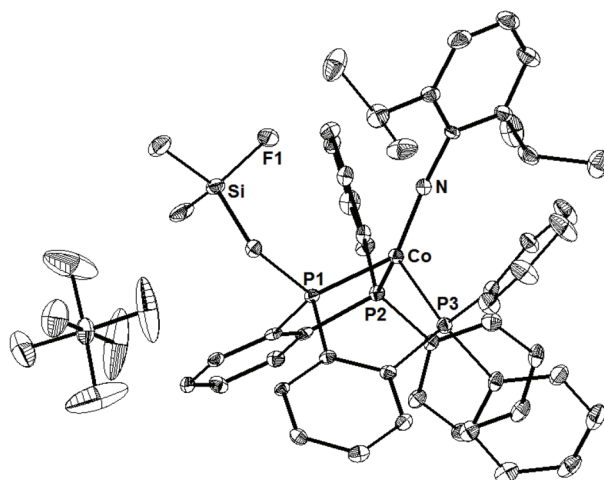
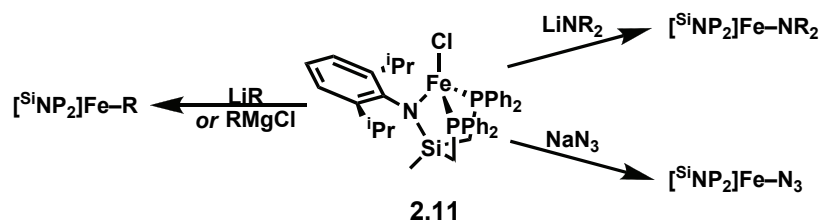


Figure 2.11. Displacement ellipsoid (35%) representation of imido complex **2.18** with hydrogen atoms omitted for clarity. Selected bond lengths (Å) and angles (°): Co–N, 1.641(3); Co–P1, 2.150(1); Co–P2, 2.193(1); Co–P3, 2.189(1); N–Co–P1, 130.3(1); N–Co–P2, 123.2(1); N–Co–P3, 112.7(1); P1–Co–P2, 87.61(5); P1–Co–P3, 88.24(5); P2–Co–P3, 108.07(5).

The imido complex can be imagined to be formed via two discrete steps: oxidation and S_N2 cleavage of the Si–N bond by fluoride (from PF_6^-). Since pseudo-tetrahedral cobalt(III) imides are best formulated as 18-electron complexes,^{5a} the neutral cobalt(II) imide would not be expected to be stable. Thus, we favor a pathway where initial oxidation of $[^SiNP_3]CoCl$ to its cation, $\{[^SiNP_3]CoCl\}^+$, is followed by attack of fluoride ion at the fluorophilic silicon to cause Si–N cleavage and chloride loss, ultimately affording **2.18**. We attribute the reasonably high yields obtained even in the presence of small excesses of PF_6^- to the possibility that PF_6^- may serve as a source of six fluoride equivalents.

Taken as a whole, these findings indicate that relative weakness of the Si–N linkage is likely to provide a major hurdle to implementation of $[^SiNP_3]$ ligands in small-molecule activation reactions, both catalytic and stoichiometric. However, formation of the cobalt(III) imide by Si–N cleavage may provide an interesting and unprecedented route to metal–imido complexes using silylamides as imide delivery agents.³¹

Reactivity of $[\text{Si}^{\text{Si}}\text{NP}_2]\text{Fe}-\text{Cl}$: Ligand Substitution. A number of complexes of the general formula $[\text{Si}^{\text{Si}}\text{NP}_2]\text{Fe}-\text{X}$ are readily prepared by metathetical reaction of $[\text{Si}^{\text{Si}}\text{NP}_2]\text{FeCl}$ (**2.11**) with anionic nucleophiles that will displace chloride (Scheme 2.6). Although most of the resulting complexes are not in themselves novel, they may serve as starting points for reactions that yield typically elusive species such as carbenes (from alkyls), imides (from amides), and nitrides (from azides or anthracenyl amides). Moreover, these complexes afford the opportunity for comparison of these new ligands with ones that have been examined previously. As depicted in Scheme 2.4, exposure of **2.11** to an alkyllithium or Grignard (1 equiv) reagent leads to clean metathesis and affords iron alkyls such as the neopentyl adduct $[\text{Si}^{\text{Si}}\text{NP}_2]\text{Fe}(\text{Np})$ (**2.19**), for which single-crystal X-ray analysis was obtained (Figure 2.12). Likewise, reaction with secondary lithium amides affords bis(amido) iron complexes such as $[\text{Si}^{\text{Si}}\text{NP}_2]\text{Fe}(\text{NPh}_2)$ (**2.20**). Reaction of **2.11** with $\text{Li}(\text{H})\text{R}$ reagents yields amides at low temperature that quickly decompose upon warming, precluding a successive oxidation/deprotonation strategy for obtaining a terminal iron imide.³²



Scheme 2.6. Representative ligand metathesis reactions at $[\text{Si}^{\text{Si}}\text{NP}_2]\text{FeCl}$ (**2.11**).

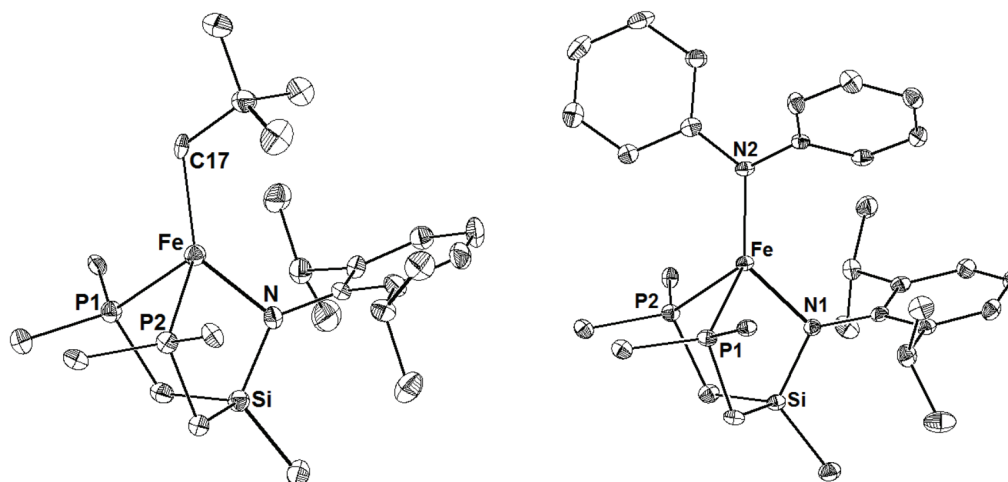


Figure 2.12. Displacement ellipsoid (35%) representation of $[\text{SiNP}_2]\text{Fe}(\text{Np})$ (**2.19**, left) and $[\text{SiNP}_2]\text{Fe}(\text{NPh}_2)$ (**2.20**, right) with phosphine substituents (except for *ipso* carbons) omitted for clarity. Selected bond lengths (Å) and angles (°) for **2.19**: Fe–N, 1.965(4); Fe–C17, 2.066(5); Fe–P1, 2.476(2); Fe–P2, 2.469(2); N–Fe–C17, 135.9(2); N–Fe–P1, 92.1(1); N–Fe–P2, 122.1(2); P1–Fe–C17, 116.1(2); P1–Fe–P2, 91.71(6); P2–Fe–C17, 122.1(2). For **2.20**: Fe–N1, 1.969(2); Fe–N2, 1.962(2); Fe–P1, 2.467(2); Fe–P2, 2.480(2); N1–Fe–N2, 133.75(9); N1–Fe–P1, 88.83(7); N1–Fe–P2, 90.10(7); P1–Fe–N2, 121.47(7); P1–Fe–P2, 92.40(5); P2–Fe–N2, 119.39(7).

A comparison of the iron–amide bond lengths in $[\text{SiNP}_2]\text{Fe}(\text{NPh}_2)$ (**2.20**) to those in **2.11** and the geometrically similar $[\text{PhBP}^{\text{iPr}}_3]\text{Fe}(\text{NPh}_2)$ ($[\text{PhBP}^{\text{iPr}}_3] = [\text{PhB}(\text{CH}_2\text{P}^{\text{iPr}}\text{Pr}_2)_3]^-$) provides some information about the $[\text{SiNP}_2]$ ligand (Table 2.1). Substitution of diphenylamide for chloride leads to an Fe–N bond lengthening of 0.02 Å in the $[\text{SiNP}_2]$ ligand. The Fe–NPh₂ bond in **2.20** is slightly (ca. 0.01 Å) shorter than that of the Fe– $[\text{SiNP}_2]$ amide bond. Compared with related tris(phosphino)borate iron(II) complexes, the Fe–NPh₂ bond in **2.20** is 0.01 Å longer than in $[\text{PhBP}^{\text{iPr}}_3]\text{Fe}(\text{NPh}_2)$ and 0.05 Å longer than the iron–amide bond in $[\text{BP}_3]\text{Fe}-\text{N}(\text{H})(p\text{-tolyl})$. These small differences highlight the electronic similarities between $[\text{SiNP}_2]$ and $[\text{BP}_3]$ complexes, indicating that the presence of a π -basic silylamido donor makes the iron center only marginally more electron rich.

Table 2.1. Comparison of N–Fe bond lengths in tetrahedral Fe(II) amido complexes

Complex	Bond	Bond Length (Å)
[^{Si} NP ₂]FeCl (2.11)	N _{lig} – Fe	1.953(3)
[^{Si} NP ₂]Fe(NPh ₂) (2.20)	N _{lig} – Fe	1.972(3)
	Ph ₂ N – Fe	1.962(2)
[PhBP ^{iPr} ₃]Fe(NPh ₂)	Ph ₂ N – Fe	1.953(2)

Reaction of **2.11** with sodium azide or the lithium amide reagent Li(dbabh)³³ yielded [^{Si}NP₂]Fe(N₃) (**2.21**, $\nu_{\text{N}_3} = 2081 \text{ cm}^{-1}$) and [^{Si}NP₂]Fe(dbabh) (**2.22**), respectively (dbabh = 2,3:5,6-dibenzo-7-aza bicyclo[2.2.1]hepta-2,5-dienide). Since azide and dbabh adducts have been shown to serve as precursors to nitrido complexes of iron,^{3,34} it was thought that these might serve a similar role for [^{Si}NP₂]-supported iron centers. Thus, **2.22** was subjected to reducing conditions (0.25% Na/Hg amalgam) and heating (3 days, 80 °C) in the hopes of preparing [^{Si}NP₂]Fe≡N with concomitant loss of anthracene. However, reduction led to no expulsion of anthracene, and the only components identifiable (by ¹H and ³¹P NMR) were starting material and free [^{Si}NP₂] ligand. Likewise, extended heating resulted in the expulsion of small amounts of anthracene with concomitant decomposition (¹H NMR). Complex **2.21** was reduced with Na/Hg amalgam (0.3%), but these conditions did not give clean reaction and led instead to ligand P–Ph bond cleavage in the only isolable products (**2.23**, Figure 2.13).

The bis(μ -phosphido) iron dimer **2.23**, which was identified only by XRD analysis, has several interesting properties. First, as mentioned above, the reductive conditions have led to cleavage of a P–Ph bond and loss of azide from **2.21**. Also interesting is the fact that the ligands have redistributed in the final dimeric product so that two amides are bound to one iron center and two phosphine ligands are bound to the other. The short Fe–Fe distance (2.54 Å) is consistent with an Fe–Fe bond, and the asymmetric nature of the phosphide bridges (P–Fe_{1,avg} =

2.24 Å whereas $\text{P}-\text{Fe}_{2_{\text{avg}}} = 2.42 \text{ \AA}$) indicates that this complex is best formulated as an $\text{Fe}^{\text{II}}-\text{Fe}^{\text{II}}$ dimer. In any case, this result further serves to highlight the instability of the $[\text{SiNP}_x]$ ligands, both to ligand cleavage and disproportionation.

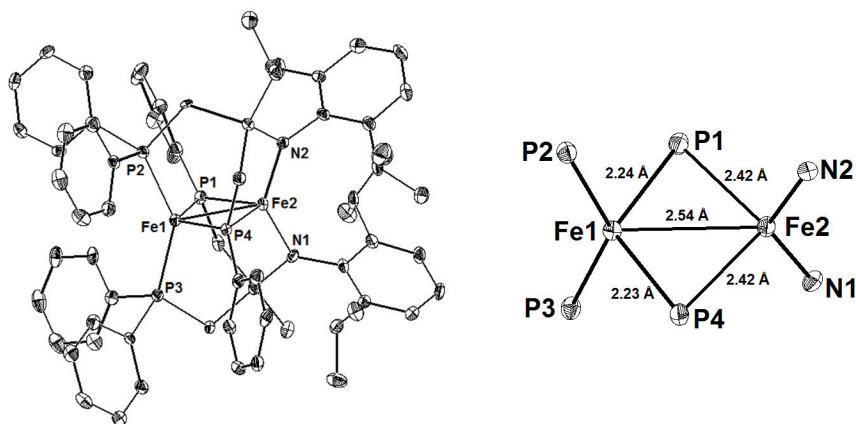


Figure 2.13. Displacement ellipsoid (35%) representation of the dimeric bis(μ -phosphido) product from Na/Hg amalgam reduction of $[\text{SiNP}_2]\text{Fe}(\text{N}_3)$ (**2.21**) (left) and a core representation of the same molecule (right). Selected bond lengths (Å) and angles ($^\circ$): Fe1-P1, 2.239(4); Fe1-P2, 2.303(5); Fe1-P3, 2.298(4); Fe1-P4, 2.234(3); Fe1-Fe2, 2.540(4); Fe2-N1, 1.956(6); Fe2-N2, 1.958(5); Fe2-P1, 2.420(3); Fe2-P4, 2.424(4); P1-Fe1-P4, 121.06(6); P2-Fe1-P3, 143.82(6); P2-Fe1-P4, 92.10(6); P3-Fe1-P4, 106.14(6); N1-Fe2-N2, 136.9(2); P1-Fe2-P4, 107.05(5); N1-Fe2-P1, 91.9(1); N2-Fe2-P1, 114.2(1).

Reactivity of $[\text{SiNP}_2]\text{Fe}-\text{Cl}$: Redox Transformations. Our interest in synthetically modeling the role that may be played by iron in biological N_2 fixation has led us to consider that ligands with a π -basic amido donor might be particularly well suited to support dinitrogen chemistry. Our group and others have shown that low-valent Fe(I) and Fe(0) complexes can serve not only as useful platforms for the activation of dinitrogen, but also for multielectron redox events that lead to the isolation of multiply bonded species.^{5,14a,35} Thus, we examined the behaviour of **2.11** under reducing conditions.

Reduction of **2.11** with Na/Hg amalgam or Mg^0 powder under dinitrogen in the absence of a strong σ -donating ligand gave a number of decomposition products, indicating that **2.11** would not show a strong propensity to bind N_2 as we had hoped. However, reduction of **2.11** (0.25% Na/Hg amalgam) in the presence of a strong phosphine donor (PMe_3) cleanly generated $[\text{SiNP}_2]\text{Fe}(\text{PMe}_3)$ (**2.24**, eq 2.3), whose crystal structure is depicted in Figure 2.14. Interestingly, the Fe–N distance increases by 0.07 \AA upon reduction and the Fe–P bonds contract by an average of 0.13 \AA , consistent with the π -acidity of the phosphines. Thus, the presence of stabilizing phosphine donors allows isolation of what is, to the best of our knowledge, the only example of an iron(I) amido complex.

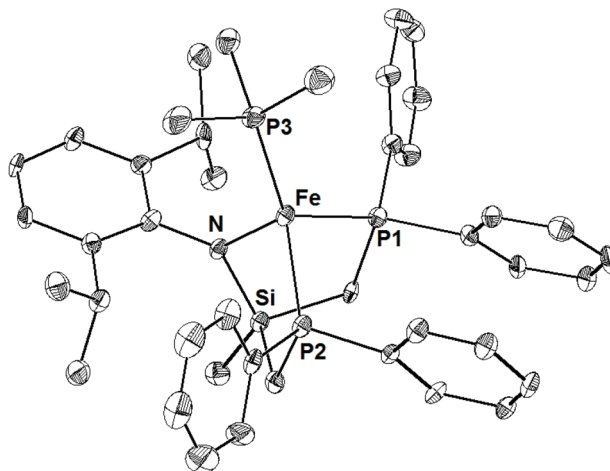
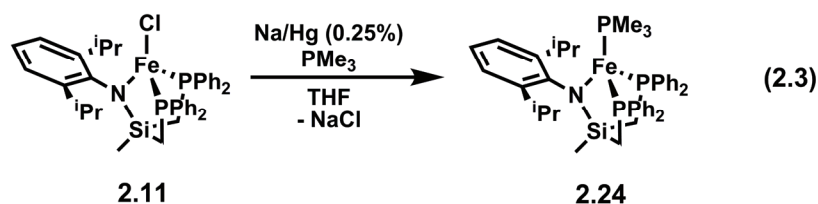


Figure 2.14. Displacement ellipsoid (35%) representation of $[\text{SiNP}_2]\text{Fe}(\text{PMe}_3)$ (**2.24**). Selected bond lengths (\AA) and angles ($^\circ$): Fe–N, 2.008(7); Fe–P1, 2.311(5); Fe–P2, 2.322(6); Fe–P3, 2.275(6); N–Fe–P1, 91.0(2); N–Fe–P2, 94.7(2); N–Fe–P3, 117.0(2); P1–Fe–P2, 98.07(8); P1–Fe–P3, 123.03(8); P2–Fe–P3, 125.00(9).

Results from our research group have shown that Fe(I) and Co(I) phosphine adducts such as **2.24** can serve as useful precursors for group transfer reactivity.⁵ Thus, a number of attempts were made to effect a two-electron oxidation by nitrene transfer, which would yield the Fe(III) imide. However, for all nitrene transfer reagents that were utilized (including adamantyl azide, *p*-tolyl azide, trimethylsilyl azide, and tosyl azide), the only product cleanly generated was the phosphinimine ($\text{Me}_3\text{P}=\text{NR}$), and free ligand was frequently observed by ^1H and ^{31}P NMR. These results indicate that, in contrast to the behavior observed for tris(phosphino)borate scaffolds, $[\text{SiNP}_2]\text{Fe}^{\text{I}}$ will likely not be a useful starting point for the generation of higher-valent multiply bonded species.

Conclusions

In conclusion, we have presented the synthesis of two new amidophosphine ligands, $[\text{SiNP}_3]$ and $[\text{SiNP}_2]$, and have explored elements of their coordination chemistry with iron and cobalt. The potentially tetradentate $[\text{SiNP}_3]$ ligand and its hexaisopropyl $[\text{SiNP}^{\text{Pr}}_3]$ relative coordinate to iron with only three donors, leaving one phosphine unbound, and these complexes have been thoroughly characterized. Coordination of $[\text{SiNP}_3]$ to cobalt(II) results in the expected trigonal-bipyramidal Co(II) complexes. One of these, $[\text{SiNP}_3]\text{CoCl}$ (**2.9**), may be reduced by one electron to afford the structurally unusual four-coordinate, trigonal-pyramidal Co(I) complex $[\text{SiNP}_3]\text{Co}$ (**2.14**), which reacts with a variety of small molecules, including CO and CO₂. Reaction of **2.14** with CO₂ results in Si–N bond cleavage and formation of isocyanate, showing one possible decomposition pathway for the $[\text{SiNP}_3]$ ligand. Ligand decomposition also occurs upon oxidation of **2.9** with ferricenium hexafluorophosphate to give an unusual cationic cobalt(III) imido complex by a related fluoride-induced Si–N bond cleavage.

The tridentate [$^{\text{Si}}\text{NP}_2$] ligand binds to both iron(II) and cobalt(II) in the desired fashion to afford the pseudo-tetrahedral complexes [$^{\text{Si}}\text{NP}_2$]FeCl (**2.11**) and [$^{\text{Si}}\text{NP}_2$]CoCl (**2.12**). The iron(II) complex **2.11** has been shown to undergo a number of metathesis reactions with X-type ligands to give the expected [$^{\text{Si}}\text{NP}_2$]Fe–X complexes, though reduction of these complexes did not give well-defined products, and they did not prove to be suitable precursors for the synthesis of multiply bonded species. Although reduction of complex **2.11** does not proceed cleanly in the absence of phosphine, reduction in the presence of PMe_3 affords the iron(I) amido complex [$^{\text{Si}}\text{NP}_2$]Fe(PMe_3) (**2.24**). However, complex **2.24** also did not prove to be a suitable precursor for multielectron redox transformations at iron.

The collective data provided in this chapter indicate that the new amidophosphine ligands presented confer a number of unusual electronic and structural properties to low-valent iron and cobalt complexes. However, the relative instability of the Si–N linkage and the propensity of [$^{\text{Si}}\text{NP}_3$] to bind in an undesirable tridentate fashion suggest that these ligands are not ideally suited for supporting well-defined multielectron redox transformations or the formation of metal–ligand multiple bonds at iron and cobalt.

Acknowledgment

The author acknowledges Dr. Eric Rivard for performing the design and first syntheses of $\text{H}[^{\text{Si}}\text{NP}_3]$ (**2.3**) and [$^{\text{Si}}\text{NP}_3$]CoI (**2.9**). Larry Henling and Neal Mankad provided crystallographic assistance.

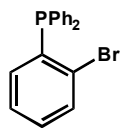
Experimental Section

General Considerations. All manipulations were carried out using standard Schlenk or glove box techniques under a dinitrogen atmosphere. Unless otherwise noted, solvents were deoxygenated and dried by thorough sparging with N₂ gas followed by passage through an activated alumina column. Nonhalogenated solvents were typically tested with a standard purple solution of sodium benzophenone ketyl in tetrahydrofuran in order to confirm effective oxygen and moisture removal. Deuterated solvents were degassed and stored over activated 3 Å molecular sieves prior to use. THF-d₈ was dried by passage through a column of activated alumina and stored over 3 Å molecular sieves prior to use. DippN(H)SiMe₂(CH₂Cl),³⁶ Li[NH(2,6-Me₂C₆H₃)],³⁷ neopentylolithium,³⁸ and Li[dbabh]³⁹ were prepared according to literature procedures. Diphenylphosphine (Strem), tetrakis(triphenylphosphine) palladium (Strem), trimethylphosphine (Strem), bis(chloromethyl)methylchlorosilane (Gelest), *n*-butyllithium (Aldrich), and sodium azide (Aldrich) were used as received without further purification. Phosphorus (III) chloride (Strem) and 2-iodobromobenzene (Alfa Aesar) were degassed via three freeze–pump–thaw cycles prior to use. Triethylamine (Aldrich) was degassed and distilled from CaH₂ prior to use. All reagents were purchased from commercial vendors and used without further purification unless explicitly stated. Elemental analyses were carried out at Desert Analytics, Tucson, Arizona. NMR spectra were recorded at ambient temperature on Varian Mercury 300 MHz spectrometers. ¹H NMR chemical shifts were referenced to residual solvent. ³¹P NMR chemical shifts are reported relative to an external standard of 85% H₃PO₄. UV-vis measurements were taken on a Hewlett Packard 8452A diode array spectrometer using a quartz crystal cell with a Teflon cap. Electrochemical analysis was performed on a CHI 600B Potentiostat/Galvanostat. X-ray diffraction studies were carried out in the Beckman Institute Crystallographic Facility on a Bruker Smart 1000 CCD diffractometer.

Magnetic Measurements. Measurements were recorded using a Quantum Designs SQUID magnetometer running MPMSR2 software (Magnetic Property Measurement System Revision 2). Data were recorded at 5000 G. Samples were suspended in the magnetometer in a clear plastic straw sealed under nitrogen with Lilly No. 4 gel caps. Loaded samples were centered within the magnetometer using the DC centering scan at 35 K and 5000 G. Data were acquired at 2–10 K (one data point every 2 K), 10–60 K (one data point every 5 K), and 60–310 K (one data point every 10 K). The magnetic susceptibility was adjusted for diamagnetic contributions using the constitutive corrections of Pascal's constants. The molar magnetic susceptibility (χ_m) was calculated by converting the calculated magnetic susceptibility (χ) obtained from the magnetometer to a molar susceptibility (using the multiplication factor $\{(\text{molecular weight})/[(\text{sample weight}) * (\text{field strength})]\}$). Curie-Weiss behavior was verified by a plot of χ_m^{-1} versus T. Effective magnetic moments were calculated using Equation 2.4. Solution magnetic moments were measured using Evans' method.¹⁶

$$\mu_{\text{eff}} = \text{sqrt}(7.997 \chi_m T) \quad \text{(2.4)}$$

Synthesis of (2-bromophenyl)diphenylphosphine (2.1). 2-Ph₂PC₆H₄Br was prepared by



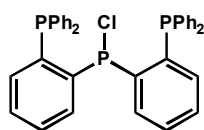
2.1

modification of a literature procedure.⁴⁰ 2-iodobromobenzene (24.1337 g, 85.3070 mmol), diphenylphosphine (15.8848 g, 85.3150 mmol), triethylamine (10.0945 g, 99.7579 mmol), and a catalytic amount of Pd(PPh₃)₄ (513.0 mg, 0.4439 mmol) were

dissolved in 150 mL of toluene to give a clear, bright-yellow solution. The solution was heated at 80 °C with stirring for 16 hours in a sealed bomb, resulting in the precipitation of triethylammonium iodide. The resulting orange solution was dried *in vacuo* at 50 °C, extracted into diethyl ether (400 mL), and filtered through a 1" pad of silica gel to give a clear, pale-yellow solution, from which the volatiles were removed *in vacuo* to yield phosphine **2.1** as a creamy

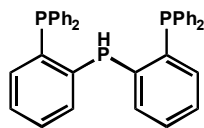
white powder (24.9352 g, 86%). Characterization data matched those previously reported for the complex.⁴⁰

Synthesis of bis(2-(diphenylphosphino)phenyl)chlorophosphine. To a colorless solution of **2.1**



(1.170 g, 3.42 mmol) in 30 mL of diethyl ether stirring at $-80\text{ }^{\circ}\text{C}$, *n*-butyllithium (1.60 M solution in hexanes, 2.15 mL, 3.44 mmol) was added dropwise by syringe, causing the solution to become deep orange and cloudy. The reaction was stirred at $-80\text{ }^{\circ}\text{C}$ for 15 min and at ambient temperature for 35 min. The orange suspension of $\text{Li}[2\text{-Ph}_2\text{PC}_6\text{H}_4]$ was added slowly by pipette (over 20 min) to a stirring solution of PCl_3 (230 mg, 1.67 mmol) in 5 mL of diethyl ether at $-80\text{ }^{\circ}\text{C}$. After the addition, the cloudy, pale-yellow suspension was allowed to stir at room temperature for 3 h and evaporated to dryness *in vacuo*. The resulting pale-yellow powder was extracted into benzene (40 mL) and filtered through celite to remove LiCl . The volatiles were removed *in vacuo* and the orange residue dissolved in 3 mL CH_2Cl_2 and layered with 2 mL of petroleum ether. A pale-yellow microcrystalline solid was obtained by cooling the solution to $-35\text{ }^{\circ}\text{C}$ for 16 h (0.667 g, 66%). ^1H NMR (C_6D_6): δ 7.76 (d, 2H, Ar-H), 7.33 (m, 4H, Ar-H), 7.17 (m, 6H, Ar-H), 6.99 (m, 6H, Ar-H), 6.80–6.94 (m, 10H, Ar-H). $^{13}\text{C}\{^1\text{H}\}$ NMR (CD_2Cl_2): δ 134.8 (d), 134.4–133.6 (m), 132.9, 130.6 (d), 129.4–128.4 (m). $^{31}\text{P}\{^1\text{H}\}$ NMR (C_6D_6): δ 68.6 (t, $^3J_{\text{PP}} = 245.6\text{ Hz}$, Ar_2PCl), -15.7 (d, $^3J_{\text{PP}} = 245.6\text{ Hz}$, $-\text{PPh}_2$). Attempts to obtain combustion analysis data repeatedly yielded low results for carbon, likely due to the presence of small amounts of $(2\text{-Ph}_2\text{PC}_6\text{H}_4)_2\text{Br}$ (evident by ^{31}P NMR spectroscopy).

Synthesis of bis(2-(diphenylphosphino)phenyl)phosphine (2.2). Pale-yellow bis(2-

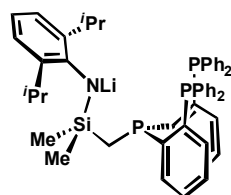


2.2

(diphenylphosphino)phenyl)chlorophosphine (485.2 mg, 0.8238 mmol) was added in portions to a solution of lithium aluminum hydride (40.2 mg, 1.06 mmol) in 35 mL of diethyl ether at $-35\text{ }^{\circ}\text{C}$. The reaction immediately became

cloudy while remaining colorless and was allowed to proceed at room temperature with stirring for 2 h. The volatiles were removed and the reaction mixture was extracted into 40 mL of benzene and filtered through a 1" pad of silica to give a colorless solution that was dried to a white foam (369.4 mg, 81 %). ^1H NMR (C_6D_6): δ 7.30 (m, 9H, Ar-H), 7.15 (m, 3H, Ar-H), 6.80 (m, 5H, Ar-H), 5.68 (dt, $^1J_{\text{PH}} = 221.8\text{ Hz}$, $^4J_{\text{PH}} = 8.0\text{ Hz}$, P-H). $^{13}\text{C}\{^1\text{H}\}$ NMR (C_6D_6): 138.0 (m), 136.2 (m), 135.0–134.2 (m), 129.5, 129.3–128.8 (m). $^{31}\text{P}\{^1\text{H}\}$ NMR (C_6D_6): δ -10.9 (d, $^3J_{\text{PP}} = 116.6\text{ Hz}$, $-\text{PPh}_2$), -53.8 (dt, $^1J_{\text{HP}} = 222.2\text{ Hz}$, $^3J_{\text{PP}} = 116.0\text{ Hz}$, Ar_2PH). MS (ESI): 555.1 ((M+H) $^+$). Anal. calcd. for $\text{C}_{36}\text{H}_{29}\text{P}_3$: C, 77.97; H, 5.27. Found: C, 77.75; H, 5.23.

Synthesis of $[(2\text{-Ph}_2\text{PC}_6\text{H}_4)_2\text{PCH}_2\text{Si}(\text{CH}_3)_2\text{N}(\text{Dipp})]\text{Li}(\text{Et}_2\text{O})_{1.5}$ ($\text{Li}[\text{Si}^{\text{NP}}_3]$, 2.3). To a stirring solution

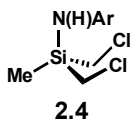
Li[Si^{NP}₃] (2.3)

of **2.2** (1.6029 g, 2.8905 mmol) in 30 mL of THF at $-35\text{ }^{\circ}\text{C}$ was added dropwise a solution of *n*-butyllithium (1.60 M in hexanes, 1.890 mL, 3.024 mmol). The mixture immediately adopted a deep-orange hue. After 1 h, this phosphide solution was added dropwise to a stirring solution of

DippN(H)SiMe₂(CH₂Cl) (820.7 mg, 2.891 mmol) in THF (20 mL). The deep-orange color of the solution quickly faded, and after 3 hours volatiles were removed from the pale-yellow solution to give a yellow foam. The foam was dissolved in Et₂O (30 mL), filtered through a pad of celite to remove LiCl, and chilled to $-35\text{ }^{\circ}\text{C}$. *n*-Butyllithium (1.60 M in hexanes, 1.890 mL, 3.024 mmol) was added dropwise with stirring, and after 2 h stirring at room temperature the solution was diluted with 50 mL of petroleum ether and chilled to $-35\text{ }^{\circ}\text{C}$ for 12 h to yield a crop of white

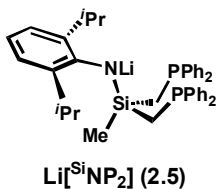
crystals, which were isolated on a frit and washed with petroleum ether (3 × 10 mL) (2.0968 mg, 79%). ^1H NMR (C_6D_6): δ 7.50 (m, 2H, Ar-H), 7.20–7.40 (m, 8H, Ar-H), 7.05 (t, 4H, Ar-H), 6.80–7.05 (m, 17H, Ar-H), 4.25 (septet, $J = 6.9$ Hz, 2H, $-\text{CH}(\text{CH}_3)_2$), 3.11 (q, 6H, Et_2O), 1.60 (d, $^2J_{\text{PH}} = 5.4$ Hz, 2H, $-\text{CH}_2$), 1.38 (d, $J = 6.0$ Hz, 12H, $-\text{CH}(\text{CH}_3)_2$), 0.82 (t, 9H, Et_2O), 0.20 (s, 6H, $\text{Si}(\text{CH}_3)_2$). $^{13}\text{C}\{^1\text{H}\}$ NMR (THF-d_8): δ 143.8, 135.5–134.5 (m), 134.0–133.0 (m), 129.5, 129.0–128.8 (m), 128.7, 122.7, 115.4, 66.5 (Et_2O), 27.4 ($-\text{CH}(\text{CH}_3)_2$), 25.7 ($-\text{CH}(\text{CH}_3)_2$), 20.2–19.0 (d, $-\text{CH}_2\text{P}$), 15.9 (Et_2O), 4.4 ($-\text{Si}(\text{CH}_3)_2$). $^{31}\text{P}\{^1\text{H}\}$ NMR (C_6D_6): δ -15.9 (d, $^3J_{\text{PP}} = 165$ Hz, PPh_2), -29.0 (t, $^3J_{\text{PP}} = 165$ Hz, Ar_2PCH_2). Anal. calcd. for $\text{C}_{57}\text{H}_{68}\text{LiNO}_{1.5}\text{P}_3\text{Si}$: C, 74.49; H, 7.46; N, 1.52. Found: C, 73.23; H, 7.17; N, 1.60.

Synthesis of $\text{HN}(\text{Dipp})\text{SiMe}(\text{CH}_2\text{Cl})_2$ (2.4). Lithium (2,6-diisopropyl)anilide (623.0 mg, 3.400



mmol) was added in portions to a stirring solution of $(\text{ClCH}_2)_2\text{SiMeCl}$ (603.9 mg, 3.401 mmol) in Et_2O (10 mL) at -35 °C. A white solid formed, and the reaction was stirred overnight at room temperature. The volatiles were removed *in vacuo* and the residues extracted into 15 mL of petroleum ether, filtered through a pad of celite, and solvent was removed *in vacuo* to give a clear, slightly yellow oil (1.0397, 96%). ^1H NMR (C_6D_6): δ 6.95–7.05 (m, 3H, Ar-H), 3.20–3.40 (septet, $J = 6.9$ Hz, 2H, $-\text{CH}(\text{CH}_3)_2$), 2.74 (s, 4H, $-\text{Si}(\text{CH}_2)_2$), 2.37 (s, 1H, $-\text{NH}$), 1.09 (d, $J = 6.0$ Hz, 12H, $-\text{CH}(\text{CH}_3)_2$), -0.02 (s, 3H, SiCH_3). $^{13}\text{C}\{^1\text{H}\}$ NMR (C_6D_6): δ 145.9, 125.9, 123.9, 28.8, 28.6, 24.2 ($-\text{CH}(\text{CH}_3)_2$), -6.6 ($-\text{SiCH}_3$). MS (CI): 317 (M^+ , 100%), 318 (26%), 319 (67%).

Synthesis of $\text{LiN}(\text{Dipp})\text{SiMe}(\text{CH}_2\text{PPh}_2)_2$ ($\text{Li}[\text{SiNP}_2]$, **2.5).** Diphenylphosphine (1.2786 g, 6.8672



mmol) was dissolved in 10 mL of THF and chilled to -80°C . *n*-Butyllithium

(1.60 M in hexanes, 4.30 mL, 6.88 mmol) was added dropwise to the stirring

solution, causing a color change to orange and then to red. After 10 min, the

solution was warmed to room temperature and stirred for 40 min. The red phosphide solution

was cooled to -35°C and added dropwise to a cold (-35°C) solution of **2.4** (1.0927 mg, 3.4316

mmol), and the color rapidly dissipated with each drop. The reaction was allowed to proceed for

5 h, and volatiles were removed *in vacuo* to leave a yellow oil. The residues were extracted into

petroleum ether (60 mL), filtered through a pad of celite, and chilled to -35°C . *n*-Butyllithium

(1.60 M in hexanes, 2.00 mL, 3.20 mmol) was added dropwise to the stirring solution, causing a

white solid to precipitate. After 2 h, the solid was isolated on a frit and washed with petroleum

ether (3×10 mL) to yield the pure lithium amide (1.3700 g, 64%). ^1H NMR (C_6D_6): δ 7.36–7.52

(m, 8H, Ar-H), 6.88–7.10 (m, 14H, Ar-H), 3.72 (br s, 2H, $-\text{CH}(\text{CH}_3)_2$), 1.40–1.80 (dd, 4H,

$-\text{Si}(\text{CH}_2)_2$), 1.10–1.20 (d, $J = 5.7$ Hz, 6H, $-\text{CH}(\text{CH}_3)_2$), 1.00 (br s, 6H, $-\text{CH}(\text{CH}_3)_2$), -0.20 (s, 3H,

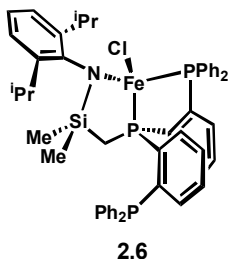
$-\text{SiCH}_3$). $^{13}\text{C}\{^1\text{H}\}$ NMR (THF- d_8): δ 155.1, 144.0–143.0 (m), 134.0 (d), 133.0 (d), 129.2–128.6 (m),

128.5, 122.9, 116.0, 27.2 ($-\text{CH}(\text{CH}_3)_2$), 25.6 ($-\text{CH}(\text{CH}_3)_2$), 17.8 (dd, $^1J_{\text{CP}} = 28.0$ Hz, $^3J_{\text{CP}} = 2.6$ Hz).

$^{31}\text{P}\{^1\text{H}\}$ NMR (C_6D_6): δ -23.4 (s). Anal. calcd. for $\text{C}_{39}\text{H}_{44}\text{LiNP}_2\text{Si}$: C, 75.10; H, 7.11; N, 2.25. Found: C,

75.06; H, 7.22; N, 2.33.

Synthesis of $[\text{Si}^{\text{NP}}_3]\text{FeCl}$ (2.6**).** A yellow solution of $\text{Li}[\text{Si}^{\text{NP}}_3]$ (**2.3**) (171.9 mg, 0.1870 mmol) in THF



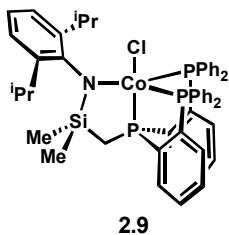
(2 mL) was added to a suspension of FeCl_2 (23.9 mg, 0.1886 mmol) in THF (5 mL). The mixture immediately gained a dark-brown hue and was allowed to stir for 12 h. The volatiles were removed and the resulting dark-brown oily residue was extracted into benzene (10 mL), filtered through a pad of

celite, dried *in vacuo*, triturated with petroleum ether (3 × 5 mL), isolated on a frit and washed with petroleum ether (3 × 10 mL) to give a brown powder (106.9 mg, 64%). Yellow-green crystals suitable for X-ray diffraction were obtained by vapor diffusion of petroleum ether into a concentrated benzene solution of **2.6**. ^1H NMR (C_6D_6): δ 50.8, 25, 16.1, 15.0, 13.1, 10.8, 8.0, 3.1, -4.0, -4.7, -6.5, -8.5, -49.1. UV-vis (C_6H_6) λ_{max} , nm (ϵ , $\text{M}^{-1} \text{cm}^{-1}$): 387 (3640). μ_{eff} (C_6D_6): 4.57 μB . MS (ESI): 856.2 ($[\text{Si}^{\text{NP}}_3]\text{Fe}^+$, 100%), 857.2 (64%), 858.3 (18%). Anal. calcd. for $\text{C}_{51}\text{H}_{53}\text{ClFeNP}_3\text{Si}$: C, 68.65; H, 5.99; N, 1.57. Found: C, 68.30; H, 5.90; N, 1.69.

Synthesis of $[(2\text{-}^i\text{Pr}_2\text{PC}_6\text{H}_4)_2\text{PCH}_2\text{Si}(\text{CH}_3)_2\text{N}(\text{Dipp})]\text{Li}$ ($\text{Li}[\text{Si}^{\text{NP}^i\text{Pr}}_3]$, **2.7).** $\text{Li}[\text{Si}^{\text{NP}^i\text{Pr}}_3]$ (**2.7**) was prepared from the previously reported bis(2-(diisopropylphosphino)phenyl)phosphine¹⁸ via a procedure analogous to that used in the synthesis of **2.3**.

Synthesis of $[\text{Si}^{\text{NP}^i\text{Pr}}_3]\text{FeCl}$ (2.8**).** Complex **2.8** was prepared from **2.7** and FeCl_2 in the same manner as $[\text{Si}^{\text{NP}}_3]\text{FeCl}$, and X-ray quality crystals were obtained by vapor diffusion of petroleum ether into a concentrated benzene solution of **2.8**.

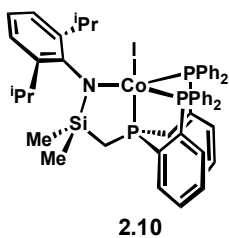
Synthesis of $[\text{Si}^{\text{NP}_3}\text{CoCl}]$ (2.9**).** A yellow solution of $\text{Li}[\text{Si}^{\text{NP}_3}]$ (**2.3**) (560.8 mg, 0.6102 mmol) in THF



(8 mL) was added to a light-blue suspension of CoCl_2 (79.2 mg, 0.610 mmol) in THF (8 mL). The mixture immediately gained a dark-maroon hue and was allowed to stir for 12 h. The volatiles were removed and the resulting dark-red oil was extracted into benzene (100 mL), filtered through

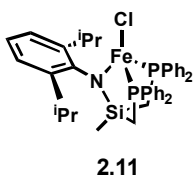
a pad of celite to remove salts, dried *in vacuo*, triturated with petroleum ether (2×10 mL), isolated on a frit and washed with 9:1 petroleum ether/ CH_2Cl_2 (3×10 mL) to give a maroon powder (120.0 mg, 22%). X-ray quality crystals were obtained by vapor diffusion of petroleum ether into a concentrated benzene solution of **2.9**. ^1H NMR (CD_2Cl_2): δ 10.8, 9.2, 8.3, 7.6, 7.4, 7.2, 7.0, 3.7, 1.3, 1.0, 0.5, 0.1, -3.0. UV-vis (C_6H_6) λ_{max} , nm (ϵ , $\text{M}^{-1} \text{cm}^{-1}$): 820 (480), 490 (3300), 422 (4500), 335 (8125). Anal. calcd. for $\text{C}_{51}\text{H}_{53}\text{ClCoNP}_3\text{Si}$: C, 68.41; H, 5.97; N, 1.56. Found: C, 68.24; H, 5.90; N, 1.37.

Synthesis of $[\text{Si}^{\text{NP}_3}\text{CoI}]$ (2.10**).** This compound was generated in the same manner as described



for **2.9**. Although analytically pure samples were not be obtained, dark-red plates suitable for XRD analysis were obtained by vapor diffusion of petroleum ether into a concentrated benzene solution of **2.10**.

Synthesis of $[\text{Si}^{\text{NP}_2}\text{FeCl}]$ (2.11**).** A yellow solution of $\text{Li}[\text{Si}^{\text{NP}_2}]$ (**2.5**) (232.8 mg, 0.3732 mmol) in

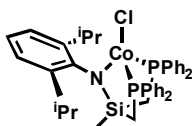


THF (5 mL) was added to a slurry of FeCl_2 (47.4 mg, 0.374 mmol) in THF (5 mL), causing an immediate color change to dark brown. After 3 h, the solution had lightened to a golden hue, and volatiles were removed *in vacuo*, leaving a

dark-yellow oil. The residues were extracted into benzene (10 mL), filtered through a pad of

celite, lyophilized to a golden powder, and washed with petroleum ether to give a canary-yellow powder (219.0 mg, 83%). Crystals suitable for X-ray diffraction were grown by diffusion of petroleum ether into a concentrated benzene solution of **2.11**. ^1H NMR (C_6D_6): δ 64.0, 55.0, 21.0, 18.1, 13.4, 10.4, 1.9, 0.9, -7.9, -45.1, -56.0. UV-vis (Et_2O) λ_{max} , nm (ϵ , $\text{M}^{-1} \text{cm}^{-1}$): 370 (2300). μ_{eff} (C_6D_6): $4.80 \mu_{\text{B}}$. Anal. calcd. for $\text{C}_{39}\text{H}_{44}\text{ClFeNP}_2\text{Si}$: C, 66.15; H, 6.26; N, 1.98. Found: C, 66.53; H, 6.26; N, 1.69.

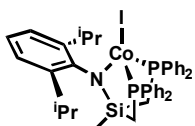
Synthesis of $[\text{SiNP}_2]\text{CoCl}$ (2.12**).** A yellow solution of $\text{Li}[\text{SiNP}_2]$ (**2.5**) (360.0 mg, 0.5771 mmol) in



2.12

Et_2O (8 mL) was added to a slurry of CoCl_2 (74.9 mg, 0.5769 mmol) in Et_2O (5 mL), causing an immediate change in color from light blue to dark green. After 5 hours, the solution was filtered to remove LiCl , dried *in vacuo*, extracted into benzene (10 mL), filtered through a pad of celite, and dried to a green oil. The oil was dissolved in Et_2O (1 mL), and 15 mL of petroleum ether was added, causing a green solid to precipitate. The solid was isolated on a frit and washed with petroleum ether (3×10 mL) to give **2.12** as a green powder (231.1 mg, 58%). ^1H NMR (THF-d_8): 44.6, 35.0, 26.5, 22.1, 12.3, 11.4, 9.2, 7.3, -1.0, -20.0, -58.4. UV-vis (Et_2O) λ_{max} , nm (ϵ , $\text{M}^{-1} \text{cm}^{-1}$): 735 (510), 600 (660), 490 (980), 360 (2900). μ_{eff} (C_6D_6): $3.74 \mu_{\text{B}}$. Anal. calcd. for $\text{C}_{39}\text{H}_{44}\text{ClCoNP}_2\text{Si}$: C, 65.86; H, 6.24; N, 1.97. Found: C, 64.15; H, 5.98; N, 1.88.

$[\text{SiNP}_2]\text{CoI}$ (2.13**).** A yellow solution of $\text{Li}[\text{SiNP}_2]$ (**2.5**) (209.4 mg, 0.3357 mmol) in Et_2O (5 mL) was

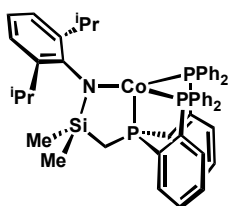


2.12

added to a dark-blue solution of CoI_2 (0.3357) in Et_2O (5 mL), causing an immediate change in color to dark brown. The reaction was allowed to proceed 5 h, filtered through a pad of celite, and dried *in vacuo* to a brown oil. The oil was triturated with petroleum ether to give a brown powder, which was isolated on a frit

and washed with 5:1 petroleum ether/Et₂O (2 × 5 mL) to afford **2.13** as a light-brown powder (125.0 mg, 46%). Dark-brown blocks of crystalline **2.13** suitable for XRD analysis were obtained by slow evaporation of Et₂O from a concentrated solution. ¹H NMR (C₆D₆): 77.1, 26.5, 20.7, 20.2, 11.4, 5.7, 3.5, 1.3, -4.3, -7.4, -8.7, -13.5, -59.0, -79.4. UV-vis (Et₂O) λ_{max}, nm (ε, M⁻¹ cm⁻¹): 790 (320), 620 (1000), 500 (1900), 320 (6700). μ_{eff} (C₆D₆): 4.04 μ_B. Anal. calcd. for C₃₉H₄₄CoINP₂Si: C, 58.36; H, 5.53; N, 1.75. Found: C, 57.53; H, 5.20; N, 1.73. Attempts to obtain combustion analyses of compounds **2.12** and **2.13** repeatedly yielded low results in carbon, even with recrystallized samples.

Synthesis of [⁵¹NP₃]Co (2.14). A 0.32 weight % Na/Hg amalgam (325.9 mg, 0.045 mmol) was

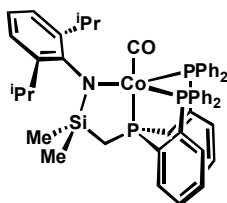


2.14

stirred in THF (2 mL). To this was added a red solution of [⁵¹NP₃]CoCl (**2.9**) (38.3 mg, 0.0428 mmol) in THF (5 mL). The reaction was allowed to proceed 15 h, causing a color change from dark red to brown, and the solution was filtered away from the amalgam. Volatiles were removed *in vacuo* to give a brown oil that was extracted into benzene, filtered, and dried *in vacuo* to a

brown oil. X-ray quality crystals were grown from a concentrated petroleum ether solution of **2.14** (16 mg, 43%). ¹H NMR (C₆D₆): δ 30.3, 21.5, 19.2, 16.5, 15.8, 13.0, 11.3, 9.8, 8.8, 4.0, 3.7, 0.2, 0.0, -1.8, -4.5, -10.1. μ_{eff} (C₆D₆): 2.73 μ_B. Anal. Calcd. For C₅₁H₅₃CoNP₃Si: C, 71.23; H, 6.21; N, 1.63. Found: C, 71.06; H, 6.46; N, 1.37.

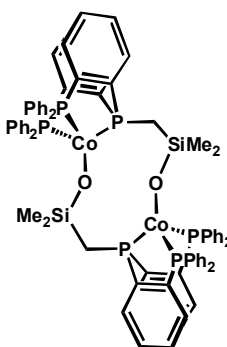
Synthesis of $[\text{}^{\text{Si}}\text{NP}_3]\text{Co}(\text{CO})$ (2.15). A sample of **2.14** was dissolved in THF (800 μL) and



2.15

transferred to a resealable NMR tube. The solution was frozen and the headspace evacuated and backfilled with carbon monoxide (1 equiv), causing a slight lightening of the solution as it melted. $^{31}\text{P}\{^1\text{H}\}$ NMR (C_6D_6): δ 121.6 (t, $^3J_{\text{PP}} = 55$ Hz, 1P), 61.9 (d, $^3J_{\text{PP}} = 55$ Hz, 2P). IR (THF, KBr, cm^{-1}) $\nu(\text{CO})$: 1932.

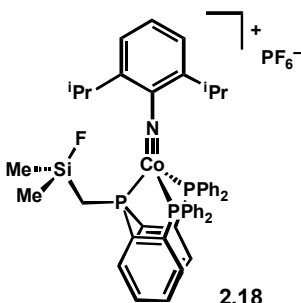
Synthesis of Siloxide Dimer (2.16). A sample of **2.14** (ca. 20 mg) was dissolved in benzene (800



2.16

μL) and transferred to a resealable NMR tube. The solution was frozen and the headspace evacuated and backfilled with carbon dioxide (1 atm). The solution was allowed to melt and stirred at ambient temperature for 2 h. Volatiles were removed *in vacuo* and the residues were redissolved in pentane, filtered, and chilled at -35 $^\circ\text{C}$ to produce a small crop of dark crystals of complex **2.16**.

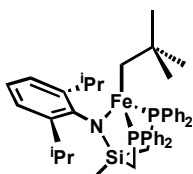
Synthesis of Cobalt Imide (2.18). $[\text{}^{\text{Si}}\text{NP}_3]\text{CoCl}$ (**2.9**) was dissolved in THF and ferricenium



2.18

hexafluorophosphate (1.1 equiv) added as a solution in THF, causing a darkening of the solution. The reaction was allowed to proceed with stirring for 12 h, volatiles were removed *in vacuo*, and residues redissolved in Et_2O , filtered, and chilled to afford a crop of dark X-ray quality crystals of complex **2.18**.

Synthesis of $[\text{SiNP}_2]\text{Fe}(\text{Np})$ (2.19**).** To a frozen solution of $[\text{SiNP}_2]\text{FeCl}$ (**2.11**) (46.7 mg, 0.0659



2.19

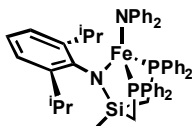
mmol) in THF (5 mL) was added solid neopentyllithium (5.2 mg, 0.0666 mmol).

The mixture was allowed to warm to ambient temperature with stirring, causing an immediate color change to orange as the solvent melted. The

reaction was allowed to proceed 1 h, then volatiles were removed *in vacuo* to

leave an orange oil, which was extracted into benzene, filtered through a glass plug, and lyophilized to an orange powder (44.3 mg, 90%). X-ray quality crystals were grown by chilling a concentrated petroleum ether solution of the product to $-35\text{ }^\circ\text{C}$ for 12 h. ^1H NMR (C_6D_6): δ 99.0, 44.2, 34.4, 24.0, 15.5, 12.4, 8.5, 1.7, 0.1, -3.0 , -6.4 , -40.0 , -43.0 . μ_{eff} (C_6D_6): $4.80\ \mu_{\text{B}}$.

Synthesis of $[\text{SiNP}_2]\text{Fe}(\text{NPh}_2)$ (2.20**).** A solution of lithium diphenylamide (3.3 mg, 0.019 mmol) in



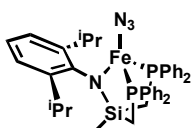
2.20

Et_2O (2 mL) was chilled to $-80\text{ }^\circ\text{C}$ and added to a stirring solution of **2.11** (13.2 mg, 0.0186 mmol) in Et_2O (5 mL), causing an immediate color change from

yellow to orange. The reaction was allowed to proceed for 3 h at $-80\text{ }^\circ\text{C}$, then

brought to room temperature, causing the solution to become cloudy. After 12 h, the cloudy solution was filtered and volatiles were removed *in vacuo* to give an orange oil. X-ray quality crystals were grown from a concentrated petroleum ether solution of **2.20**. ^1H NMR (C_6D_6): δ 93.0, 47.1, 40.8, 20.8, 17.3, 12.1, 8.1, 3.6, -2.9 , -8.3 , -11.1 , -36.5 , -52.6 , -55.6 .

Synthesis of $[\text{SiNP}_2]\text{Fe}(\text{N}_3)$ (2.21**).** $[\text{SiNP}_2]\text{FeCl}$ (**2.11**) (82.1 mg, 0.116 mmol) was dissolved in THF



2.20

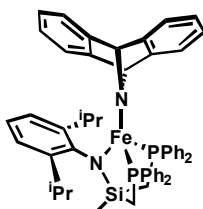
(5 mL) and added to a stirring solution of sodium azide (7.6 mg, 0.12 mmol), causing a color change from light yellow to golden over a period of 15 min.

After 4 h, the mixture was filtered to remove dark solids and dried to a golden

oil. The oil was extracted into benzene, filtered, and lyophilized to afford a golden powder. ^1H

NMR (C_6D_6): δ 62.9, 54.3, 20.7, 17.9, 13.5, 10.3, 1.8, 0.1, -7.6, -44.7, -54.2. IR (THF, cm^{-1}): $\nu(N_3)$ 2081.

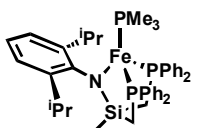
Synthesis of $[^{Si}NP_2]Fe(dbabh)$ (2.22**).** Lithium 2,3:5,6-dibenzo-7-aza bicyclo[2.2.1]hepta-2,5-



2.22

diene diethyl etherate (14.1 mg, 0.0516 mmol) was dissolved in THF (2 mL) and added to a frozen solution of $[^{Si}NP_2]FeCl$ (**2.11**) (36.1 mg, 0.0510 mmol) in THF (5 mL). The solution was brought to room temperature, and as melting began, the color darkened to a red-orange hue. The reaction was allowed to continue 4 h, and the solution was filtered and the volatiles removed *in vacuo*, leaving a dark-yellow residue. The residue was extracted into benzene, filtered, and lyophilized to yield a golden powder (35.0 mg, 79%). 1H NMR (C_6D_6): δ 111.0, 45.2, 20.3, 17.3, 11.9, 8.9, 3.2, 1.5, -2.4, -9.1, -11.3, -42.7, -45.5.

Synthesis of $[^{Si}NP_2]Fe(PMe_3)$ (2.24**).** A 0.27 weight % Na/Hg amalgam (2.0 g, 0.23 mmol) was



2.24

stirred in THF (2 mL). To this was added $[^{Si}NP_2]FeCl$ (**2.11**) (155.2 mg, 0.2192 mmol) and PMe_3 (68 μ L, 0.66 mmol) in THF (5 mL), causing a gradual color change from yellow to dark red-orange over a period of 10 min. The reaction was allowed to proceed 4 h, and the solution was filtered away from the amalgam. The solution was dried *in vacuo*, extracted into benzene and filtered to remove salts. Volatiles were removed from the dark-orange solution *in vacuo*, leaving an orange foam. Brown crystals were grown by chilling a concentrated solution of **2.24** in petroleum ether at -35 $^{\circ}C$ for 2 days (67.7 mg, 41%). 1H NMR (C_6D_6): δ 85.5, 67.5, 30.4, 14.4, 12.6, 10.1, 8.2, 5.4, 3.7, 0.0, -0.6, -1.4, -25.2, -28.5.

X-ray Crystallography Procedures. X-ray quality crystals were grown as indicated in the experimental procedures for each complex. The crystals were mounted on a glass fiber with Paratone-N oil. Structures were determined using direct methods with standard Fourier techniques using the Bruker AXS software package. In some cases, Patterson maps were used in place of the direct methods procedure. Table 2.2 contains the X-ray diffraction experimental details.

Table 2.2. X-ray crystallographic data

complex	2.6	2.8	2.10
Empirical Formula	C ₅₁ H ₅₃ ClFeNP ₃ Si · 0.5 (C ₆ H ₆) · 0.5 (C ₅ H ₁₀)	C ₃₉ H ₆₁ ClFeNP ₃ Si	C ₅₁ H ₅₃ CoINP ₃ Si · 2 (C ₆ H ₆)
Formula Weight	966.36	756.19	1141.98
λ (Å)	0.71073	0.71073	0.71073
T (K)	100(2)	100(2)	100(2)
a (Å)	10.8604(17)	11.0059(16)	13.0107(10)
b (Å)	20.831(3)	23.266(3)	19.1387(15)
c (Å)	23.586(4)	16.749(2)	22.1493(16)
α (deg)	72.318(3)	90	90
β (deg)	83.313(3)	102.779(4)	102.943(3)
γ (deg)	89.880(3)	90	90
V (Å ³)	5046.3(14)	4182.6(10)	5399.8(7)
Z	4	4	4
Crystal System	Triclinic	Monoclinic	Monoclinic
Space Group	P-1	P2(1)/n	P2(1)/c
d _{calc} (g/cm ³)	1.272	1.201	1.405
GOF on F ²	1.006	0.939	1.254
R1, wR2 ^a (I > 2 σ (I))	0.1253, 0.2861	0.0587, 0.0826	0.0717, 0.1089

complex	2.11	2.13	2.14
Empirical Formula	C ₃₉ H ₄₄ ClFeNP ₂ Si · C ₆ H ₆	C ₃₉ H ₄₄ CoINP ₂ Si · C ₄ H ₁₀ O	C ₅₁ H ₅₃ CoNP ₃ Si
Formula Weight	786.19	876.73	859.87
λ (Å)	0.71073	0.71073	0.71073
T (K)	100(2)	100(2)	100(2)
a (Å)	9.793(3)	11.6071(8)	24.862(7)
b (Å)	9.371(3)	21.6762(15)	13.975(4)
c (Å)	44.610(12)	16.8895(12)	12.669(4)
α (deg)	90	90	90
β (deg)	94.581(4)	92.988(2)	90
γ (deg)	90	90	90
V (Å ³)	4080.9(19)	4243.6(5)	4402(2)
Z	4	4	4
Crystal System	Monoclinic	Monoclinic	Orthorhombic
Space Group	P2(1)/n	P2(1)/c	Pna2(1)
d _{calc} (g/cm ³)	1.28	1.372	1.297
GOF on F ²	1.305	3.006	1.619
R1, wR2 ^a (I > 2σ (I))	0.0456, 0.0682	0.0700, 0.1290	0.1422, 0.2250

complex	2.16	2.18	2.19
Empirical Formula	C ₃₉ H ₃₆ CoOP ₃ Si	C ₅₁ H ₅₃ CoF ₇ NP ₄ Si	C ₅₄ H ₅₅ FeNP ₂ Si
Formula Weight	700.61	1023.84	743.77
λ (Å)	0.71073	0.71073	0.71073
T (K)	100(2)	100(2)	100(2)
a (Å)	14.438(9)	10.5082(12)	26.8547(13)
b (Å)	14.563(10)	22.014(2)	26.8547(13)
c (Å)	18.348(13)	21.559(2)	11.1680(8)
α (deg)	90	90	90
β (deg)	95.732(13)	99.548(2)	90
γ (deg)	90	90	90
V (Å ³)	3839(4)	4917.9(9)	8054.1(8)
Z	4	4	8
Crystal System	Monoclinic	Monoclinic	Tetragonal
Space Group	P2(1)/n	P2(1)/c	P-42(1)c
d _{calc} (g/cm ³)	1.212	1.383	1.227
GOF on F ²	1.113	0.986	1.358
R1, wR2 ^a (I > 2 σ (I))	0.0631, 0.0954	0.0606, 0.0888	0.0667, 0.0950

complex	2.20	2.21	2.24
Empirical Formula	C ₅₁ H ₅₄ FeN ₂ P ₂ Si	C ₆₆ H ₃₃ FeNP ₂ Si · C ₅ H ₁₂	C ₅₄ H ₅₅ FeNP ₂ Si
Formula Weight	840.84	1263.22	743.77
λ (Å)	0.71073	0.71073	0.71073
T (K)	100(2)	100(2)	100(2)
a (Å)	9.834(5)	13.579(2)	26.8547(13)
b (Å)	11.416(4)	15.663(3)	26.8547(13)
c (Å)	22.530(11)	16.181(3)	11.1680(8)
α (deg)	102.54(5)	90.198(3)	90
β (deg)	94.33(4)	102.448(3)	90
γ (deg)	106.56(3)	100.579(3)	90
V (Å ³)	2341.0(19)	3300.1(9)	8054.1(8)
Z	2	2	8
Crystal System	Triclinic	Triclinic	Tetragonal
Space Group	P-1	P-1	P-42(1)c
d _{calc} (g/cm ³)	1.193	1.271	1.227
GOF on F ²	1.184	1.073	1.358
R1, wR2 ^a (I > 2 σ (I))	0.0520, 0.0775	0.0516, 0.0787	0.0667, 0.0950

References and Notes

- (1) (a) Evans, D. J.; Pickett, C. J. *Chem. Soc. Rev.* **2003**, *32*, 268. (b) Tard, C.; Liu, X. M.; Ibrahim, S. K.; Bruschi, M.; De Gioia, L.; Davies, S. C.; Yang, X.; Wang, L. S.; Sawers, G.; Pickett, C. J. *Nature* **2005**, *433*, 610. (c) MacKay, B. A.; Fryzuk, M. D. *Chem. Rev.* **2004**, *104*, 385. (d) Laplaza, C. E.; Odom, A. L.; Davis, W. M.; Cummins, C. C.; Protasiewicz, J. D. *J. Am. Chem. Soc.* **1995**, *117*, 4999.
- (2) (a) Yandulov, D. V.; Schrock, R. R. *J. Am. Chem. Soc.* **2002**, *124*, 6252. (b) Yandulov, D. V.; Schrock, R. R.; Rheingold, A. L.; Ceccarelli, C.; Davis, W. M. *Inorg. Chem.* **2003**, *42*, 796. (c) Laplaza, C. E.; Cummins, C. C. *Science* **1995**, *268*, 861. (d) Laplaza, C. E.; Johnson, M. J. A.; Peters, J. C.; Odom, A. L.; Kim, E.; Cummins, C. C.; George, G. N.; Pickering, I. J. *J. Am. Chem. Soc.* **1996**, *118*, 8623.
- (3) Betley, T. A.; Peters, J. C. *J. Am. Chem. Soc.* **2004**, *126*, 6252.
- (4) (a) Piers, W. E.; Emslie, D. J. H. *Coord. Chem. Rev.* **2002**, *233*, 131. (b) Gade, L. H. *Acc. Chem. Res.* **2002**, *35*, 575.
- (5) (a) Jenkins, D. M.; Betley, T. A.; Peters, J. C. *J. Am. Chem. Soc.* **2002**, *124*, 11238. (b) Brown, S. D.; Betley, T. A.; Peters, J. C. *J. Am. Chem. Soc.* **2003**, *125*, 322.
- (6) (a) Jenkins, D. M.; Di Bilio, A. J.; Allen, M. J.; Betley, T. A.; Peters, J. C. *J. Am. Chem. Soc.* **2002**, *124*, 15336. (b) Jenkins, D. M.; Peters, J. C. *J. Am. Chem. Soc.* **2003**, *125*, 11162. (c) Jenkins, D. M.; Peters, J. C. *J. Am. Chem. Soc.* **2005**, *127*, 7148.
- (7) (a) Fryzuk, M. D.; MacNeil, P. A. *J. Am. Chem. Soc.* **1981**, *103*, 3592. (b) Fryzuk, M. D.; Love, J. B.; Rettig, S. J. *Chem. Commun.* **1996**, 2783. (c) Fryzuk, M. D.; Johnson, S. A.; Rettig, S. J. *J. Am. Chem. Soc.* **1998**, *120*, 11024.
- (8) (a) Fryzuk, M. D. *Can. J. Chem.* **1992**, *70*, 2839. (b) Fryzuk, M. D.; Love, J. B.; Rettig, S. J.; Young, V. G. *Science* **1997**, *275*, 1445.
- (9) (a) Fryzuk, M. D.; Leznoff, D. B.; Ma, E. S. F.; Rettig, S. J.; Young, V. G. *Organometallics* **1998**, *17*, 2313. (b) Fryzuk, M. D.; Leznoff, D. B.; Thompson, R. C.; Rettig, S. J. *J. Am. Chem. Soc.* **1998**, *120*, 10126. (c) Ingleson, M.; Fan, H. J.; Pink, M.; Tomaszewski, J.; Caulton, K. G. *J. Am. Chem. Soc.* **2006**, *128*, 1804. (d) Ingleson, M. J.; Pink, M.; Caulton, K. G. *J. Am. Chem. Soc.* **2006**, *128*, 4248. (e) Ingleson, M. J.; Pink, M.; Fan, H.; Caulton, K. G. *J. Am. Chem. Soc.* **2008**, *130*, 4262.
- (10) For related studies of PPN ligands (N = amine, pyrazole) on iron and cobalt, cf. the work of Huttner et al.: (a) Faissner, R.; Huttner, G.; Kaifer, E.; Rutsch, P. *Eur. J. Inorg. Chem.* **2003**, 1681. (b) Jacobi, A.; Huttner, G.; Winterhalter, U. *Chem. Ber. Recl.* **1997**, *130*, 1279.

- (11) (a) Ozerov, O. V.; Guo, C. Y.; Papkov, V. A.; Foxman, B. M. *J. Am. Chem. Soc.* **2004**, *126*, 4792. (b) Walstrom, A.; Pink, M.; Yang, X. F.; Tomaszewski, J.; Baik, M. H.; Caulton, K. G. *J. Am. Chem. Soc.* **2005**, *127*, 5330.
- (12) (a) Venanzi, L. M. *Angew. Chem., Int. Ed.* **1964**, *3*, 453. (b) Halfpenny, B. T.; Hartley, J. G.; Venanzi, L. M. *J. Chem. Soc. A* **1967**, 627. (c) King, R. B.; Kapoor, R. N.; Saran, M. S.; Kapoor, P. N. *Inorg. Chem.* **1971**, *10*, 1851. (d) Sacconi, L.; Divaira, M. *Inorg. Chem.* **1978**, *17*, 810.
- (13) (a) Stoppioni, P.; Mani, F.; Sacconi, L. *Inorg. Chim. Acta* **1974**, *11*, 227. (b) George, T. A.; Rose, D. J.; Chang, Y. D.; Chen, Q.; Zubieta, J. *Inorg. Chem.* **1995**, *34*, 1295.
- (14) (a) Betley, T. A.; Peters, J. C. *J. Am. Chem. Soc.* **2003**, *125*, 10782. (b) Daida, E. J.; Peters, J. C. *Inorg. Chem.* **2004**, *43*, 7474.
- (15) (a) Barney, A. A.; Heyduk, A. F.; Nocera, D. G. *Chem. Commun.* **1999**, 2379. (b) Shapiro, I. R.; Jenkins, D. M.; Thomas, J. C.; Day, M. W.; Peters, J. C. *Chem. Commun.* **2001**, 2152. (c) Betley, T. A.; Peters, J. C. *Inorg. Chem.* **2003**, *42*, 5074.
- (16) (a) Evans, D. F. *J. Chem. Soc.* **1959**, 2003. (b) Sur, S. K. *J. Magn. Reson.* **1989**, *82*, 169.
- (17) MacBeth, C. E.; Harkins, S. B.; Peters, J. C. *Can. J. Chem.* **2005**, *83*, 332.
- (18) Mankad, N. P.; Rivard, E.; Harkins, S. B.; Peters, J. C. *J. Am. Chem. Soc.* **2005**, *127*, 16032.
- (19) For a similar approach to enforcing a *fac*-only geometry, cf. the diamido-pyridyl ligands developed by Gade: (a) Gade, L. H. *Chem. Commun.* **2000**, 173. (b) Mehrkhodavandi, P.; Bonitatebus, P. J.; Schrock, R. R. *J. Am. Chem. Soc.* **2000**, *122*, 7841.
- (20) Trofimenko, S. *Scorpionates: The Coordination Chemistry of Polypyrazolyl Borates*; Imperial College Press: London, 1999.
- (21) (a) Ge, P. H.; Haggerty, B. S.; Rheingold, A. L.; Riordan, C. G. *J. Am. Chem. Soc.* **1994**, *116*, 8406. (b) Schebler, P. J.; Mandimutsira, B. S.; Riordan, C. G.; Liable-Sands, L. M.; Incarvito, C. D.; Rheingold, A. L. *J. Am. Chem. Soc.* **2001**, *123*, 331.
- (22) In the time since this work was performed, a closely related example of a tetracoordinate, trigonal pyramidal cobalt(I) complex supported by a monoanionic, tetradentate ligand has been reported: Chomitz, W. A.; Arnold, J. *Chem. Commun.* **2008**, 3648.
- (23) Sacconi, L.; Orlandin, A.; Midollin, S. *Inorg. Chem.* **1974**, *13*, 2850.
- (24) (a) Hu, X.; Meyer, K. *J. Am. Chem. Soc.* **2004**, *126*, 16322. (b) Hu, X. L.; Castro-Rodriguez, I.; Meyer, K. *J. Am. Chem. Soc.* **2004**, *126*, 13464.

- (25) (a) Ray, M.; Yap, G. P. A.; Rheingold, A. L.; Borovik, A. S. *J. Chem. Soc. Chem. Commun.* **1995**, 1777. (b) Ray, M.; Hammes, B. S.; Yap, G. P. A.; Rheingold, A. L.; Borovik, A. S. *Inorg. Chem.* **1998**, *37*, 1527.
- (26) Castro-Rodriguez, I.; Nakai, H.; Zakharov, L.; Rheingold, A.L.; Meyer, K. *Science* **2004**, *305*, 1757.
- (27) Sigma-Aldrich Spectral Database: 2,6-diisopropylphenyl isocyanate (376930). <http://www.sigmaaldrich.com/spectra/ftir/FTIR005149.PDF> (accessed Dec 1, 2008).
- (28) (a) Schrock, R. R.; Seidel, S. W.; Mösch-Zanetti, N. C.; Dobbs, D. A.; Shih, K.-Y.; Davis, W. M. *Organometallics* **1997**, *16*, 5195. (b) Schrock, R. R. *Acc. Chem. Res.* **1997**, *30*, 9.
- (29) Fryzuk, M. D.; MacNeil, P. A. *J. Am. Chem. Soc.* **1984**, *106*, 6993.
- (30) (a) Ozerov, O. V.; Gerard, H. F.; Watson, L. A.; Huffman, J. C.; Caulton, K. G. *Inorg. Chem.* **2002**, *41*, 5615. (b) Fullmer, B. C.; Fan, H.; Pink, M.; Caulton, K. G. *Inorg. Chem.* **2008**, *47*, 1865.
- (31) For another example of imide formation by Si–N cleavage, see reference 28a.
- (32) Mindiola, D. J.; Hillhouse, G. L. *J. Am. Chem. Soc.* **2001**, *123*, 4623.
- (33) Mindiola, D. J.; Cummins, C. C. *Angew. Chem., Int. Ed.* **1998**, *37*, 945.
- (34) Hendrich, M. P.; Gunderson, W.; Behan, R. K.; Green, M. T.; Mehn, M. P.; Betley, T. A.; Lu, C. C.; Peters, J. C. *Proc. Natl. Acad. Sci. U.S.A.* **2006**, *103*, 17107.
- (35) Lu, C. C.; Saouma, C. T.; Day, M. W.; Peters, J. C. *J. Am. Chem. Soc.* **2007**, *129*, 4.
- (36) Schrock, R. R.; Seidel, S. W.; Schrodi, Y.; Davis, W. M. *Organometallics* **1999**, *18*, 428.
- (37) Patton, J. T.; Feng, S. G. G.; Abboud, K. A. *Organometallics* **2001**, *20*, 3399.
- (38) Carpino, L. A.; Padykula, R. E.; Barr, D. E.; Hall, F. H.; Krause, J. G.; Dufresne, R. F.; Thoman, C. J. *J. Org. Chem.* **1988**, *53*, 2565.
- (39) Negishi, E.; Swanson, D. R.; Rousset, C. J. *J. Org. Chem.* **1990**, *55*, 5406.
- (40) Brauer, D. J.; Hingst, M.; Kottsieper, K. W.; Like, C.; Nickel, T.; Tepper, M.; Stelzer, O.; Sheldrick, W. S. *J. Organomet. Chem.* **2002**, *645*, 14.

Chapter 3

Dinitrogen Complexes Supported by Tris(phosphino)silyl Ligands

The text in this chapter is reproduced in part with permission from:

Whited, M. T.; Mankad, N. P.; Lee, Y.; Oblad, P. F.; Peters, J. C. *Inorg. Chem.* **2009**, *48*, 2507–2517.

Copyright 2009 American Chemical Society

and

Mankad, N. P.; Whited, M. T.; Peters, J. C. *Angew. Chem., Int. Ed.* **2007**, *46*, 5768–5771.

Copyright 2007 Wiley Interscience

Introduction

A great deal of biochemical, theoretical, and synthetic research has recently been focused on exploring the nature of the inorganic cofactors of nitrogenase enzymes.^{1,2} Given the presence of iron and molybdenum in FeMo-nitrogenase, particular emphasis has been placed on elucidating the roles these elements may play in N₂ reduction.^{2,3} Yandulov and Schrock recently reported a catalytic cycle for N₂ reduction involving a trivalent triamidoamine [NN₃]Mo–N₂ species that is thought to shuttle between four different formal oxidation states.⁴

We and others have established that, given a suitable set of supporting ligands, single low-coordinate iron sites can exhibit the necessary redox flexibility to facilitate multielectron small-molecule reductions,^{5,6} and we have begun to target a synthetic scheme akin to the Chatt cycle in which a monovalent iron center binds N₂ and mediates its reduction via proton/electron equivalents.^{2,6,7} In this context it is interesting to consider terminal Fe^I–N₂ complexes as synthetic targets. Our group and Holland's group have reported the preparation of μ -N₂ complexes of three- and four-coordinate iron in which the iron centers may be formally regarded as iron(I).^{5d,f} More detailed spectroscopic studies have suggested that the Holland system, supported by β -diketiminato ligands, is perhaps better described as a diiron(II) species with a reduced dinitrogen dianion.⁸ In contrast, our phosphine-supported diiron system appears to be better described by two $S = 3/2$ iron centers that are weakly ferromagnetically coupled.⁶

We have recently begun to consider whether monoanionic, tetradentate ligands might stabilize *terminally* bonded N₂ adducts of monovalent iron. Accordingly, we have explored two complementary approaches to introduce a single X-type donor into a phosphine-rich, tetradentate framework (Figure 3.1).^{9,10} Ligands of this type, the sole example of which was first reported by Stobart,¹¹ are also of general interest for catalytic studies since the presence of a strongly *trans*-influencing silyl donor should labilize bound substrates to facilitate turnover.

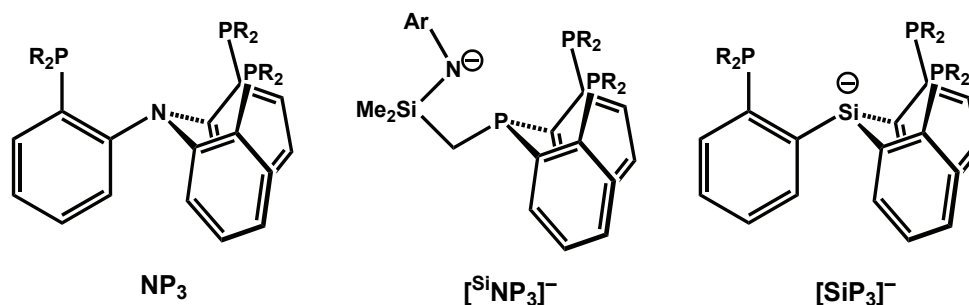


Figure 3.1. Neutral and anionic tetradentate ligands related to the chemistry described herein.

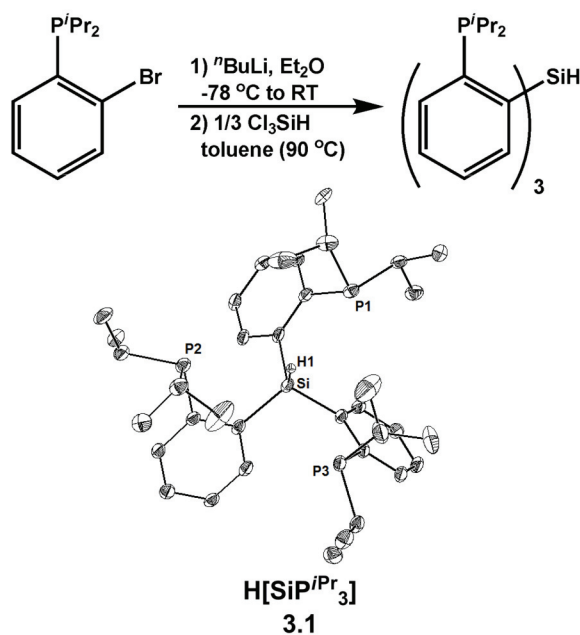
Herein we discuss the preparation and characterization of the isopropyl-substituted $[\text{SiP}^{i\text{Pr}}_3]$ ligand derivative and probe aspects of its fundamental coordination chemistry with di- and trivalent iron, cobalt, nickel, and iridium. We present complementary strategies for metalation of the silane ligand and examine the monovalent, terminal dinitrogen complexes $[\text{SiP}^{i\text{Pr}}_3]\text{M}-\text{N}_2$ ($\text{M} = \text{Fe}, \text{Co}, \text{Ir}$). Comparisons are made where informative to related $[\text{SiP}^{\text{Ph}}_3]$ systems.

Results and Discussion

Synthesis and Characterization of $\text{H}[\text{SiP}^{i\text{Pr}}_3]$

(2-bromophenyl)phosphines serve as excellent precursors for a variety of phosphine ligands since they are readily lithiated with a single equivalent of *n*-butyllithium in diethyl ether at low temperature.^{9,12} Although the (2-bromophenyl)diphenylphosphine precursor required for the synthesis of $\text{H}[\text{SiP}^{\text{Ph}}_3]$ is most easily obtained by a Pd-catalyzed coupling reaction,^{9,13} we were unable to access the diisopropylphosphine derivative by such a route, and it was instead synthesized by the addition of $i\text{PrMgCl}$ to the previously reported (2-bromophenyl)dichlorophosphine.¹⁴ To prepare the desired silane, 2-(diisopropylphosphino)phenyllithium was generated at low temperature and isolated without further purification as an orange solid. Quenching this lithio species with trichlorosilane (1/3

equiv) in toluene, followed by heating at 90 °C, afforded the target $\text{H}[\text{SiP}^i\text{Pr}_3]$ ligand (**3.1**, Scheme 3.1). Combustion analysis, ^1H and ^{31}P NMR spectroscopy, and an XRD study confirm the assignment of the desired silane. The silyl proton is obscured by aromatic-proton resonances in the ^1H NMR spectrum. However, the Si–H vibration ($\nu_{\text{SiH}} = 2218 \text{ cm}^{-1}$) is prominent in the infrared spectrum and provides a convenient handle with which to monitor consumption of the silane ligand during metalation reactions (*vide infra*).



Scheme 3.1. Synthesis and displacement ellipsoid (35%) representation of $\text{H}[\text{SiP}^i\text{Pr}_3]$ (**3.1**).

The solid-state molecular structure of **3.1** obtained by X-ray diffraction analysis (Scheme 3.1) reveals an arrangement in which the phosphine arms adopt a propeller-like orientation trisected by the Si–H unit with the H-atom approximately equidistant from each P-atom ($\text{P}-\text{H}_{\text{Si}}(\text{avg.}) = 3.14(2) \text{ \AA}$), suggesting a convenient metal binding site upon substitution of the silyl proton by a transition-metal ion. The $\text{P}-\text{H}_{\text{Si}}$ distances are sufficiently long that no interaction in the solid state can be inferred.

Synthesis and Characterization of Di- and Trivalent [SiP^{*i*Pr}₃]M Complexes

Metalation of polydentate silyl ligands has often been accomplished via chelate-assisted Si–H bond oxidative addition at late metal precursors.¹⁵ This method is a straightforward route for installing the [SiP^{*i*Pr}₃] ligand on Co, Ni, and Ir precursors, as shown in Scheme 3.2. For instance, monitoring a slurry of either CoCl₂ or NiCl₂ in the presence of the neutral silane **3.1** and a sacrificial amine base (e.g., Et₃N or ^{*i*}Pr₂NEt) by IR spectroscopy established the gradual decay of the Si–H vibration over a period of 16 h for CoCl₂ at ambient temperature and 12 h for NiCl₂ in refluxing THF. By this method red [SiP^{*i*Pr}₃]CoCl (**3.2**) and pale-red [SiP^{*i*Pr}₃]NiCl (**3.3**) could be isolated in analytically pure form and high yields (80% and 96%, respectively). The presence of a single resonance (δ 35.6 ppm) in the ³¹P NMR spectrum of diamagnetic complex **3.3** suggested a C₃-symmetric solution structure, and XRD analysis confirmed this assignment for both **3.2** and **3.3** in the solid state (Figure 3.2).

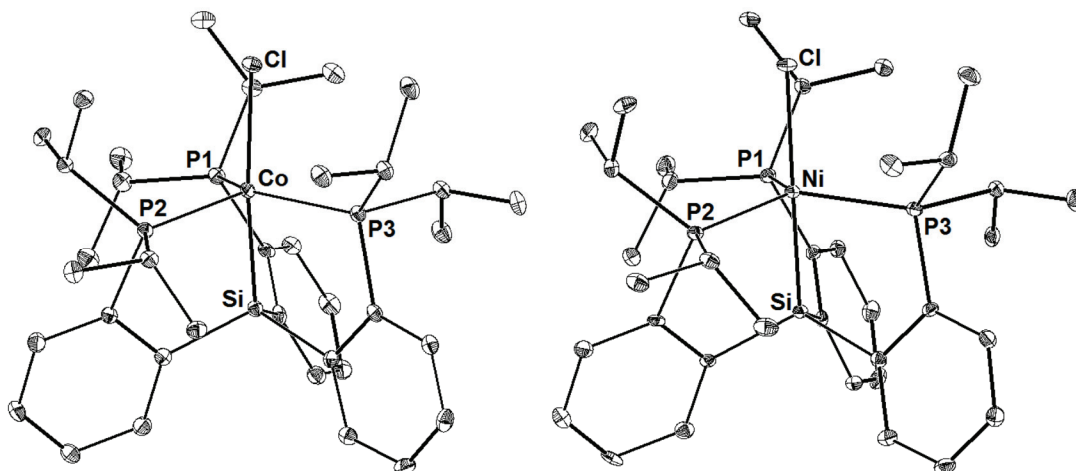
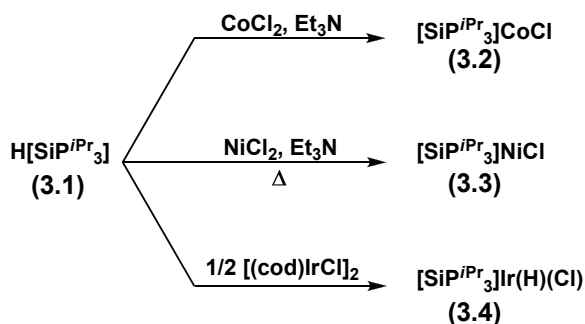


Figure 3.2. Displacement ellipsoid (35%) representations of $[\text{SiP}^{i\text{Pr}}_3]\text{CoCl}$ (**3.2**, left) and $[\text{SiP}^{i\text{Pr}}_3]\text{NiCl}$ (**3.3**, right). Solvent molecules and hydrogen atoms have been omitted for clarity. Selected bond distances (\AA) and angles ($^\circ$), for **3.2**: Co–Si, 2.2262(9); Co–P1, 2.3684(8); Co–P2, 2.3080(9); Co–P3, 2.2734(8); Co–Cl, 2.3091(8); P1–Co–P2, 110.16(3); P1–Co–P3, 131.26(3); P2–Co–P3, 114.07(3); Si–Co–Cl, 174.16(3). For **3.3**: Ni–Si, 2.2134(9); Ni–P1, 2.2980(9); Ni–P2, 2.2836(9); Ni–P3, 2.2840(9); Ni–Cl, 2.3143(9); P1–Ni–P2, 117.09(3); P1–Ni–P3, 118.66(3); P2–Ni–P3, 120.27(3); Si–Ni–Cl, 178.59(3).



Scheme 3.2. Metalation of $\text{H}[\text{SiP}^{i\text{Pr}}_3]$ ligand by chelate-assisted Si–H oxidative addition.

A potentially useful iridium synthon was prepared by the addition of **3.1** to a stirring solution of orange $[(\text{cod})\text{IrCl}]_2$ (cod = 1,4-cyclooctadiene), providing after 12 h the pale-yellow complex $[\text{SiP}^{i\text{Pr}}_3]\text{Ir}(\text{H})(\text{Cl})$ (**3.4**) in 95% yield. A single crystal of **3.4** was analyzed by X-ray diffraction methods. The hydride was not located in the difference map, but its presence was indicated by infrared spectroscopy ($\nu_{\text{Ir-H}} = 2145 \text{ cm}^{-1}$). The distinctive hydride signal observed by ^1H NMR at $\delta -10.83$ ppm (dt, $^2J_{\text{HP}(\text{trans})} = 118 \text{ Hz}$, $^2J_{\text{HP}(\text{cis})} = 24 \text{ Hz}$) reveals coupling to two inequivalent ^{31}P nuclei, and in combination with XRD data this suggests a geometry in which the

chloride ligand is situated *trans* to the silyl donor and the hydride ligand sits in the plane of the three phosphines, *trans* to one and *cis* to the other two (Figure 3.3). This complex is similar to octahedral iridium(III) hydrido chloride complexes of chelating silyl ligands previously reported, in which the weakly *trans*-influencing chloride ligand prefers the site opposite the silyl donor.^{15c}

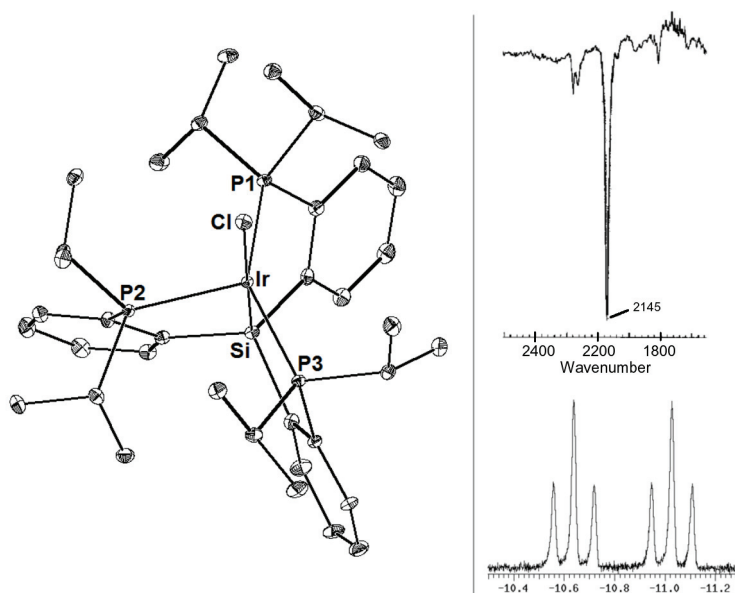
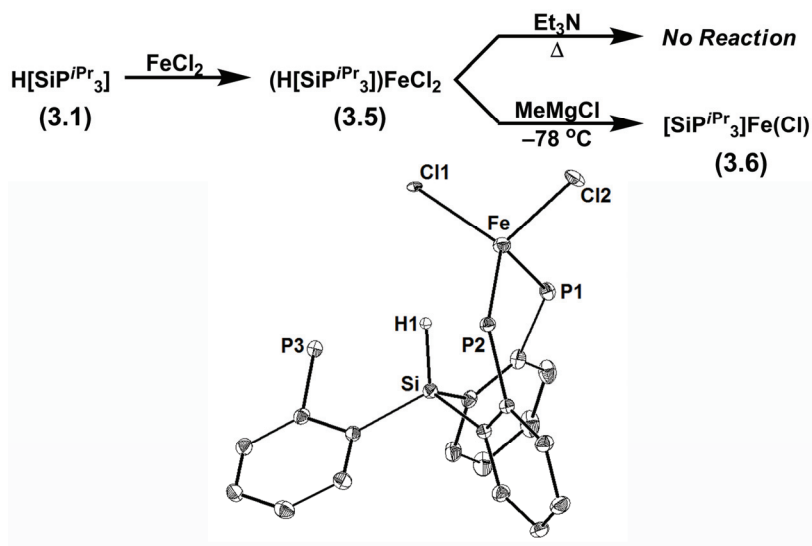


Figure 3.3. Displacement ellipsoid (35%) representation of $[\text{SiP}^{i\text{Pr}}_3]\text{Ir}(\text{H})(\text{Cl})$ (**3.4**) with inset of IR stretch and ^1H NMR signal for the Ir–H. Hydrogen atoms and a molecule of benzene have been omitted for clarity. Selected bond distances (Å) and angles (°): Ir–Si, 2.2749(8); Ir–P1, 2.3597(8); Ir–P2, 2.3848(8); Ir–P3, 2.3151(8); Ir–Cl, 2.5433(7); P1–Ir–P2, 107.43(3); P1–Ir–P3, 145.05(3); P2–Ir–P3, 103.95(3); Si–Ir–Cl, 178.46(3).

Installation of the silyl ligand at iron precursors in high yield proved more challenging. For instance, the reaction of **3.1** with Fe_2Mes_4 , which proved successful in the preparation of $[\text{SiP}^{\text{Ph}}_3]\text{Fe}(\text{Mes})$, gave rise to an ill-defined reaction mixture from which $[\text{SiP}^{i\text{Pr}}_3]\text{Fe}(\text{Mes})$ could not be readily isolated. The reaction of **3.1** with a single equivalent of ferrous chloride in THF generated the bis(phosphine) adduct complex $(\text{H}[\text{SiP}^{i\text{Pr}}_3])\text{FeCl}_2$ (**3.5**), whose structure was established by X-ray crystallography (Scheme 3.3). For comparison, the phenyl-substituted derivative $\text{H}[\text{SiP}^{\text{Ph}}_3]$ did not react with FeCl_2 under similar conditions. No dehydrohalogenation was observed upon exposure of **3.5** to amine bases such as Et_3N , even at elevated

temperatures. To induce successful activation of the Si–H unit and thus install the desired Fe–Si bond we explored the generation of a mixed alkyl-chloride complex, akin to those examined by Kauffmann and co-workers,¹⁶ hoping that alkane elimination might drive Fe–Si bond formation. Slow dropwise addition of MeMgCl to a stirring solution of **3.5** at $-78\text{ }^{\circ}\text{C}$ led to an immediate color change from pale yellow to bright orange, characteristic of the trigonal-bipyramidal $[\text{SiP}^{i\text{Pr}}_3]\text{FeCl}$ (**3.6**, Scheme 3.3), which was characterized by single-crystal XRD analysis. The chloride complex **3.6** has been prepared in a one-pot synthesis in respectable yield (43%) first by addition of $\text{H}[\text{SiP}^{i\text{Pr}}_3]$ to FeCl_2 at room temperature, followed by cooling and addition of the Grignard reagent. This method of installing the $\text{H}[\text{SiP}^{i\text{Pr}}_3]$ ligand appears to be of broad utility and can also be used for the independent synthesis of $[\text{SiP}^{\text{Ph}}_3]\text{FeCl}$ (**3.8**).



Scheme 3.3. Metalation of $\text{H}[\text{SiP}^{i\text{Pr}}_3]$ ligand at iron and displacement ellipsoid (35%) representation of $(\text{H}[\text{SiP}^{i\text{Pr}}_3])\text{FeCl}_2$ (**3.5**) with hydrogen atoms and phosphine $i\text{Pr}$ substituents omitted for clarity.

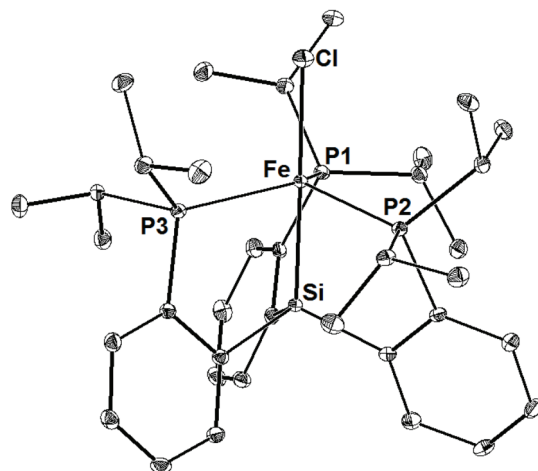


Figure 3.4. Displacement ellipsoid (35%) representation of $[\text{SiP}^{i\text{Pr}}_3]\text{FeCl}$ (**3.6**) with solvent molecules and hydrogen atoms omitted for clarity. Selected bond distances (Å) and angles ($^\circ$): Fe–Si, 2.305(1); Fe–P1, 2.3627(7); Fe–P2, 2.3438(7); Fe–P3, 2.3489(7); Fe–Cl, 2.2820(9); P1–Fe–P2, 115.67(2); P1–Fe–P3, 116.70(2); P2–Fe–P3, 118.09(2); Si–Fe–Cl, 178.53(2).

The solution magnetic moments and solid-state structural data (Figures 3.2 and 3.4) for the $[\text{SiP}^{i\text{Pr}}_3]\text{M–Cl}$ complexes (Fe, Co, Ni) indicate that the ligand confers a ground-state preference for trigonal-bipyramidal geometries at later first-row metals, in contrast to several previously reported, potentially tetradentate ligands that show a tendency to dissociate a donor to accommodate higher spin states with four-coordinate geometries.^{7,9,17} The spin states of the divalent iron (triplet, $\mu_{\text{eff}} = 3.3 \mu_{\text{B}}$), cobalt (doublet, $\mu_{\text{eff}} = 1.8 \mu_{\text{B}}$), and nickel (singlet) chloride complexes are in accord with the expected d-orbital splitting pattern for trigonal-bipyramidal complexes supported by strong-field donor sets.¹⁸

Compared to our series of previously reported 4-coordinate tris(phosphino)borate $[\text{PhBP}^{\text{R}}_3]\text{M–X}$ complexes (M = Mn,¹⁹ Fe,^{5a,20} Co,²¹ Ni²²), the presence of the silyl donor draws the coordinated metal ion into the plane of the three phosphine donors and creates a far more sterically encumbered binding site. To illustrate this point, space-filling models for the hexaisopropyl tris(phosphino)borate and tris(phosphino)silyl iron(II) chloride complexes $[\text{PhBP}^{i\text{Pr}}_3]\text{FeCl}$ ²⁰ and $[\text{SiP}^{i\text{Pr}}_3]\text{FeCl}$ (**3.6**) are provided in Figure 3.5. The figure reveals a substantially

more protected chloride ligand for the case of **3.6**. A comparison of the solid-state molecular structures of these complexes reveals slightly shorter Fe–P bonds for complex **3.6** ($\text{Fe–P}_{\text{avg}} = 2.35 \text{ \AA}$) relative to $[\text{PhBP}^{i\text{Pr}}_3]\text{FeCl}$ ($\text{Fe–P}_{\text{avg}} = 2.43 \text{ \AA}$), consistent with the lower spin state of **3.6** (doublet versus quartet). Thus, it may be possible to ascribe the slightly longer Fe–Cl bond in **3.6** (2.28 \AA versus 2.22 \AA for $[\text{PhBP}^{i\text{Pr}}_3]\text{FeCl}$) at least in part to the presence of a *trans*-disposed silyl donor. In any case, the steric properties of the tris(phosphino)silyl ligands, combined with the relatively soft nature of the donors, suggest that monovalent, monomeric dinitrogen adducts might be generally accessible.

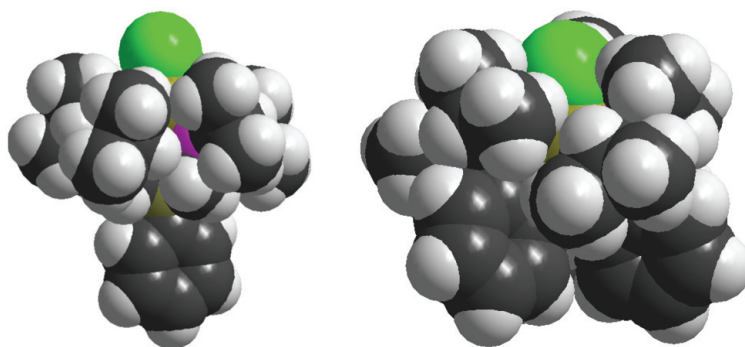


Figure 3.5. Space-filling models of $[\text{PhBP}^{i\text{Pr}}_3]\text{FeCl}$ (left) and $[\text{SiP}^{i\text{Pr}}_3]\text{FeCl}$ (**3.6**; right); $[\text{PhBP}^{i\text{Pr}}_3]^- = [\text{PhB}(\text{CH}_2\text{P}^i\text{Pr}_2)_3]^-$.

Electrochemical Characterization of Divalent Iron and Cobalt Complexes

Comparative cyclic voltammetry data for the divalent iron complexes $[\text{SiP}^{i\text{Pr}}_3]\text{FeCl}$ (**3.6**) and $[\text{SiP}^{\text{Ph}}_3]\text{FeCl}$ (**3.8**) are shown in Figure 3.6 and establish a reversible $\text{Fe}^{\text{III/II}}$ redox couple for each complex. The oxidation of divalent **3.6** occurs at $E_{1/2} = -670 \text{ mV}$, a 270 mV cathodic shift relative to the phenyl-substituted derivative **3.8** ($E_{1/2} = -400 \text{ mV}$). This difference was anticipated due to the greater electron-releasing character of alkyl versus aryl phosphines, and a similar magnitude shift has been observed for the $\text{Fe}^{\text{III/II}}$ couple upon substitution of isopropyl for phenyl substituents in tris(phosphino)borate systems.²⁰

Complexes **3.6** and **3.8** display quite different behavior in their cyclic voltammograms when scanned cathodically under N_2 . Whereas phenyl-substituted complex **3.8** displays a reversible $Fe^{II/I}$ redox couple ($E_{1/2} = -2.10$ V; Figure 3.6c), the reduction of complex **3.6** at $E_{max} = -2.55$ V is not fully reversible and instead appears to generate three distinct products, even at scan rates as fast as 500 mV/s, whose respective oxidations can be seen at -2.40 , -2.14 , and -1.04 V on the return scan (Figure 3.6a). In order to shed light on the identities of these species, complex **6** was subjected to electrochemical interrogation in the absence of N_2 (Figure 3.6b), and under these conditions both the $Fe^{III/II}$ and $Fe^{II/I}$ couples were found to be reversible and no other species were observed. We assign the anodic wave observed -2.40 V to the reoxidation of $\{[SiP^{iPr}_3]FeCl\}^-$ and the wave at -1.04 V to the oxidation of monovalent $[SiP^{iPr}_3]Fe(N_2)$ (**3.10**) to its cation, $\{[SiP^{iPr}_3]Fe(N_2)\}^+$. These results also indicate that the species which is oxidized at -2.14 V is generated only in the presence of N_2 . Thus, since the position of the anodic wave is consistent with a solvento $[SiP^{iPr}_3]Fe(THF)$ or a chloride-dissociated “[SiP^{iPr}_3]Fe” complex,²³ the fact that the species is only observed under N_2 may indicate that chloride loss from $\{[SiP^{iPr}_3]FeCl\}^-$ occurs by an associative, N_2 -assisted mechanism. Since this hypothesis would invoke an unstable 19-electron intermediate complex, further studies will be required to definitively assign this species.

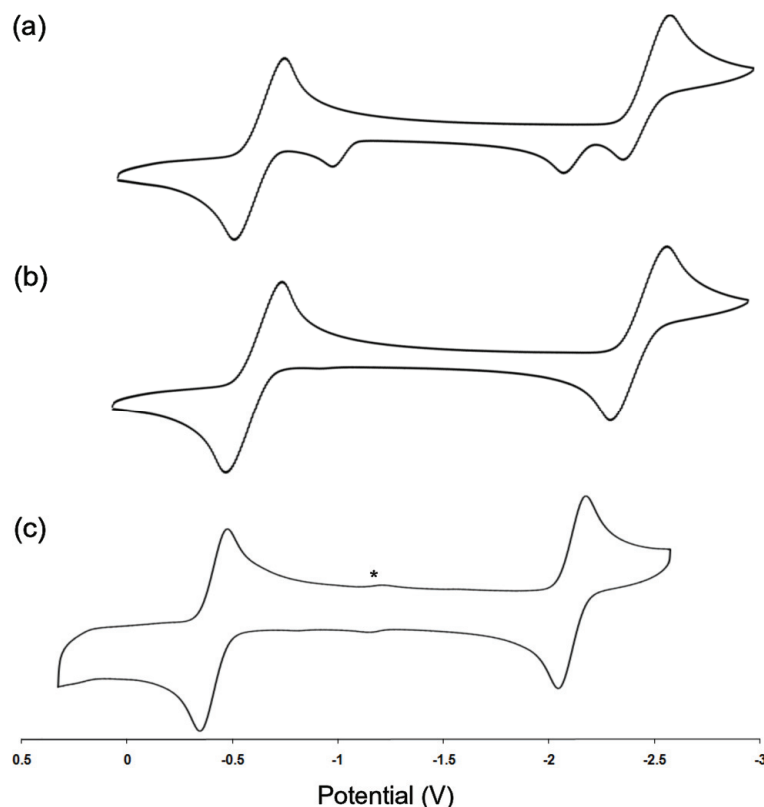


Figure 3.6. Cyclic voltammograms of (a) $[\text{SiP}^{\text{iPr}}_3]\text{FeCl}$ (**3.6**) under N_2 , (b) $[\text{SiP}^{\text{iPr}}_3]\text{FeCl}$ (**3.6**) under Ar, and (c) $[\text{SiP}^{\text{Ph}}_3]\text{FeCl}$ (**3.8**) under N_2 (* denotes a trace impurity in **3.8**). Scans (a) and (b) were recorded at a scan rate of 500 mV/s, and scan (c) was recorded at 100 mV/s. All data were acquired in THF and potentials are referenced to Fc/Fc^+ .

Figure 3.7 shows related voltammetry data for the $[\text{SiP}^{\text{R}}_3]\text{CoCl}$ derivatives ($\text{R} = \text{iPr}$ (**3.2**) or Ph (**3.9**)), where **3.9** can be prepared in a fashion analogous to **3.2**. As with the iron systems, both complexes exhibit reversible $\text{Co}^{\text{III/II}}$ redox couples with the half-wave potential for **3.2** ($E_{1/2} = -710$ mV) being ca. 260 mV negative of that for **3.9** ($E_{1/2} = -450$ mV). Additionally, while **3.9** exhibits a quasi-reversible $\text{Co}^{\text{II/I}}$ event, the electrochemical reduction of **3.2** is completely irreversible. Both are connected with reoxidation events slightly negative of the III/II couple, consistent with the generation of a new Co(I) species by halide expulsion. By analogy with **3.6**, we assign the new waves to $[\text{SiP}^{\text{R}}_3]\text{Co}(\text{N}_2)$ complexes in each case. This assignment is supported by the observation that, as with complex **3.6** (*vide supra*), electrochemical reduction of **3.9** in

the absence of N_2 is fully reversible and the oxidation wave ascribed to the $[SiP^{Ph}_3]Co(N_2)$ species is no longer present. Interestingly, neither **3.2** nor **3.9** displays electrochemical evidence for the generation of an alternative species such as that observed for the $[SiP^{iPr}_3]Fe$ system.

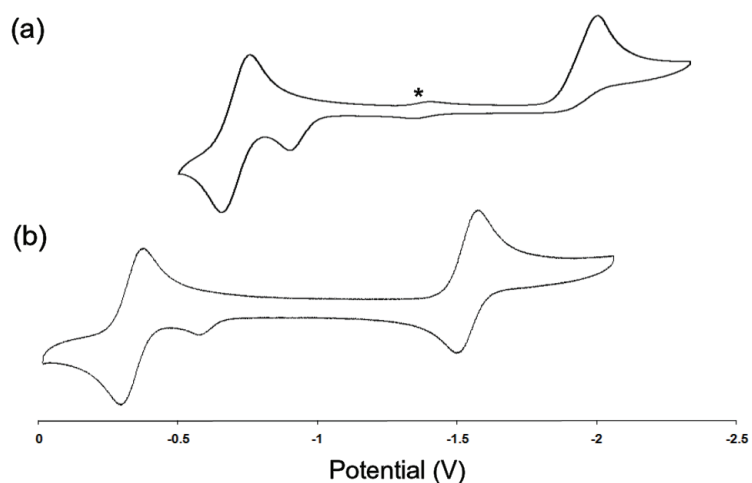


Figure 3.7. Cyclic voltammograms of (a) $[SiP^{iPr}_3]CoCl$ (**3.2**) and (b) $[SiP^{Ph}_3]CoCl$ (**3.9**) recorded at a scan rate of 100 mV/s (* denotes a trace impurity in **3.2**). Both scans were recorded in THF under an N_2 atmosphere. Potentials are referenced to Fc/Fc^+ .

As with all of the iron and cobalt complexes described, cyclic voltammetry of $[SiP^{iPr}_3]NiCl$ (**3.3**) revealed a reversible $Ni^{III/II}$ redox couple at $E_{1/2} = -245$ mV (Figure 3.8), indicating that chemical oxidation of this complex should be relatively facile. However, as expected for an 18-electron complex, **3.3** was not well behaved upon electrochemical reduction.

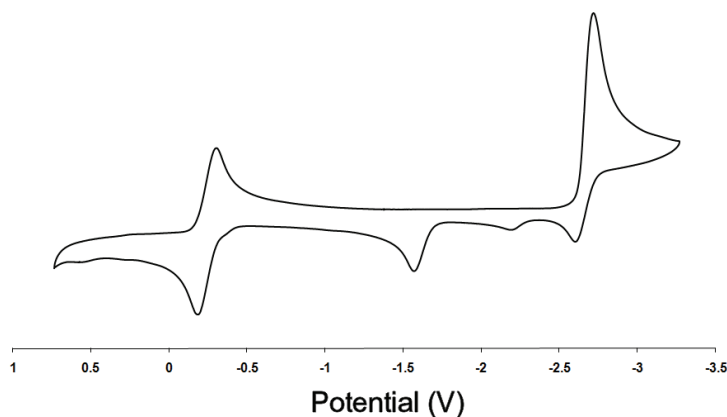


Figure 3.8. Cyclic voltammogram of $[\text{SiP}^{i\text{Pr}}_3]\text{NiCl}$ (**3.3**) recorded at a scan rate of 100 mV/s in THF under an N_2 atmosphere. Potentials are referenced to Fc/Fc^+ .

Chemical Reduction to Generate Monovalent $[\text{SiP}^{i\text{Pr}}_3]\text{M}(\text{N}_2)$ ($\text{M} = \text{Fe}, \text{Co}, \text{Ir}$)

At the outset of our work, it was not clear whether a strongly *trans*-influencing silyl ligand would support a coordinated dinitrogen ligand in a position *trans* to the silyl linkage. Indeed, there have been few examples of $\text{M}-\text{N}_2$ complexes that also feature a supporting silyl ligand.²⁴ None of these contains an N_2 ligand and silyl donor in a *trans* orientation.

Exposure of $[\text{SiP}^{i\text{Pr}}_3]\text{FeCl}$ (**3.6**) to an equivalent of sodium naphthalide results in an immediate darkening of the bright-orange solution and the appearance of a prominent infrared stretch ($\nu_{\text{NN}} = 2008 \text{ cm}^{-1}$) consistent with a terminal dinitrogen ligand. NMR and XRD analyses reveal the desired $S = 1/2$ terminal N_2 complex, $[\text{SiP}^{i\text{Pr}}_3]\text{Fe}(\text{N}_2)$ (**3.10**) (Figure 3.9).²⁵ The hexaphenyl complex **3.8** can be reduced in the same fashion, though the reaction is effected by a weaker reductant (Na/Hg amalgam), consistent with the cyclic voltammetry data. The resulting N_2 complex, $[\text{SiP}^{\text{Ph}}_3]\text{Fe}(\text{N}_2)$ (**3.11**), reveals an intense infrared stretch at higher energy ($\nu_{\text{NN}} = 2041 \text{ cm}^{-1}$), indicating that the N_2 ligand is coordinated to a substantially less electron-rich metal center in this complex. Complexes **3.10** and **3.11** are the first examples of d^7 iron complexes containing terminally bonded dinitrogen ligands. Cyclic voltammetry of dinitrogen

adduct **3.10** revealed a reversible $\text{Fe}^{\text{I}}/\text{Fe}^0$ redox couple at $E_{1/2} = -2.68$ V (Figure 3.10), a significant cathodic shift relative to the hexaphenyl $[\text{SiP}^{\text{Ph}}_3]\text{Fe}(\text{N}_2)$ (**3.11**), which exhibits a reversible $\text{Fe}^{\text{I}}/\text{Fe}^0$ couple at $E_{1/2} = -1.92$ V. This dramatic shift is somewhat surprising given the gross structural and electronic similarities between the complexes, but is likely attributable to the better σ -donating and worse π -accepting abilities of alkyl versus aryl phosphines since the resulting d^8 complex contains an additional electron in an $\text{Fe-P } \sigma^*/\pi$ orbital set.

As indicated by its cyclic voltammetry, the hexaphenyl complex **3.11** may be chemically reduced with Na/Hg amalgam (1 equiv) in the presence of [12]crown-4 to afford its anion, $\{[\text{SiP}^{\text{Ph}}_3]\text{Fe}(\text{N}_2)\}\{\text{Na}([\text{12}]\text{c-4})_2\}$ (**3.12**). This complex was assigned on the basis of a strong N_2 vibration at 1967 cm^{-1} in its IR spectrum, its diamagnetic ^1H and $^{31}\text{P}\{^1\text{H}\}$ (δ 84.3 ppm) NMR spectra, and combustion analysis. Since the $\text{Fe}^{\text{I}/0}$ redox wave is shifted so dramatically (760 mV cathodic shift) for dinitrogen adduct **3.10** compared with **3.11**, reduction of the hexaisopropyl species was not attempted.

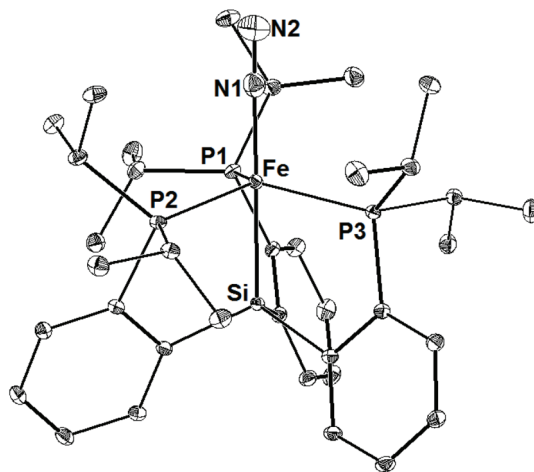


Figure 3.9. Displacement ellipsoid (35%) representation of $[\text{SiP}^{\text{Pr}}_3]\text{Fe}(\text{N}_2)$ (**3.10**).²⁵ Hydrogen atoms and solvent molecules have been omitted for clarity. Selected bond distances (\AA) and angles ($^\circ$): Fe–Si, 2.2918(6); Fe–P1, 2.3174(5); Fe–P2, 2.2954(5); Fe–P3, 2.3078(5); Fe–N1, 1.817(4); N1–N2, 1.065(5); P1–Fe–P2, 115.14(1); P1–Fe–P3, 119.18(2); P2–Fe–P3, 117.82(2); Si–Fe–N1, 178.83(6).

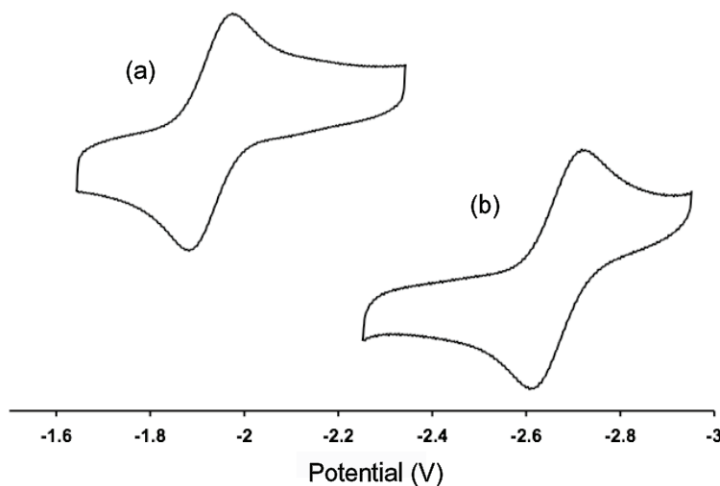


Figure 3.10. Cyclic voltammograms of (a) [SiP^{Ph}₃]Fe(N₂) (**3.11**) and (b) [SiP^{iPr}₃]Fe(N₂) (**3.10**) recorded at a scan rate of 100 mV/s in THF under N₂. Potentials are referenced to Fc/Fc⁺.

The cobalt complexes [SiP^{iPr}₃]CoCl (**3.2**) and [SiP^{Ph}₃]CoCl (**3.9**) are reduced by Na/Hg amalgam in a similar fashion to afford the diamagnetic d⁸ dinitrogen complexes [SiP^{iPr}₃]Co(N₂) (**3.13**) and [SiP^{Ph}₃]Co(N₂) (**3.14**). Again, the N₂ stretching frequencies provide a quantitative measure of the relative electron-releasing properties of each ligand, as a 32 cm⁻¹ difference is observed between **3.13** ($\nu_{\text{NN}} = 2063 \text{ cm}^{-1}$) and **3.14** ($\nu_{\text{NN}} = 2095 \text{ cm}^{-1}$). Complex **3.13** was analyzed by single-crystal XRD, and its molecular structure is presented in Figure 3.11. The N–N bond length of 1.12 Å is slightly elongated relative to free N₂, as expected based on the infrared stretching frequency.

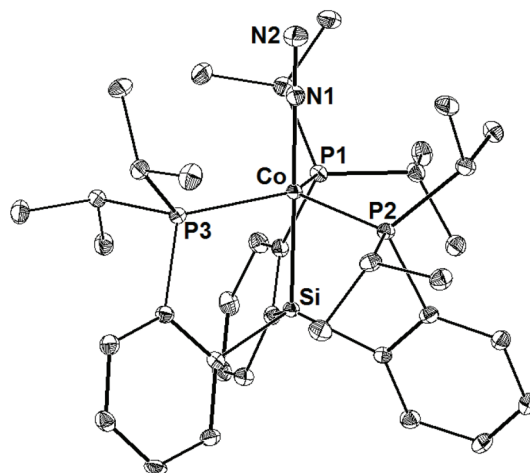
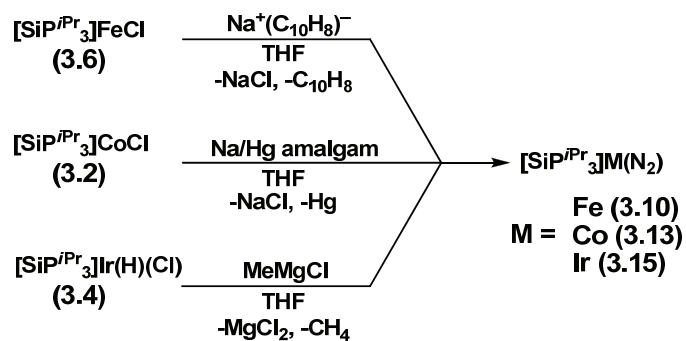


Figure 3.11. Displacement ellipsoid (35%) representation of $[\text{SiP}^{i\text{Pr}}_3]\text{Co}(\text{N}_2)$ (**3.13**) with hydrogen atoms and solvent molecules omitted for clarity. Selected bond distances (Å) and angles (°): Co–Si, 2.2327(6); Co–P1, 2.2376(6); Co–P2, 2.2277(6); Co–P3, 2.2342(6); Co–N1, 1.813(2); N1–N2, 1.123(3); P1–Co–P2, 117.48(2); P1–Co–P3, 118.01(2); P2–Co–P3, 119.51(2); Si–Co–N1, 179.13(6).

Since divalent iridium halide complexes of $[\text{SiP}^{i\text{Pr}}_3]$ were not readily available, a somewhat different synthetic strategy was required to access the $\text{Ir}^{\text{I}}\text{-N}_2$ complex. In a reaction reminiscent of that utilized by Stobart and co-workers to prepare the tris(phosphinoalkyl)silyl rhodium monocarbonyl $((\text{Ph}_2\text{PCH}_2\text{CH}_2)_3\text{Si})\text{Rh}(\text{CO})$,¹¹ $[\text{SiP}^{i\text{Pr}}_3]\text{Ir}(\text{H})(\text{Cl})$ (**3.4**) was found to react with methyl Grignard (1 equiv) under a dinitrogen atmosphere to afford the diamagnetic N_2 adduct $[\text{SiP}^{i\text{Pr}}_3]\text{Ir}(\text{N}_2)$ (**3.15**) (Scheme 3.4). The presence of **3.15** was indicated by a single resonance in the ^{31}P NMR spectrum (δ 38.7 ppm) and an intense N_2 infrared stretch ($\nu_{\text{NN}} = 2122 \text{ cm}^{-1}$). Its identity was confirmed by XRD analysis, revealing a structurally unusual example of a trigonal-bipyramidal dinitrogen adduct of iridium(I) (Figure 3.12).²⁶ The $\text{N}\equiv\text{N}$ bond length (1.094 Å) in the iridium complex is somewhat shorter than that observed for the cobalt–dinitrogen adduct and only slightly longer than that observed for free N_2 ,³ consistent with its significantly higher energy $\text{N}\equiv\text{N}$ infrared absorption.



Scheme 3.4. Generation of $[\text{SiP}^{i\text{Pr}}_3]\text{M}(\text{N}_2)$ complexes from corresponding di- and trivalent metal halides (M = Fe, Co, Ir).

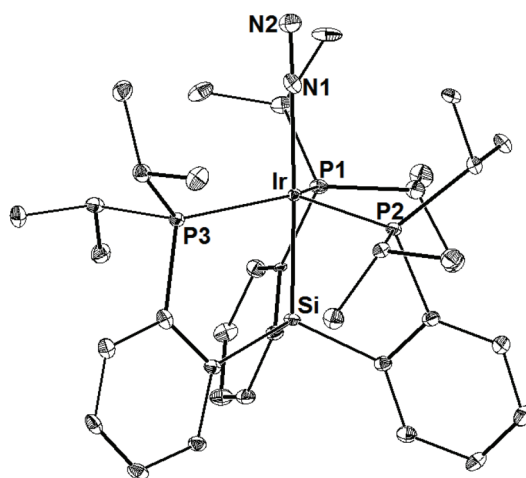


Figure 3.12. Displacement ellipsoid (35%) representation of $[\text{SiP}^{i\text{Pr}}_3]\text{Ir}(\text{N}_2)$ (**3.15**). Hydrogen atoms and solvent molecules have been omitted for clarity. Selected bond lengths (Å) and angles (°): Ir–Si, 2.304(2); Ir–P1, 2.336(2); Ir–P2, 2.328(2); Ir–P3, 2.315(2); Ir–N1, 2.033(4); N1–N2, 1.094(4); P1–Ir–P2, 116.00(4); P1–Ir–P3, 121.61(6); P2–Ir–P3, 117.31(5); Si–Ir–N1, 177.05(9).

Table 3.1 summarizes some pertinent parameters for the N_2 adducts **3.10–3.15** reported here and related literature compounds.

Table 3.1. Representative dinitrogen stretching frequencies for complexes of Fe, Co, and Ir

Entry	Complex	ν_{NN} (cm ⁻¹)	Reference
1	[SiP ^{Ph} ₃]Fe(N ₂) (3.11)	2041	this work
2	{[SiP ^{Ph} ₃]Fe(N ₂)}{Na([12]c-4) ₂ } (3.12)	1967	this work
3	[SiP ^{iPr} ₃]Fe(N ₂) (3.10)	2008	this work
4	[SiP ^{Ph} ₃]Co(N ₂) (3.14)	2095	this work
5	[SiP ^{iPr} ₃]Co(N ₂) (3.13)	2063	this work
6	[SiP ^{iPr} ₃]Ir(N ₂) (3.15)	2122	this work
7	[NP ^{Ph} ₃]Fe(N ₂) ^a	1967	27
8	{[NP ^{Ph} ₃]Fe(H)(N ₂)} ^{+a}	2090	27
9	{[NP ^{iPr} ₃]Fe(H)(N ₂)} ^{+a}	2090	7
10	{[PP ₃]Co(N ₂)} ^{+b}	2128	28
11	IrCl(N ₂)(C ₈ H ₁₂ O ₄)(PPh ₃) ₂	2190	26
12	[PCP]Ir(N ₂) ^c	2078	29
13	[Tp [*]]Ir(Ph) ₂ (N ₂) ^d	2190	30

^a [NP^R₃] = N(CH₂CH₂PR₂)₃; ^b [PP₃] = P(CH₂CH₂PPh₂)₃; ^c [PCP] = C₆H₃-2,6-(CH₂P^tBu₂)₂; ^d [Tp^{*}] = tris(3,5-dimethylpyrazol)yl borate

Having prepared the desired dinitrogen complexes of iron, cobalt, and iridium, we briefly canvassed the lability of the N₂ unit. Early evidence that the *trans* silyl donor would serve to labilize the bound dinitrogen ligand came from the results of combustion analysis data, which consistently indicated lower levels of nitrogen than expected for the empirical formulae of **3.10**, **3.11**, and **3.13–3.15** (between 25% and 50% of the values predicted for the monomeric N₂ complexes). This lability is particularly evident for [SiP^{iPr}₃]Ir(N₂) (**3.15**), where N₂ loss is quickly apparent upon application of vacuum by a color change of the solution from light yellow to dark green. The change in color is reversed upon reintroduction of nitrogen, both in solution and in the solid state. While it is possible that application of vacuum results in the formation of the μ -N₂ dimer species {[SiP^{iPr}₃]Ir}₂(μ -N₂), similar to complexes known for rhodium and iridium pincer

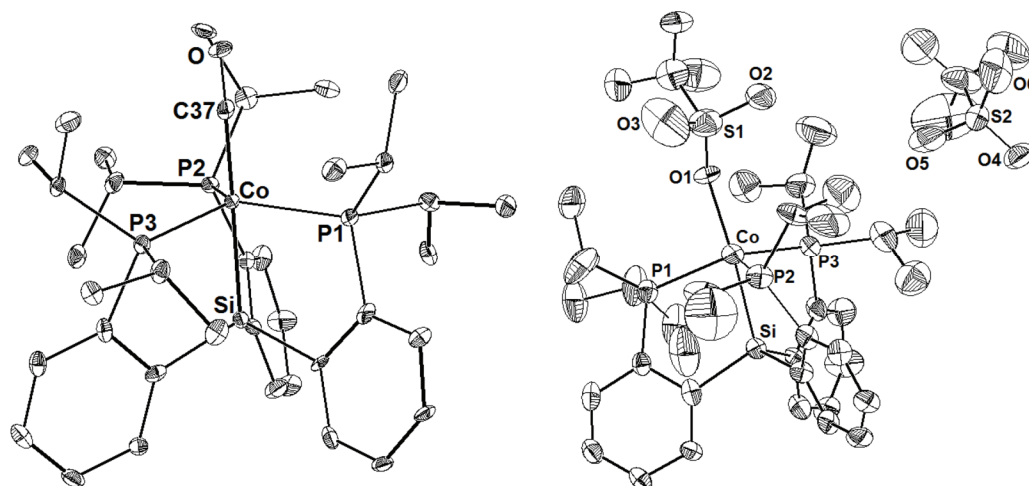


Figure 3.13. Displacement ellipsoid (35%) representations of $[\text{SiP}^{\text{iPr}}_3]\text{Co}(\text{CO})$ (**3.16**, left) and $\{[\text{SiP}^{\text{iPr}}_3]\text{Co}(\text{OTf})\}\{\text{OTf}\}$ (**3.17**, right) with hydrogen atoms and solvent molecules omitted for clarity. Selected bond lengths (Å) and angles (°), for **3.16**: Co–P1, 2.241(2); Co–P2, 2.218(3); Co–P3, 2.208(2); Co–Si, 2.256(3); Co–C37, 1.753(6); C37–O, 1.163(6); Si–Co–C37, 176.7(2); Si–Co–P1, 82.65(10); P1–Co–P2, 116.09(8); P1–Co–P3, 121.45(9); P1–Co–C37, 96.2(2); P2–Co–P3, 117.73(8). For **3.17**: Co–P1, 2.416(3); Co–P2, 2.403(3); Co–P3, 2.415(4); Co–Si, 2.355(3); Co–O1, 2.014(6); Si–Co–O1, 175.2(2); Si–Co–P1, 78.36(11); P1–Co–P2, 119.14(12); P1–Co–P3, 117.16(12); P1–Co–O1, 96.9(2); P2–Co–P3 113.43(13).

Related chemistry is also prevalent for the iron system. For instance, $[\text{SiP}^{\text{Ph}}_3]\text{Fe}(\text{N}_2)$ reacts with CO rapidly to afford the terminal carbonyl $[\text{SiP}^{\text{Ph}}_3]\text{Fe}(\text{CO})$ ($\nu_{\text{CO}} = 1881 \text{ cm}^{-1}$). $[\text{SiP}^{\text{Ph}}_3]\text{Fe}(\text{N}_2)$ can also be oxidized by AgOTf to provide the divalent, structurally characterized triflate species $[\text{SiP}^{\text{Ph}}_3]\text{Fe}(\text{OTf})$ (**3.18**) with release of N_2 (Figure 3.14).

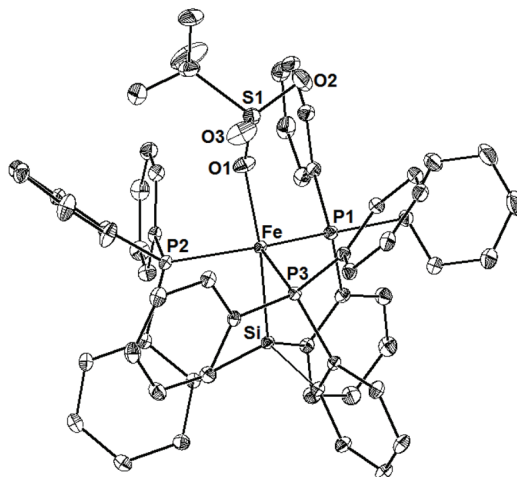


Figure 3.14. Displacement ellipsoid (35%) representation of $[\text{SiP}^{\text{Ph}}_3]\text{Fe}(\text{OTf})$ (**3.18**). All hydrogen atoms and cosolvent molecules omitted for clarity. Selected bond lengths (\AA) and angles ($^\circ$): Fe–P1, 2.3017(5); Fe–P2, 2.3044(5); Fe–P3, 2.3144(5); Fe–Si, 2.3002(5); Fe–O1, 1.9880(15); Si–Fe–O1, 173.47(5); Si–Fe–P1, 103.20(5); P1–Fe–P2, 114.669(19); P1–Fe–P3, 114.710(18); P1–Fe–O1, 103.20(5); P2–Fe–P3, 121.396(19).

Protonolysis of $[\text{SiP}^{\text{R}}_3]\text{Fe}(\text{N}_2)$ Complexes

Previously characterized iron dinitrogen complexes have been reported to release low yields (less than 15% per Fe equivalent) of hydrazine and/or ammonia under strongly protolytic conditions.^{27,32} However, the addition of protic reagents to either the previously reported diiron(I) systems $[\{(\text{PhBP}^{\text{Pr}})_3\text{Fe}\}_2(\mu\text{-N}_2)]$ or the diiron(I) β -diketiminato complex $[(\text{L}^{\text{R}}\text{Fe})_2(\mu\text{-N}_2)]^{5h}$ did not lead to any detectable production of either NH_3 or N_2H_4 . Therefore, our observation of low yields of hydrazine upon addition of acids HX to **3.11** (17% per Fe equivalent for $\text{X} = \text{BF}_4$; 7% per Fe equivalent for $\text{X} = \text{Cl}$) represents a promising initial lead for the $[\text{SiP}^{\text{R}}_3]\text{Fe}$ systems. More interesting is the observation that performing such protonations in the presence of CrX_2 as a one-electron reductant increases yields of hydrazine significantly (47% per Fe equivalent for $\text{X} = \text{Cl}$; 42% per Fe equivalent for $\text{X} = \text{Cp}^*$). The addition of similar protic reagents to **3.12** rapidly and cleanly regenerates **3.11** with no evidence for protonation at the N_2 ligand. Analogous

conditions result in substantially lower yields of hydrazine for **3.10** (9% per Fe equivalent), even in the presence of CrCp*₂, presumably because the more reducing nature of **3.10** causes direct H⁺ reduction to H₂ to vastly outcompete N₂ reduction. Complex **3.10** is more basic than **3.11**, and therefore weaker acids that fail to react with **3.11** instead provide low yields of hydrazine with **3.10** (e.g., 13% per Fe equivalent for HX = [HNⁱPr₂Et][BPh₄]). Full results of protonolysis experiments are presented in Table 3.2. One key to further advancing this N₂ reduction chemistry will be to control the delivery of protons and electrons more carefully so that N₂ reduction is favored over H₂ evolution.

Table 3.2. Summary of protonolytic hydrazine formation experiments for [SiP^R₃]Fe(N₂)

Complex	H ⁺	e ⁻	Solvent	Yield of N ₂ H ₄ per Fe
3.11	HCl	none	THF	7%
3.11	HBf ₄	none	THF	17%
3.11	HBf ₄	CrCl ₂	THF	47%
3.11	HBf ₄	CrCp* ₂	THF	42%
3.11	HBf ₄	CrCp* ₂	THF, 0 °C	28%
3.11	HBf ₄	CrCp* ₂	THF, add H ⁺ dropwise	23%
3.11	HBf ₄	CrCp* ₂	Et ₂ O	15%
3.11	HBf ₄	CrCp* ₂	C ₆ H ₆	<5%
3.11	[LutH]BPh ₄	CrCp* ₂	THF	0%
3.11	[LutH]BPh ₄	CrCp* ₂	C ₆ H ₆	0%
3.10	HBf ₄	CrCp* ₂	THF	9%
3.10	[HN ⁱ Pr ₂ Et][BPh ₄]	CrCp* ₂	THF	13%
3.10	[HN ⁱ Pr ₂ Et][BPh ₄]	CrCp* ₂	C ₆ H ₆	0%
3.10	[LutH]BPh ₄	CrCp* ₂	C ₆ H ₆	0%

Conclusions

We have described synthetic methods and characterization data for a family of complexes supported by tetradentate tris(phosphino)silyl ligands. In particular, we have introduced the newly prepared hexaisopropyl $[\text{SiP}^{i\text{Pr}}_3]$ ligand and characterized several coordination complexes derived from this scaffold. The collective spectroscopic and electrochemical data indicate that, as expected, $[\text{SiP}^{i\text{Pr}}_3]$ is considerably more electron rich than the related hexaphenyl $[\text{SiP}^{\text{Ph}}_3]$ derivative. Importantly, complementary strategies for the installation of the M–Si linkage on later transition metals have been developed, and these strategies provide access to $[\text{SiP}^{\text{R}}_3]$ complexes of iron, cobalt, nickel, and iridium. Reduction of the di- and trivalent $[\text{SiP}^{\text{R}}_3]\text{M}$ halide complexes also provides access to unusual trigonal-bipyramidal dinitrogen adducts of monovalent iron, cobalt, and iridium, and in all three cases the N_2 ligand appears to be labilized by a strongly *trans*-influencing silyl donor. However, protonolysis of the N_2 adducts of iron has been shown to result in formation of small amounts (up to 47% per Fe center) of hydrazine, a reaction without precedent for dinitrogen adducts of monovalent iron. The propensity of the $[\text{SiP}^{\text{R}}_3]$ ligand to give rise to a single and labile reaction site is one we hope to exploit in the context of future reactivity studies. Specifically, it will be of interest to examine group transfer reactions to both the mid- and low-valent synthons described.

Acknowledgment

The author acknowledges Neal Mankad for the design and syntheses of the $\text{H}[\text{SiP}^{\text{Ph}}_3]$ ligand (**3.7**) and complexes **3.8**, **3.11**, and **3.12**, as well as for performing the protonolysis experiments described in this chapter. Paul Oblad performed the syntheses of **3.9** and **3.14** and Dr. Yunho Lee prepared **3.18**. Larry Henling provided crystallographic assistance.

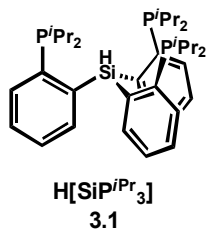
Experimental Section

General Considerations. All manipulations were carried out using standard Schlenk or glove box techniques under a dinitrogen atmosphere. Unless otherwise noted, solvents were deoxygenated and dried by thorough sparging with N₂ gas followed by passage through an activated alumina column. Nonhalogenated solvents were typically tested with a standard purple solution of sodium benzophenone ketyl in tetrahydrofuran in order to confirm effective oxygen and moisture removal. (2-bromophenyl)diisopropylphosphine¹² and (2-bromophenyl)diphenylphosphine⁹ were prepared according to literature procedures. All other reagents were purchased from commercial vendors and used without further purification unless otherwise noted. Deuterated solvents were purchased from Cambridge Isotopes Laboratories and were degassed and stored over activated 3 Å molecular sieves prior to use.

Physical Methods. Elemental analyses were performed by Desert Analytics, Tucson, AZ. A Varian Mercury-300 spectrometer was used to record ¹H, ³¹P{¹H}, and ¹³C{¹H} spectra at room temperature unless otherwise noted. ¹H and ¹³C{¹H} chemical shifts were referenced to residual solvent. ³¹P{¹H} NMR are reported relative to an external standard of 85% H₃PO₄ (0 ppm). Abbreviations for reported signal multiplicities are as follows: s, singlet; d, doublet; t, triplet; q, quartet; m, multiplet; br, broad. IR spectra were recorded on a Bio-Rad Excalibur FTS 3000 spectrometer controlled by Win-IR Pro software using a KBr solution cell. Solution magnetic moments were measured at 298 K following the Evans method.³³ UV-vis measurements were recorded on a Varian Cary 50 Bio Spectrophotometer controlled by Cary WinUV Software. All measurements were recorded using a quartz cell fitted with a Teflon cap. X-ray diffraction studies were carried out in the Beckman Institute Crystallographic Facility on a Bruker Smart 1000 CCD diffractometer. Electrochemical analysis was performed on a CHI 600B

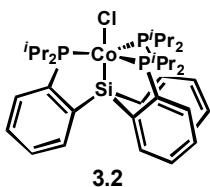
Potentiostat/Galvanostat using a glassy carbon working electrode, a platinum wire auxiliary electrode and an Ag/AgNO₃ nonaqueous reference electrode filled with THF and Bu₄NPF₆.

Synthesis of Tris(*o*-(diisopropylphosphino)phenyl)silane (H[SiP^{*i*Pr}]₃), **3.1.** (2-



bromophenyl)diisopropylphosphine (4.1429 g, 15.164 mmol) was dissolved in 100 mL of diethyl ether and chilled to $-78\text{ }^\circ\text{C}$, and *n*-butyllithium (1.60 M in hexanes, 9.50 mL, 15.2 mmol) was added dropwise, causing a darkening of the mixture and gradual precipitation of solids. After 15 min, the slurry was brought to room temperature and stirred for 2 h, after which volatiles were removed *in vacuo* to yield a pale-red powder. The powder was redissolved in toluene (80 mL), chilled to $-35\text{ }^\circ\text{C}$, and trichlorosilane (511 μL , 5.06 mmol) was added in one portion, resulting in the immediate precipitation of white solids and lightening of the solution. The mixture was stirred at room temperature for 30 min, then at $90\text{ }^\circ\text{C}$ for 15 h, and filtered through celite to give a clear, light-orange solution. Solvents were removed *in vacuo* to give an orange oil, and the addition of petroleum ether (20 mL) caused the precipitation of white solids. These were isolated on a frit and washed with petroleum ether ($2 \times 5\text{ mL}$) to yield **3.1** as a white powder. Subsequent crops could be isolated by crystallization from concentrated petroleum ether solutions at $-35\text{ }^\circ\text{C}$ (0.5439 g, 18%). ¹H NMR (C₆D₆): δ 7.46–7.34 (m, 3H, Ar–H), 7.30–7.20 (m, 3H, Ar–H), 7.20–7.10 (td, $J = 1.2$ and 7.2 Hz , 3H, Ar–H), 7.02–6.92 (tt, $J = 1.5$ and 7.5 Hz , 3H, Ar–H), 2.05–1.85 (doublet of septets, ² $J_{\text{PH}} = 6.9\text{ Hz}$, ³ $J_{\text{HH}} = 3.0\text{ Hz}$, 6H, $-\text{CH}(\text{CH}_3)_2$), 1.20–1.02 (m, 18H, $-\text{CH}(\text{CH}_3)_2$), 1.00–0.88 (m, 18H, $-\text{CH}(\text{CH}_3)_2$). ³¹P NMR (C₆D₆): δ 1.7 (s). IR (THF, KBr, cm^{-1}) $\nu(\text{Si-H})$: 2218. Anal. calcd. for C₃₆H₅₅P₃Si: C, 71.02; H, 9.11. Found: C, 71.09; H, 9.38.

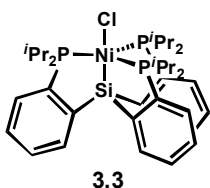
[SiP^{iPr}₃]CoCl (3.2). H[SiP^{iPr}₃] (3.1) (102.6 mg, 0.1685 mmol) and triethylamine (100 μ L, 1.35



mmol) were dissolved in THF (5 mL) and added by pipette to a stirring solution of CoCl₂ (21.9 mg, 0.169 mmol) in THF (10 mL), causing an immediate color change from light blue to dark green. Over a period of 30

min, the solution gradually adopted a maroon hue and was allowed to stir 12 h. Volatiles were removed *in vacuo* and the residues extracted into diethyl ether (15 mL), filtered, and dried to an analytically pure red powder (95.2 mg, 80%). Crystals suitable for X-ray diffraction were grown by slow evaporation of benzene from a concentrated solution. ¹H NMR (C₆D₆): δ 8.7, 8.0, 7.8, 7.4, 7.3, 6.7, 2.8, 2.6, 2.3, 1.6, 1.4, 1.2, 1.0, 0.6. UV-vis (THF) λ_{max} , nm (ϵ , M⁻¹ cm⁻¹): 508 (1100), 420 (1700). μ_{eff} (C₆D₆): 1.8 μ_{B} . Anal. calcd. for C₃₆H₅₄ClCoP₃Si: C, 61.58; H, 7.75. Found: C, 61.29; H, 7.61.

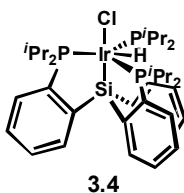
[SiP^{iPr}₃]NiCl (3.3). To a stirring slurry of NiCl₂ (7.3 mg, 0.056 mmol) in THF (5 mL) was added a



solution of H[SiP^{iPr}₃] (3.1) (34.5 mg, 0.0567 mmol) in THF (3 mL). Triethylamine (ca. 200 μ L) was added and the solution was heated at reflux for 12 h with stirring, causing a color change to bright red. Volatiles were

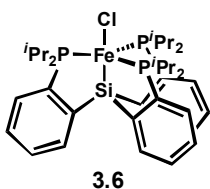
removed *in vacuo* and the residues extracted into benzene (5 mL), filtered through celite and lyophilized to yield **3.3** as a pale-red powder (38.0 mg, 96%). Crystals suitable for X-ray diffraction were grown by slow evaporation of benzene from a concentrated solution. ¹H NMR (C₆D₆): δ 7.78–7.70 (m, 3H, Ar-H), 7.30–7.24 (m, 6H, Ar-H), 7.15–7.00 (m, 3H, Ar-H), 2.70–2.55 (m, 6H, -CH(CH₃)₂), 1.35–1.20 (m, 18H, -CH(CH₃)₂), 1.00–0.80 (m, 18H, -CH(CH₃)₂). ³¹P NMR (C₆D₆): δ 35.6 (s). UV-vis (THF) λ_{max} , nm (ϵ , M⁻¹ cm⁻¹): 482 (1500), 349 (2000). Anal. calcd. for C₃₆H₅₄ClNiP₃Si: C, 61.60; H, 7.75. Found: C, 61.55; H, 7.73.

[SiP^{iPr}₃]Ir(H)(Cl) (3.4). To a stirring solution of [(cod)IrCl]₂ (60.1 mg, 0.0895 mmol) was added a



solution of H[SiP^{iPr}₃] (**3.1**) (108.8 mg, 0.1787 mmol) in THF (3 mL), causing an immediate color change from orange to yellow. After 12 h, volatiles were removed *in vacuo* and the residues dissolved in benzene (10 mL), filtered through celite, and lyophilized to yield **3.4** as a pale-yellow powder (142.4 mg, 95%). Analytically pure sample was obtained as colorless crystals by vapor diffusion of petroleum ether into a concentrated benzene solution, and analysis is reported for **3.4**·(C₆H₆). ¹H NMR (C₆D₆): δ 8.10 (d, *J* = 7.2 Hz, 2H, Ar-*H*), 7.92 (d, *J* = 6.9 Hz, 1H, Ar-*H*), 7.38–7.28 (m, 2H, Ar-*H*), 7.26–7.20 (m, 1H, Ar-*H*), 7.14–6.94 (m, 6H, Ar-*H*), 3.00–2.85 (m, 2H, -CH(CH₃)₂), 2.80–2.65 (m, 2H, -CH(CH₃)₂), 2.55–2.40 (m, 2H, -CH(CH₃)₂), 1.90–1.75 (m, 6H, -CH(CH₃)₂), 1.45–1.25 (m, 12H, -CH(CH₃)₂), 1.05–0.90 (m, 12H, -CH(CH₃)₂), 0.60–0.45 (m, 6H, -CH(CH₃)₂), -10.83 (dt, ²*J*_{HP(trans)} = 118 Hz, ²*J*_{HP(cis)} = 24 Hz, 1H, Ir-*H*). ³¹P NMR (THF): δ 28.9 (br s, 2P, P-Ir-*H*_{cis}), 25.5 (d, ²*J*_{PH} = 100 Hz, 1P, P-Ir-*H*_{trans}). UV-vis (THF) λ_{max}, nm (ε, M⁻¹ cm⁻¹): 495 (18), 428 (48), 367 (120). IR (THF, KBr, cm⁻¹) ν(Ir-*H*): 2145. Anal. calcd. for C₄₂H₆₁ClP₃IrSi: C, 55.15; H, 6.72. Found: C, 55.11; H, 6.66.

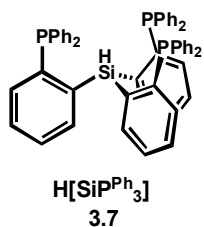
[SiP^{iPr}₃]FeCl (3.6). To a stirring slurry of FeCl₂ (30.6 mg, 0.241 mmol) in THF (10 mL) was added a



solution of H[SiP^{iPr}₃] (**3.1**) (147.2 mg, 0.2418 mmol) in THF (5 mL), causing a color change to yellow as complex **3.5** was generated (n.b., crystalline samples of **3.5** could be isolated at this point by removal of solvent and crystallization from benzene). The resulting solution was chilled to -78 °C, and MeMgCl (3.0 M in THF, 81 μL, 0.24 mmol) was diluted in THF (1 mL) and added dropwise, causing an immediate darkening of the solution. The mixture was stirred at -78 °C for 1 h, then warmed to room temperature and stirred 3 h to give a dark-orange solution. The solution was filtered through celite and concentrated to an orange film *in vacuo*. The residues were extracted into benzene,

filtered, lyophilized, and washed with petroleum ether (3 x 3 mL) to yield **3.6** as an orange powder (72.5 mg, 43%). Crystals suitable for X-ray diffraction were obtained by slow evaporation of benzene from a concentrated solution. ^1H NMR (C_6D_6): δ 7.3, 5.4, 2.6, -2.7. UV-vis (THF) λ_{max} , nm (ϵ , $\text{M}^{-1} \text{cm}^{-1}$): 471 (990), 379 (2100). μ_{eff} (C_6D_6): 3.3 μ_{B} . Anal. calcd. for $\text{C}_{36}\text{H}_{54}\text{ClFeP}_3\text{Si}$: C, 61.85; H, 7.79. Found: C, 62.34; H, 7.96.

Tris(*o*-(diphenylphosphino)phenyl)silane (H[SiP^{Ph}]₃, 3.7). (2-bromophenyl)diphenylphosphine

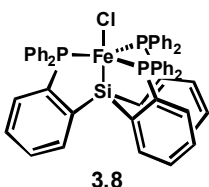


(10.24 g, 30.0 mmol) was dissolved in diethyl ether (150 mL) and cooled to -78 °C. *n*-Butyllithium (1.60 M in hexanes, 18.8 mL, 30.0 mmol) was added slowly, giving a light-orange solution with a tan-colored precipitate. This mixture was allowed to warm gradually to room temperature and then stirred for 1 h, after which the volatiles were removed *in vacuo*. Toluene (150 mL) was added, and the cloudy orange solution was cooled back to -78 °C. Trichlorosilane (1.01 mL, 10.0 mmol) was added in one portion, and the resulting mixture was warmed to room temperature gradually. After stirring for 30 min, the reaction was heated in a sealed vessel to 110 °C for 15 h. The resulting yellow solution and white precipitate were cooled to ambient temperature and filtered through celite, and the filtrate was concentrated to white solids. Petroleum ether (100 mL) was added and the resulting mixture was stirred vigorously for 20 min, at which point tan solids were collected on a sintered glass frit and washed with additional petroleum ether (2 x 30 mL) to afford **3.7** as a fine tan powder (6.15 g, 76%). ^1H NMR (C_6D_6): δ 7.63 (dm, $J_1 = 6.3$ Hz, $J_2 = 1.5$ Hz, 3H), 7.34 (ddm, $J_1 = 7.8$ Hz, $J_2 = 3.9$ Hz, $J_3 = 1.0$ Hz, 3H), 7.25–7.20 (m, 12H), 7.05 (td, $J_1 = 7.3$ Hz, $J_2 = 1.5$ Hz, 6H), 7.02–6.95 (m, 19H). ^{13}C NMR (C_6D_6): δ 145.5 (d, $J = 11.4$ Hz), 144.3 (t, $J = 4.0$ Hz), 144.0 (t, $J = 4.0$ Hz), 138.8 (d, $J = 14.6$ Hz), 138.5 (d, $J = 12.8$ Hz), 134.7, 134.5 (d, $J = 19.2$

Hz), 130.4, 128.8, 128.6 (d, $J = 17.3$ Hz). ^{31}P NMR (C_6D_6): $\delta -10.4$ (s). IR (KBr, cm^{-1}) $\nu(\text{Si-H})$: 2170.

Anal. calcd. for $\text{C}_{54}\text{H}_{43}\text{P}_3\text{Si}$: C, 79.78; H, 5.33. Found: C, 79.39; H, 5.61.

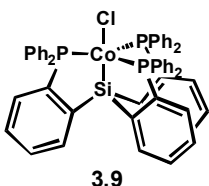
[SiP^{Ph}₃]FeCl (3.8). H[SiP^{Ph}₃] (**3.7**) (2.19 g, 2.69 mmol) and FeCl₂ (0.341 g, 2.69 mmol) were



combined in THF (50 mL) and cooled to -78 °C. *n*-Butyllithium (1.60 M in hexanes, 1.68 mL, 2.69 mmol) was added slowly, resulting in an immediate color change to dark red. The mixture was allowed to warm to room

temperature, and after stirring for 2 h was concentrated to oily red solids. Benzene (50 mL) was added, and the resulting solution was filtered through celite and concentrated. Diethyl ether (40 mL) was added and the mixture was stirred vigorously, yielding an orange precipitate and a red supernatant. The orange solids were collected on a sintered glass frit and washed with additional diethyl ether portions, yielding pure **3.8** as a light-orange powder (1.28 g, 53%). Crystals suitable for X-ray diffraction were obtained by slow diffusion of petroleum ether vapors into a dichloromethane solution. ^1H NMR (C_6D_6): δ 12.32, 7.61, 6.99, 4.67, 3.29, -2.09 , -5.03 . μ_{eff} (C_6D_6): $2.9 \mu_{\text{B}}$. UV-vis (toluene) λ_{max} , nm (ϵ , $\text{M}^{-1} \text{cm}^{-1}$): 479 (5700), 426 (4700). Anal. calcd. for $\text{C}_{54}\text{H}_{42}\text{ClFeP}_3\text{Si}$: C, 71.81; H, 4.69. Found: C, 71.82; H, 4.41.

[SiP^{Ph}₃]CoCl (3.9). H[SiP^{Ph}₃] (**3.7**) (0.483 g, 0.595 mmol) and CoCl₂ (0.0830 g, 0.639 mmol) were



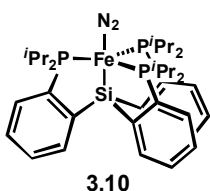
combined in THF (30 mL) with *i*Pr₂NEt (110 μL , 0.666 mmol). After several minutes, the blue solution adopted a red hue and was then stirred for 16 h. Solvent was removed under reduced pressure and the remaining solid was

dissolved in benzene (30 mL). This solution was filtered through a glass microfilter and lyophilized to yield spectroscopically pure **3.9** as a fluffy red powder (0.4686 g, 87%). Crystals suitable X-ray diffraction were obtained by vapor diffusion of petroleum ether into a saturated

solution of **3.9** in methylene chloride. ^1H NMR (C_6D_6): δ 10.3, 8.1, 7.7, 5.6, 3.0, -1.2 . UV-vis (C_6H_6) λ_{max} , nm (ϵ , $\text{M}^{-1} \text{cm}^{-1}$): 402 (5700), 506 (3800).

Complexes **3.10**, **3.11**, and **3.13–3.15** proved unstable to extended exposure to vacuum due to the lability of the N_2 ligand. Although the reported complexes were spectroscopically pure, suitable elemental analyses were not obtained.

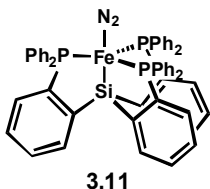
[SiP^{*i*Pr}₃]Fe(N₂) (3.10). A dark-green solution of sodium naphthalide was prepared by stirring a



colorless solution of naphthalene (8.6 mg, 0.067 mmol) in THF (3 mL) over excess sodium metal (8.0 mg, 0.35 mmol) for 3 h. The resulting naphthalide solution was filtered away from sodium and added dropwise to an orange

solution of **3.6** (46.8 mg, 0.0669 mmol) in THF (5 mL), causing the color of the solution to change to dark orange over a period of several minutes. The reaction was allowed to proceed overnight, filtered, and volatiles removed *in vacuo* to give an orange-red film. The residues were extracted into benzene (5 mL), filtered, and dried. The remaining film was triturated with petroleum ether (1 x 5 mL) to give a red powder that was washed with petroleum ether (2 x 3 mL) to yield spectroscopically pure **3.10** (10.5 mg, 23%). Crystals suitable for X-ray diffraction were obtained by slow evaporation of benzene from a concentrated solution. ^1H NMR (C_6D_6): δ 10, 7.1, 7.0, 3.8, 2.1, 1.1 ppm. μ_{eff} (C_6D_6): 2.2 μ_{B} . IR (THF, KBr, cm^{-1}) $\nu(\text{N}_2)$: 2008. UV-vis (THF) λ_{max} , nm (ϵ , $\text{M}^{-1} \text{cm}^{-1}$): 468 (1800), 380 (3500).

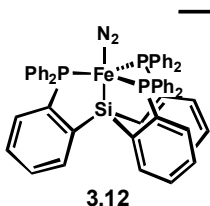
[SiP^{Ph}₃]Fe(N₂) (3.11). Sodium (8.3 mg, 0.36 mmol) and mercury (0.714 g) were combined in THF



(1 mL). Solid **3.8** (0.322 g, 0.357 mmol) was added, and the total volume was brought up to 15 mL. After vigorous stirring for 6 h at room temperature, a brown supernatant was decanted off the Na/Hg amalgam and concentrated

in vacuo to brown solids. Benzene (10 mL) was added, and the resulting cloudy solution was filtered through celite. The resulting red-orange filtrate was lyophilized, providing spectroscopically pure **3.11** as a fluffy red-orange solid (0.278 g, 87%). Crystals suitable for X-ray diffraction were obtained by slow diffusion of petroleum ether vapors into a THF solution. ¹H NMR (C₆D₆): δ 10.48, 7.98, 7.42, 6.17, 4.46, -1.85 (br), -1.86. μ_{eff} (C₆D₆): 1.8 μ_B. UV-vis (toluene) λ_{max}, nm (ε, M⁻¹ cm⁻¹): 347 (9400). IR (KBr, cm⁻¹) ν(N₂): 2041.

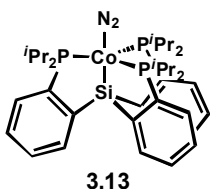
{[SiP^{Ph}₃]Fe(N₂)}{Na([12]crown-4)₂} (3.12). Sodium (2.3 mg, 0.10 mmol) and mercury (0.552 g)



were combined in THF (1 mL). A THF solution (8 mL) of [SiP^{Ph}₃]Fe(N₂) (**3.11**) (73.5 mg, 0.0821 mmol) and then 12-crown-4 (40.0 mL, 0.247 mmol) were added, resulting in a red-purple solution. The reaction was stirred

vigorous for 6.5 h, the deep-purple supernatant was decanted off the Na/Ha amalgam, filtered through celite, and concentrated *in vacuo* to purple solids. The residue was triturated with diethyl ether (10 mL), and a purple microcrystalline solid was collected on a sintered glass frit. Additional diethyl ether washes (2 × 10 mL) yielded analytically pure {[SiP^{Ph}₃]Fe(N₂)}{Na(12-crown-4)₂} (**3.12**) (63.5 mg, 71%). ¹H NMR (THF-d₈): δ 8.22 (d, *J* = 10.5 Hz, 3H), 7.4–6.4 (m, 39H), 3.55 (s, 32H, 12-crown-4). ³¹P{¹H} NMR (THF-d₈): δ 84.3 (s). UV-vis (THF) λ_{max}, nm (ε, M⁻¹ cm⁻¹): 415 (6100), 460 (6300). IR (KBr, cm⁻¹) ν(N₂): 1967. Anal. calcd. for C₇₀H₇₄FeN₂O₈P₃Si: C, 66.14; H, 5.87; N, 2.20. Found: C, 66.35; H, 5.85; N, 1.77.

[SiP^{iPr}₃]Co(N₂) (3.13). A red solution of **3.2** (154.3 mg, 0.2197 mmol) in THF (10 mL) was added



onto a 0.27 weight % Na/Hg amalgam (0.0057 g, 0.25 mmol sodium dissolved in 2.0875 g of mercury) with stirring. Over a period of 2 h, the color of the solution changed from red to golden. After 12 h, the solution was

filtered to remove insoluble residues and volatiles were removed *in vacuo* to give a golden film.

The residues were extracted into benzene, filtered, and lyophilized to an orange powder, which was subsequently washed with petroleum ether (3 × 10 mL) to yield **3.13** as a bright-orange

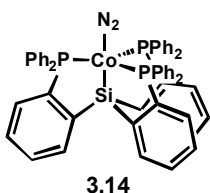
powder (90.4 mg, 60%). Crystals suitable for X-ray diffraction were obtained by slow

evaporation of benzene from a concentrated solution. ¹H NMR (C₆D₆): δ 7.89 (d, *J* = 6.9 Hz, 3H, Ar-*H*), 7.21 – 6.95 (m, 9H, Ar-*H*), 2.51 (br, 6H, -CH(CH₃)₂), 1.11 (br, 18H, -CH(CH₃)₂), 0.65 (br,

18H, -CH(CH₃)₂). ³¹P NMR (C₆D₆): δ 65.7 (s). IR (THF, KBr, cm⁻¹) ν(N₂): 2063. UV-vis (THF) λ_{max}, nm

(ε, M⁻¹ cm⁻¹): 381 (2800).

[SiP^{Ph}₃]Co(N₂) (3.14). A red solution of **3.9** (0.035 g, 0.039 mmol) in THF (10 mL) was added onto



a 0.5 weight % Na/Hg amalgam (0.0015 g, 0.066 mmol sodium dissolved in 0.3025 g of mercury) with stirring, causing a gradual color change to brown.

After 12 h, the mixture was decanted from the amalgam and filtered

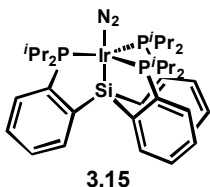
through celite to give an orange solution. Volatiles were removed *in vacuo*, and the residues

were extracted into benzene, filtered, and lyophilized to afford **3.14** as an orange powder

(0.014 g, 45%). ¹H NMR (C₆D₆): δ 8.1, 7.4, 7.2, 7.0, 6.9, 6.8. ³¹P NMR (C₆D₆): δ 63.5. UV-vis (C₆H₆)

λ_{max}, nm (ε, M⁻¹ cm⁻¹): 378 (2000). IR (KBr, cm⁻¹) ν(N₂): 2095.

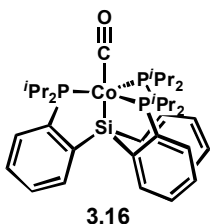
[SiP^{iPr}₃]Ir(N₂) (3.15). A colorless solution of **3.4** (101.2 mg, 0.1210 mmol) in THF (5 mL) was



chilled to $-78\text{ }^{\circ}\text{C}$. MeMgCl (3.0 M in THF, 44 μL , 0.132 mmol) was diluted in 1 mL of THF and added dropwise to the stirring solution. The reaction was

allowed to proceed at $-78\text{ }^{\circ}\text{C}$ for 30 min with no color change, then warmed to room temperature and stirred for 4 h, causing a change in color to bright yellow. The mixture was concentrated *in vacuo* to give a green film which was subsequently extracted into benzene/petroleum ether (2:1, 20 mL). The solution was filtered through celite and dried to afford **3.15** as an electric yellow powder (87.5 mg, 87%). ¹H NMR (C₆D₆): δ 8.09 (d, $J = 6.9$ Hz, 3H, Ar-H), 7.30–7.20 (m, 3H, Ar-H), 7.20–7.10 (m, 3H, Ar-H), 7.10–7.00 (m, 3H, Ar-H), 2.52 (br, 6H, $-\text{CH}(\text{CH}_3)_2$), 1.06 (br, 18H, $-\text{CH}(\text{CH}_3)_2$), 0.69 (br, 18H, $-\text{CH}(\text{CH}_3)_2$). ³¹P NMR (C₆D₆): δ 38.7 (s). UV-vis (THF) λ_{max} , nm (ϵ , M⁻¹ cm⁻¹): 310 (7600). IR (THF, KBr, cm⁻¹) $\nu(\text{N}_2)$: 2122.

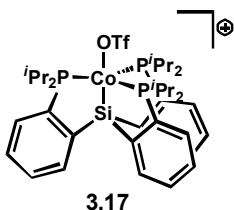
[SiP^{iPr}₃]Co(CO) (3.16). In a sealed NMR tube, an orange solution of **3.13** in THF (1 mL) was frozen



and the headspace evacuated and backfilled with carbon monoxide. Over a period of 12 h, the hue of the solution lightened from orange to yellow.

Consumption of **3.13** and appearance of **3.16** was confirmed by NMR (³¹P) and IR, and yellow X-ray quality crystals were grown by storing a concentrated solution of **3.16** in petroleum ether at $-35\text{ }^{\circ}\text{C}$. ³¹P NMR (THF): δ 78.2 (s). IR (THF, KBr, cm⁻¹) $\nu(\text{CO})$: 1896.

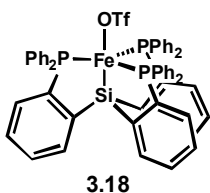
[[SiP^{iPr}₃]Co(OTf)]⁺(OTf)⁻ (3.17). To a solution of **3.13** (45.1 mg, 0.0649 mmol) in THF (5 mL) was



added a colorless solution of silver triflate (33.4 mg, 0.130 mmol) in THF (5 mL). The color of the mixture immediately changed from orange to green as it became cloudy. After 5 h, the solution was filtered through celite and

concentrated *in vacuo* to a green film. The product was triturated with petroleum ether (1 x 5 mL) and washed with petroleum ether (3 x 5 mL) and benzene (1 x 5 mL) to give **3.17** as a fine green powder (81.0 mg, 84%). X-ray quality crystals were grown by vapor diffusion of petroleum ether into a concentrated solution of **3.17** in THF. ¹H NMR (CD₃CN): δ 11.9, 7.8, 7.4, 7.2, 7.0, 3.8, 3.4, 3.0, 2.7, 1.9, 1.2, 0.9, 0.6, -3.5. UV-vis (THF) λ_{max}, nm (ε, M⁻¹ cm⁻¹): 810 (220), 611 (330), 517 (390), 373 (2300). μ_{eff} (THF-d₈): 3.3 μ_B. Anal. calcd. for C₃₈H₅₄CoF₆O₆P₃S₂Si: C, 47.30; H, 5.64. Found: C, 47.17; H, 5.73.

[SiP^{Ph}₃]Fe(OTf) (3.18). In separate scintillation vials, [SiP^{Ph}₃]FeN₂ (**3.11**) (29.5 mg, 0.0329 mmol)



and AgOTf (8.5 mg, 33 mmol) were dissolved in THF (1 mL each) and cooled to -35 °C. The AgOTf solution was then added slowly to the [SiP^{Ph}₃]FeN₂ solution with stirring. After stirring for 5 h at room temperature, volatiles

were removed *in vacuo*. Et₂O (10 mL) was added, and black solids were filtered away from the resulting suspension to yield an orange filtrate. Volatiles were removed *in vacuo* to yield **3.18** as an orange powder (22.2 mg, 66%). ¹H NMR (C₆D₆): 12.4, 5.4, 5.1, -4.3. μ_{eff} (C₆D₆): 3.0 μ_B. UV-Vis (toluene) λ_{max}, nm (ε, M⁻¹ cm⁻¹): 432 (1440), 489 (1840). IR (KBr, cm⁻¹): 3050, 2958, 1586, 1482, 1435, 1324, 1232 (OTf), 1210 (OTf), 1179 (OTf), 1108, 1027. Anal. calcd for C₅₅H₄₂F₃FeO₃P₃SSi: C, 64.97; H, 4.16. Found: C, 64.08; H, 3.76.

Reaction of 3.10 and 3.11 with acids. $[\text{SiP}_3^{\text{R}}]\text{FeN}_2$ (R = *i*Pr, **3.10**; R = Ph, **3.11**) (approx 10 mg), and in some cases a sacrificial Cr(II) reagent (10 equiv per Fe), were dissolved in THF (3 mL) in a 2-neck 25 mL round-bottom flask and sealed with septa. An ethereal solution of the acid (10 equiv per Fe) was added via syringe, and the resulting solution was stirred overnight under septum seal. Volatiles were then vacuum transferred onto a frozen HCl solution (5 mL, 1.0 M in Et₂O). A solution of NaO^tBu (>15 equiv) in THF (5 mL) was then added to the source flask via syringe through the second neck, and the mixture was stirred vigorously for 30 min. The volatiles were again vacuum transferred into the same receiving flask. The combined distillates were concentrated to white solids by rotary evaporation and analyzed by ¹H NMR (DMSO-d₆) with mesitylene added as an internal integration standard. $[\text{N}_2\text{H}_6]\text{Cl}_2$ was identified by comparison with an authentic sample and its concentration quantified by integration versus mesitylene. The results of these experiments are summarized in Table 3.2.

X-ray Crystallography Procedures. X-ray quality crystals were grown as indicated in the experimental procedures for each complex. The crystals were mounted on a glass fiber with Paratone N oil. Structures were determined using direct methods with standard Fourier techniques using the Bruker AXS software package. In some cases, Patterson maps were used in place of the direct methods procedure. Table 3.3 contains the X-ray diffraction experimental details.

Table 3.3. X-ray crystallographic data

complex	3.1	3.2	3.3
Empirical Formula	C ₃₆ H ₅₅ P ₃ Si	C ₃₆ H ₅₄ ClCoP ₃ Si	C ₃₆ H ₅₄ ClNiP ₃ Si · C ₆ H ₆
Formula Weight	608.80	702.17	780.06
λ (Å)	0.71073	0.71073	0.71073
T (K)	100(2)	100(2)	100(2)
a (Å)	11.3718(3)	16.149(5)	12.916(4)
b (Å)	11.5291(4)	17.085(4)	15.540(3)
c (Å)	16.4561(5)	25.497(6)	20.130(5)
α (deg)	96.135(2)	90	90
β (deg)	105.964(2)	90	92.32(3)
γ (deg)	116.084(2)	90	90
V (Å ³)	1797.03(10)	7035(3)	4037.1(17)
Z	2	8	4
Crystal System	Triclinic	Orthorhombic	Monoclinic
Space Group	P-1	Pbca	P2(1)/c
d_{calc} (g/cm ³)	1.125	1.326	1.283
GOF on F ²	1.026	1.308	1.164
R1, wR2 ^a (I > 2 σ (I))	0.0722, 0.1839	0.0546, 0.0877	0.0509, 0.0820

complex	3.4	3.5	3.6
Empirical Formula	$C_{36}H_{55}ClIrP_3Si \cdot C_6H_6$	$C_{36}H_{55}Cl_2FeP_3Si$	$C_{36}H_{54}ClFeP_3Si \cdot C_6H_6$
Formula Weight	914.56	735.55	777.20
λ (Å)	0.71073	0.71073	0.71073
T (K)	100(2)	100(2)	100(2)
a (Å)	19.5771(15)	13.0548(19)	12.913(4)
b (Å)	11.0445(9)	13.718(3)	15.513(4)
c (Å)	18.5937(14)	22.356(6)	20.296(8)
α (deg)	90	90	90
β (deg)	90	104.102(11)	92.33(3)
γ (deg)	90	90	90
V (Å ³)	4020.3(5)	3883.0(15)	4062(2)
Z	4	4	4
Crystal System	Orthorhombic	Monoclinic	Monoclinic
Space Group	Pna2(1)	P2(1)/n	P2(1)/c
d_{calc} (g/cm ³)	1.511	1.258	1.271
GOF on F ²	1.077	1.089	1.367
R1, wR2 ^a (I > 2 σ (I))	0.0394, 0.0802	0.0688, 0.2052	0.0510, 0.0872

complex	3.10	3.13	3.15
Empirical Formula	0.96 (C ₃₆ H ₅₄ FeN ₂ P ₃ Si) 0.04 (C ₃₆ H ₅₄ ClFeP ₃ Si) · C ₆ H ₆	C ₃₆ H ₅₄ CoN ₂ P ₃ Si · C ₆ H ₆	C ₃₆ H ₅₄ IrN ₂ P ₃ Si
Formula Weight	769.77	772.85	828.01
λ (Å)	0.71073	0.71073	0.71073
T (K)	100(2)	100(2)	100(2)
a (Å)	12.759(2)	12.6932(9)	15.98(2)
b (Å)	15.4865(19)	15.4021(11)	17.151(12)
c (Å)	20.561(4)	20.6008(15)	25.95(2)
α (deg)	90	90	90
β (deg)	92.006(16)	91.9160(10)	90
γ (deg)	90	90	90
V (Å ³)	4060.1(11)	4025.2(5)	7112(12)
Z	4	4	8
Crystal System	Monoclinic	Monoclinic	Orthorhombic
Space Group	P2(1)/c	P2(1)/c	Pbca
d _{calc} (g/cm ³)	1.259	1.275	1.546
GOF on F ²	1.033	1.032	1.210
R1, wR2 ^a (I > 2σ (I))	0.0521, 0.1287	0.0475, 0.1050	0.0496, 0.0767

complex	3.16	3.17	3.18
Empirical Formula	C ₃₇ H ₅₄ CoN ₂ OP ₃ Si	C ₃₈ H ₅₄ CoF ₆ O ₆ P ₃ S ₂ Si	C ₅₄ H ₄₂ F ₃ FeO ₃ P ₃ SSi · C ₄ H ₈ O
Formula Weight	694.73	964.86	1088.91
λ (Å)	0.71073	0.71073	0.71073
T (K)	100(2)	100(2)	100(2)
a (Å)	16.13(2)	10.8159(10)	22.7568(7)
b (Å)	17.050(14)	14.3316(13)	16.8912(5)
c (Å)	25.54(2)	28.152(3)	26.7730(8)
α (deg)	90	90	90
β (deg)	90	90	90
γ (deg)	90	90	90
V (Å ³)	7023(13)	4363.9(7)	10291.3(5)
Z	8	4	8
Crystal System	Orthorhombic	Orthorhombic	Orthorhombic
Space Group	Pbca	P2(1)2(1)2(1)	Pbca
d _{calc} (g/cm ³)	1.314	1.469	1.385
GOF on F ²	1.096	1.007	1.043
R1, wR2 ^a (I > 2σ(I))	0.0707, 0.1150	0.0783, 0.1895	0.0446, 0.1106

References and Notes

- (1) (a) Howard, J. B.; Rees, D. C. *Chem. Rev.* **1996**, *96*, 2965; Burgess, B. K., Lowe, D. J. *Chem. Rev.* **1996**, *96*, 2983. (b) Chatt, J.; Dilworth, J. R.; Richards, R. L. *Chem. Rev.* **1978**, *78*, 589.
- (2) Peters, J. C.; Mehn, M. P. In *Activation of Small Molecules*; Tolman, W. B., Ed.; Wiley: New York, 2006, p 81–120.
- (3) MacKay, B. A.; Fryzuk, M. D. *Chem. Rev.* **2004**, *104*, 385.
- (4) (a) Yandulov, D. V.; Schrock, R. R. *Science* **2003**, *301*, 76. (b) Yandulov, D. V.; Schrock, R. R. *J. Am. Chem. Soc.* **2002**, *124*, 6252. (c) Schrock, R. R. *Acc. Chem. Res.* **2005**, *38*, 955.
- (5) (a) Brown, S. D.; Betley, T. A.; Peters, J. C. *J. Am. Chem. Soc.* **2003**, *125*, 322. (b) Brown, S. D.; Peters, J. C. *J. Am. Chem. Soc.* **2005**, *127*, 1913. (c) Brown, S. D.; Mehn, M. P.; Peters, J. C. *J. Am. Chem. Soc.* **2005**, *127*, 13146. (d) Betley, T. A.; Peters, J. C. *J. Am. Chem. Soc.* **2003**, *125*, 10782. (e) Betley, T. A.; Peters, J. C. *J. Am. Chem. Soc.* **2004**, *126*, 6252. (f) Smith, J. M.; Lachicotte, R. J.; Pittard, K. A.; Cundari, T. R.; Lukat-Rodgers, G.; Rodgers, K. R.; Holland, P. L. *J. Am. Chem. Soc.* **2001**, *123*, 9222. (g) Holland, P. L. *Can. J. Chem.* **2005**, *83*, 296. (h) Smith, J. M.; Sadique, A. R.; Cundari, T. R.; Rodgers, K. R.; Lukat-Rodgers, G.; Lachicotte, R. J.; Flaschenriem, C. J.; Vela, J.; Holland, P. L. *J. Am. Chem. Soc.* **2006**, *128*, 756.
- (6) Hendrich, M. P.; Gunderson, W.; Behan, R. K.; Green, M. T.; Mehn, M. P.; Betley, T. A.; Lu, C. C.; Peters, J. C. *Proc. Natl. Acad. Sci. U. S. A.* **2006**, *103*, 17107.
- (7) MacBeth, C. E.; Harkins, S. B.; Peters, J. C. *Can. J. Chem.* **2005**, *83*, 332.
- (8) Stoian, S. A.; Vela, J.; Smith, J. M.; Sadique, A. R.; Holland, P. L.; Munck, E.; Bominaar, E. L. *J. Am. Chem. Soc.* **2006**, *128*, 10181.
- (9) Whited, M. T.; Rivard, E.; Peters, J. C. *Chem. Commun.* **2006**, 1613.
- (10) Arnold and co-workers have recently adopted a similar approach in their synthesis of monoanionic, tetradentate ligands: (a) Chomitz, W. A.; Arnold, J. *Chem. Commun.* **2007**, 4797. (b) Chomitz, W. A.; Mickenberg, S. F.; Arnold, J. *Inorg. Chem.* **2008**, *47*, 373.
- (11) Joslin, F. L.; Stobart, S. R. *J. Chem. Soc., Chem. Commun.* **1989**, 504.
- (12) Mankad, N. P.; Rivard, E.; Harkins, S. B.; Peters, J. C. *J. Am. Chem. Soc.* **2005**, *127*, 16032.
- (13) Brauer, D. J.; Hingst, M.; Kottsieper, K. W.; Liek, C.; Nickel, T.; Tepper, M.; Stelzer, O.; Sheldrick, W. S. *J. Organomet. Chem.* **2002**, *645*, 14.
- (14) Talay, R.; Rehder, D. *Zeit. f. Natur. B: Anorg. Chemie* **1981**, *36*, 451.

- (15) (a) Grundy, S. L.; Holmessmith, R. D.; Stobart, S. R.; Williams, M. A. *Inorg. Chem.* **1991**, *30*, 3333. (b) Okazaki, M.; Ohshitanai, S.; Iwata, M.; Tobita, H.; Ogino, H. *Coord. Chem. Rev.* **2002**, *226*, 167. (c) Gossage, R. A.; McLennan, G. D.; Stobart, S. R. *Inorg. Chem.* **1996**, *35*, 1729.
- (16) Kauffmann, T.; Laarmann, B.; Menges, D.; Neiteler, G. *Chem. Ber. Recl.* **1992**, *125*, 163.
- (17) (a) Sacconi, L.; Divaira, M. *Inorg. Chem.* **1978**, *17*, 810. (b) Stoppioni, P.; Mani, F.; Sacconi, L. *Inorg. Chim. Acta* **1974**, *11*, 227.
- (18) Cotton, F. A. *Chemical Applications of Group Theory*; 3rd ed.; Wiley: New York, 1990.
- (19) Lu, C. C.; Peters, J. C. *Inorg. Chem.* **2006**, *45*, 8597.
- (20) Betley, T. A.; Peters, J. C. *Inorg. Chem.* **2003**, *42*, 5074.
- (21) (a) Shapiro, I. R.; Jenkins, D. M.; Thomas, J. C.; Day, M. W.; Peters, J. C. *Chem. Commun.* **2001**, 2152. (b) Jenkins, D. M.; Di Bilio, A. J.; Allen, M. J.; Betley, T. A.; Peters, J. C. *J. Am. Chem. Soc.* **2002**, *124*, 15336. (c) Jenkins, D. M.; Peters, J. C. *J. Am. Chem. Soc.* **2005**, *127*, 7148.
- (22) MacBeth, C. E.; Thomas, J. C.; Betley, T. A.; Peters, J. C. *Inorg. Chem.* **2004**, *43*, 4645.
- (23) A similarly dramatic shift in redox potential upon binding of N₂ at an available Mo(III) coordination site has been described by Peters et al.: Peters, J. C.; Cherry, J. P. F.; Thomas, J. C.; Baraldo, L.; Mindiola, D. J.; Davis, W. M.; Cummins, C. C. *J. Am. Chem. Soc.* **1999**, *121*, 10053.
- (24) (a) Dioumaev, V. K.; Plossl, K.; Carroll, P. J.; Berry, D. H. *J. Am. Chem. Soc.* **1999**, *121*, 8391. (b) Yoo, H.; Carroll, P. J.; Berry, D. H. *J. Am. Chem. Soc.* **2006**, *128*, 6038. (c) Trovitch, R. J.; Lobkovsky, E.; Chirik, P. J. *Inorg. Chem.* **2006**, *45*, 7252. (d) Gusev, D. G.; Fontaine, F. G.; Lough, A. J.; Zargarian, D. *Angew. Chem. Int. Ed.* **2003**, *42*, 216.
- (25) Compound **3.10** cocrystallized with a small amount of [SiP^{Pr}₃]₃FeCl (**3.6**) (refined to 4% occupancy). In Figure 3.9, the chloride ligand (which was refined isotropically due to low occupancy) has been omitted. Due to this disorder, N≡N bond lengths are not discussed in the text.
- (26) Collman, J. P.; Kubota, M.; Vastine, F. D.; Sun, J. Y.; Kang, J. W. *J. Am. Chem. Soc.* **1968**, *90*, 5430.
- (27) George, T. A.; Rose, D. J.; Chang, Y. D.; Chen, Q.; Zubieta, J. *Inorg. Chem.* **1995**, *34*, 1295.
- (28) Bianchini, C.; Mealli, C.; Meli, A.; Peruzzini, M.; Zanobini, F. *J. Am. Chem. Soc.* **1988**, *110*, 8725.
- (29) Lee, D. W.; Kaska, W. C.; Jensen, C. M. *Organometallics* **1998**, *17*, 1.

- (30) Gutierrez-Puebla, E.; Monge, A.; Nicasio, M. C.; Perez, P. J.; Poveda, M. L.; Carmona, E. *Chem. Eur. J.* **1998**, *4*, 2225.
- (31) (a) Cohen, R.; Rybtchinski, B.; Gandelman, M.; Rozenberg, H.; Martin, J. M. L.; Milstein, D. *J. Am. Chem. Soc.* **2003**, *125*, 6532. (b) Van der Boom, M. E.; Liou, S. Y.; Ben-David, Y.; Shimon, L. J. W.; Milstein, D. *J. Am. Chem. Soc.* **1998**, *120*, 6531. (c) Ghosh, R.; Kanzelberger, M.; Emge, T. J.; Hall, G. S.; Goldman, A. S. *Organometallics* **2006**, *25*, 5668.
- (32) (a) Gilbertson, J. D.; Szymczak, N. K.; Tyler, D. R. *J. Am. Chem. Soc.* **2005**, *127*, 10184. (b) Leigh, G. J. *Acc. Chem. Res.* **1992**, *25*, 177.
- (33) (a) Evans, D. F. *J. Chem. Soc.* **1959**, 2003. (b) Sur, S. K. *J. Magn. Reson.* **1989**, *82*, 169.

Chapter 4
C–H, C–O, and C–C Bond Activation at Pincer-Supported Iridium Frameworks

The text in this chapter is reproduced in part with permission from:

Romero, P. E.; Whited, M. T.; Grubbs, R. H. *Organometallics* **2008**, *27*, 3422–3429.

Copyright 2008 American Chemical Society

and

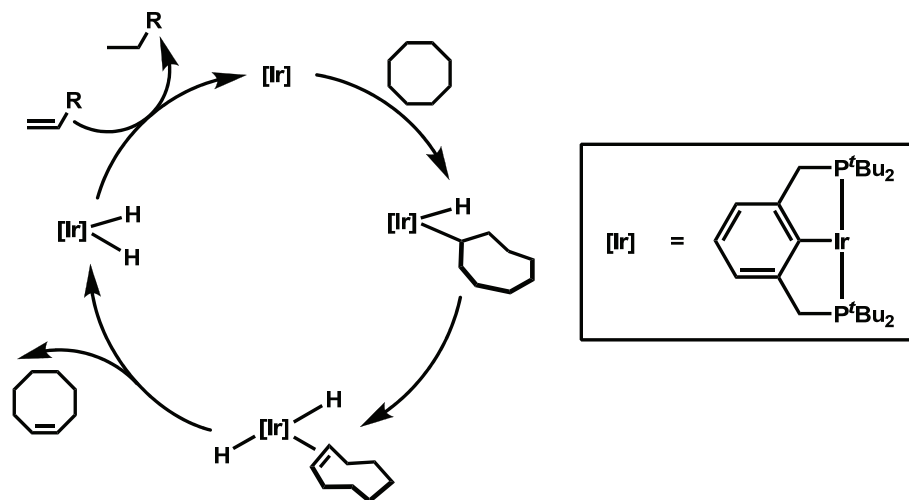
Whited, M. T.; Zhu, Y.; Timpa, S. D.; Chen, C.-H.; Foxman, B. M.; Ozerov, O. V.; Grubbs, R. H. *Organometallics*, submitted.

Unpublished material copyright 2009 American Chemical Society

Introduction

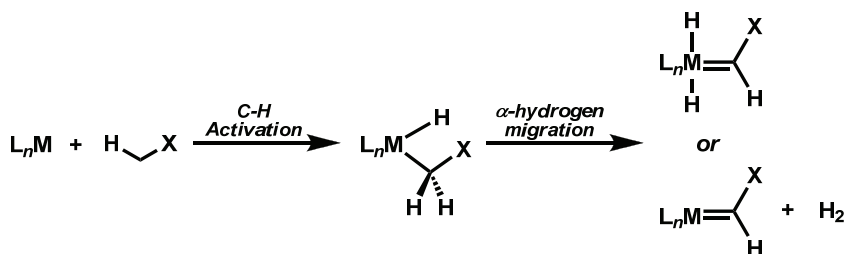
The catalytic activation and functionalization of otherwise inert C–H bonds of discrete molecules continues to be an area of active research in organometallic chemistry.¹ One particular approach that has received increasing attention in recent years is the catalytic, dehydrogenative conversion of alkanes into alkenes.² This transformation generates a functionalized product which can be further elaborated but, due to its thermodynamically uphill nature, it is usually accomplished in the presence of a sacrificial olefin that functions as a hydrogen acceptor. In recent years, significant progress has been made in this area due the introduction of thermally robust pincer-type complexes, and iridium variants in particular have been found to be exceptionally active catalysts.^{2,3}

The commonly accepted mechanism for this transformation involves (1) C–H oxidative addition of the alkane at a highly reactive 14-electron iridium intermediate, (2) β -hydrogen elimination with formation of the corresponding alkene, (3) release of the alkene and regeneration of the metal dihydride precursor, and (4) transfer of hydrogen from the latter to a sacrificial olefin to regenerate the active catalytic species (Scheme 4.1, cyclooctane as substrate).^{2,4} Tuning of the steric bulk around the metal center and reaction conditions have a major impact on catalytic activity and catalyst lifetime, and in some cases such tuning has allowed the dehydrogenation of alkanes to occur in the absence of a hydrogen acceptor.^{2b}



Scheme 4.1. Accepted mechanism for alkane dehydrogenation at pincer-supported iridium.

In comparison to alkane dehydrogenation, progress in the dehydrogenation of heteroatom-containing substrates has lagged.⁵ This is somewhat surprising given the high versatility demonstrated by pincer-type complexes in several areas of catalysis.^{3,6} As outlined above, β -hydrogen elimination allows for the generation of an alkene from an alkane. In the absence of β -hydrogens, α -hydrogen migration is likely to ensue, giving access to unsaturated Fischer-type carbenes which could be further elaborated (Scheme 4.2). While most C–H activation protocols rely on the generation of an $M-C_{sp^3}$ bond for potential functionalization,¹ the construction of a reactive $M=C_{sp^2}$ fragment via direct C–H activation provides new mechanisms for entry into C–C coupling and other bond-forming reactions.



Scheme 4.2. Formation of heteroatom-substituted carbenes by double C–H activation.

We have begun to explore this subject and have selected pincer iridium platforms as a starting point for the generation of Fischer-type carbenes from methyl ethers. In this contribution we present our initial efforts in this area using the pincer ligands **4.1** and **4.2** (Figure 4.1).

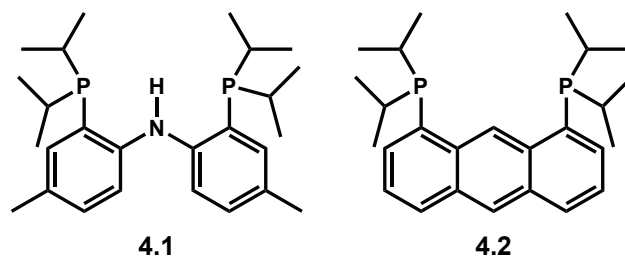
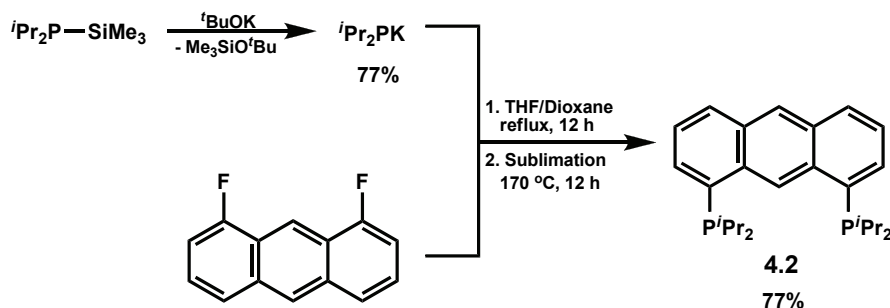
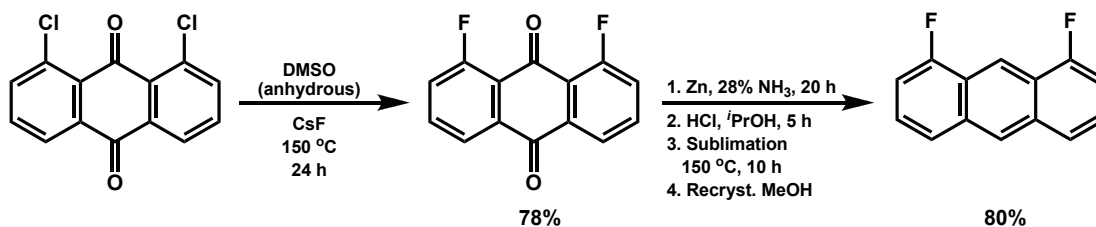


Figure 4.1. Pincer-type ligands used in this study.

Results and Discussion

Preparation of Anthraphos Ligands

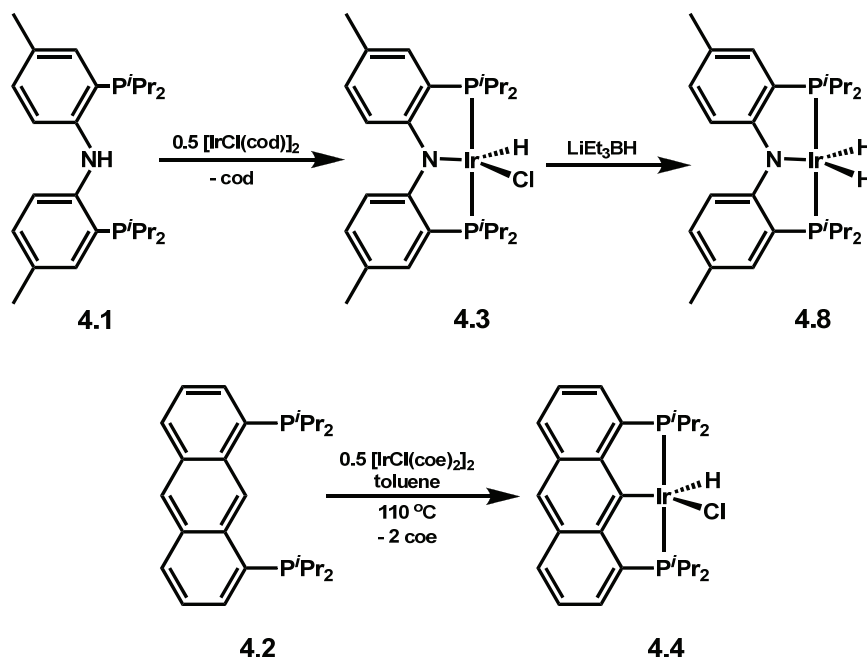
Although originally claimed by Haenel et al. in the context of alkane dehydrogenation,⁷ neither synthetic details nor characterization for **4.2** or its complexes has been furnished. Therefore, we start by discussing some of the details of the preparation of **4.2**. As reported, the key 1,8-difluoroanthraquinone can be conveniently prepared from commercially available 1,8-dichloroanthraquinone and subsequently reduced to 1,8-difluoroanthracene in good yields.⁸ Additionally, we have found that both 1,8-difluoroanthraquinone and 1,8-difluoroanthracene can be conveniently purified by sublimation, circumventing the need for chromatographic purification. Subsequent reaction of ⁱPr₂PK (obtained from metathesis of ⁱPr₂P-SiMe₃ and ^tBuOK) with 1,8-difluoroanthracene in a 1:1 mixture of THF/dioxane affords the desired ligand (ca. 75%–80% yield), which can also be readily purified by sublimation. Anthraphos ligand **4.2** is an air stable solid and can be routinely prepared on a 3–5 g scale (Scheme 4.3).



Scheme 4.3. Preparation of $f^{i\text{Pr}}$ Anthrathos ligand **4.2**.

Preparation of Iridium Precursors

Hydrido chloride complex **4.3** bearing a diarylamido unit has been prepared by Ozerov and co-workers by reaction of the free ligand with $[\text{IrCl}(\text{cod})]_2$ (Scheme 4.4),⁹ and dihydride complex **4.8** can be obtained by direct reaction of **4.3** with LiEt_3BH .¹⁰ Anthrathos complex **4.4** was prepared in high yield by direct metalation of the ligand with $[\text{IrCl}(\text{coe})_2]_2$ in refluxing toluene (Scheme 4.4). Multinuclear NMR spectroscopy analysis revealed a complex of C_s symmetry with a diagnostic triplet hydride signal at -35.9 ppm ($^2J_{\text{PH}} = 12$ Hz) and a singlet resonance in the ^{31}P NMR spectrum (δ 61 ppm). The high-field position of the Ir–H resonance in the ^1H NMR spectrum, as well as the symmetry displayed, is consistent with a square-pyramidal complex with the apical site occupied by the hydride and a mirror plane bisecting the backbone anthracene ligand. Red complex **4.4** is air sensitive in solution but can be handled in air as a solid.

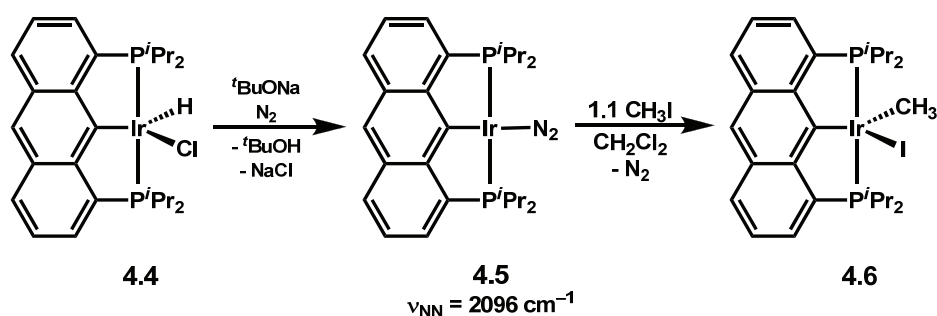


Scheme 4.4. Metalation of pincer ligands and precursor syntheses.

Haenel et al. have prepared the dihydride (^tBu Anthraphos)IrH₂ complex, which can be used as a precatalyst for the C–H activation of alkanes,⁷ from the corresponding hydrido chloride precursor. Alternatively, access to the 14-electron unsaturated intermediate responsible for C–H activation is possible directly from the hydrido chloride precursor. Following a protocol reported by Brookhart and co-workers,¹¹ reductive dehydrochlorination of **4.4** with the soluble base ^tBuONa proceeds smoothly in aromatic solvents. When this procedure is carried out under an atmosphere of N₂, dinitrogen complex **4.5** forms rapidly (Scheme 4.5). Although generation of **4.5** in solution is quantitative as judged by NMR, isolation of pure compound is difficult due to its lack of crystallinity. Therefore, **4.5** was characterized in solution. The ¹H NMR spectrum of dark-green complex **4.5** showed a complex of C_{2v} symmetry consistent with a symmetrical environment around the iridium center, and the ³¹P NMR spectrum revealed a single resonance at 64 ppm. Solution IR spectroscopy (C₆H₆) of **4.5** showed a band at 2096 cm⁻¹ assigned to the bound dinitrogen ligand. This value is slightly higher than the previously reported complex

(^tBuPCP)IrN₂ ($\nu_{\text{NN}} = 2079 \text{ cm}^{-1}$),¹² but is lower in energy than stretches reported for five-coordinate iridium(I)–dinitrogen adducts.¹³ The observed $\Delta\nu$ of 17 cm^{-1} is likely a reflection of the weaker donor ability of the ligand **4.2** due to the presence of less basic phosphines (ⁱPr versus ^tBu) and a more electron-withdrawing anthracene backbone (compared to *m*-xylyl). This translates into a lower $d\pi\text{--}p\pi^*$ backbonding from the (PCP)Ir center to the terminal N₂ ligand. The appearance of an IR-active band for **4.5** also indicates that, in solution, the product corresponds to the terminal dinitrogen adduct since the symmetric Ir–N≡N–Ir dimer should be IR silent.

The identity of dinitrogen complex **4.5** has also been inferred by derivatization with CH₃I (Scheme 4.5). Oxidative addition to the iridium(I) center in **4.5** occurs smoothly at room temperature to give **4.6** in 96% isolated yield. Air- and moisture-stable **4.6** shows a diagnostic triplet (δ 1.37 ppm) in its ¹H NMR spectrum corresponding to the iridium-bound methyl group (³*J*_{PH} = 6.0 Hz, CD₂Cl₂) along with C_s symmetry for the ligand environment and a single ³¹P NMR resonance at 39.6 ppm. IR spectroscopy showed the disappearance of the N≡N stretch observed in **4.5**.



Scheme 4.5. Synthesis and derivatization of (ⁱPr Anthrphos)Ir(N₂) (**4.5**).

X-ray characterization of a single crystal of **4.6** obtained by slow evaporation of a CH₂Cl₂ solution confirmed the proposed structure. The structure shows a distorted square-pyramidal configuration wherein the apical methyl group is slightly canted toward the ligand backbone

with a C13–Ir–C27 angle of $83.3(1)^\circ$, while the vector defined by C13–Ir–I is deviated from linearity with an angle of $168.65(8)^\circ$. This is likely a consequence of the rigid geometry imposed by the ligand which distorts the square-pyramidal structure to avoid unfavorable steric interactions with the isopropyl groups. The iridium atom resides slightly above the mean plane defined by C13–P1–I–P2 by 0.22 Å. Both the Ir–CH₃ (2.086(3) Å) and the Ir–C13 (2.017(3) Å) distances are unremarkable and compare well with related complexes.^{12,14} The anthracene ligand backbone deviates from planarity and is slightly puckered in the solid state.

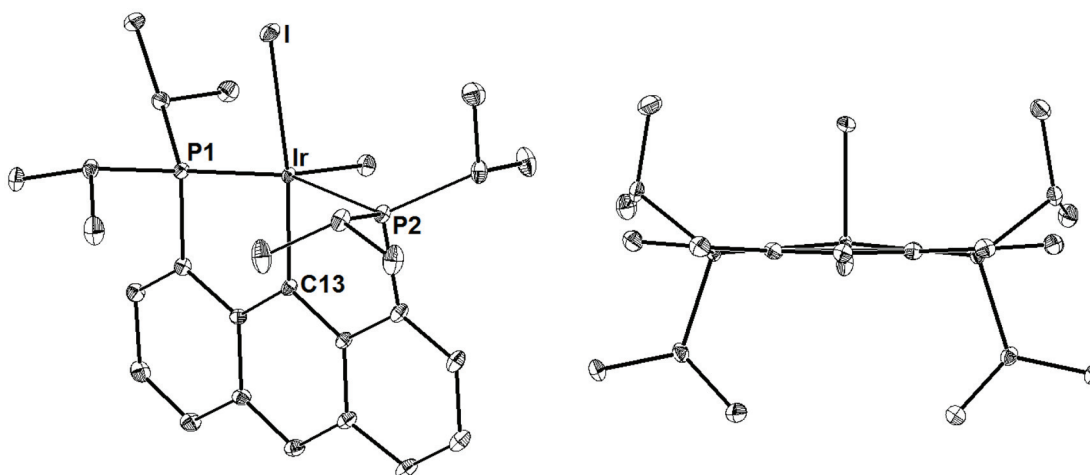


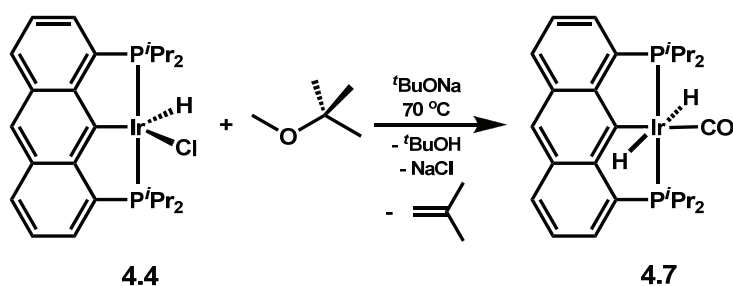
Figure 4.2. Displacement ellipsoid (35%) representation of (*i*PrAnthraphos)Ir(CH₃)I (**4.6**) (top and side view) with hydrogen atoms omitted for clarity. Selected bond lengths (Å) and angles (°): Ir–C13, 2.017(3); Ir–P1, 2.3009(8); Ir–P2, 2.3119(8); Ir–C27, 2.086(3); Ir–I, 2.6935(2); C13–Ir–I, 168.65(8); P1–Ir–P2, 163.78(3); C13–Ir–C27, 83.3(1); C27–Ir–I, 107.99(8).

Dehydrogenation of *tert*-Butyl Methyl Ether

To access the desired Fischer carbenes, reaction of the (PCP)Ir and (PNP)Ir fragments with *tert*-butyl methyl ether (MTBE) was investigated. MTBE is an ideal candidate since it can be used as both reacting partner and solvent. Furthermore, the bulky *tert*-butyl group should bias C–H activation events toward the desired and more accessible CH₃ group.

Initial experiments showed that the dinitrogen complex **4.5** was inactive toward C–H activation of MTBE, consistent with previous observations that the catalytic activity of PCP-supported catalysts in alkane dehydrogenation is strongly inhibited by the presence of dinitrogen.^{2,4,12} Despite rigorous exclusion of N₂ from the system, formation of **4.5** was also observed under an atmosphere of argon. Therefore, subsequent experiments were performed in evacuated systems using carefully degassed solvents.

Vacuum transfer of MTBE onto a mixture of **4.4** and ^tBuONa, followed by brief heating, generated a clear, brown solution from which an orange powder was isolated. ¹H NMR analysis of this material showed clean formation of a complex evidencing C_{2v} symmetry along with a diagnostic triplet hydride signal at –9.45 ppm (²J_{PH} = 15.0 Hz), and the ³¹P NMR spectrum showed a single resonance at 66.1 ppm. Solution IR spectroscopy (THF) showed a strong absorption in the carbonyl region at 1989 cm⁻¹. An absorption band assigned to the H–Ir–H asymmetric stretch was also observed at 1763 cm⁻¹, consistent with *trans*-disposed hydride ligands.¹⁵ Based on the spectroscopic evidence, the structure of this material was assigned as the *trans*-dihydrido carbonyl complex **4.7** (Scheme 4.6).



Scheme 4.6. Decarbonylation of MTBE at (^{iPr}AnthrPhos)Ir to give *trans*-dihydrido carbonyl complex **4.7**.

The identity of **4.7** was further confirmed by single-crystal X-ray diffraction. The analysis showed a carbonyl ligand located in the plane of the PCP ligand, although the hydride atoms

could not be located. Bond distances and angles in **4.7** are unremarkable and selected metrical parameters are shown in Figure 4.3.

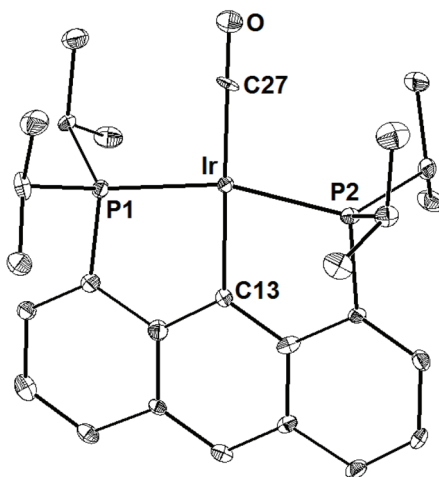
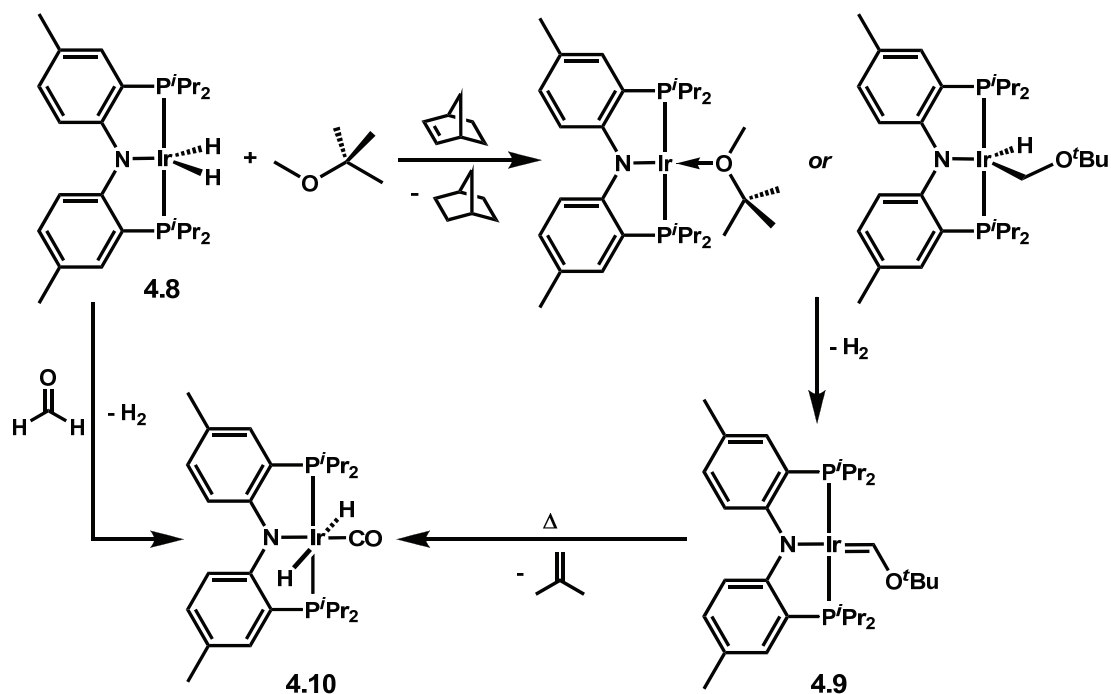


Figure 4.3. Structural representation of *trans*-(^{*i*}Pr-Anthraphos)Ir(H)₂(CO) (**4.7**) with thermal ellipsoids at 35% probability. Selected bond distances (Å) and angles (°): Ir–C13, 2.094(6); Ir–P1, 2.2941(15); Ir–P2, 2.3041(15); Ir–C27, 1.876(6); C13–Ir–C27, 178.7(2); P1–Ir–P2, 163.29(5).

In contrast to (PCP)Ir complexes, pincer derivatives of PNP ligand **4.1** show no tendency to form dinitrogen adducts, facilitating the study of C–H activation processes.^{6,10,16} Complex **4.8** reacts cleanly with norbornene in MTBE at room temperature to generate an intermediate observable by ³¹P NMR spectroscopy (45 ppm), which is formulated as the iridium(I)–MTBE adduct or its reactive equivalent, (PNP)Ir(H)(CH₂O^{*t*}Bu). This complex gradually converts to the desired Fischer carbene, (PNP)Ir=C(H)O^{*t*}Bu (**4.9**), over a period of 16 h at ambient temperature with loss of hydrogen (Scheme 4.7). Two equivalents of norbornene is necessary to ensure complete conversion because regeneration of **4.8** occurs readily upon exposure of the intermediate species to the generated hydrogen. The ¹H NMR spectrum of **4.9** contains a characteristic triplet shifted far downfield that represents the carbene proton (13.8 ppm, ³J_{PH} = 7.5 Hz).



Scheme 4.7. Formation and decarbonylative decomposition of (PNP)Ir=C(H)O^tBu (**4.9**).

Single-crystal XRD analysis confirmed the identity of **4.9** as the Fischer carbene and revealed a square-planar Ir(I) center with the carbene situated *trans* to the amido donor (Figure 4.4). The short Ir=C bond (1.88 Å) is consistent with those of previously reported iridium–carbon double bonds.¹⁷ Although a number of Fischer-type iridium carbenes are known, most examples feature an Ir(III) center.^{17,18} Complex **4.9** represents an unusual example of a square-planar Ir(I) center featuring this moiety.¹⁹ Interestingly, though the carbene substituents and C–N–C linkage are canted slightly out of the square plane, they are precisely aligned with each other, allowing a strong interaction between the filled π orbital of the amido donor and the empty π orbital of the *tert*-butoxymethylidene ligand (Figure 4.4).

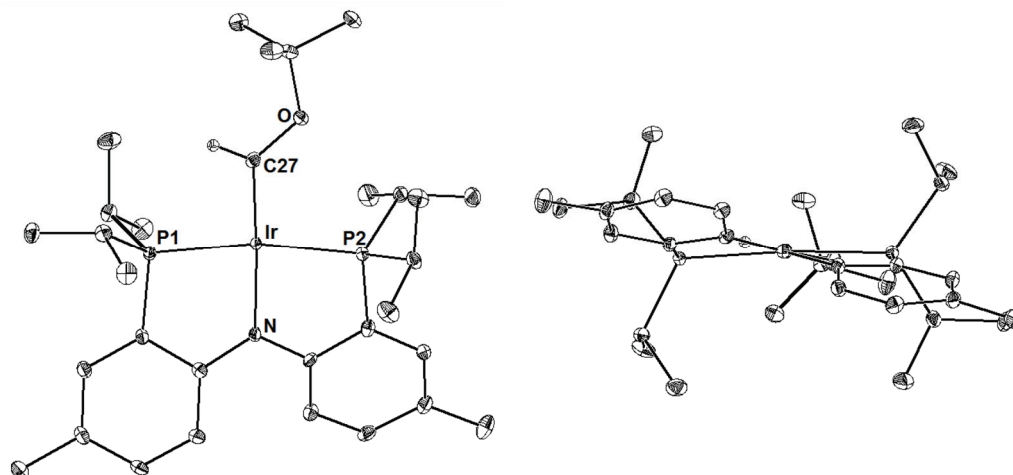


Figure 4.4. Displacement ellipsoid (35%) representation of (PNP)Ir=C(H)O^tBu (**4.9**) (top and side views) with hydrogen atoms omitted for clarity. Selected bond lengths (Å) and angles (°): Ir–N, 2.067(3); Ir–C27, 1.882(4); Ir–P1, 2.273(1); Ir–P2, 2.280(1); P1–Ir–P2, 165.80(4); N–Ir–C27, 177.4(1).

Carbene **4.9** undergoes smooth conversion to the *trans*-dihydrido carbonyl complex **4.10** upon thermolysis in C₆D₆ over a period of hours with concomitant elimination of isobutylene (detected by ¹H NMR spectroscopy). We have observed that **4.9** is thermally unstable both in solution and in the solid state, and crystalline samples of **4.9** are stored at –35 °C to avoid decomposition. The thermolysis of complex **4.8** in the presence of MTBE without a hydrogen acceptor can be readily monitored by NMR spectroscopy. The initial formation of carbene **4.9** and its subsequent decomposition to **4.10** are graphically shown in Chart 4.1. Under these conditions (sealed system), the reaction reaches a maximum of 50% conversion to the final product **4.10** due to reaction inhibition by generated hydrogen (*vide supra*).

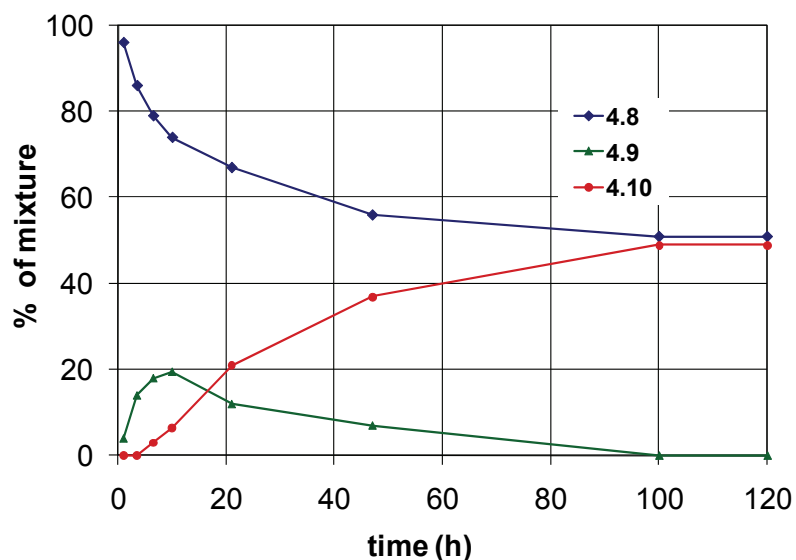


Chart 4.1. Thermolysis of **4.8** in neat MTBE.

The identity of **4.10** was confirmed by XRD analysis (Figure 4.5). The Ir–C14 bond (1.84 Å) is slightly shorter than the Ir–C27 bond of Fischer carbene complex **4.9** (1.88 Å), indicating that the effective bond orders in these complexes are similar. The infrared spectrum of compound **4.10** features a prominent carbonyl stretch ($\nu_{\text{CO}} = 1990 \text{ cm}^{-1}$) similar to that observed for the isostructural **4.7**.

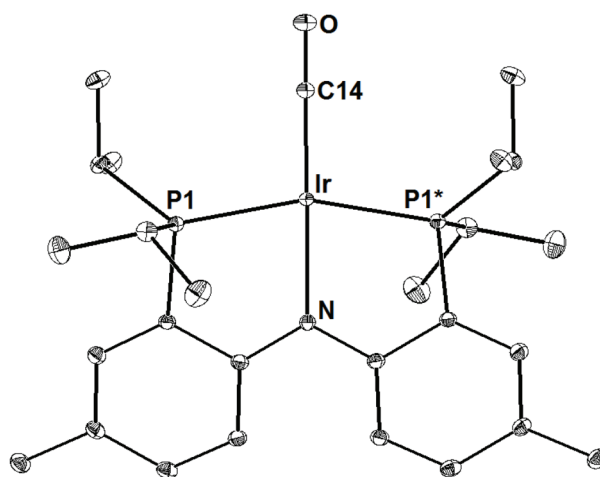
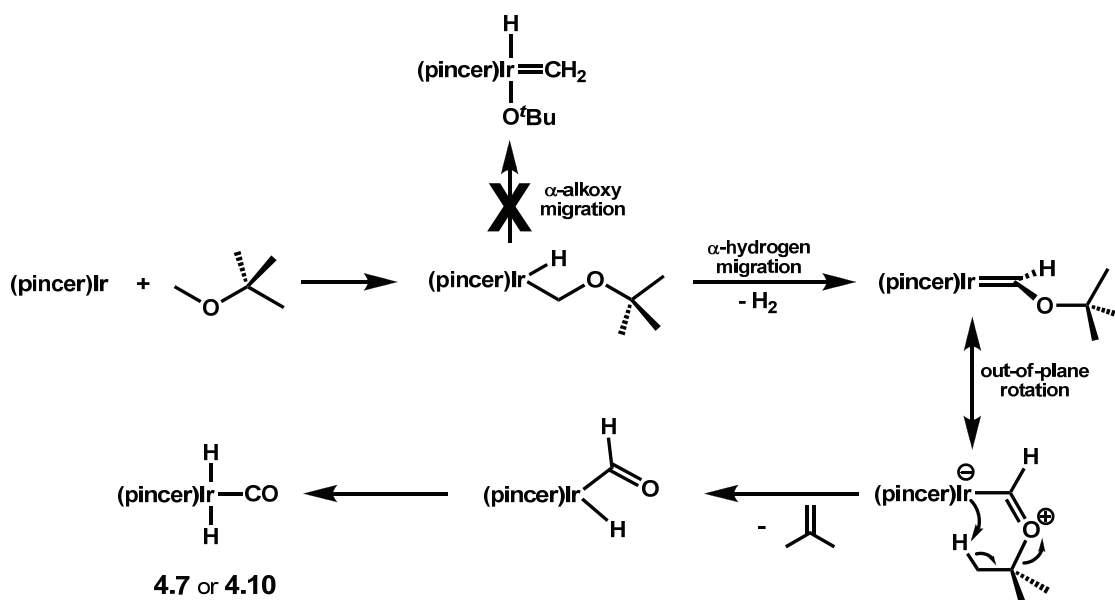


Figure 4.5. Displacement ellipsoid (35%) representation of *trans*-(PNP)Ir(H)₂(CO) (**4.10**) with hydrogen atoms and solvent molecules omitted for clarity. Selected bond lengths (Å) and angles (°): Ir–N 2.109(2), Ir–P1 2.3057(6), Ir–C14 1.841(2), N–Ir–C14 180.000, P1–Ir–P1* 160.18(2).

Mechanism of MTBE Decarbonylation

Complexes **4.7** and **4.10** are structurally related to Milstein's (ⁱPrPCP)Ir(H)₂(CO)^{15a} and Goldberg's [(^tBuPNP)Ir(H)₂(CO)]⁺,²⁰ with the latter being obtained by decarbonylation of methanol. This decarbonylation is thought to occur by β-hydrogen elimination of a metal-bound methoxide, followed by C–H activation of the newly formed formaldehyde.

In analogy to the results of Goldberg, we find that exposure of **4.8** to formaldehyde (37 weight % solution in H₂O) results in the immediate formation of **4.10** with loss of H₂ (Scheme 4.7). Based on this observation, we propose that the decarbonylation processes mediated by the (PCP)Ir and (PNP)Ir systems share common intermediates. Thus, thermodynamically favored **4.7** likely arises from a series of C–H activation events involving the intermediacy of an unobserved iridium Fischer-carbene complex. A plausible mechanism is depicted in Scheme 4.8.



Scheme 4.8. Proposed mechanism for decarbonylation of MTBE by (pincer)Ir frameworks.

Either reductive dehydrochlorination of **4.4** or dihydrogen elimination from **4.8** leads to the active 14-electron species which undergoes C–H oxidative addition, followed by α-hydrogen

migration and H₂ elimination to yield an alkoxy carbene. The fact that the hydride ligands in **4.7** and **4.10** are in a *trans* arrangement suggests a mechanism with a predisposition of the carbene fragment to afford this geometry. Therefore, we propose that the decarbonylation of **4.9** (as well as that of the unobserved carbene derived from **4.4**) occurs via an oxocarbenium-type zwitterionic species, where proton transfer from the *tert*-butyl substituent in a rigid intermediate leads to elimination of isobutylene. In solution we only observe a single resonance in the ³¹P NMR spectrum, indicating that the out-of-plane rotation required by this mechanism is facile. Even at -80 °C, only broadening of the ³¹P NMR resonance is observed, suggesting a low barrier for rotation. The mechanism proposed in Scheme 4.8 is further supported by the fact that the X-ray structure of carbene **4.9** shows a C27–O distance of 1.351(5) Å, suggesting a sizable degree of multiple bond character and therefore a significant contribution of the oxocarbenium-type canonical form. The unobserved formyl complex undergoes further stereoselective C–H activation, yielding the *trans*-dihydrido carbonyl species, in line with the observation that reaction of **4.8** and formaldehyde yields **4.10** cleanly. Notably, a potential α -alkoxy migration is not a competitive pathway after the first C–H activation event, and only α -hydrogen migration is observed to occur.

The key proton-transfer event in Scheme 4.8 which leads to elimination of isobutylene is also consistent with the predicted ground-state electronic structure of *tert*-butoxycarbene **4.9**. Seminal work by Vaska²¹ and later by Shriver and others²² showed that square-planar, d⁸ complexes generally possess a high-lying molecular orbital of d_{z²}-origin, causing square-planar iridium(I) complexes to exhibit a high degree of nucleophilicity and basicity. Thus, simple molecular-orbital considerations indicate that a high-energy Ir(d_{z²}) orbital should be competent to initiate the decarbonylation of carbene complex **4.9** by deprotonation of the *tert*-butoxy carbene substituent to eliminate isobutylene. As shown in Figure 4.6, the high-lying filled

orbitals are expected to be derived from Ir(d_{xz}) and Ir(d_{z^2}) orbitals since the Ir(d_{xz}) orbital should have strong π^* interactions with the diarylamido ligand. However, since the d_{xz} orbital may be significantly delocalized over the molecule, reactivity is expected to be dominated by the nucleophilic d_{z^2} that is oriented out of the square plane. As mentioned above, this finding would be consistent with the classical studies of Vaska and others.

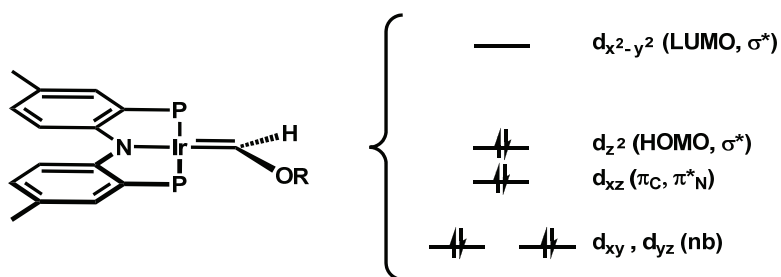
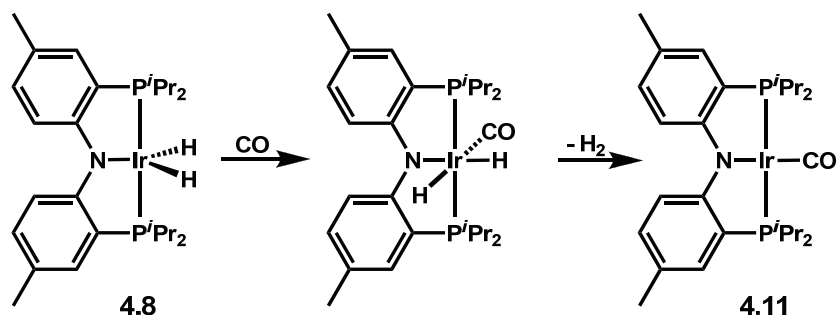


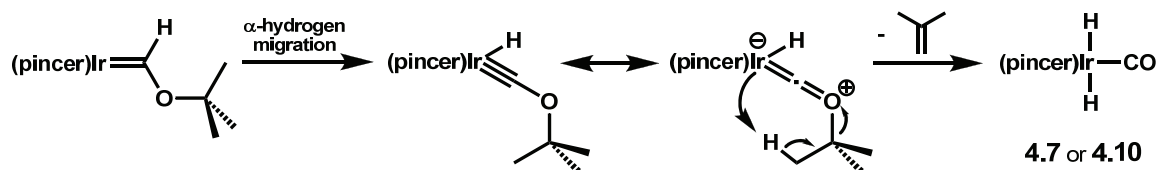
Figure 4.6. Predicted ground-state molecular-orbital diagram for carbene **4.9**.

Milstein and co-workers have reported that, under certain conditions, *cis*-(i^{Pr} PCP)Ir(H)₂(CO) undergoes thermal isomerization into the thermodynamically favored *trans*-(i^{Pr} PCP)Ir(H)₂(CO) isomer.^{15a} The intermediacy of a *cis*-dihydride for these systems was ruled out by a separate experiment. Reaction of **4.8** with CO leads to the exclusive formation of Ir(I) carbonyl complex **4.11** via formation of an unstable *cis*-dihydride which slowly eliminates H₂ (Scheme 4.9). This dihydride intermediate is characterized by a prominent IR band ($\nu_{\text{CO}} = 1960 \text{ cm}^{-1}$) and distinct high-field triplets of doublets in the ¹H NMR spectrum at -9.1 ppm ($^2J_{\text{PH}} = 18 \text{ Hz}$, $^2J_{\text{HH}} = 3.9 \text{ Hz}$) and -16.5 ppm ($^2J_{\text{PH}} = 11 \text{ Hz}$, $^2J_{\text{HH}} = 3.9 \text{ Hz}$). Carbonyl complex **4.11** shows a strong CO absorption at 1930 cm^{-1} .



Scheme 4.9. Reaction of (PNP)IrH₂ (**4.8**) with excess carbon monoxide.

Alternatively, a second decarbonylation mechanism could also be operative. The Fischer carbene in both systems could undergo a second α -hydrogen migration event to give a Fischer-type alkoxy-carbyne (Scheme 4.10). This step would install the first hydride and would be immediately followed by hydrogen delivery from the *tert*-butyl group on the opposite side of the metal center, with elimination of isobutylene.



Scheme 4.10. An alternative mechanism for carbene decarbonylation by generation of an alkoxy-carbyne.

Terminal alkoxy-carbynes are rare, and certainly unknown for Group 9 metals, but recent work by Templeton and co-workers has shown that for certain tungsten complexes they are indeed isolable species.²³ Protonation of Templeton's alkoxy-carbyne leads to formation of a tungsten Fischer carbene, and the carbene proton engages in an agostic interaction with the metal center, suggesting an intermediate situation where the hydrogen is shared by both the metal and the carbene carbon.²³ In the solid state, we find no evidence of an agostic contact in carbene **4.9**. This is largely because, as mentioned above, the carbene fragment is found in the plane of the pincer framework due to conjugation with the amido group. Such an agostic

interaction would be expected to precede the proposed formation of the hydrido-alkoxycarbyne intermediate in Scheme 4.10. Although the Ir=C bond is indeed fluxional in solution, no evidence for a C–H agostic interaction is observed in the ^1H NMR spectrum. Although we cannot rule out this mechanism, based on the available evidence, we favor the path delineated in Scheme 4.8.

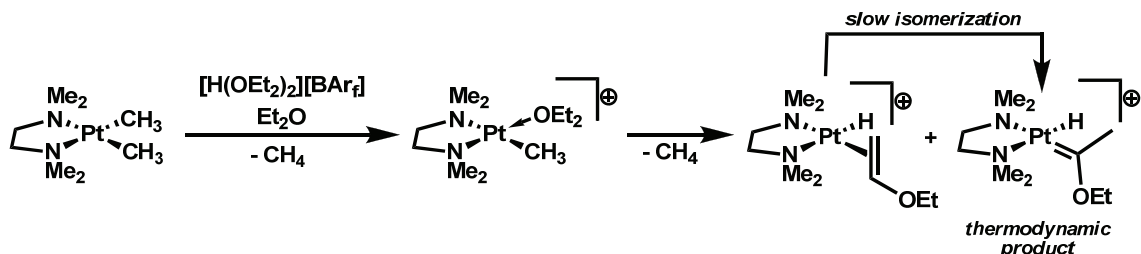
Reaction of (PNP)Ir with Other Linear and Cyclic Ethers

Encouraged by these initial results indicating that the (PNP)Ir framework is capable of generating heteroatom-substituted carbene complexes by multiple C–H activations, we endeavored to explore the generality of this reactivity. Development of a double C–H activation route as a general method for the preparation of heteroatom-substituted carbenes would have at least two distinct advantages. First, if catalytic group transfer chemistry could be realized as a route to C–H functionalization, it would be critical to expand the substrate scope beyond MTBE. Second, the elimination process that leads to decomposition of the *tert*-butoxymethylidene complex **4.9** might be less favorable for carbenes with other substituents, so these complexes may be significantly more stable than the original *tert*-butoxymethylidene **4.9**.

In our previous studies of ether C–H activation, MTBE was utilized as a substrate in order to preclude the possibility of β -hydrogen elimination, thereby favoring an α,α -dehydrogenative process to afford a carbene adduct. However, we were interested in whether such a process might be observed for other ethereal substrates, especially those containing β -hydrogen atoms. Several reports have demonstrated that α -hydrogen elimination can be kinetically favored at sterically congested early metal centers.²⁴ Although systems that are amenable to the study of competitive α - and β - processes at late metals have only recently been developed,²⁵ it is clearly necessary to develop an understanding of the factors controlling these

steps if catalytic reactions involving multiple C–H activations and metal carbene generation are to be realized.

In this context, two salient examples of selective carbene formation at late metal centers merit attention. Bercau and co-workers have demonstrated that dehydrogenation of diethyl ether at TMEDA-supported Pt(II) occurs via both α,α - and α,β -modes, initially affording a mixture of carbene and vinyl ether adducts of Pt(II) (TMEDA = *N,N,N',N'*-tetramethylethylenediamine).²⁶ However, slow isomerization of the vinyl ether complex led to isolation of the diethyl ether-derived carbene as the thermodynamic product (Scheme 4.11). On the other hand, Carmona and co-workers have reported that a relatively more encumbered tris(pyrazolyl)borate iridium(III) system reacts with diethyl ether and a number of cyclic ethers to afford Fischer-type carbenes as the sole products, and in these instances vinyl ethers are not observed.^{18a,c,27}



Scheme 4.11. Dehydrogenation of diethyl ether at (tmeda)Pt to afford vinyl ether and carbene adducts.

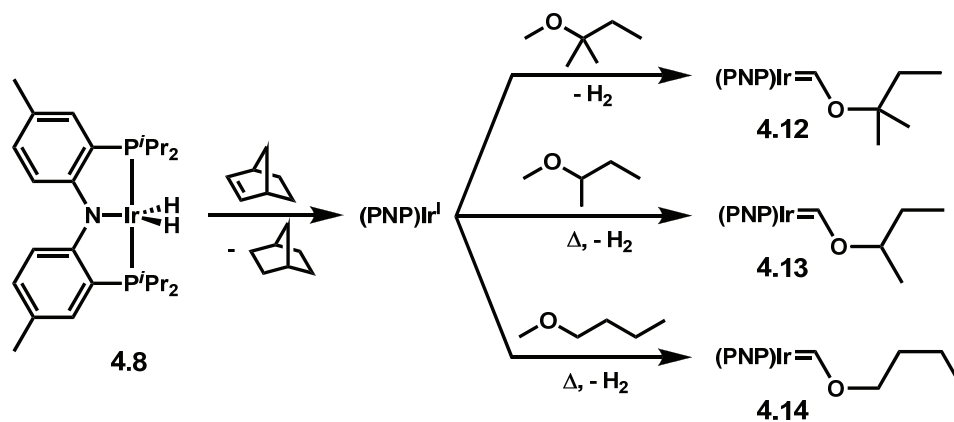
Here we report on the C–H activation of a series of linear and cyclic ethers by (PNP)Ir. Depending on the substrate, this process affords the products of α,α -dehydrogenation (carbenes), α,β -dehydrogenation (vinyl ethers), or decarbonylation. Examination of these reactions has led to the characterization of a number of species along the reaction profile for carbene formation and has also provided insight into the variety of pathways utilized by the

electron-rich, unsaturated (PNP)Ir fragment to stabilize itself by transferring electron density to ethereal substrates through oxidative addition and/or the formation of π -acidic ligands.

α,α -Dehydrogenation of Ethers at (PNP)Ir. In light of our previous success generating *tert*-butoxymethylidene **4.9** by double C–H activation of MTBE, several other methyl ethers were initially targeted as potential carbene precursors. As expected, reaction of (PNP)IrH₂ (**4.8**) with norbornene in *tert*-amyl methyl ether led to facile generation of the corresponding carbene complex **4.12** with loss of hydrogen (Scheme 4.12). As with **4.9**, immediate formation of a long-lived intermediate is observed by ³¹P NMR spectroscopy (δ 45 ppm), followed by slow appearance of **4.12**. Like carbene **4.9**, complex **4.12** is unstable to thermolysis, decomposing by a similar mechanism to afford *trans*-(PNP)Ir(H)₂(CO) upon heating for several hours at 70 °C. The spectroscopic parameters of **4.12** are remarkably similar to those of **4.9**, particularly the distinctive carbene ¹H (δ 13.8 ppm, t, ³J_{PH} = 7.5 Hz) and ¹³C (δ 210 ppm) chemical shifts observed by NMR spectroscopy.

Encouraged by this result, we turned our attention to *sec*-butyl methyl ether (SBME) and *n*-butyl methyl ether (NBME) as linear ethers with multiple protons α - to oxygen that might serve as sites for an initial C–H cleavage event. In the case of SBME, methyl activation would be expected to lead to carbene formation, as with MTBE, whereas methine C–H activation should afford only vinyl ethers since double C–H activation at this site is not possible. For NBME, carbene formation should likewise be favored after an initial methyl C–H activation event, whereas methylene C–H activation could yield either the corresponding vinyl ether or carbene. In light of the many possible products that could be formed by upon interaction of (PNP)Ir with these linear ethers, we were pleased to find that both SBME and NBME were dehydrogenated exclusively to (PNP)Ir=C(H)O^{sec}Bu (**4.13**) and (PNP)Ir=C(H)OⁿBu (**4.14**), respectively, upon

addition of excess norbornene (3 equiv) to a solution of dihydride **4.8** in the appropriate solvent, followed by brief heating (Scheme 4.12). Like compound **4.12**, the carbene complexes **4.13** and **4.14** are similar spectroscopically to *tert*-butoxymethylidene **4.9**, exhibiting diagnostic ^{13}C NMR signals that are slightly downfield from that of **4.9** (δ 216.4 ppm for **4.13**, 216.3 ppm for **4.14**).

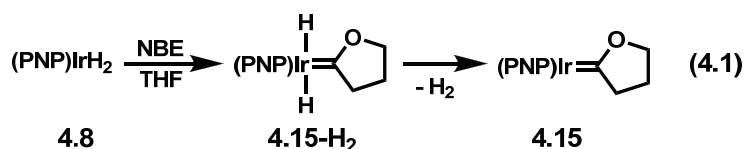


Scheme 4.12. Formation of carbenes from methyl ethers at (PNP)Ir.

Several systems have been reported for which methyl C–H activation occurs with high selectivity in the presence of methylene and/or methine protons, though this is not an entirely general observation.²⁸ In this case, the observation of carbenes as the sole products from C–H activation of SBME and NBME shows that (PNP)Ir either exhibits a high affinity for the less encumbered H–CH₂O bonds or, if methylene or methine C–H activation is accomplished, such a pathway is unproductive. Since the complete conversion of **4.8** to **4.13** and **4.14** occurs only in the presence of excess norbornene, it is possible that some equivalents of NBE are consumed in a competing transfer dehydrogenation process such as those previously reported for heteroatom-containing substrates at (PCP)Ir²⁹ and observed for our (PNP)Ir system with diethyl ether (*vide infra*). The possibility of competing transfer dehydrogenation and the factors dictating selectivity in these reactions are currently the subject of theoretical studies.³⁰ In any

case, these results point to the possible use of SBME and NBME as well as more highly functionalized methyl ethers in catalytic oxidation schemes involving multiple C–H activations.

Encouraged by these results with methyl ethers and inspired by previous reports of carbene formation from tetrahydrofuran (THF), dehydrogenation of THF by (PNP)Ir was examined. Generation of the (PNP)Ir fragment in THF resulted in the immediate appearance of a new species which was observed by ^{31}P NMR (δ 46.7 ppm). This complex could not be cleanly isolated due to slow decomposition to another species, observed at δ 43.1 ppm by ^{31}P NMR. Thermolysis of the solution (60 °C, 7 h) resulted in complete conversion to the second species, which was identified as the carbene complex derived from α,α -dehydrogenation of THF (**4.15**, eq 4.1). As expected, this complex is quite thermally stable since any decarbonylation pathways, such as those observed for **4.9** and **4.12**, would necessarily invoke an unfavorable carbon–carbon bond cleavage, and this thermal stability may have important implications on catalytic reactions involving cyclic carbenes such as **4.15**.



Carbene **4.15** was analyzed by single crystal X-ray diffraction (XRD), revealing a structure remarkably similar to that of the MTBE-derived carbene **4.9** (Figure 4.7). As previously noted for **4.9**, the carbene cants slightly to allow a push–pull interaction between the filled π amido and empty π carbene orbitals. The Ir–C14 bond is only slightly longer than that observed for complex **4.9** (1.92 Å versus 1.88 Å). The structure of **4.15** suffers from disorder due to a crystallographically-imposed C_2 axis containing the C14, Ir, and N atoms, resulting in positional disorder between the O1 and C15 atoms of the cyclic carbene. Nevertheless, this disorder was

satisfactorily modeled with partially occupied C15 and O1 atomic positions, as described in the Experimental Section.

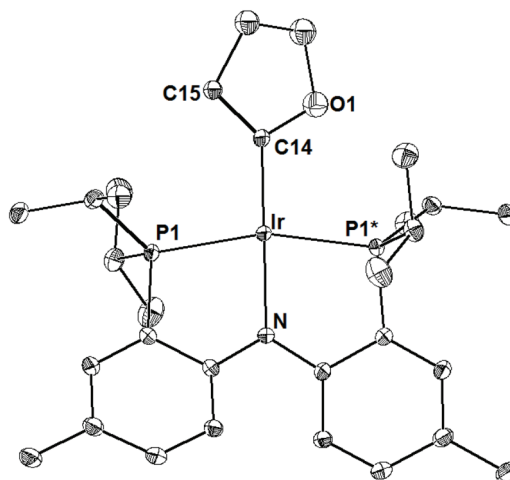
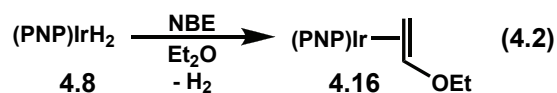


Figure 4.7. Structural representation of (PNP)Ir=CO(CH₂)₃ (**4.15**) with ellipsoids at 35% probability. Selected bond lengths (Å) and angles (°): Ir–N, 2.073(3); Ir–P1, 2.287(1); Ir–C14, 1.921(4); C27–O, 1.357(7); N–Ir–C14, 180.0; N–Ir–P1, 81.56(2); P1–Ir–P1*, 163.12(3).

The intermediate species in the reaction leading to **4.15** was also accessible via an alternate synthesis, allowing its full solution characterization and identification. Addition of excess 2,3-dihydrofuran (3 equiv) to a solution of dihydride **4.8** in benzene-*d*₆ led to quantitative generation of the same intermediate observed in the formation of carbene **4.15**, which was identified as the *trans*-dihydrido carbene complex **4.15-H₂** (eq 4.1), a structural and electronic relative of the *trans*-dihydrido aminocarbenes previously reported.³¹ **4.15-H₂** exhibits *C*_{2v} symmetry in solution, indicating that rotation about the iridium–carbon bond is fast on the NMR time-scale, as expected based on the similar behavior of **4.9** and related aminocarbenes.³¹ The ¹H NMR spectrum of **4.15-H₂** shows a triplet hydride resonance characteristic of such a complex (δ –7.86 ppm, t, ²J_{PH} = 15 Hz, 2H), as well as a distinctive carbene resonance in its ¹³C NMR spectrum (δ 261.2 ppm). In order to lose hydrogen and generate **4.15**, complex **4.15-H₂** must isomerize to place the hydride ligands in a *cis* configuration to allow for reductive elimination of

hydrogen, but a buildup of the *cis*-dihydrido isomer *cis*-**4.15-H₂** is not observed.³² The loss of hydrogen is likely a thermodynamically uphill process, as previously indicated in computational studies of a related system by Yates and co-workers.³³ Thus, the rate of formation of **4.15** is probably governed both by the isomerization of **4.15-H₂** and by a hydrogen-scavenging process that is similar to that outlined by Yates and co-workers in the dehydrogenation of MTBE,³³ and the role of these processes is discussed in more detail below.

α,β -Dehydrogenation of Ethers at (PNP)Ir. The findings described above demonstrated that THF exhibits a strong preference for α - over β -elimination at (PNP)Ir. This result is in contrast with previous reports regarding the transfer dehydrogenation of THF to 2,3-dihydrofuran and furan at pincer-supported iridium centers,³⁴ though there are a number of other systems that preferentially generate cyclic carbenes via C–H activation of THF.^{17a,27,35} Thus, we endeavored to determine whether such a preference for carbene formation in the presence of β -hydrogen atoms would be general, as with Carmona's tris(pyrazolyl)borate complexes,^{18a,c,35} or limited to THF, as was observed for Bergman's Cp*(PMe₃)Ir system.^{17a} Reaction of (PNP)IrH₂ (**4.8**) with norbornene in diethyl ether leads to the immediate formation of two products observed by ³¹P NMR spectroscopy at 47.5 ppm (sharp singlet) and 29.5 ppm (broad singlet). Over a period of 16 h, these convert cleanly to the ethyl vinyl ether adduct of iridium(I), (PNP)Ir(H₂C=C(H)OEt) (**4.16**) (eq 4.2). This divergent behavior with respect to THF and diethyl ether resembles that observed for the Cp*(PMe₃)Ir system of Bergman, which effects α,α -dehydrogenation and carbene formation from dimethyl ether, MTBE, and THF, but affords an ethyl vinyl ether adduct by α,β -dehydrogenation of diethyl ether.



Single crystals of vinyl ether adduct **4.16** were characterized by XRD analysis, and a molecular representation of **4.16** is provided in Figure 4.8. Of particular note is the orientation of the vinyl ether fragment, which is canted slightly to allow through-metal interaction of the filled amido π orbital and the empty π^* orbital of the ethyl vinyl ether. The consequences of this interaction as well as strong π -donation from the electron-rich iridium(I) center are manifested in the C27–C28 bond,³⁶ which at 1.46 Å is significantly elongated relative to crystallographically characterized free vinyl ethers (typically ca. 1.30 Å)³⁷ and other metal-bound vinyl ethers (e.g., 1.36 Å in a Pd(II) vinyl ether complex).³⁸ The complex also exhibits C_1 symmetry by NMR spectroscopy due to slow rotation of the vinyl ether ligand.

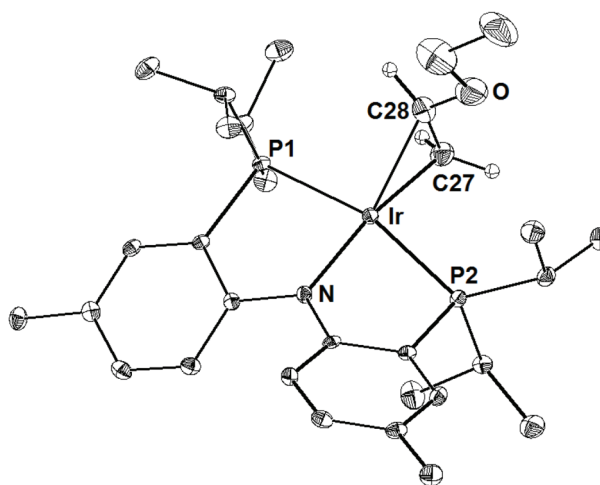


Figure 4.8. Displacement ellipsoid (35%) representation of ethyl vinyl ether adduct **4.16** with hydrogen atoms (except those attached to C27 and C28) omitted for clarity. Selected bond lengths (Å) and angles (°): Ir–N, 2.056(3); Ir–P1, 2.2827(10); Ir–P2, 2.2987(10); Ir–C27, 2.125(3); Ir–C28, 2.174(4); C27–C28, 1.464(7); N–Ir–P1, 82.27(8); N–Ir–P2, 80.92(8); P1–Ir–P2, 162.54(3); N–Ir–C27, 165.37(12); N–Ir–C28, 154.79(12).

In order to probe whether preference for carbene versus olefin formation is related to whether the ether is cyclic, the C–H activation of 1,4-dioxane and of tetrahydropyran (THP) by (PNP)Ir was explored. Reaction of (PNP)IrH₂ (**4.8**) with norbornene in the presence of THP inevitably leads to regeneration of **4.8** as the major product, even when an excess of NBE is

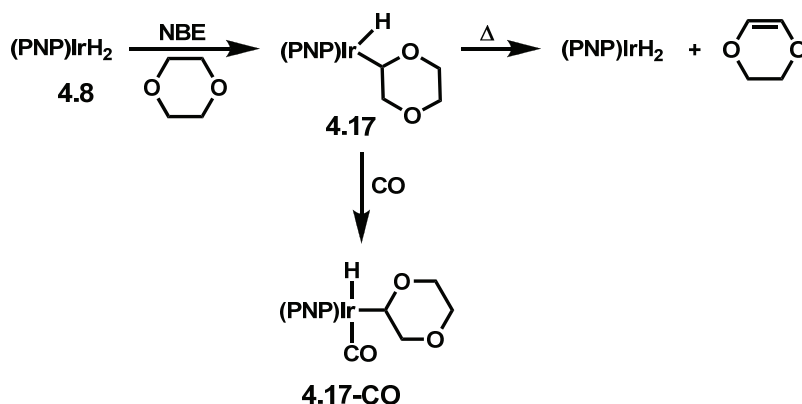
utilized. Unfortunately, this reaction does not proceed cleanly and the products have not been thoroughly characterized. Nonetheless, it is likely that THP participates in a facile transfer dehydrogenation process.

Reaction of (PNP)IrH₂ (**4.8**) with norbornene in 1,4-dioxane resulted in the immediate formation of a new product exhibiting two doublet resonances in its ³¹P NMR spectrum (δ 46.5 and 43.7 ppm, ²J_{PP} = 322 Hz). However, direct isolation of this species proved elusive, as complete removal of solvent or thermolysis led to regeneration of starting material **4.8** with expulsion of 2,3-dihydro-1,4-dioxine.

The product from reaction of (PNP)Ir with 1,4-dioxane was ultimately characterized by a combination of methods. Partial removal of solvent and reconstitution of the mixture in benzene-d₆ allowed characterization of the intermediate by ¹H NMR, revealing a distinct triplet hydride signal at -34.2 ppm (²J_{PH} = 13 Hz). The position of this resonance is consistent with a Y geometry, a highly distorted trigonal bipyramidal structure with an acute H-Ir-X angle.³⁹ This orientation might be expected for a hydrido alkyl complex of (PNP)Ir based on the presence of a π -basic amido donor as well as comparison to (PNP)Ir(Ph)(H)¹⁰ and similar Y-shaped dialkyl complexes reported by Fryzuk and co-workers.⁴⁰ Thus, on the basis of comparison to similar complexes as well as the symmetry of the species, it seemed most likely that this intermediate was the product of a single C-H oxidative addition of 1,4-dioxane to (PNP)Ir, affording (PNP)Ir(H)(1,4-dioxan-2-yl) (**4.17**) (Scheme 4.13).

Goldman has shown that the five-coordinate (PCP)Ir(H)(Ph), which easily undergoes reductive elimination of benzene, may be trapped by addition of CO to afford the stable six-coordinate iridium(III) adduct.⁴¹ Such a route to stabilization of a five-coordinate species is consistent with previous studies by Goldberg and others indicating that reductive elimination from d⁶ transition metals preferentially occurs from five- rather than six-coordinate

intermediates,⁴² a finding that has previously been confirmed for complexes of (PNP)Ir.⁴³ Thus, we found that trapping of **4.17** with carbon monoxide (1 atm) allowed isolation and full spectroscopic characterization of (PNP)Ir(H)(1,4-dioxan-2-yl)(CO) (**4.17-CO**, Scheme 4.13), further supporting the assignment of **4.17** as the single C–H oxidative addition product of 1,4-dioxane. This complex is structurally related to a previously reported carbonyl adduct of a (PNP)-supported aminoalkyl hydride complex of iridium(III) and exhibits a diagnostic carbonyl stretch in its infrared absorbance spectrum ($\nu_{\text{CO}} = 1980 \text{ cm}^{-1}$).³¹



Scheme 4.13. C–H activation of dioxane at (PNP)Ir.

These findings regarding the reactivity of (PNP)Ir with 1,4-dioxane and THP indicate that the preference for carbene versus olefin formation in this system cannot be ascribed simply to whether the ether is linear or cyclic. The observed product selectivity is due to a subtle combination of factors, and thus it is possible that the preference of THF for carbene formation in the presence of β -hydrogen atoms is substrate-specific. In related work, Caulton and co-workers have reported that the $(^i\text{Pr}_3\text{P})_2\text{Ru}(\text{H})(\text{Cl})$ converts THF and piperidine into heteroatom-substituted carbenes but not their six-membered counterparts.³⁵ Thus, although six-membered rings have been reported to form metal carbenes by multiple C–H activations,²⁷ our findings point to the possibility that five-membered ring systems are especially predisposed to α,α -dehydrogenation and carbene complex formation.

Decarbonylation of Ethers at (PNP)Ir. The α,β -dehydrogenation process that was observed for diethyl ether and 1,4-dioxane suggested that other substrates should be examined for which such a reaction would not be possible, or at least would not be facile. In this context, benzyl methyl ether was an attractive candidate since no β -elimination would be possible and, if a benzyloxymethylidene were to be formed, it would be incapable of decomposing by the decarbonylative pathways observed for carbene complexes **4.9** and **4.12** (*vide supra*). Thus, we were surprised to find that exposure of (PNP)IrH₂ (**4.8**) to norbornene in benzyl methyl ether resulted in the immediate formation of a new iridium complex containing hydride and carbonyl ligands, as judged by NMR and IR spectroscopy ($\nu_{\text{CO}} = 1995 \text{ cm}^{-1}$). Single crystals of the complex were analyzed by XRD, allowing definitive identification of the product as (PNP)Ir(Ph)(CO)(H) (**4.18**) (Figure 4.9).

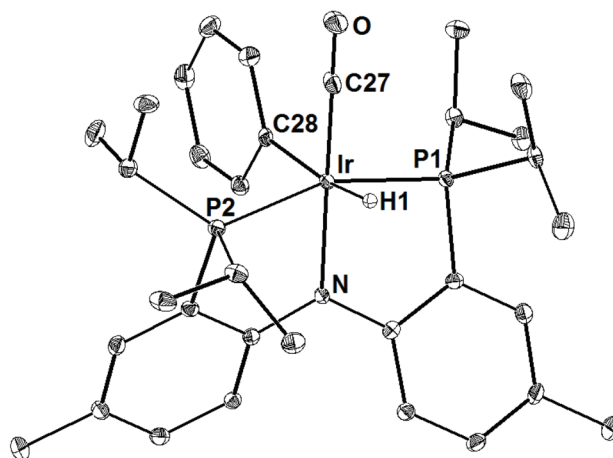
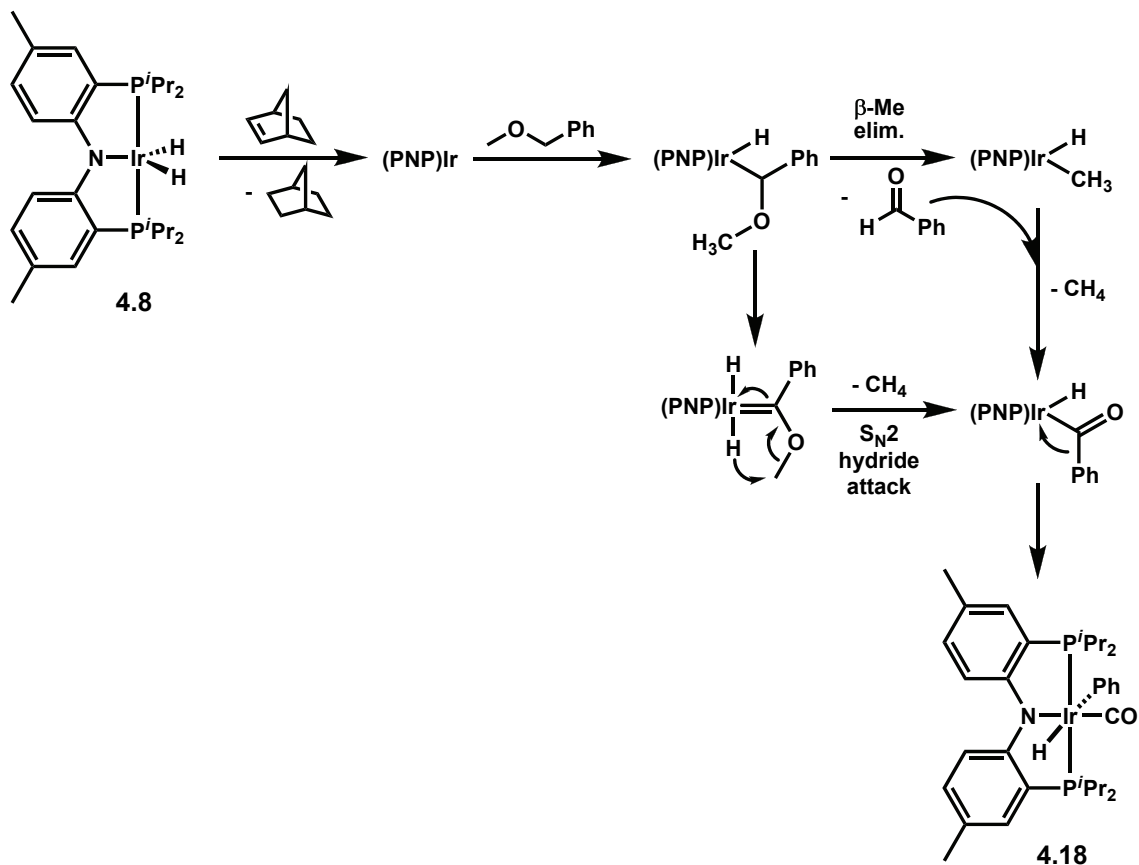


Figure 4.9. Structural representation of (PNP)Ir(Ph)(CO)(H) (**4.18**) with ellipsoids at 35% probability. Selected bond lengths (Å) and angles (°): Ir–N, 2.1083(16); Ir–P1, 2.3204(5); Ir–P2, 2.3223(5); Ir–C27, 1.847(2); Ir–C28, 2.1595(19); C27–O, 1.148(3); N–Ir–C27, 176.86(9); N–Ir–P1, 82.55(4); N–Ir–C28, 90.13(7); P1–Ir–P2, 161.194(19); P1–Ir–C27, 98.52(7); P1–Ir–C28, 91.62(5); C27–Ir–C28, 92.79(9).

This decarbonylation is quite remarkable, in that it involves the cleavage of C_{sp3}–H, C_{sp3}–O, and C_{sp3}–C_{sp2} bonds. The carbon–carbon bond cleavage is particularly unusual. Although scission of C_{sp3}–C_{sp2} bonds at Group 9 metals has been reported,⁴⁴ these processes typically

occur only in systems where the bond is tied into a polydentate pincer-type ligand that preorganizes the complex for C–C activation.^{45,46} In this case, the structural similarities between complex **4.18** and the previously characterized *trans*-(PNP)Ir(H)₂(CO) (**4.10**), which was shown to be formed stereoselectively from a hydrido formyl complex of iridium(III), suggested that a hydrido benzoyl iridium(III) complex might be the immediate precursor of **4.18**. 1,2-Alkyl migration at late metal acyls is a step with considerable precedent⁴⁷ and is important in the catalytic decarbonylation of aldehydes.⁴⁸

Thus, we propose that the unusual decarbonylation of benzyl methyl ether is in this case made possible by a series of bond activations and rearrangements that lead to formation of benzaldehyde (Scheme 4.14). The reaction is likely initiated by oxidative addition of a weak benzylic C–H bond to the (PNP)Ir fragment. Subsequent β -methyl elimination, with C–O bond cleavage, leads to loss of benzaldehyde and generation of an iridium(III) methyl hydride,⁴⁹ which is expected to reductively eliminate methane readily, regenerating the (PNP)Ir fragment. The reactive fragment should oxidatively add the acyl C–H bond easily, and stereoselective 1,2-phenyl migration at the resulting benzoyl hydride iridium(III) complex affords the observed complex **4.18**.⁵⁰



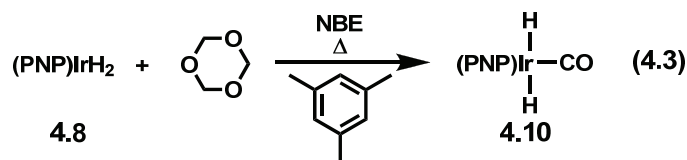
Scheme 4.14. Proposed mechanisms of benzyl methyl ether decarbonylation at $(\text{PNP})\text{Ir}$.

An alternative possible mechanism that avoids the unusual thermodynamically uphill release of benzaldehyde involves formation of a dihydrido carbene complex by double C–H activation at the benzylic position. Subsequent nucleophilic attack by the bound hydride at the methoxy position would lead to release of methane with formation of a $(\text{PNP})\text{Ir}$ -supported benzoyl hydride complex, which could undergo 1,2-phenyl migration to afford the observed complex **4.18**. This mechanism is somewhat problematic in that the $\text{S}_{\text{N}}2$ -type nucleophilic attack of hydride would be expected to be disfavored by Baldwin's rules,⁵¹ even with the allowance that a large iridium center expands the ring size of the intermediate. Additionally, it does not explain why other related dihydrido carbene species reported previously and in this paper do not undergo similar decomposition mechanisms.³¹

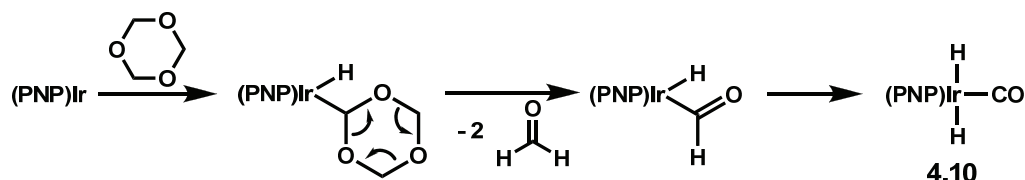
Both mechanistic proposals are supported by the observation that (PNP)IrH₂ (**4.8**) reacts immediately with benzaldehyde to afford complex **4.18** upon loss of H₂. They are also substantiated by the detection of methane (¹H NMR spectroscopy) upon vacuum transfer of volatile components from the decarbonylation reaction onto frozen C₆D₆ in a J. Young tube. At this point, however, we have not been able to distinguish between these two mechanistic possibilities.

The overall course of this reaction is quite similar to the decarbonylation of alcohols with C–C cleavage observed by Kubas and Caulton⁵² and Tilley and Bergman.⁵³ It also resembles the conversion of secondary amines to isocyanides investigated by Goldman.⁵⁴ However, this reaction is distinct in that oxidation occurs via C_{sp3}–O cleavage rather than the typically much more facile O–H or N–H cleavage, and it may point to new mechanistic possibilities for carbon functionalization via C–C activation.⁵⁵

The C–H activation of 1,3,5-trioxane was also investigated with the motivation of blocking β-hydrogen elimination and favoring carbene generation, since such a substrate would provide a rough estimate for the difficulty in realizing α-elimination from 1,4-dioxane, which is also a six-membered cyclic ether. These reactions were made slightly more difficult by the fact that 1,3,5-trioxane is a solid at ambient temperature, so they were carried out in mesitylene. Addition of a mesitylene solution of norbornene and 1,3,5-trioxane to solid (PNP)IrH₂ (**4.8**) leads to the generation of three products at ambient temperature: the previously characterized (PNP)Ir(H)(mes) (60%),⁴³ *trans*-(PNP)Ir(H)₂(CO) (**4.10**, 15%), and a third unknown species (25%). However, at elevated temperatures, all three complexes cleanly convert to *trans*-(PNP)Ir(H)₂(CO) (**4.10**, eq 4.3), which was previously characterized as the product generated upon thermolytic decomposition of *tert*-butoxymethylidene **4.9**.



This result is not unexpected when considering that 1,3,5-trioxane is a formal trimer of formaldehyde, with which (PNP)IrH₂ (**4.8**) reacts to generate complex **4.10**. Previous reports have shown that the depolymerization of 1,3,5-trioxane may be promoted by strongly acidic catalysts.⁵⁶ In contrast, it seems most likely in this case that a compound derived from C–H activation of 1,3,5-trioxane readily disproportionates to release formaldehyde. One possible mechanism for this transformation is depicted in Scheme 4.15.



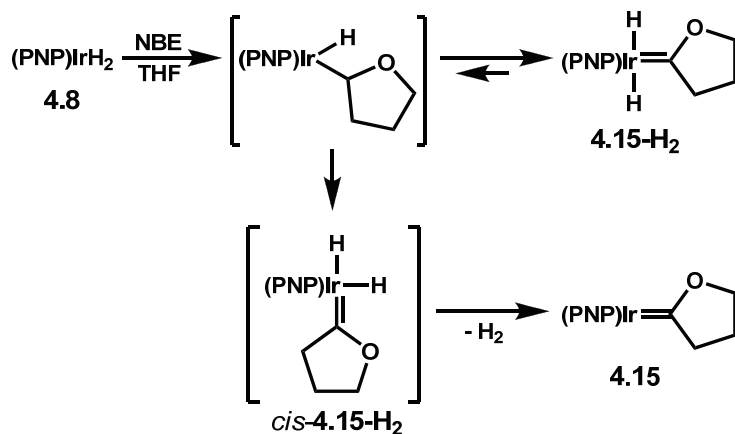
Scheme 4.15. Possible mechanism for decarbonylation of 1,3,5-trioxane at (PNP)Ir.

Probing the Mechanism of Carbene Formation

The results described in the preceding sections begin to provide a framework for understanding and predicting the ultimate course that C–H activation reactions at (PNP)Ir will take with a variety of cyclic ethers. Perhaps more interesting is that these reactions, especially those involving THF and 1,4-dioxane, have allowed characterization of species believed to be important intermediates in the α,α - and α,β -dehydrogenation processes and have prompted reexamination of the previously reported dehydrogenation of MTBE to afford carbene **4.9**.

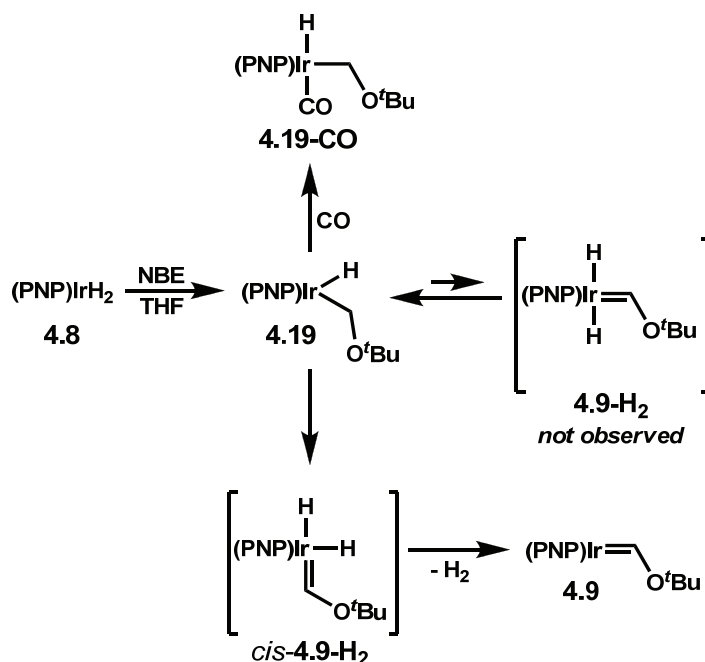
As noted above, the dehydrogenation of THF proceeds by immediate generation of the carbene **4.15-H₂**, which contains hydride ligands in a *trans* orientation and gradually converts to the thermodynamic product **4.15** with loss of hydrogen. Thus, the formation of **4.15** proceeds by

a pathway, as depicted in Scheme 4.16, where C–H oxidative addition at (PNP)Ir and α -hydrogen elimination to form the kinetically favored **4.15-H₂** occur quickly. The α -elimination step is reversible, and the rate of H₂ loss to generate **4.15** is limited by isomerization from **4.15-H₂** to *cis*-**4.15-H₂**. That the isomerization of **4.15-H₂** to *cis*-**4.15-H₂** is slow and requires elevated temperatures is not surprising when compared to similar results regarding the *trans* to *cis* isomerization dihydrido aminocarbene complexes of (PNP)Ir.³¹ In the case of the aminocarbenes, H₂ loss is not observed because the more electron-releasing aminocarbene ligand confers proportionally greater basicity to the iridium center and precludes the reductive elimination of hydrogen. However, our failure to observe any intermediate species corresponding to *cis*-dihydrido isomers of **4.15-H₂** likely indicates that hydrogen loss from *cis*-**4.15-H₂** is facile for the less basic alkoxy-carbenes. Additionally, our failure to observe a product of the first C–H oxidative addition of THF such as **4.17**, which formed from 1,4-dioxane, suggests that the selective formation of a carbene from THF is due at least in part to the greater stability of carbene relative to α -oxoalkyl hydride at (PNP)Ir for this five-membered cyclic ether. This behavior may be general, especially since it is in accord with the findings of Bergman for Cp*(PMe₃)Ir^{17a} and Caulton for (iPr₃P)₂Ru(H)(Cl).³⁵



Scheme 4.16. Proposed mechanism of formation for carbene **4.15**.

These findings concerning the formation of **4.15** prompted us to reexamine the formation of *tert*-butoxymethylidene **4.9** from MTBE. We wondered whether the long-lived intermediate observed during the preparation of **4.9** was a dihydrido carbene such as **4.15-H₂**, an α -oxoalkyl hydride such as **4.17**, or a simple adduct of MTBE coordinated to iridium through oxygen as we had originally postulated based on similar intermediates observed by Bercaw and co-workers at cationic Pt(II) centers.²⁶ The identity of the intermediate was ultimately determined by two related experiments. First, upon addition of norbornene and a small amount of MTBE (ca. 50 μ L) to a solution of dihydride **4.8** in cyclohexane-d₁₂, ³¹P NMR spectroscopy revealed generation of the intermediate species (δ 45 ppm), and ¹H NMR spectroscopy showed a hydride signal (δ -34.7 ppm, ²J_{PH} = 13 Hz) nearly identical to that observed for the α -oxoalkyl hydride complex **4.17**. Additionally, trapping of the intermediate with carbon monoxide resulted in the formation of (PNP)Ir(H)(CH₂O^tBu)(CO) (**4.19-CO**, Scheme 4.17). These results strongly indicate that the observable intermediate in the dehydrogenation of MTBE is the product of the first oxidative addition (**4.19**), followed by a slow and rate-determining second C-H activation step and loss of hydrogen to afford the isolated carbene complex **4.9** (Scheme 4.17). These findings are consistent with recent theoretical studies suggesting that the formation of **4.19** should be facile and that it is likely the dominant species in solution before formation of the observed carbene product **4.9** and that **4.19** plays an important role in controlling the favorable thermodynamic parameters of the reaction.³³



Scheme 4.17. Proposed mechanisms of formation for carbene **4.9** and trapped intermediate **4.19-CO**.

Another important consideration, which has previously been discussed in greater detail by Yates and co-workers,³³ is that reactions described above that result in carbene formation must necessarily involve the loss of hydrogen. Simple considerations would indicate that, in spite of the small entropic benefit, this reaction should be thermodynamically uphill. In fact, the necessity of scavenging the hydrogen evolved in such reactions using a suitable sink has been noted previously for related chemistry.^{35,57} This rationalizes the need for at least two equivalents of norbornene in all of the carbene reactions described and suggests that hydrogen scavenging may provide a further limitation on the rate of carbene formation. Yates and co-workers have provided theoretical evidence that interaction of hydrogen with complex **4.19** to regenerate dihydride **4.8** is facile, and thus this step is probably not rate-limiting for the substrates that closely mirror MTBE. However, it is worth considering that, if isomerization of **4.15-H₂** must occur prior to interaction with evolved hydrogen, this step may be considerably slower in the

generation of carbene **4.15**. At the present time, we have no direct evidence regarding the consumption of evolved hydrogen by intermediates in the formation of **4.15**, and we simply note that this sort of process clearly plays an important role for all of the carbene formation reactions described.

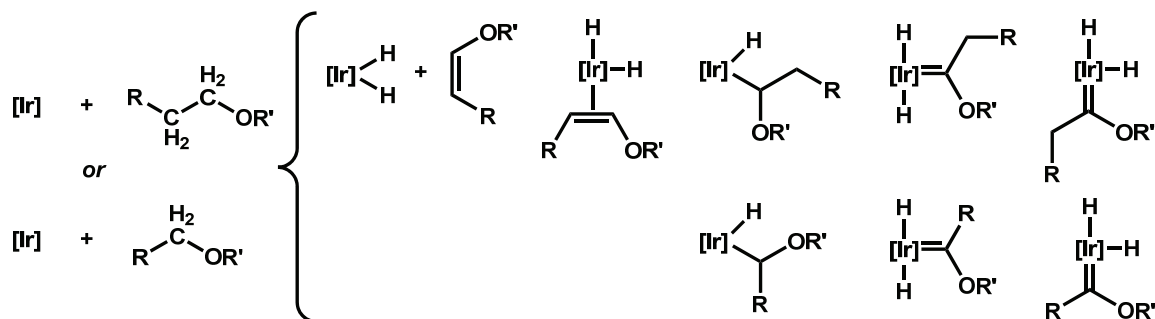
Finally, although it is somewhat counterintuitive that the generation of two otherwise similar carbene complexes (**4.9** and **4.15**) would involve different observed intermediates, this finding seems to be related to the observation that five-membered heterocycles often form carbenes much more readily than their six-membered and acyclic counterparts. Additionally, it rationalizes the elevated temperatures required for generation of THF-derived carbene **4.15**, since it has previously been shown that isomerization of *trans*-dihydrido aminocarbene complexes of (PNP)Ir is only observed upon thermolysis. These studies do not allow definitive assignments of rate-limiting steps for each reaction, but they certainly underscore the importance of numerous subtle factors in the thermodynamic stabilization of one isomer relative to another for related substrates at (PNP)Ir.

Conclusions

Pincer iridium complexes derived from PCP ligand **4.1** and PNP ligand **4.2** are suitable platforms for the C–H activation of *tert*-butyl methyl ether (MTBE). Although Anthrphos ligand **4.1** proved to be unsuitable for the stabilization of MTBE-derived Fischer carbenes, dehydrogenation of (PNP)IrH₂ (**4.8**) in MTBE afforded a square-planar, formally d⁸ iridium(I) carbene in high yield as a kinetic product. For both systems, the final thermodynamic product is a *trans*-(pincer)Ir(H)₂(CO) complex arising from thermal decomposition of the corresponding Fischer carbene. A mechanism involving an oxocarbenium intermediate has been proposed based on structural evidence and indirect experiments. In the case of the thermodynamic

products **4.7** and **4.10**, it appears that the preferred *trans* configuration of hydride ligands is due to a kinetic preference for this and related elimination events to position a second hydride ligand in the open site *trans* to the first hydride. This geometry is thermodynamically counterintuitive given the positioning of two strongly *trans*-influencing hydride ligands, but recent results by Milstein, Goldberg, and others suggest this to be a general trend for these architectures.^{15a,20,58}

These results have been extended to a detailed synthetic study of the reactivity of the (PNP)Ir fragment with a series of linear and cyclic ethers, providing reaction mechanisms that rationalize a number of distinct but related α,α -dehydrogenation, α,β -dehydrogenation, and decarbonylation pathways. In general, these findings support the notion that the (PNP)Ir fragment is extremely unsaturated and electron rich, and it participates in a variety of reactions that allow the transfer of electron density to various substrates, either through oxidative addition or conversion of the substrates to π -acidic ligands. In Scheme 4.18, a number of relevant isomers of the elemental content [(PNP)Ir + ether] are depicted. For those isomers that contain *cis*-coordinated hydride ligands, there is also the possibility of hydrogen loss and consumption by iridium-mediated transfer to a sacrificial olefin, which is often a thermodynamically downhill process.



Scheme 4.18. Possible isomers of the elemental content [(PNP)Ir + ether] ([Ir] = (PNP)Ir).

Given this range of possible options, the fate of a particular ether upon interaction with (PNP)Ir depends intricately on its structure and cannot easily be rationalized by simple linear versus cyclic arguments, giving rise to a fascinating complexity of outcomes within a rather narrow substrate scope. The development of catalytic protocols involving C–H activation and functionalization of ethers depends on understanding the subtle reasons underlying this complexity, some of which we have elucidated herein. Thus, further study promises to illuminate more effectively the factors controlling α - versus β -elimination processes, allowing the development of new catalytic reactions relying on the selective use of one or the other.

In general, the reactivity of Fischer carbenes stabilized by group 9 metals has received little attention.^{17,18} Complexes **4.9**, **4.13–4.15**, and **4.17** are unusual examples of square-planar iridium(I) carbenes and currently the only examples of such species prepared by multiple C–H activations. Simple molecular-orbital considerations as well as studies of the decomposition of **4.9** indicate that the carbene complexes described in this work should possess a HOMO of largely Ir(d_{z^2})-parentage due to their formally d^8 , square-planar configuration. The orientation of this orbital perpendicular to the plane of the complex may lead to metal-based reactivity rather than the ligand-based reactivity more commonly discussed for metal-bound carbenes.⁵⁹ In addition to providing fundamental information and interesting structural possibilities, this work opens new catalytic pathways for hydrocarbon functionalization.

Acknowledgment

The author acknowledges Dr. Patricio Romero for the synthesis of the [ⁱPr Anthraphos] ligand and its complexes described in this chapter. Professor Oleg Ozerov, Yanjun Zhu, and Samuel Timpa (Texas A&M University, Brandeis University) performed the work described with respect to C–H activation of cyclic ethers (THF, 1,4-dioxane, and 1,3,5-trioxane) and Professor

Bruce Foxman and Josh Chen (Brandeis University) solved the X-ray crystal structure of complex **4.15**. Larry Henling provided crystallographic assistance and Nigel Brookes (University of Tasmania) provided helpful insight concerning the dehydrogenation of diethyl ether.

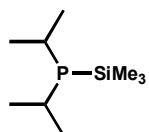
Experimental Section

General Considerations. All operations were performed under inert atmosphere in a nitrogen-filled glove box or by using standard Schlenk techniques unless otherwise specified. *tert*-Amyl methyl ether, *sec*-butyl methyl ether, and *n*-butyl methyl ether were purchased from Aldrich and dried from calcium hydride or by passage through activated alumina followed by degassing via three freeze–pump–thaw cycles. All commercial reagents were used without further purification. (PNP)IrH₂ (**4.8**) was synthesized according to a published procedure.¹⁰ Unless otherwise noted, solvents were deoxygenated and dried by thorough sparging with Ar gas followed by passage through an activated alumina column.⁶⁰ NMR spectra were obtained at ambient temperature on a Mercury-300 spectrometer. ³¹P NMR chemical shifts are reported relative to an external standard of 85% H₃PO₄. Infrared spectra were recorded on a Perkin-Elmer Paragon 1000 FT-IR spectrometer. HRMS were acquired using an Agilent 6200 Series TOF with an Agilent G1978A Multimode source in electrospray ionization (ESI), atmospheric pressure chemical ionization (APCI) or mixed (MM) ionization mode. Elemental analyses were carried out at Desert Analytics, Tucson, Arizona. X-ray diffraction studies were carried out in the Beckman Institute Crystallographic Facility on a Bruker Smart 1000 CCD diffractometer.

Notes on the preparation of 1,8-difluoroanthraquinone and 1,8-difluoroanthracene. Although reliable protocols for both of these starting materials have been reported,⁸ we have also found that they can be readily purified by sublimation under dynamic vacuum (10⁻³ torr, 1,8-

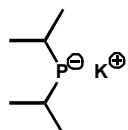
difluoroanthraquinone = 150 °C; 1,8-difluoroanthracene = 100 °C) without the need for chromatographic purification. 1,8-difluoroanthracene can be further purified by recrystallization from hot methanol followed by cooling at -35 °C.

Synthesis of ${}^i\text{Pr}_2\text{PSiMe}_3$. This phosphine was prepared according to the method developed by



Werner and co-workers⁶¹ with some modifications. Under nitrogen, ${}^i\text{Pr}_2\text{PH}$ (5.00 g, 42.3 mmol) was loaded into a two-neck round-bottom flask fitted with a rubber septum, and the flask was connected to a swivel-frit apparatus. The flask was cooled to -78 °C and THF (30 mL) was vacuum transferred to the system. At this temperature, *n*-butyllithium (31.9 mL, 51 mmol, 1.6 M in hexanes) was added dropwise and the system was allowed to warm to room temperature and stirred for 2 h. During this time, a bright-yellow solution developed. The system was cooled to -78 °C, chlorotrimethylsilane (7.0 mL, 55 mmol) was added dropwise, and the solution stirred overnight. The volatiles were removed *in vacuo* and pentane (20 mL) was transferred onto the mixture. The LiCl was separated by filtration and upon removal of the solvent the product was obtained as a clear, viscous oil (7.6 g, 95%). Characterization data matched those previously reported for the compound.⁶¹

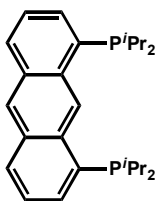
Synthesis of ${}^i\text{Pr}_2\text{PK}$. In a nitrogen-filled glove box, freshly sublimed ${}^t\text{BuOK}$ (2.03 g, 18.1 mmol)



was dissolved in dry THF (20 mL) and placed into a sealable glass bomb. To this solution, ${}^i\text{Pr}_2\text{PSiMe}_3$ (3.28 g, 17.2 mmol) dissolved in dry THF (20 mL) was added in one portion. The bomb containing the homogenous yellow solution was removed from the glove box and heated in an oil bath at 70 °C overnight. The resulting orange solution was transferred under nitrogen to a swivel frit apparatus via cannula and the volatiles removed *in vacuo*. 10 mL of dry toluene was added to the mixture, followed by 40 mL of pentane, causing

the precipitation of solid $i\text{Pr}_2\text{PK}$. The mixture was stirred for 30 min and filtered. The creamy solid was washed with fresh pentane until the washes became colorless and dried *in vacuo* (2.06 g, 77%). ^1H NMR spectrum matched those previously reported.⁶² The ^{31}P NMR resonance did not match the reported value as it was recorded in a different solvent. ^1H NMR (THF- d_8): δ 2.31 (m, 2H, $-\text{CH}(\text{CH}_3)_2$), 1.06 (dd, 12H, $^3J_{\text{HH}} = 6.6$ Hz, $^3J_{\text{PH}} = 11.4$ Hz, $-\text{CH}(\text{CH}_3)_2$). $^{31}\text{P}\{^1\text{H}\}$ NMR (THF- d_8): δ 21.3 (s).

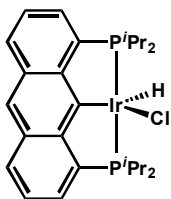
Synthesis of Anthrphos Ligand (4.2). 1,8-difluoroanthracene (1.7 g, 7.94 mmol) was dissolved



4.2

in dry dioxane (20 mL) and placed in a sealable glass bomb. To this solution, a solution of $i\text{Pr}_2\text{PK}$ (2.48 g, 15.87 mmol) in 20 mL of dry THF was added via cannula at room temperature. The flask was closed and the resulting red solution was heated at 105 °C for 5 h, then cooled to room temperature. The system was opened to air, the solution was transferred to a round-bottom flask, and the volatiles were removed *in vacuo*. The solid residue was transferred to a sublimation apparatus and heated to 170 °C under dynamic vacuum (10^{-3} torr) overnight. Pure ligand deposited as a bright-yellow solid on the cold finger. Although this material is adequate for preparative purposes, it separated as a very fine powder that was difficult to handle. Recrystallization from hot ethanol followed by cooling at -30 °C afforded a crystalline, manageable solid (2.60 g, 80%). Spectral features match those reported in the literature.⁶³

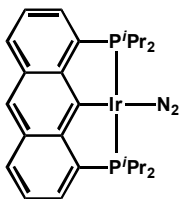
Synthesis of Complex (4.4). $[\text{IrCl}(\text{coe})_2]_2$ (164 mg, 0.183 mmol) and **4.2** (158 mg, 0.365 mmol)



4.4

were weighed into a 20 mL glass bomb fitted with a Kontes valve and suspended in 8 mL of toluene. The sealed bomb was then placed in an oil bath and the mixture heated at 120 °C overnight. Under nitrogen, the red solution obtained was transferred to a round-bottom flask and the solvent removed *in vacuo*. In air, pentane was added to the residue and the solid was broken up with a spatula. Filtration through a medium porosity frit afforded a bright-red solid, which was washed with several portions of pentane and dried under high vacuum (203 mg, 83%). This complex is sensitive to air in solution but can be handled as a solid in air. ^1H NMR (C_6D_6): δ 7.93 (m, 1H, Ar-H), 7.86 (d, 2H, $^3J_{\text{HH}} = 8.4$ Hz, Ar-H), 7.35–7.29 (m, 2H, Ar-H), 7.22 (m, 2H, Ar-H), 3.24 (m, 2H, $-\text{CH}(\text{CH}_3)_2$), 2.56 (m, 2H, $-\text{CH}(\text{CH}_3)_2$), 1.43 (dd, 6H, $^3J_{\text{HH}} = 6.6$ Hz, $^3J_{\text{PH}} = 16$ Hz, $-\text{CH}(\text{CH}_3)_2$), 1.08 (dd, 6H, $^3J_{\text{HH}} = 6.9$ Hz, $^3J_{\text{PH}} = 13$ Hz, $-\text{CH}(\text{CH}_3)_2$), 1.01 (dd, 6H, $^3J_{\text{HH}} = 7.2$ Hz, $^3J_{\text{PH}} = 17$ Hz, $-\text{CH}(\text{CH}_3)_2$), 0.85 (dd, 6H, $^3J_{\text{HH}} = 6.6$ Hz, $^3J_{\text{PH}} = 17$ Hz, $-\text{CH}(\text{CH}_3)_2$), -35.9 (t, 1H, $^2J_{\text{PH}} = 12$ Hz, Ir-H). $^{31}\text{P}\{^1\text{H}\}$ NMR (C_6D_6): δ 61.1 (s). Anal. calcd. for $\text{C}_{26}\text{H}_{36}\text{ClIrP}_2$: C, 48.93; H, 5.29. Found: C, 48.76; H, 5.54.

Characterization of ($^{i\text{Pr}}$ Anthraphos)Ir(N₂) (4.5). In a nitrogen-filled glove box, a 50 mL round-

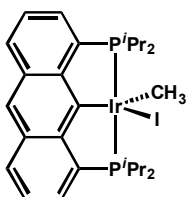


4.5

bottom flask was charged with a mixture of **4.4** (150 mg, 0.216 mmol), $^t\text{BuONa}$ (23 mg, 0.24 mmol), and 15 mL of benzene. The solution was stirred under nitrogen for 3 h at room temperature, during which time a dark-green color developed. ^1H and ^{31}P NMR as well as IR analysis of this mixture indicates the presence of a single species assigned as the monomeric dinitrogen complex **4.5**. Spectral features for **4.5**: ^1H NMR (CD_2Cl_2): δ 7.96–7.94 (m, 2H, Ar-H), 7.92 (s, 1H, Ar-H), 7.65–7.60 (m, 2H, Ar-H), 7.42–7.37 (m, 2H, Ar-H), 2.82 (m, 4H, $-\text{CH}(\text{CH}_3)_2$), 1.32 (dd, 12H, $^3J_{\text{HH}} = 7.2$ Hz, $^3J_{\text{PH}} =$

15.7 Hz, $-\text{CH}(\text{CH}_3)_2$), 1.24 (dd, 12H, $^3J_{\text{HH}} = 7.2$ Hz, $^3J_{\text{PH}} = 14.5$ Hz, $-\text{CH}(\text{CH}_3)_2$). $^{31}\text{P}\{^1\text{H}\}$ NMR (CD_2Cl_2): δ 64 (s). IR (C_6H_6 , KBr, cm^{-1}) $\nu(\text{N}_2)$: 2096.

Synthesis of ($^{i\text{Pr}}$ Anthraphos)Ir(CH_3)(I) (4.6). To a solution containing **4.5**, methyl iodide (20 μL ,

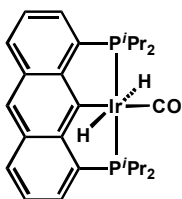


4.6

0.32 mmol) was added, causing an immediate color change to red-purple. The solution was stirred at room temperature for 1 h and the volatiles were removed *in vacuo*. The solid residue was dissolved in 15 mL of CH_2Cl_2 and filtered through celite. The solvent was removed under high vacuum and the

solid residue was triturated with pentane (15 mL) and filtered to afford **4.6** (154 mg, 96%). This material is of sufficient quality for preparative purposes. Analytically pure material can be obtained by recrystallization from toluene at -35 $^\circ\text{C}$. Spectral features for **4.6**: ^1H NMR (CD_2Cl_2): δ 8.14 (m, 1H, Ar-H), 8.12 (s, 1H, Ar-H), 8.09 (s, 1H, Ar-H), 7.77–7.72 (m, 2H, Ar-H), 7.54–7.49 (m, 2H, Ar-H), 3.38–3.26 (m, 2H, $-\text{CH}(\text{CH}_3)_2$), 3.22–3.13 (m, 2H, $-\text{CH}(\text{CH}_3)_2$), 1.81 (dd, 6H, $^3J_{\text{HH}} = 6.9$ Hz, $^3J_{\text{PH}} = 15.1$ Hz, $-\text{CH}(\text{CH}_3)_2$), 1.37 (t, 3H, $^3J_{\text{PH}} = 6.0$ Hz, Ir-Me), 1.25 (dd, overlap, 12H, $-\text{CH}(\text{CH}_3)_2$), 0.62 (dd, 6H, $^3J_{\text{HH}} = 7.2$ Hz, $^3J_{\text{PH}} = 16.2$ Hz, $-\text{CH}(\text{CH}_3)_2$). $^{31}\text{P}\{^1\text{H}\}$ NMR (CD_2Cl_2): δ 39.6 (s). Anal. calcd. for $\text{C}_{27}\text{H}_{38}\text{IrP}_2$: C, 43.61; H, 5.15. Found: C, 43.76; H, 5.38.

Synthesis of *trans*-($^{i\text{Pr}}$ Anthraphos)Ir(H) $_2$ (CO) (4.7). In a nitrogen-filled glove box, **4.4** (120 mg,

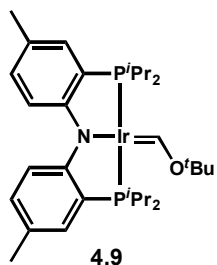


4.7

0.188 mmol) and $^t\text{BuONa}$ (22 mg, 0.23 mmol, 1.2 eq) were weighed into a 20 mL glass bomb. The system was fully evacuated and refilled with argon. The process was repeated twice and the bomb was left under full vacuum and cooled to -78°C . Dry, nitrogen-free *tert*-butyl methyl ether (ca. 10 mL) was condensed onto the solids and the system was closed under vacuum. The solution was heated to 70°C for 2.5 h, causing a brown color to develop. The volatiles were removed *in vacuo* and the

resulting solid residue was dissolved in CH_2Cl_2 (10 mL) and filtered through celite. The solvent was removed and the mixture triturated with pentane. The supernatant was decanted, yielding an orange powder, which was dried under vacuum (101 mg, 85%). ^1H NMR (C_6D_6): δ 7.91 (s, 1H, Ar-H), 7.85–7.81 (m, 2H, Ar-H), 7.27–7.18 (m, 4H, Ar-H), 2.08 (m, 4H, $-\text{CH}(\text{CH}_3)_2$), 1.27 (dd, 12H, $^3J_{\text{HH}} = 6.6$ Hz, $^3J_{\text{PH}} = 17$ Hz, $-\text{CH}(\text{CH}_3)_2$), 0.90 (dd, 12H, $^3J_{\text{HH}} = 6.9$ Hz, $^3J_{\text{PH}} = 16$ Hz, $-\text{CH}(\text{CH}_3)_2$), -9.45 (t, 2H, $^2J_{\text{PH}} = 15$ Hz, Ir-H). $^{13}\text{C}\{^1\text{H}\}$ NMR (C_6D_6): δ 149.3 (s, $^2J_{\text{PC}(\text{cis})} = 15$ Hz, Ir-CO). $^{31}\text{P}\{^1\text{H}\}$ NMR (C_6D_6): δ 66.1 (s). IR (THF, KBr, cm^{-1}) $\nu(\text{CO})$: 1989. Anal. calcd. for $\text{C}_{27}\text{H}_{37}\text{IrOP}_2$: C, 51.33; H, 5.90. Found: C, 49.46; H, 5.56. HRMS (FAB+) calcd. for $\text{C}_{27}\text{H}_{37}\text{IrOP}_2$ [$(\text{M}+\text{H})-2\text{H}^+$] 631.1870, found 631.1876.

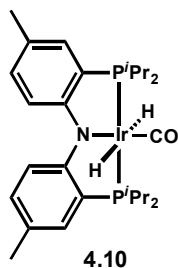
Synthesis of (PNP)Ir=C(H)O^tBu (4.9). To a red solution of (PNP)IrH₂ (**4.8**) (175.8 mg, 0.2823



mmol) in *tert*-butyl methyl ether (6 mL) was added norbornene (49.0 mg, 0.520 mmol) in *tert*-butyl methyl ether (6 mL). After several hours, the solution gradually darkened and gained a purple hue. After 18 h, volatiles were removed *in vacuo* to yield a dark red film which was redissolved in

pentane (10 mL), filtered and dried to afford **4.9** as a purple solid. Analytically pure crystals of **4.9** were obtained by slow evaporation of pentane from a concentrated solution at -35 °C (107.0 mg, 54%). Compound **4.9** was stored at -35 °C to prevent decomposition. ^1H NMR (C_6D_6): δ 13.78 (t, $^3J_{\text{HP}} = 7.5$ Hz, 1H, $-\text{C}(\text{H})\text{O}^t\text{Bu}$), 7.80 (d, $^3J_{\text{HH}} = 8.4$ Hz, 2H, Ar-H), 7.17 (s, 2H, Ar-H), 6.82 (d, $^3J_{\text{HH}} = 8.4$ Hz, 2H, Ar-H), 2.62 (m, 4H, $-\text{CH}(\text{CH}_3)_2$), 2.24 (s, 6H, Ar- CH_3), 1.30 (m, 12H, $-\text{CH}(\text{CH}_3)_2$), 1.21 (m, 12H, $-\text{CH}(\text{CH}_3)_2$), 1.10 (s, 9H, $-\text{C}(\text{CH}_3)_3$). $^{13}\text{C}\{^1\text{H}\}$ NMR (C_6D_6): δ 210.0 (Ir=CHO^tBu). $^{31}\text{P}\{^1\text{H}\}$ NMR (C_6D_6): δ 40.8 (s). Anal. calcd. for $\text{C}_{31}\text{H}_{50}\text{IrNOP}_2$: C, 52.67; H, 7.13; N, 1.98. Found: C, 52.74; H, 7.05; N, 2.04.

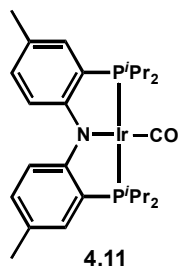
Synthesis of *trans*-(PNP)Ir(H)₂(CO) (4.10). A dark-purple solution of **4.9** (20.0 mg, 0.0283 mmol)



in C₆D₆ (600 μL) was heated at 80 °C in a sealed NMR tube for 48 h, causing a color change to dark golden. Volatiles were removed *in vacuo*, leaving a golden film. **4.10** was isolated in analytically pure crystalline form as yellow needles by slow evaporation of pentane at –35 °C (13.7 mg, 71%). ¹H NMR (C₆D₆): δ 7.68

(d, ³J_{HH} = 8.7 Hz, 2H, Ar–H), 6.86 (s, 2H, Ar–H), 6.70 (d, ³J_{HH} = 8.7 Hz, 2H, Ar–H), 2.18 (s, 6H, Ar–CH₃), 2.02 (m, 12H, –CH(CH₃)₂), 1.21 (m, 12H, –CH(CH₃)₂), 1.07 (m, 12H, –CH(CH₃)₂), –7.25 (t, ³J_{PH} = 15.3 Hz, 2H, Ir–H). ¹³C{¹H} NMR (C₆D₆): δ 174.6 (t, ²J_{PC} = 7 Hz, Ir–CO). ³¹P{¹H} NMR (C₆D₆): δ 51.2 (s). IR (THF, KBr, cm^{–1}) ν(CO): 1990. Anal. calcd. for C₂₇H₄₂IrNOP₂: C, 49.83; H, 6.50; N, 2.15. Found: C, 50.23; H, 6.73; N, 2.03.

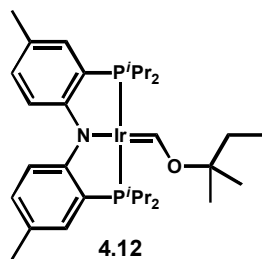
Synthesis of (PNP)Ir(CO) (4.11). In a sealed NMR tube, a red solution of **4.8** (40 mg, 0.064 mmol)



in C₆D₆ was frozen and the headspace evacuated and backfilled with carbon monoxide (1 atm). As the solution melted, an immediate color change to pale yellow was observed. The reaction was allowed to proceed 24 h and complete formation of **4.11** confirmed by NMR. Lyophilization of the solution yielded **4.11**

as an analytically pure yellow powder (41 mg, 98%). X-ray quality crystals were grown at room temperature from a concentrated solution of **4.3** in benzene/hexamethyldisiloxane (1:1). ¹H NMR (C₆D₆): δ 7.72 (d, ³J_{HH} = 8.4 Hz, 2H, Ar–H), 6.92 (s, 2H, Ar–H), 6.83 (d, ³J_{HH} = 8.4 Hz, 2H, Ar–H), 2.27 (m, 4H, –CH(CH₃)₂), 2.18 (s, 6H, Ar–CH₃), 1.29 (m, 12H, –CH(CH₃)₂), 1.05 (m, 12H, –CH(CH₃)₂). ³¹P{¹H} NMR (C₆D₆): δ 57.3 (s). IR (THF, KBr, cm^{–1}) ν(CO): 1930. Anal. calcd. for C₂₇H₄₀IrNOP₂: C, 49.98; H, 6.21; N, 2.16. Found: C, 49.97; H, 5.73; N, 2.05.

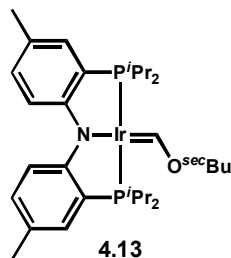
Synthesis of (PNP)Ir=C(H)O^tAm (4.12). (PNP)IrH₂ (**4.8**) (42.1 mg, 0.0676 mmol) and norbornene



(13.8 mg, 0.147 mmol) were combined in *tert*-amyl methyl ether (700 μ L) and transferred to an NMR tube. The sample was allowed to react at ambient temperature for 2 h and heated at 80 °C for 20 min until complete conversion to **4.12** was observed by ³¹P NMR with

concomitant color change from brown to purple. Volatile components were removed *in vacuo* and the residues were redissolved in pentane (5 mL), filtered, and dried to afford carbene **4.12** as a viscous purple oil (42.2 mg, 87%). ¹H NMR (C₆D₆): δ 13.80 (t, ³J_{PH} = 7.5 Hz, -C(H)O^tAm), 7.83 (d, *J* = 8 Hz, 2H, Ar-H), 7.22 (s, 2H, Ar-H), 6.86 (d, *J* = 8 Hz, 2H, Ar-H), 2.68 (m, 4H, -CH(CH₃)₂), 2.29 (s, 6H, Ar-CH₃), 1.47 (q, ³J_{HH} = 7.5 Hz, 2H, and -OC(CH₃)₂(CH₂CH₃)), 1.37 (dvt, 12H, -CH(CH₃)₂), 1.26 (dvt, 12H, -CH(CH₃)₂), 0.81 (t, ³J_{HH} = 7.5 Hz, 3H, -OC(CH₃)₂(CH₂CH₃)), 0.12 (s, 6H, -OC(CH₃)₂(CH₂CH₃)). ¹³C{¹H} NMR (C₆D₆): δ 210.1 (Ir=C(H)O^tAm), 164.5 (t, *J* = 10.5 Hz), 133.0, 131.6, 126.7 (t, *J* = 21 Hz), 127.7, 116.8, 83.8, 33.8, 26.5, 26.4, 26.3, 20.9, 20.3, 19.2, 8.8. ³¹P{¹H} NMR (C₆D₆): δ 40.7 (s). HRMS (MM: ESI-APCI) calcd. for C₃₂H₅₂IrNOP₂ [(M+Na)⁺] 744.3047, found 744.3065.

Synthesis of (PNP)Ir=C(H)O^{sec}Bu (4.13). A solution of norbornene (17.9 mg, 0.190 mmol) in *n*-

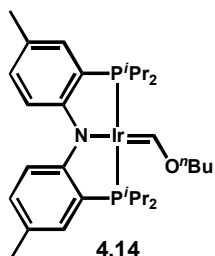


butyl methyl ether (1 mL) was added to a vial containing (PNP)IrH₂ (**4.8**) (39.5 mg, 0.0634 mmol), and an immediate color change from red to brown was observed. The solution was transferred to an NMR tube and heated at 90 °C for 2 h. Volatile components were removed *in vacuo* and

the residues were redissolved in pentane (5 mL), filtered, and dried to afford **4.13** as a viscous purple oil (38.5 mg, 86%). ¹H NMR (C₆D₆): δ 13.46 (t, ³J_{PH} = 7.4 Hz, -C(H)O^{sec}Bu), 7.84 (dt, *J*₁ = 8.4 Hz, *J*₂ = 2.1 Hz, 2H, Ar-H), 7.22 (d, *J* = 1.8 Hz, 2H, Ar-H), 6.87 (dd, *J*₁ = 8.4 Hz, *J*₂ = 1.8 Hz, 2H, Ar-

H), 3.41 (sextet, $^3J_{\text{HH}} = 6.0$ Hz, 1H, $-\text{OCH}(\text{CH}_3)(\text{CH}_2\text{CH}_3)$), 2.68 (m, 4H, $-\text{CH}(\text{CH}_3)_2$), 2.29 (s, 6H, Ar- CH_3), 1.55–1.13 (m, 26H, $-\text{CH}(\text{CH}_3)_2$ and $-\text{OCH}(\text{CH}_3)(\text{CH}_2\text{CH}_3)$), 1.07 (d, $^3J_{\text{HH}} = 6.6$ Hz, 3H, $-\text{OCH}(\text{CH}_3)(\text{CH}_2\text{CH}_3)$), 0.80 (t, $^3J_{\text{HH}} = 7.5$ Hz, $-\text{OCH}(\text{CH}_3)(\text{CH}_2\text{CH}_3)$). $^{13}\text{C}\{^1\text{H}\}$ NMR (C_6D_6): δ 216.4 ($\text{Ir}=\text{C}(\text{H})\text{O}^{\text{sec}}\text{Bu}$), 164.5, 133.1, 131.6, 126.6 (t, $J = 25$ Hz), 125.8, 116.8, 89.0, 30.3, 26.5 (t, $J = 11$ Hz), 21.0, 20.9, 20.3, 20.2, 19.2, 19.1, 10.6, 10.5. $^{31}\text{P}\{^1\text{H}\}$ NMR (C_6D_6): δ 40.9 (s). HRMS (MM: ESI-APCI) calcd. for $\text{C}_{31}\text{H}_{50}\text{IrNOP}_2$ $[(\text{M}+\text{H})^+]$ 708.3071, found 708.3050.

Synthesis of (PNP)Ir=C(H)OⁿBu (4.14). (PNP)IrH₂ (**4.8**) (72.1 mg, 0.116 mmol) and norbornene

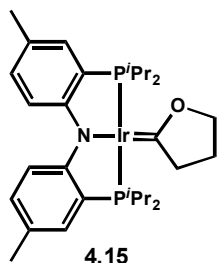


(32.7 mg, 0.347 mmol) were combined in *n*-butyl methyl ether (2 mL), causing an immediate color change from red to brown. The solution was heated at 90 °C for 2.5 h in a sealed vial, resulting in a color change to purple. Volatile components were removed *in vacuo*, and the residues were

redissolved in pentane, filtered, and dried to afford **4.14** as a viscous purple oil (72.3 mg, 88%).

^1H NMR (C_6D_6): δ 13.49 (t, $^3J_{\text{PH}} = 7.2$ Hz, 1H, $-\text{C}(\text{H})\text{O}^n\text{Bu}$), 7.85 (dt, $J_1 = 8.4$ Hz, $J_2 = 2.1$ Hz, 2H, Ar- H), 7.23 (m, 2H, Ar- H), 6.88 (d, $J = 8.4$ Hz, 2H, Ar- H), 3.48 (t, $^3J_{\text{HH}} = 6.5$ Hz, 2H, $-\text{OCH}_2(\text{CH}_2)_2\text{CH}_3$), 2.68 (m, 4H, $-\text{CH}(\text{CH}_3)_2$), 2.30 (s, 6H, Ar- CH_3), 1.50–0.95 (m, 28H, $-\text{CH}(\text{CH}_3)_2$ and $-\text{OCH}_2(\text{CH}_2)_2\text{CH}_3$), 0.79 (t, $^3J_{\text{HH}} = 7.2$ Hz, 3H, $-\text{OCH}_2(\text{CH}_2)_2\text{CH}_3$). $^{13}\text{C}\{^1\text{H}\}$ NMR (C_6D_6): 216.3 ($\text{Ir}=\text{C}(\text{H})\text{O}^n\text{Bu}$), 164.5, 133.1, 131.6, 126.6 (t, $J = 20$ Hz), 125.8, 116.8, 89.0, 30.3, 26.4, 21.0, 20.9, 20.2, 19.2, 19.1, 10.5. $^{31}\text{P}\{^1\text{H}\}$ NMR (C_6D_6): 41.1 (s). HRMS (MM: ESI-APCI) calcd. for $\text{C}_{31}\text{H}_{50}\text{IrNOP}_2$ $[(\text{M}+\text{H})^+]$ 708.3071, found 708.2962.

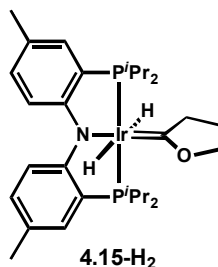
Synthesis of (PNP)Ir=C(O(CH₂)₂CH₂) (4.15). (PNP)Ir(H)₂ (4.8) (76 mg, 0.12 mmol) and norbornene



(83 mg, 0.86 mmol) were dissolved in tetrahydrofuran (600 μ L) and transferred to a J. Young tube. An immediate color change to brown was accompanied by the appearance of a singlet in the ³¹P{¹H} NMR spectrum at δ 46.7 ppm. Thermolysis of the solution (60 $^{\circ}$ C, 7 h) resulted in a color change to dark red and ca. 97% conversion to another product at δ 43.1 ppm. The solution was

filtered through celite and the filtrate was collected. Volatiles were removed *in vacuo* and **4.15** was obtained as a pure solid by slow evaporation of pentane from a concentrated solution at -35 $^{\circ}$ C (21.6 mg, 24%). ¹H NMR (C₆D₆): δ 7.87 (d, J = 8.4 Hz, 2H, Ar-H), 7.25 (s, 2H, Ar-H), 6.86 (d, J = 8.4 Hz, 2H, Ar-H), 3.50 (t, ³ J_{HH} = 6.9 Hz, 2H, -C₃H₆O), 2.67 (m, 4H, CH(CH₃)₂), 2.29 (s, 6H, Ar-CH₃), 1.39 (quintet, ³ J_{HH} = 7.2 Hz, 2H, C₃H₆O), 1.30 (dvt, 12H, CH(CH₃)₂), 1.24 (dvt, 12H, CH(CH₃)₂), 0.39 (t, ³ J_{HH} = 7.5 Hz, 2H, C₃H₆O). ¹³C{¹H} NMR (C₆D₆): δ 232.6 (t, ² J_{PC} = 11 Hz, Ir=C), 164.1 (t, J = 17 Hz, C-N), 132.5 (PNP aryl C), 131.2 (PNP-aryl C), 125.3 (PNP aryl C), 124.7 (PNP aryl C), 116.4 (PNP aryl C), 74.6, 60.3, 26.2, 24.2, 20.6, 19.8, 18.7. ³¹P{¹H} NMR: δ 42.9 (s). Anal. calcd. for C₃₀H₄₆NOP₂Ir: C, 51.98; H, 6.66; N, 1.90. Found: C, 52.16; H, 6.71; N, 2.03.

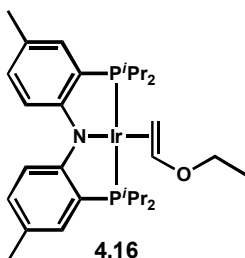
Solution Characterization of *trans*-(PNP)Ir(H)₂=C(C₃H₆O) (4.15-H₂). (PNP)IrH₂ (4.8) (39 mg, 0.062



mmol) was dissolved in 0.6 mL C₆D₆ in a J. Young tube followed by the addition of 2,3-dihydrofuran (14 μ L, 0.19 mmol). ³¹P{¹H} NMR spectroscopy showed >97% conversion to **4.15-H₂** (δ 46.7 ppm). ¹H NMR(C₆D₆): δ 7.78 (d, J = 8 Hz, 2H, Ar-H), 7.02 (s, 2H, Ar-H), 6.73 (d, J = 8 Hz, 2H, Ar-H), 3.66 (t, ³ J_{HH} = 6 Hz, 2H, C₃H₆O), 2.14 – 2.24 (m, 10H, Ar-CH₃ and -CH(CH₃)₂), 1.02–1.22 (m, 28H, -CH(CH₃)₂ and C₃H₆O), -7.86 (t, ³ J_{PH} = 15 Hz, 2H, Ir-H). ¹³C{¹H} NMR (C₆D₆): δ 261.2

(br, Ir=C), 161.9 (t, $J = 9$ Hz, C–N), 130.7 (PNP aryl C), 124.7 (t, $J = 25$ Hz, PNP aryl C), 122.8 (t, $J = 24$ Hz, PNP aryl C), 115.6 (t, $J = 4$ Hz, PNP aryl C), 79.7, 65.4, 26.4 (t, $J = 16$ Hz), 23.7, 20.6, 18.9, 18.6. $^{31}\text{P}\{^1\text{H}\}$ NMR: δ 46.7 (s). ^1H NMR (CD_2Cl_2): δ 7.29 (d, $J = 8$ Hz, 2H, Ar–H), 6.89 (s, 2H, Ar–H), 6.65 (d, $J = 8$ Hz, 2H, Ar–H), 4.41 (t, $J = 7$ Hz, 2H, $\text{C}_3\text{H}_6\text{O}$), 2.62 (t, $J = 8$ Hz, 2H, $\text{C}_3\text{H}_6\text{O}$), 2.33 (m, 4H, $\text{CH}(\text{CH}_3)_2$), 2.18 (s, 6H, Ar– CH_3), 1.80 (m, 2H, $\text{C}_3\text{H}_6\text{O}$), 1.10 (m, 24H, $\text{CH}(\text{CH}_3)_2$), –8.58 (t, $J = 15$ Hz, 2H, Ir–H). $^{31}\text{P}\{^1\text{H}\}$ NMR (CD_2Cl_2): δ 46.7 (s).

Synthesis of Ethyl Vinyl Ether Adduct (4.16). To a red solution of (PNP)IrH₂ (**4.8**) (63.3 mg, 0.102

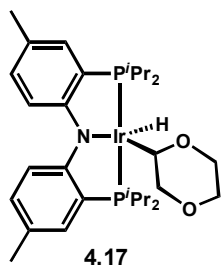


mmol) in diethyl ether (5 mL) was added norbornene (18.6 mg, 0.198 mmol) in diethyl ether (3 mL). The color of the solution initially lightened to a golden hue and turned dark red over a period of 12 h. To ensure complete reaction, excess norbornene (10.0 mg, 0.106 mmol) was added

and the solution stirred for an additional 24 h. Volatiles were removed *in vacuo* to give a red film which was redissolved in pentane (5 mL), filtered, and dried to give **4.16** as a red-orange solid.

An analytically pure, crystalline sample of **4.16** was obtained by slow evaporation of pentane from a concentrated solution (22.3 mg, 32%). ^1H NMR (C_6D_6): δ 7.73 (d, $J = 5.5$ Hz, 2H, Ar–H), 6.94 (m, 2H, Ar–H), 6.84 (d, $J = 8.0$ Hz, 2H, Ar–H), 5.13 (m, 1H, $-\text{OC}_2\text{H}_3$), 4.01 (m, 1H, $-\text{OC}_2\text{H}_3$), 3.60 (m, 1H, $-\text{OC}_2\text{H}_3$), 2.56 (m, 2H, $-\text{OCH}_2$), 2.52–2.27 (m, 3H, $-\text{CH}(\text{CH}_3)_2$), 2.22 (s, 6H, Ar– CH_3), 2.11 (m, 1H, $-\text{CH}(\text{CH}_3)_2$), 1.40 (m, 6H, $-\text{CH}(\text{CH}_3)$), 1.21 (t, $^3J_{\text{HH}} = 5.0$ Hz, 3H, $-\text{OCH}_2\text{CH}_3$), 1.12 (m, 6H, $-\text{CH}(\text{CH}_3)$), 1.02 (m, 6H, $-\text{CH}(\text{CH}_3)$), 0.96 (m, 6H, $-\text{CH}(\text{CH}_3)$). $^{13}\text{C}\{^1\text{H}\}$ NMR (C_6D_6): 164.6, 164.1, 132.2, 132.0, 131.7, 131.5, 125.9, 125.6, 124.6 (d, $J = 39$ Hz), 123.4 (d, $J = 40$ Hz), 115.6, 115.3, 77.3, 66.3, 24.2, 23.8, 20.5, 19.6, 18.6, 17.9, 17.4, 16.7, 15.3, 9.6. $^{31}\text{P}\{^1\text{H}\}$ NMR (C_6D_6): δ 36.6 (d, $^2J_{\text{PP}} = 340$ Hz), 30.4 (d, $^2J_{\text{PP}} = 340$ Hz). Anal. calcd. for $\text{C}_{30}\text{H}_{48}\text{IrNOP}_2$: C, 52.00; H, 6.98; N, 2.02. Found: C, 51.87; H, 6.68; N, 1.97.

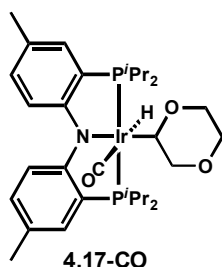
Solution Characterization of (PNP)Ir(H)(1,4-dioxan-2-yl) (4.17). (PNP)IrH₂ (**4.8**) (14.8 mg, 0.024



mmol) was combined with norbornene (14 mg, 0.14 mmol) in a J. Young tube and dissolved in 0.6 mL 1,4-dioxane. ³¹P NMR of the sample immediately displayed two doublets and an unidentified compound with a singlet at 42.9 ppm (ca. 15% by ³¹P NMR). The volatiles were partially

removed and the residues redissolved in C₆D₆. ³¹P NMR in C₆D₆ showed the same percentage of a singlet at 41.9 ppm (ca. 15%) and two doublets of representing **4.17** together with some amount of (PNP)IrH₂. ¹H NMR(C₆D₆): δ 7.75 (m, 2H, Ar-H), 7.02 (d, *J* = 6 Hz, 1H, Ar-H), 6.97 (d, *J* = 6 Hz, 1H, Ar-H), 6.83 (d, *J* = 8 Hz, 2H, Ar-H), 5.65 (m, 1H, C₄H₇O), 4.02 (m, 2H, C₄H₇O), 3.80 (m, 2H, C₄H₇O), 3.74 (d, *J* = 10 Hz, 1H), 3.52 (d, *J* = 11 Hz, 1H), -34.2 (t, ³*J*_{PH} = 13 Hz, 1H). All other protons of **4.17** were obscured by the unknown compound and traces of (PNP)IrH₂. ³¹P{¹H} NMR: δ 46.5(d, *J* = 322 Hz), 43.7 (d, *J* = 322 Hz). Thermolysis of **4.17** in 1,4-dioxane leads to the transformation back to (PNP)IrH₂. Removal of solvent *in vacuo* also regenerates (PNP)IrH₂.

Synthesis of (PNP)Ir(H)(1,4-dioxan-2-yl)(CO) (4.17-CO). (PNP)IrH₂ (**4.8**) (53 mg, 0.085 mmol) was

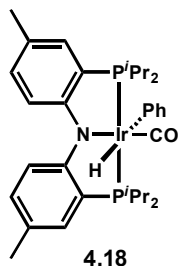


combined with norbornene (26 mg, 0.26 mmol) in a J. Young tube and dissolved in 0.6 mL 1,4-dioxane. A ³¹P NMR spectrum of the sample immediately revealed two doublets and an unidentified compound with a singlet at 42.9 ppm (ca. 15% by ³¹P NMR). The solution was frozen and the

headspace evacuated and backfilled with carbon monoxide (1 atm). As the solution thawed, a gradual change in color from brown to yellow was observed, and a ³¹P NMR spectrum showed that the mixture contained 80% of **4.17-CO**. The volatiles were removed *in vacuo* and the residue was crystallized in toluene/pentane to obtain analytically pure **4.17-CO** (26 mg, 43%). ¹H NMR (C₆D₆): δ 7.64 (d, *J* = 8 Hz, 2H, Ar-H), 6.95 (s, 1H, Ar-H), 6.82 (s, 1H, Ar-H), 6.71 (t, *J* = 8 Hz,

2H, Ar-H), 5.27 (m, 1H, C₄H₇O), 3.94 (m, 2H, C₄H₇O), 3.78 (m, 2H, C₄H₇O), 3.68 (d, ³J_{HH} = 8 Hz, 1H), 3.54 (d, ³J_{HH} = 9 Hz, 1H, C₄H₇O), 2.43 (m, 1H, CH(CH₃)₂), 2.37 (m, 2H, CH(CH₃)₂), 2.19 (s, 3H, Ar-CH₃), 2.16 (s, 3H, Ar-CH₃), 2.07 (m, 1H, CH(CH₃)₂), 1.36 (q, ³J_{HH} = 8 Hz, 3H, CH(CH₃)₂), 1.20 (q, ³J_{HH} = 8 Hz, 9H, CH(CH₃)₂), 1.12 (q, ³J_{HH} = 8 Hz, 9H, CH(CH₃)₂), 0.91 (q, ³J_{HH} = 8 Hz, 3H, CH(CH₃)₂), -8.34 (t, ³J_{PH} = 17 Hz, 1H, Ir-H). ¹³C{¹H} NMR (C₆D₆): δ 179.7 (t, ²J_{PC} = 5 Hz), 161.1 (t, J = 8 Hz, C-N), 160.9 (t, J = 8 Hz, C-N), 131.7 (PNP aryl C), 131.5 (PNP aryl C), 130.7 (PNP aryl C), 130.6 (PNP aryl C), 124.4 (t, J = 6 Hz, PNP aryl C), 124.1 (t, J = 3 Hz, PNP aryl C), 124.0 (t, J = 3 Hz, PNP aryl C), 123.1 (t, J = 6 Hz, PNP aryl C), 115.8 (t, J = 4 Hz, PNP aryl C), 115.2 (t, J = 4 Hz, PNP aryl C), 81.6, 70.5, 67.1, 51.8 (t, J = 2 Hz), 26.6 (t, J = 16 Hz), 26.5, 25.9 (t, J = 15 Hz), 25.8, 20.5, 20.4, 18.7, 18.4, 18.2, 18.0, 17.6, 17.5, 17.1, 17.0. ³¹P{¹H} NMR: δ 28.6 (s). IR (cm⁻¹) ν(CO): 1980. Anal. calcd. for C₃₁H₄₈NO₃P₂Ir: C, 50.69; H, 6.54; N, 1.85. Found: C, 50.53; H, 6.57; N, 1.90.

Synthesis of (PNP)Ir(Ph)(CO)(H) (**4.18**).



Method A. To a solution of (PNP)IrH₂ (**4.8**) (18.6 mg, 0.0299 mmol) in benzyl methyl ether/pentane (6 mL, 1:5) was added norbornene (2.8 mg, 0.030 mmol) in benzyl methyl ether (2 mL). Over a period of several hours, a color change from red to golden was observed. After 4 h, the volatiles were removed by

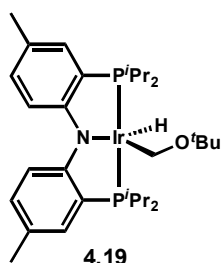
vacuum distillation at 60 °C. Analytically pure **4.18** was recovered as yellow crystals by slow evaporation of pentane from a concentrated solution at ambient temperature (18.0 mg, 83%).

¹H NMR (C₆D₆): δ 8.32 (br, 1H, -C₆H₅), 7.89 (d, J = 8.4 Hz, 2H, PNP aryl H), 7.60 (br, 1H, -C₆H₅), 7.16–6.96 (m, 3H, PNP aryl H and -C₆H₅), 6.78 (m, 1H -C₆H₅), 6.75 (d, J = 8.4 Hz, 2H, PNP aryl H), 2.25 (m, 2H, -CH(CH₃)₂), 2.13 (s, 6H, Ar-CH₃), 1.93 (m, 2H, -CH(CH₃)₂), 1.18 (dvt, 6H, -CH(CH₃)₂), 1.08 (dvt, 6H, -CH(CH₃)₂), 0.92 (dvt, 6H, -CH(CH₃)₂), 0.66 (dvt, 6H, -CH(CH₃)₂), -9.83 (t, ³J_{PH} = 15 Hz, 1H, Ir-H). ¹³C{¹H} NMR (C₆D₆): δ 175.6 (t, ²J_{PC} = 7 Hz, Ir-CO), 161.5 (t, J = 10

Hz), 132.4, 132.1, 128.9, 128.7, 127.8, 127.3, 125.9 (t, $J = 4$ Hz), 123.3, 122.4 (t, $J = 25$ Hz), 118.0 (t, $J = 5$ Hz), 29.2 (t, $J = 18$ Hz), 28.6 (t, $J = 16$ Hz), 20.7, 20.3, 20.1, 19.7, 19.4, 19.0. $^{31}\text{P}\{^1\text{H}\}$ NMR (C_6D_6): δ 39.6 (s). IR (THF, KBr, cm^{-1}) $\nu(\text{CO})$: 1995. Anal. calcd. for $\text{C}_{33}\text{H}_{46}\text{IrNOP}_2$: C, 54.53; H, 6.38; N, 1.93. Found: C, 53.45; H, 6.35; N, 1.88.

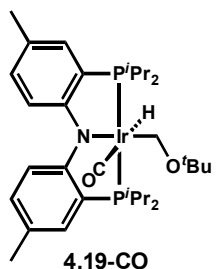
Method B. To a vial containing (PNP)IrH₂ (**4.8**) (20.7 mg, 0.0332 mmol) was added an excess of benzaldehyde (ca. 2 mL). As the red solids dissolved, the solution adopted a golden hue. After 20 min, volatile components were removed by vacuum distillation at 60 °C to leave a golden residue. Quantitative generation of **4.18** was confirmed by ^1H and ^{31}P NMR spectroscopy.

Observation of (PNP)Ir(H)(CH₂O^tBu) (4.19). To a vial containing (PNP)IrH₂ (**4.8**) (23.4 mg, 0.0376



mmol) and MTBE (ca. 50 μL) was added a solution of norbornene (12.5 mg, 0.133 mmol) in cyclohexane- d_{12} (ca. 700 μL), causing an immediate color change from red to brown. ^{31}P NMR spectroscopy revealed generation of an intermediate species (δ 45 ppm), and ^1H NMR spectroscopy showed a distinct hydride signal at δ -34.7 ppm (t, $^2J_{\text{PH}} = 12.6$ Hz), consistent with similar previously characterized complexes as well as the analogous α -oxoalkyl hydride complex **4.17**.¹⁰

Solution Characterization of (PNP)Ir(H)(CH₂O^tBu)(CO) (4.19-CO). (PNP)IrH₂ (**4.8**) (25.0 mg,



0.0401 mmol) and norbornene (8.1 mg, 0.086 mmol) were combined in MTBE (800 μL) and the resulting brown solution was transferred to a J. Young tube. ^{31}P NMR spectroscopy after 10 min revealed quantitative generation of the previously observed intermediate species (δ 45 ppm). The solution was frozen and the headspace evacuated and backfilled with carbon monoxide (1 atm). As the solution thawed, an immediate color change from brown to yellow was observed, and ^{31}P

NMR revealed a mixture containing a new species (δ 30 ppm) and the previously characterized (PNP)Ir–CO (**4.11**) in a >9:1 ratio. Volatile components were removed *in vacuo* and the yellow residues redissolved in C_6D_6 , allowing characterization of the new product, **4.19-CO**. 1H NMR (C_6D_6): δ 7.70 (dt, $J_1 = 8.4$ Hz, $J_2 = 2.1$ Hz, 2H, Ar–H), 6.96 (m, 2H, Ar–H), 6.75 (dd, $J_1 = 8.4$ Hz, $J_2 = 2.1$ Hz), 4.45 (t, $^3J_{PH} = 4.2$ Hz, 2H, $-CH_2O^tBu$), 2.55 (m, 2H, $-CH(CH_3)_2$), 2.21 (s, 6H, Ar– CH_3), 2.20 (m, 2H, $-CH(CH_3)_2$), 1.32 (dvt, 6H, $-CH(CH_3)_2$), 1.27–1.12 (m, 12H, $-CH(CH_3)_2$), 1.22 (s, 9H, $-OC(CH_3)_3$), 1.04 (dvt, 6H, $-CH(CH_3)_2$), -8.19 (t, $^2J_{PH} = 1H, 1H, Ir-H$). $^{13}C\{^1H\}$ NMR (C_6D_6): δ 180.3 (Ir–CO), 161.7 (t, $J = 7.4$ Hz), 131.8, 131.3, 125.1 (t, $J = 25$ Hz), 124.3, 116.1, 73.7, 27.9, 27.2, 27.1, 27.0, 20.9, 19.1, 18.7, 18.5. $^{31}P\{^1H\}$ NMR (C_6D_6): δ 30.4 (s). IR (THF, KBr, cm^{-1}) $\nu(CO)$: 1976 cm^{-1} .

Synthesis of *trans*-(PNP)Ir(H)₂(CO) (4.10) from 1,3,5-trioxane. (PNP)IrH₂ (**4.8**) (16.5 mg, 0.026 mmol) was placed in a J. Young tube followed by the addition of a mesitylene solution of 1,3,5-trioxane (33 mg, 0.36 mmol) and norbornene (5 mg, 0.053 mmol). $^{31}P\{^1H\}$ showed instantaneous generation of a reaction mixture containing 60% of the known compound (PNP)Ir(H)(mes),⁴³ 15% of the *trans*-(PNP)Ir(H)₂(CO), and 25% of an unidentified compound (42.1 ppm). The reaction mixture was heated at 85°C for 30 min, after which time ^{31}P and 1H NMR showed quantitative generation of *trans*-(PNP)Ir(H)₂(CO) from all three intermediates.

X-ray Crystallography Procedures. X-ray quality crystals were grown as indicated in the experimental procedures for each complex. For complexes other than **4.15**, the crystals were mounted on a glass fiber with Paratone-N oil. Structures were determined using direct methods with standard Fourier techniques using the Bruker AXS software package. In some cases, Patterson maps were used in place of the direct methods procedure.

For complex **4.15**, all operations were performed on a Bruker-Nonius Kappa Apex2 diffractometer using graphite-monochromated MoK α radiation. All diffractometer manipulations, including data collection, integration, scaling, and absorption corrections were carried out using the Bruker Apex2 software.⁶⁴ Preliminary cell constants were obtained from three sets of 12 frames. Data collection was carried out at 120K, using a frame time of 10 sec and a detector distance of 60 mm. The optimized strategy used for data collection consisted of three phi and nine omega scan sets, with 0.5° steps in phi or omega; completeness was 99.9%. A total of 3173 frames were collected. Final cell constants were obtained from the xyz centroids of 9725 reflections after integration.

From the systematic absences, the observed metric constants and intensity statistics, space group *Pbca* was chosen initially; subsequent solution and refinement confirmed the correctness of this choice. The structure was solved using SIR-92,⁶⁵ and refined (full-matrix-least squares) using the Oxford University *Crystals for Windows* program.⁶⁶ All ordered non-hydrogen atoms were refined using anisotropic displacement parameters; hydrogen atoms were fixed at calculated geometric positions and allowed to ride on the corresponding carbon atoms.

The carbene ring was placed such that the O atom was in the 2-position (as established from spectroscopic evidence). The carbene ring lies on a crystallographic twofold axis containing the Ir and C14 atoms, and thus the O and C atoms must be disordered in the 2- and 5-positions. Beyond this expected disorder, it was noted that the oxygen atom (O1) and the carbon atom in the 5-position (C15) are not strictly related by the crystallographic 2 axis; further, the atoms in the 3- and 4-positions (C17, C16) are also not related by the twofold axis. In the final model the occupancies of atoms O1, C15, C16 and C17 were fixed at 0.5 and refined by using isotropic displacement parameters. In addition, both angular and distance restraints were made to various atoms on the ring, with an angular restraint for C14-O1-C17 to be 110.0(5)°, the distance

restrain of C(15) to C(16), C(17) to O(1), C(14) to C(15), C(16) to C(17), and C(14) to O(1) to be 1.500, 1.490, 1.400, 1.480, and 1.350, (with esd's of 0.005), respectively.

Table 4.1 contains the X-ray diffraction experimental details for all complexes.

Table 4.1. X-ray crystallographic data

complex	4.6	4.7	4.9
Empirical Formula	C ₂₇ H ₃₈ IrP ₂	C ₂₇ H ₃₇ IrOP ₂	C ₃₁ H ₅₀ IrNOP ₂
Formula Weight	743.61	631.71	706.86
λ (Å)	0.71073	0.71073	0.71073
T (K)	100(2)	100(2)	100(2)
a (Å)	7.4979(4)	8.2807(6)	15.554(4)
b (Å)	16.7508(10)	14.1531(10)	11.303(3)
c (Å)	20.6495(12)	11.5174(9)	18.303(4)
α (deg)	90	90	90
β (deg)	90	106.646(2)	91.557(8)
γ (deg)	90	90	90
V (Å ³)	2593.5(3)	1293.24(17)	3216.6(13)
Z	4	2	4
Crystal System	Orthorhombic	Monoclinic	Monoclinic
Space Group	P2(1)2(1)2(1)	P2(1)	P2(1)/c
d _{calc} (g/cm ³)	1.904	1.622	1.46
GOF on F ²	1.039	1.060	1.314
R1, wR2 ^a (I > 2 σ (I))	0.0442, 0.0986	0.0559, 0.1075	0.0526, 0.0888

complex	4.10	4.15	4.16
Empirical Formula	C ₂₇ H ₄₂ IrNOP ₂ · C ₆ H ₆	C ₃₀ H ₄₆ IrNOP ₂	C ₃₀ H ₄₈ IrNOP ₂
Formula Weight	728.86	690.87	692.83
λ (Å)	0.71073	0.71073	0.71073
T (K)	100(2)	100(2)	100(2)
a (Å)	11.0661(3)	10.6616(6)	10.650(3)
b (Å)	14.3670(4)	17.4949(10)	11.288(3)
c (Å)	20.2719(5)	15.7215(9)	14.491(4)
α (deg)	90	90	67.416(6)
β (deg)	90	90	70.097(6)
γ (deg)	90	90	72.263(7)
V (Å ³)	3222.96(15)	2932.4(3)	1481.7(7)
Z	4	4	2
Crystal System	Orthorhombic	Orthorhombic	Triclinic
Space Group	Pccn	Pbcn	P-1
d _{calc} (g/cm ³)	1.502	1.565	1.553
GOF on F ²	1.527	1.085	1.661
R1, wR2 ^a (I > 2σ (I))	0.0365, 0.0722	0.0298, 0.0599	0.0403, 0.0551

complex	4.18
Empirical Formula	C ₃₃ H ₄₆ IrNOP ₂
Formula Weight	726.85
λ (Å)	0.71073
T (K)	100(2)
a (Å)	9.3928(4)
b (Å)	15.9869(6)
c (Å)	20.6970(9)
α (deg)	90
β (deg)	90
γ (deg)	90
V (Å ³)	3107.9(2)
Z	4
Crystal System	Orthorhombic
Space Group	P2(1)2(1)2(1)
d_{calc} (g/cm ³)	1.553
GOF on F ²	0.992
R1, wR2 ^a (I > 2 σ (I))	0.0257, 0.0359

References and Notes

- (1) (a) Labinger, J. A.; Bercaw, J. E. *Nature* **2002**, *417*, 507. (b) Fekl, U.; Goldberg, K. I. *Adv. Inorg. Chem.* **2003**, *54*, 259. (c) Crabtree, R. H. *J. Chem. Soc., Dalton. Trans.* **2001**, 2437. (d) Arndtsen, B. A.; Bergman, R. G.; Mobley, T. A.; Peterson, T. H. *Acc. Chem. Res.* **1995**, *28*, 154. (e) Shilov, A. E.; Shul'pin, G. B. *Chem. Rev.* **1997**, *97*, 2879.
- (2) (a) Xu, W.-w.; Rosini, G. P.; Gupta, M.; Jensen, C. M.; Kaska, W. C.; Krogh-Jespersen, K.; Goldman, A. S. *Chem. Commun.* **1997**, 2273. (b) Liu, F.; Goldman, A. S. *Chem. Commun.* **1999**, 655. (c) Jensen, C. M. *Chem. Commun.* **1999**, 2443. (d) Goldman, A. S.; Renkema, K. B.; Czerw, M.; Krogh-Jespersen, K. Alkane Transfer-Dehydrogenation Catalyzed by a Pincer-Ligated Iridium Complex. In *Activation and Functionalization of C-H Bonds*; Goldberg, K. I., Goldman, A. S., Eds.; ACS Symposium Series 885; American Chemical Society: Washington, DC, 2004; pp 198–215.
- (3) (a) Van der Boom, M. E.; Milstein, D. *Chem. Rev.* **2003**, *103*, 1759. (b) Singleton, J. T. *Tetrahedron* **2003**, *59*, 1837.
- (4) Gupta, M.; Hagen, C.; Flesher, R. J.; Kaska, W. C.; Jensen, C. M. *Chem. Commun.* **1996**, 2083.
- (5) (a) West, N. M.; White, P. S.; Templeton, J. L. *J. Am. Chem. Soc.* **2007**, *129*, 12372. (b) Gupta, M.; Kaska, W. C.; Jensen, C. M. *Chem. Commun.* **1997**, 461. (c) Zhang, X.; Fried, A.; Knapp, S.; Goldman, A. S. *Chem. Commun.* **2003**, 2060.
- (6) For general references on catalysis utilizing PNP pincer-type ligands, see: Liang, L.-C. *Coord. Chem. Rev.* **2006**, *250*, 1152.
- (7) Haenel, M. W.; Oevers, S.; Angermund, K.; Kaska, W. C.; Fan, H. J.; Hall, M. B. *Angew. Chem. Int. Ed.* **2001**, *40*, 3596.
- (8) Haenel, M. W.; Oevers, S.; Bruckmann, J.; Kuhnigk, J.; Kruger, C. *Synlett* **1998**, 301.
- (9) Ozerov, O. V.; Guo, C.; Papkov, V. A.; Foxman, B. M. *J. Am. Chem. Soc.* **2004**, *126*, 4792.
- (10) Fan, L.; Parkin, S.; Ozerov, O. V. *J. Am. Chem. Soc.* **2005**, *127*, 16772.
- (11) (a) Gottker-Schnetmann, I.; Brookhart, M. *J. Am. Chem. Soc.* **2004**, *126*, 9330. (b) Gottker-Schnetmann, I.; White, P.; Brookhart, M. *J. Am. Chem. Soc.* **2004**, *126*, 1804.
- (12) Ghosh, R.; Kanzelberger, M.; Emge, T. J.; Hall, G. S.; Goldman, A. S. *Organometallics* **2006**, *25*, 5668.
- (13) (a) Collman, J. P.; Kubota, M.; Vastine, F. D.; Sun, J. Y.; Kang, J. W. *J. Am. Chem. Soc.* **1968**, *90*, 5430. (b) Whited, M. T.; Mankad, N. P.; Lee, Y.; Oblad, P. F.; Peters, J. C. *Inorg. Chem.* **2009**, *48*, 2507.

- (14) Fryzuk, M. D.; Macneil, P. A.; Rettig, S. J. *Organometallics* **1986**, *5*, 2469.
- (15) (a) Rybtchinski, B.; Ben-David, Y.; Milstein, D. *Organometallics* **1997**, *16*, 3786. (b) Fryzuk, M. D.; Macneil, P. A. *Organometallics* **1983**, *2*, 682.
- (16) (a) Demott, J. C.; Basuli, F.; Kilgore, U. J.; Foxman, B. M.; Huffman, J. C.; Ozerov, O. V.; Mindiola, D. J. *Inorg. Chem.* **2007**, *46*, 6271. (b) Zhu, Y. J.; Fan, L.; Chen, C. H.; Finnell, S. R.; Foxman, B. M.; Ozerov, O. V. *Organometallics* **2007**, *26*, 6701.
- (17) (a) Luecke, H. F.; Arndtsen, B. A.; Burger, P.; Bergman, R. G. *J. Am. Chem. Soc.* **1996**, *118*, 2517. (b) Gutiérrez-Puebla, E.; Monge, Á.; Nicasio, M. C.; Pérez, P. J.; Poveda, M. L.; Carmona, E. *Chem.—Eur. J.* **1998**, *4*, 2225.
- (18) (a) Carmona, E.; Paneque, M.; Santos, L. L.; Salazar, V. *Coord. Chem. Rev.* **2005**, *249*, 1729. (b) Alvarez, E.; Paneque, M.; Petronilho, A. G.; Poveda, M. L.; Santos, L. L.; Carmona, E.; Mereiter, K. *Organometallics* **2007**, *26*, 1231. (c) Slugovc, C.; Mereiter, K.; Trofimenko, S.; Carmona, E. *Angew. Chem. Int. Ed.* **2000**, *39*, 2158. (d) Paneque, M.; Poveda, M. L.; Santos, L. L.; Salazar, V.; Carmona, E. *Chem. Commun.* **2004**, 1838. (e) Carmona, E.; Paneque, M.; Poveda, M. L. *J. Chem. Soc., Dalton Trans.* **2003**, 4022. (f) Santos, L. L.; Mereiter, K.; Paneque, M.; Slugovc, C.; Carmona, E. *New J. Chem.* **2003**, *27*, 107. (g) Luecke, H. F.; Bergman, R. G. *J. Am. Chem. Soc.* **1997**, *119*, 11538.
- (19) (a) Fraser, P. J.; Roper, W. R.; Stone, F. G. A. *J. Chem. Soc., Dalton Trans.* **1974**, 760. (b) Ozerov, O. V., Brandeis University, Waltham, MA. Personal communication, 2007. (c) Fan, L. PNP Pincer Ligands and their Late Transition Metal Complexes in the Context of Strong Bond Activation and Catalysis. Ph.D. Thesis, Brandeis University, 2006.
- (20) Kloek, S. M.; Heinekey, D. M.; Goldberg, K. I. *Organometallics* **2006**, *25*, 3007.
- (21) (a) Vaska, L.; DiLuzio, J. W. *J. Am. Chem. Soc.* **1961**, *83*, 2784. (b) Vaska, L. *Science* **1963**, *140*, 809. (c) Vaska, L.; Bath, S. S. *J. Am. Chem. Soc.* **1966**, *88*, 1333.
- (22) (a) Scott, R. N.; Shriver, D. F.; Vaska, L. *J. Am. Chem. Soc.* **1968**, *90*, 1079. (b) Shriver, D. F. *Acc. Chem. Res.* **1970**, *3*, 231.
- (23) Stone, K. C.; White, P. S.; Templeton, J. L. *J. Organomet. Chem.* **2003**, *684*, 13.
- (24) (a) Parkin, G.; Burger, B. J.; Trimmer, M. S.; Asselt, A. V.; Bercaw, J. E. *J. Mol. Catal.* **1987**, *41*, 21. (b) Schrock, R. R.; Seidel, S. W.; Mösch-Zanetti, N. C.; Shih, K.-Y.; O'Donoghue, M. B.; Davies, W. M.; Reiff, W. M. *J. Am. Chem. Soc.* **1997**, *119*, 11876.
- (25) (a) Carmona, E.; Paneque, M.; Poveda, M. L. *Dalton Trans.* **2003**, 4022. (b) Paneque, M.; Poveda, M. L.; Santos, L. L.; Carmona, E.; Lledós, A.; Ujaque, G.; Mereiter, K. *Angew. Chem., Int. Ed.* **2004**, *43*, 3708.

- (26) (a) Holtcamp, M. W.; Labinger, J. A.; Bercaw, J. E. *J. Am. Chem. Soc.* **1997**, *119*, 848. (b) Holtcamp, M. W.; Henling, L. M.; Day, M. W.; Labinger, J. A.; Bercaw, J. E. *Inorg. Chim. Acta* **1998**, *270*, 467.
- (27) Boutry, O.; Gutiérrez, E.; Monge, A.; Nicasio, M. C.; Pérez, P. J.; Carmona, E. *J. Am. Chem. Soc.* **1992**, *114*, 7288.
- (28) (a) Jones, W. D.; Hessel, E. T. *J. Am. Chem. Soc.* **1993**, *115*, 554. (b) Periana, R. A.; Bergman, R. G. *Organometallics* **1984**, *3*, 508.
- (29) (a) Gupta, M.; Kaska, W. C.; Jensen, C. M. *Chem. Commun.* **1997**, 461. (b) Zhang, X.; Fried, A.; Knapp, S.; Goldman, A. S. *Chem. Commun.* **2003**, 2060.
- (30) Brookes, N. J.; Whited, M. T.; Grubbs, R. H.; Yates, B. F., manuscript in preparation.
- (31) Whited, M. T.; Grubbs, R. H. *Organometallics* **2008**, *27*, 5737.
- (32) An alternative possibility is that hydrogen is lost directly from an α -oxoalkyl hydride intermediate via 1,2-elimination, though the previous observation of *cis*-dihydrido aminocarbenes for the (PNP)Ir system and computational studies on the MTBE reaction (ref 33) seem to discount this mechanism.
- (33) Brookes, N. J.; Ariaifard, A.; Stranger, R.; Yates, B. F. *J. Am. Chem. Soc.* **2009**, *131*, 5800.
- (34) (a) Gupta, M.; Kaska, W. C.; Jensen, C. M. *Chem. Commun.* **1997**, 461. (b) Zhang, X.; Fried, A.; Knapp, S.; Goldman, A. S. *Chem. Commun.* **2003**, 2060.
- (35) Ferrando-Miguel, G.; Coalter, J. N.; Gerard, H.; Huffman, J. C.; Eisenstein, O.; Caulton, K. G. *New J. Chem.* **2002**, *26*, 687.
- (36) The short C28–O1 bond length suggests that an alternative explanation for an elongated C27–C28 bond, namely polarization of the vinyl ether, may be operative. This type of distortion serves to increase the σ -donating ability of heteroatom-substituted olefins while reducing their π -acidity. However, the relatively similar Ir–C27 and Ir–C28 bond lengths as well as the expected low electrophilicity of the (PNP)Ir fragment indicate that the contribution from this sort of polarization is minimal. For leading references on polarization of bound vinyl ethers, see: (a) Chang, T. C. T.; Foxman, B. M.; Rosenblum, M.; Stockman, C. *J. Am. Chem. Soc.* **1981**, *103*, 7361. (b) Watson, L. A.; Franzman, B.; Bollinger, J. C.; Caulton, K. G. *New J. Chem.* **2003**, *27*, 1769.
- (37) See, for example: Gagnon, M. K. J.; St. Germain, T. R.; Vogels, C. M.; McNamara, R. A.; Taylor, N. J.; Westcott, S. A. *Aust. J. Chem.* **2000**, *53*, 693. (b) Alickmann, D.; Frohlich, R.; Maulitz, A. H.; Wurthwein, E.-U. *Eur. J. Org. Chem.* **2002**, 1523.
- (38) Nilsson, P.; Larhed, M.; Hallberg, A. *J. Am. Chem. Soc.* **2001**, *123*, 8217.

- (39) For leading references on the structural preferences of five-coordinate, d^6 metal complexes, see: (a) Lam, W. H.; Shimada, S.; Batsanov, A. S.; Lin, Z.; Marder, T. B.; Cowan, J. A.; Howard, J. A. K.; Mason, S. A.; McIntyre, G. J. *Organometallics* **2003**, *22*, 4557. (b) Rachidi, I. E.-I.; Eisenstein, O.; Jean, Y. *New J. Chem.* **1990**, *14*, 671. (c) Riehl, J.-F.; Jean, Y.; Eisenstein, O.; Pelissier, M. *Organometallics* **1992**, *11*, 729. (d) Olivan, M.; Eisenstein, O.; Caulton, K. G. *Organometallics* **1997**, *16*, 2227.
- (40) (a) Fryzuk, M. D.; MacNeil, P. A.; Ball, R. G. *J. Am. Chem. Soc.* **1986**, *108*, 6414. (b) Fryzuk, M. D.; MacNeil, P. A.; Massey, R. L.; Ball, R. G. *J. Organomet. Chem.* **1989**, *328*, 231.
- (41) Kanzelberger, M.; Singh, B.; Czerw, M.; Krogh-Jespersen, K.; Goldman, A. S. *J. Am. Chem. Soc.* **2000**, *122*, 11017.
- (42) For leading references, see: Procelewska, J.; Zahl, A.; Liehr, G.; van Eldik, R.; Smythe, N. A.; Williams, B. S.; Goldberg, K. I. *Inorg. Chem.* **2005**, *44*, 7732.
- (43) Zhu, Y.; Fan, L.; Chen, C.-H.; Finnell, S. R.; Foxman, B. M.; Ozerov, O. V. *Organometallics* **2007**, *26*, 6701.
- (44) (a) Gozin, M.; Weisman, A.; Ben-David, Y.; Milstein, D. *Nature* **1993**, *364*, 699. (b) Liou, S.-Y.; Gozin, M.; Milstein, D. *J. Am. Chem. Soc.* **1995**, *117*, 9774. (c) Rybtchinski, B.; Vigalok, A.; Ben-David, Y.; Milstein, D. *J. Am. Chem. Soc.* **1996**, *118*, 12406.
- (45) For related studies of N-C_{sp}³ cleavage in a pincer-type ligand, see reference 9 and Weng, W.; Guo, C.; Moura, C.; Yang, L.; Foxman, B. M.; Ozerov, O. V. *Organometallics* **2005**, *24*, 3487.
- (46) For an unusual case of C-C cleavage by β -phenyl elimination that does not involve a preorganized system, see: Campora, J.; Gutierrez-Puebla, E.; Lopez, J. A.; Monge, A.; Palma, P.; del Rıo, D.; Carmona, E. *Angew. Chem., Int. Ed.* **2001**, *40*, 3641.
- (47) See, for example: (a) Alaimo, P. J.; Arndtsen, B. A.; Bergman, R. G. *J. Am. Chem. Soc.* **1997**, *119*, 5269. (b) Alaimo, P. J.; Arndtsen, B. A.; Bergman, R. G. *Organometallics* **2000**, *19*, 2130.
- (48) (a) Ohno, K.; Tsuji, J. *J. Am. Chem. Soc.* **1968**, *90*, 99. (b) Abu-Hasanayn, F.; Goldman, M. E.; Goldman, A. S. *J. Am. Chem. Soc.* **1992**, *114*, 2520. (c) Beck, C. M.; Rathmill, S. E.; Park, Y. J.; Chen, J.; Crabtree, R. H.; Liable-Sands, L. M.; Rheingold, A. L. *Organometallics* **1999**, *18*, 5311. (d) Fristrup, P.; Kreis, M.; Palmelund, A.; Norrby, P.-O.; Madsen, R. *J. Am. Chem. Soc.* **2008**, *130*, 5206.
- (49) This step bears some resemblance to the β -hydrogen elimination and loss of olefin that occurs in transfer dehydrogenation schemes at pincer-supported iridium centers. For a discussion of the mechanism of these types of reactions, see: Renkema, K. B.; Kissin, Y. V.; Goldman, A. S. *J. Am. Chem. Soc.* **2003**, *125*, 7770.

- (50) Such a stereoselective 1,2-migration is similar to what we and others have previously observed in the decarbonylation of formaldehyde.
- (51) Baldwin, J. E. *J. Chem. Soc. Chem. Commun.* **1976**, 734.
- (52) Van der Sluys, L. S.; Kubas, G. J.; Caulton, K. G. *Organometallics* **1991**, *10*, 1033.
- (53) Klei, S. R.; Golden, J. T.; Tilley, T. D.; Bergman, R. G. *J. Am. Chem. Soc.* **2002**, *124*, 2092.
- (54) Zhang, X.; Emge, T. J.; Ghosh, R.; Goldman, A. S. *J. Am. Chem. Soc.* **2005**, *127*, 8250.
- (55) For leading references on C–C activation, see: Rybtchinski, B.; Milstein, D. *Angew. Chem., Int. Ed.* **1999**, *38*, 870.
- (56) Walker, J. F.; Chadwick, A. F. *Ind. Eng. Chem.* **1947**, *39*, 974.
- (57) Ozerov, O. V.; Pink, M.; Watson, L. A.; Caulton, K. G. *J. Am. Chem. Soc.* **2004**, *126*, 2105.
- (58) Nemeš, S.; Flesher, R. J.; Gierling, K.; Maichle-Mossmer, C.; Mayer, H. A.; Kaska, W. C. *Organometallics* **1998**, *17*, 2003.
- (59) Gallop, M. A.; Roper, W. R. *Adv. Organomet. Chem.* **1986**, *25*, 121.
- (60) Pangborn, A. B.; Giardello, M. A.; Grubbs, R. H.; Rosen, R. K.; Timmers, F. J. *Organometallics* **1996**, *15*, 1518.
- (61) Wolfsberger, W.; Burkart, W.; Bauer, S.; Hampp, A.; Wolf, J.; Werner, H. Z. *Naturforsch. B* **1994**, *49*, 1659.
- (62) Bangerter, B. W.; Beatty, R. P.; Kouba, J. K.; Wreford, S. S. *J. Org. Chem.* **1977**, *42*, 3247.
- (63) Kilian, P.; Slawin, A. M. Z. *J. Chem. Soc., Dalton Trans.* **2007**, 3289.
- (64) Apex2, Version 2 User Manual, M86-E01078, Bruker Analytical X-ray Systems, Madison, WI, June 2006.
- (65) Altomare, A.; Cascarano, G.; Giacovazzo, G.; Guagliardi, A.; Burla, M. C.; Polidori, G.; Camalli, M. *J. Appl. Cryst.* **1994**, *27*, 435.
- (66) Betteridge, P. W.; Carruthers, J. R.; Cooper, R. I.; Prout, K.; Watkin, D. J. *J. Appl. Cryst.* **2003**, *36*, 1487.

Chapter 5

A Distinct Class of M=C Bond Reactivity: Elucidation of Heterocumulene Activation by a Nucleophilic-at-Metal Iridium(I) Carbene

The text in this chapter is reproduced in part with permission from:

Whited, M. T.; Grubbs, R. H. *J. Am. Chem. Soc.* **2008**, *127*, 5874–5875.

Copyright 2008 American Chemical Society

and

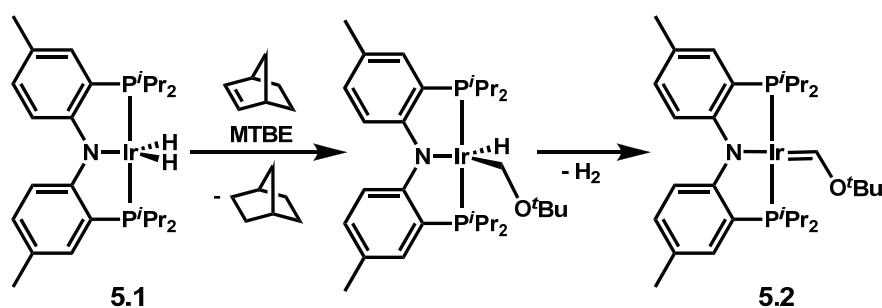
Whited, M. T.; Grubbs, R. H. *Organometallics* **2009**, *28*, 161–166.

Copyright 2009 American Chemical Society

Introduction

The reactivity of transition metal–carbon multiple bonds has been the subject of intense investigation for many years, allowing the development of a host of transformations based on reactivity of the carbene unit.¹ In general, these transformations are dominated by carbon-based frontier orbitals.² Thus, metal–carbon multiple bonds are conventionally divided into two classes, where Fischer carbenes (coordinated singlet carbenes) are electrophilic at carbon and Schrock carbenes (coordinated triplet carbenes) are nucleophilic at carbon.

We have been investigating the reactivity of iridium species supported by Ozerov's PNP ligand (PNP = $[N(2-P^iPr_2-4-Me-C_6H_3)_2]^-$),³ and recently reported that the (PNP)Ir fragment could generate a square-planar *tert*-butoxymethylidene complex by double C–H activation of *tert*-butyl methyl ether and loss of dihydrogen (Scheme 6.1). Furthermore, the unusual decomposition pathway of this and related complexes, combined with rudimentary electronic considerations, indicated that the reactivity of these types of species would be dominated by a high-lying, nucleophilic Ir(d_{22}) orbital. This would be distinct from what has been previously reported and would offer the possibility of activating electrophiles across the M=C bond of a heteroatom-substituted carbene complex.



Scheme 5.1. Generation of an iridium carbene by double C–H activation of MTBE.

As shown in Figure 5.1, there are four possible interactions between metal carbenes and nucleophiles or electrophiles. In the continuum shown, classical Fischer carbenes are considered to be electrophilic at carbon (top left), while Shrock-type carbenes fall somewhere between the two lower scenarios, electrophilic at metal and nucleophilic at carbon.^{2a} There have also been examples of Fischer-type carbenes attached to highly reduced early-metal centers where the carbene is clearly nucleophilic.⁴ However, the reactivity of carbene complexes with nucleophilic metal centers has not been explored, so we were interested in exploiting the unusual structure of complex **5.2** in the activation of electrophiles.

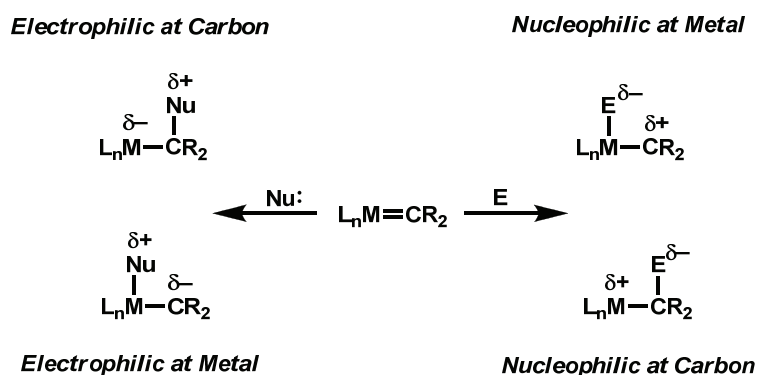


Figure 5.1. Possible modes of reactivity of metal carbenes with nucleophiles and electrophiles.

Though there is significant interest in reductive transformations of carbon dioxide,^{5,6} direct scission of the C=O bond is seldom realized due to the thermodynamic stability of the highly oxidized carbon and the bond strength (127 kcal/mol).⁷ Highly reducing early transition-metal and uranium complexes have been reported to effect the cleavage of CO₂,⁸ but it is rarely accomplished at late transition-metal centers.^{9,10} Peters and co-workers have recently described a low-valent iron complex that breaks the C=O bond, yielding a bimetallic dimer with a structurally unique μ -carbonyl/ μ -oxo core.^{9a} Additionally, Sadighi and co-workers have reported the copper-catalyzed deoxygenation of CO₂ via net oxygen-atom transfer to diborane reagents.^{9c}

In this chapter, we describe the reactivity of *tert*-butoxymethylidene complex **5.2**, which may be generated by double C–H activation of MTBE. We report that the nucleophilic complex interacts with carbon dioxide to effect quantitative oxygen-atom transfer from CO₂ to the metal carbene, yielding *tert*-butyl formate and an iridium carbonyl. The carbene has also been found to effect sulfur-atom and nitrene-group transfer from carbonyl sulfide and phenyl isocyanate, respectively. Although transition metal–carbene complexes are fundamentally important in a number of transformations, both catalytic and stoichiometric, to our knowledge the only reports of reactivity between metal-bound carbenes and CO₂ involve nucleophilic attack by the carbene.¹¹ Thus, the decarbonylative pathways described in this contribution represent a unique mode of reactivity for metal carbenes.

Results and Discussion

Oxygen-Atom Transfer from CO₂ to a Fischer Carbene at (PNP)Ir

As we have noted previously, an initial survey of the reactivity of **5.2** revealed a strong propensity to decarbonylate the carbene upon thermolysis, releasing isobutylene and forming the *trans*-dihydrido iridium carbonyl complex ($\nu_{\text{CO}} = 1991 \text{ cm}^{-1}$).¹² Also, unlike numerous reported Fischer carbenes,¹³ **5.2** does not react with nucleophiles such as amines, alkoxides, or alkyllithium reagents, indicating the low electrophilicity of the carbene bound to low-valent iridium.

In light of these findings, we anticipated that distinct reactivity might be realized. Since simple molecular-orbital considerations indicate that the square-planar Ir(I) should have a HOMO of d_{z^2} origin oriented out of the plane of the complex, we were intrigued by the possible reactivity of **5.2** with electrophiles.^{13d} Exposure of a solution of **5.2** in C₆D₆ to an atmosphere of CO₂ resulted in the quantitative formation of (PNP)Ir–CO (**5.3**, $\nu_{\text{CO}} = 1930 \text{ cm}^{-1}$), for which a

molecular representation is provided in Figure 5.2, over a period of 30 min with concomitant expulsion of *tert*-butyl formate (eq 5.1). Reaction of **5.3** with $^{13}\text{CO}_2$ afforded $(\text{PNP})\text{Ir}-^{13}\text{CO}$ ($\nu_{\text{CO}} = 1883 \text{ cm}^{-1}$), confirming that the carbonyl ligand is derived from carbon dioxide. Although oxygen-atom transfer from CO_2 to free carbenes has been reported and studied theoretically,¹⁴ this reaction represents an unusual instance of oxygen extrusion from carbon dioxide by a metal-bound carbene.

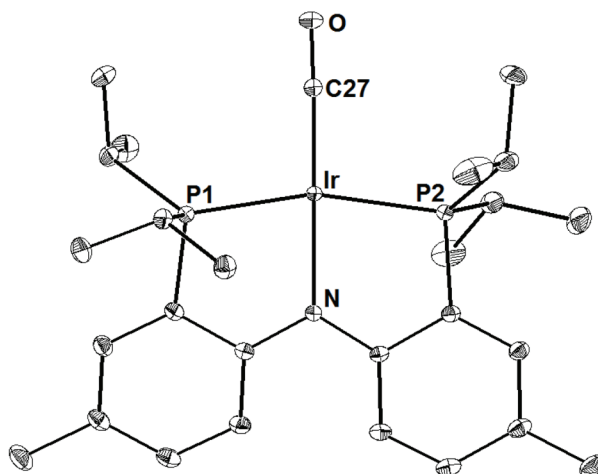
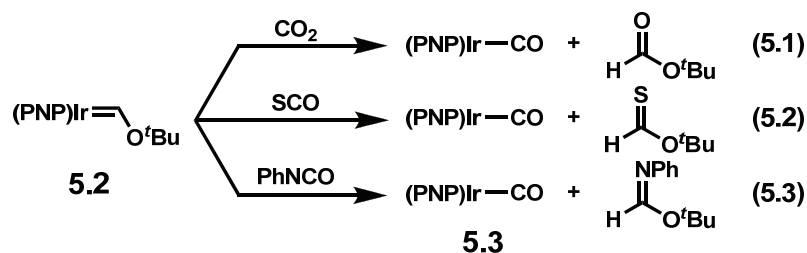
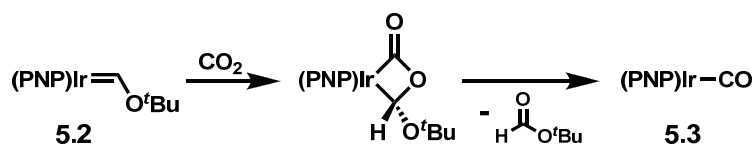


Figure 5.2. Displacement ellipsoid (35%) representation of $(\text{PNP})\text{Ir}-\text{CO}$ (**5.3**) with hydrogen atoms and solvent molecules removed for clarity. Selected bond lengths (\AA) and angles ($^\circ$): Ir–N, 2.073(1); Ir–C27, 1.826(1); Ir–P1, 2.2865(4); Ir–P2, 2.2886(4); P1–Ir–P2, 161.20(1); N–Ir–C27, 176.68(7).



We propose a mechanism wherein initial nucleophilic attack at CO_2 by iridium is followed by cyclization to form a 4-membered metallalactone analogous to the metallacyclobutane demonstrated as an intermediate in olefin metathesis.¹⁵ Subsequent elimination of *tert*-butyl formate results in an effective “oxygen-atom metathesis” from CO_2 to

the metal-bound Fischer carbene (Scheme 5.2).¹⁶ When the reaction is monitored by ^1H NMR at $-60\text{ }^\circ\text{C}$, small amounts of an intermediate species are observed. Consistent with the assignment of this species as the metallacycle is the appearance of a triplet (δ 6.5 ppm, $^3J_{\text{PH}} = 9\text{ Hz}$) formulated as the metallalactone proton.



Scheme 5.2. Proposed mechanism of CO_2 decarbonylation by carbene **5.2**.

This proposed mechanism is also supported by kinetic studies. Pseudo-first-order experiments conducted at $-20\text{ }^\circ\text{C}$ indicated that the reaction is first order in both **5.2** and CO_2 (Figure 5.3). Thus, the mechanism of the reaction is associative, as expected. Observation of the metallacycle by NMR spectroscopy (*vide supra*) suggests that the relative energetic barriers for metallacycle formation and formate elimination can be reversed or at least made very close at lower temperatures.

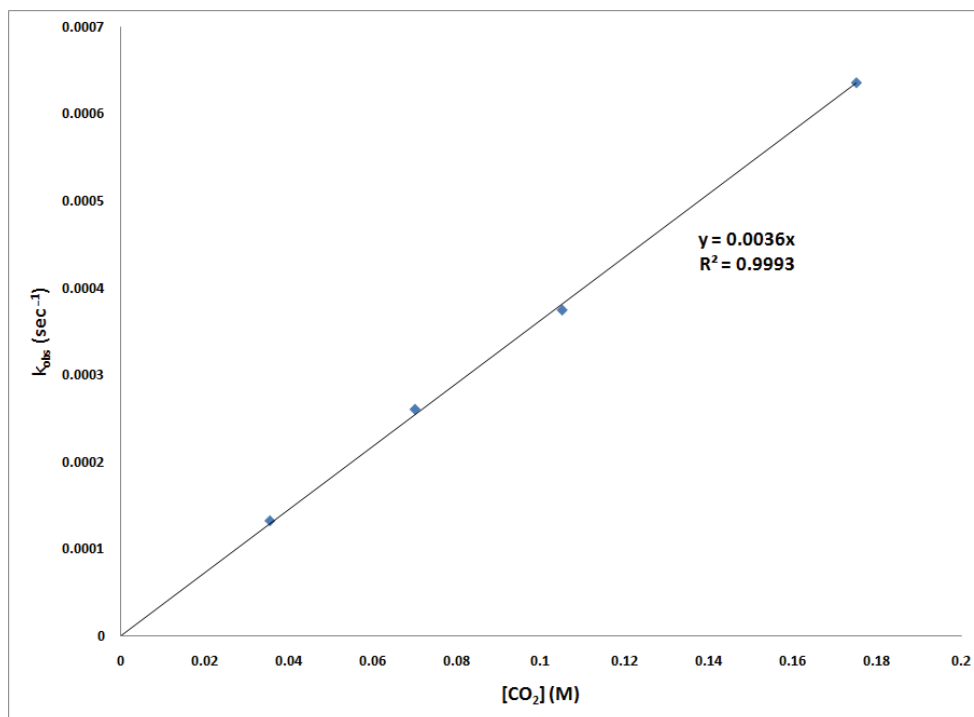
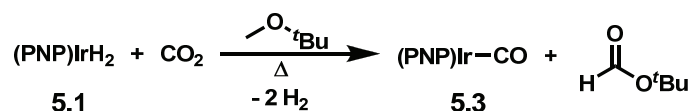


Figure 5.3. Plot of k_{obs} versus concentration of CO_2 for the reaction of **5.2** with CO_2 at $-20\text{ }^\circ\text{C}$.

In light of this finding and previous results from Mayer's laboratory,^{8b} it seemed likely that **5.2** would effect the decarbonylation of other oxygen-containing heterocumulenes. Exposure of **5.2** to carbonyl sulfide (1 atm) results in immediate and quantitative formation of **5.3** and *tert*-butyl thioformate (eq 5.2). Similarly, addition of phenyl isocyanate to a solution of **5.3** in C_6D_6 effects nitrene transfer to the Fischer carbene to generate **5.3** and *N*-phenyl *tert*-butylformimidate (eq 5.3). To our knowledge, the closest precedent for this type of reaction comes from Ibers' report of sulfur-atom transfer from SCO to triphenylphosphine at low-valent iron and ruthenium centers.¹⁷ The formation of isocyanates by the interaction of nitrenes and CO at transition metals has also been reported.¹⁸ The facility with which the SCO and PhNCO reactions proceed at low temperatures precludes the observation of reactive intermediates or thorough kinetic analysis, but 4-membered metallacyclic intermediates are proposed since carbonyl sulfide and phenyl isocyanate are isoelectronic to carbon dioxide.

The acceptorless oxidation of *tert*-butyl methyl ether to *tert*-butyl formate can be accomplished in one pot by thermolysis of (PNP)IrH₂ (**5.1**) in MTBE under an atmosphere of CO₂, generating **5.3** and one equivalent of *tert*-butyl formate (Scheme 5.3). At this time, it seems that the unusually high driving force for all of the transformations described can be attributed to the stability of (PNP)Ir–CO (**5.3**). Thus, development of catalytic reactions is likely to be hampered by the large energy input required to regenerate **5.1**.



Scheme 5.3. Acceptorless dehydrogenative oxidation of MTBE to *tert*-butyl formate via oxygen-atom transfer from CO₂.

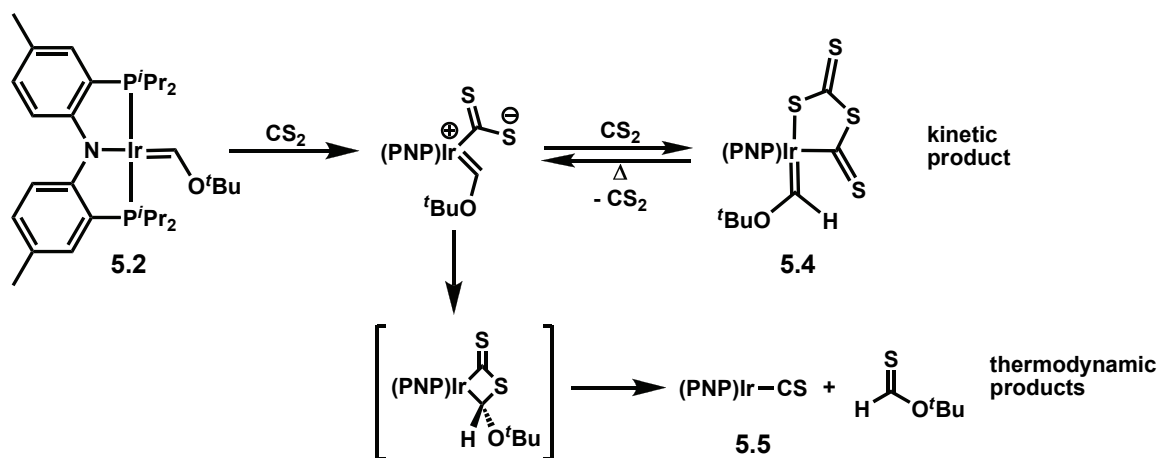
Elucidation of Heterocumulene Activation at a (PNP)Ir Fischer Carbene

The proposed mode of reactivity with carbonyl reagents implies that the high d-electron count and coordinatively unsaturated nature of carbene **5.2** confer a degree of nucleophilicity to the iridium center that controls reactivity of the complex, contrasting previous reports of heterocumulene reactivity where the metal-bound carbenes act as nucleophiles and C–C bonds are formed.^{19,20} Such behavior would not be entirely unexpected in light of Roper's previous observation, which we have confirmed for our system, that heteroatom-substituted carbenes rarely exhibit electrophilic character when attached to electron-rich, late transition metals.²⁸ Additionally, Stone has reported that a square-planar carbene of iridium(I) performs the oxidative addition of dihydrogen, affording an iridium(III) dihydrido carbene.²¹ By analogy, the electron-rich metal center in our system might be expected to play a central role in substrate activation.

Reaction of carbene **5.2** with CS₂ and PhNCS, which are isoelectronic to the carbonyl heterocumulenes previously examined (*vide supra*), allows observation and isolation of kinetically trapped intermediate species, supporting a mechanism of atom transfer that clearly requires a distinct mode of carbene reactivity. Additionally, experimental and theoretical studies indicate that a high-lying, nucleophilic Ir(d_{z²}) orbital plays a critical role in initiating these unusual transformations. Taken together, these findings suggest a new strategy for the activation of heterocumulenes and other electrophiles across metal–ligand multiple bonds at late transition metals. Interestingly, these reactivity patterns are complementary to those observed for the nucleophilic alkylidenes of the high-valent early metals.^{2a,19a,22}

Reactivity with Carbon Disulfide. In light of the high driving force for the formation of carbonyl complex **5.3**, reaction of carbene **5.2** with heterocumulenes lacking oxygen was examined with the goal of stabilizing an intermediate iridacyclic species. However, in contrast to the reactivity observed with oxygen-containing heterocumulenes, dissolution of (PNP)Ir=C(H)O^tBu (**5.2**) in neat CS₂ did not afford (PNP)Ir–CS but instead yielded the unusual CS₂ head-to-tail dimer complex **5.4** in which the iridium carbene unit remained intact (Scheme 5.4),^{23,24} as confirmed by X-ray diffraction analysis (Figure 5.4). The carbene proton retains a distinctive ¹H NMR shift (δ 15.5 ppm), consistent with an iridium–carbon multiple bond, but collapses from a triplet (in complex **5.2**) to a singlet (in complex **5.4**) due to the shifting of the C–H bond vector out of the plane of the iridium–phosphorus bonds.²⁵ The carbene is observed by ¹³C NMR at δ 266.7 ppm, shifted significantly downfield from the parent *tert*-butoxymethylidene (δ 210.0 ppm).²⁶ As a result of the change in metal oxidation state, the Ir=C bond of **5.4** is slightly elongated (1.96 Å) relative to carbene **5.2** (1.88 Å), and the C27–O1 bond is contracted by

approximately the same amount (from 1.35 to 1.28 Å), indicating a decrease in metal–carbon multiple-bond character and concomitant increase in the effective carbon–oxygen bond order.



Scheme 5.4. Reaction of carbene **5.2** with carbon disulfide.

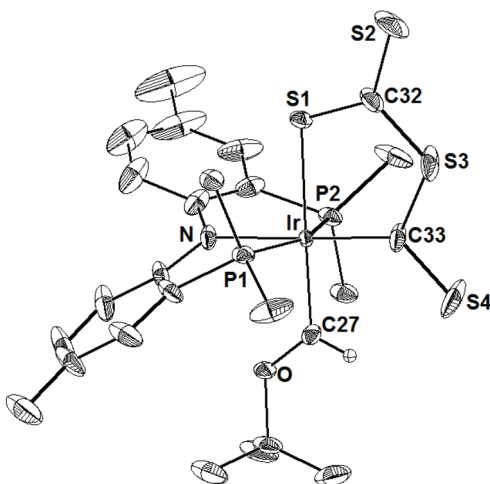


Figure 5.4. Displacement ellipsoid (35%) representation of $(\text{PNP})\text{Ir}(\text{C}_2\text{S}_4)(\text{CHO}^t\text{Bu})$ (**5.4**) with hydrogen atoms and phosphine substituents (except for *ipso* carbons) omitted for clarity. Relevant bond lengths (Å) and angles (°): Ir–C27, 1.960(4); Ir–S1, 2.397(1); Ir–N, 2.119(4); Ir–C33, 1.998(5); Ir–P1, 2.350(1); Ir–P2, 2.357(1); C27–O, 1.281(5); S1–Ir–C27, 179.1(1); N–Ir–C33, 178.5(2); P1–Ir–P2, 159.52(4).

Heating a benzene solution of **5.4** (70 °C, 16 h) caused quantitative degradation to $(\text{PNP})\text{Ir}-\text{CS}$ (**5.5**, Figure 5.5) with concomitant expulsion of *tert*-butyl thioformate and CS_2 (Scheme 5.4), indicating the potential intermediacy of CS_2 dimer **5.4** in the sulfur-atom transfer process (and suggesting CO_2 dimers as possible intermediates in previously reported oxygen-

atom transfer reactions).²⁴ However, previous studies of the kinetics of CO₂ deoxygenation by **5.2** had shown a first-order rate dependence on CO₂ concentration, indicating that such a mechanism was not operative. Additionally, the connectivity of **5.4** is more consistent with intermediates typically invoked in heterocumulene disproportionation reactions.²⁷ Thus, we were interested to see whether **5.4** was instead a kinetic product formed from the trapping of an intermediate species formed by reaction of **5.2** with CS₂.

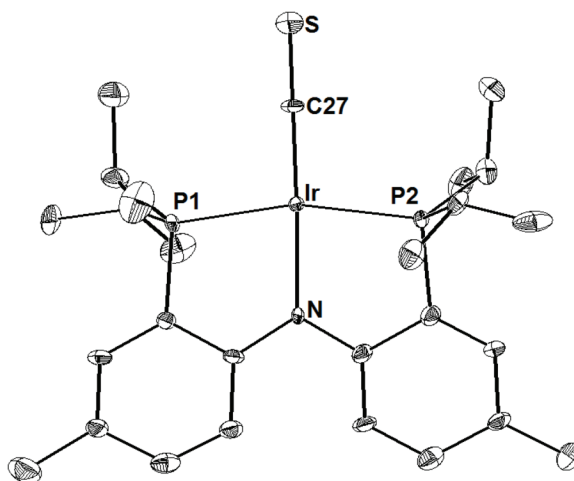


Figure 5.5. Displacement ellipsoid (35%) representation of (PNP)Ir-CS (**5.5**) with hydrogen atoms omitted for clarity. Selected bond lengths (Å) and angles (°): Ir–C27, 1.82(2); Ir–N, 2.04(1); Ir–P1, 2.290(3); Ir–P2, 2.298(3); N–Ir–C27, 170.0(7); P1–Ir–P2, 164.2(1).

Slow addition of one equivalent of CS₂ to a benzene solution of **5.2** resulted in the immediate and quantitative formation of thiocarbonyl complex **5.5** at *ambient temperature*, ruling out the intermediacy of **5.4** in the atom transfer reaction. Thus, as in our original assessment of the mechanism, we propose that reaction begins with nucleophilic attack by iridium at an electrophilic heterocumulene carbon. Depending on the concentration of CS₂, two pathways are available for this intermediate, and it can either be trapped by a second molecule of CS₂, affording **5.4**, or cyclize to the irida(dithio)lactone and decompose to give **5.5** and *tert*-butylthioformate as thermodynamic products (Scheme 5.4).²⁸ Therefore, compound **5.4** can be

viewed as a protected form of an intermediate species in the atom transfer reaction, supporting the view that atom and group transfers to carbene complex **5.2** are initiated by a nucleophilic metal rather than an electrophilic carbene ligand.^{29,30} This interpretation is also consistent with the observation that reductive condensations of CS₂ are generally promoted by nucleophilic, electron-rich metal centers.^{23a,e}

Reaction with Phenyl Isothiocyanate. The reactivity of **5.2** with isothiocyanates is considerably more complex and, depending on reaction conditions, several species were observed to form. In analogy to reaction with CS₂, slow addition of PhNCS (1 equiv) to a dilute solution of Fischer carbene **5.2** resulted in quantitative sulfur-atom transfer to generate (PNP)Ir–CNPh (**5.6**, Figure 5.6) and *tert*-butyl thioformate (Scheme 5.5). Although metal-mediated desulfurization of isothiocyanates has been reported,^{30b,31} this process typically occurs by sulfur-atom transfer to a phosphine ligand and has not been observed for metal-bound carbenes.

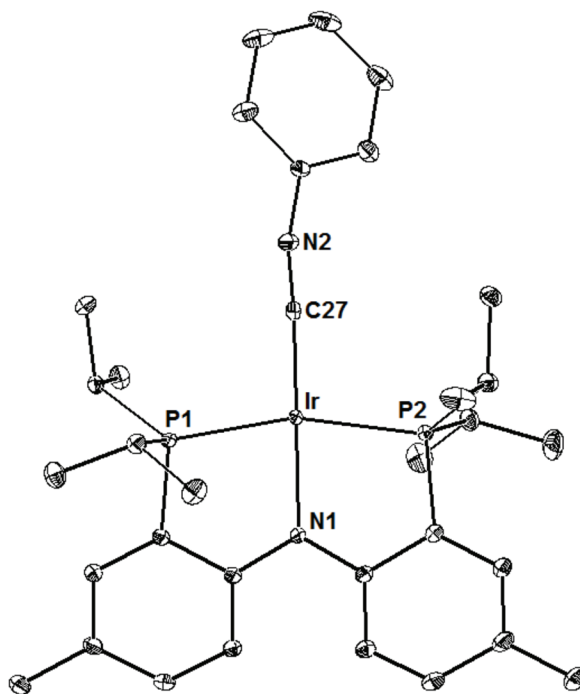
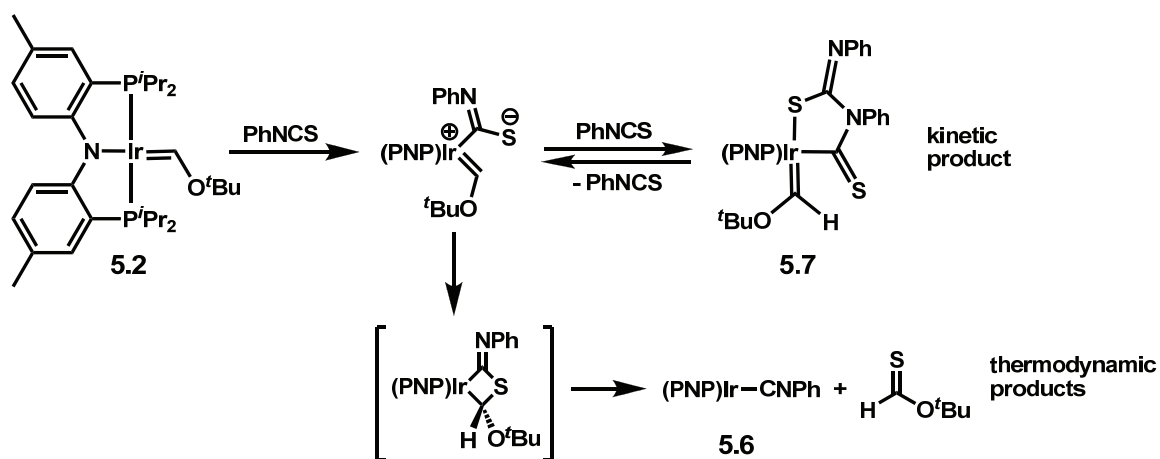


Figure 5.6. Displacement ellipsoid (35%) representation of (PNP)Ir–CNPh (**5.6**) with hydrogen atoms omitted for clarity. Selected bond lengths (Å) and angles (°): Ir–C27, 1.852(1); Ir–N, 2.071(9); Ir–P1, 2.2811(3); Ir–P2, 2.2877(3); C27–N2, 1.197(1); N1–Ir–C27, 177.09(4); P1–Ir–P2, 162.16(1).



Scheme 5.5. Reaction of carbene **5.2** with phenyl isothiocyanate.

In light of the reactivity observed for CS_2 , we were hopeful that exposure of **5.2** to an excess of PhNCS would allow the isolation of an iridium-supported PhNCS dimer similar to **5.4**. Addition of an excess (2–10 equiv) of PhNCS to concentrated solutions of **5.2** led to the

formation of species **5.7**, for which the spectroscopic data proved nearly identical to those of CS₂ dimer **5.4**, particularly the distinctive shift of the carbene proton in ¹H NMR (δ 15.5 ppm). However, this apparent PhNCS dimer was observed to decompose quickly (1 h) to isocyanide complex **5.6**, indicating the more facile reversibility of PhNCS versus CS₂ condensation in these complexes.

In the presence of excess PhNCS and *tert*-butyl thioformate, compound **5.6** converts to a new, structurally unusual species **5.8**, in which the C_s symmetry has been broken. X-ray diffraction analysis of single crystals of **5.8** revealed the structural motif depicted in Figure 5.7, which results from the reductive condensation of PhNCS and *tert*-butyl thioformate (Scheme 5.6). Based on the structure observed for complex **5.8** and the spectroscopic similarities between complexes **5.7** and **5.4**, we tentatively assign the connectivity of the unstable PhNCS dimer **5.7** as shown in Scheme 5.5. Although the isomeric metallacycle resulting from C–S bond formation is the more commonly observed product of isothiocyanate condensation (I in Figure 5.8),^{23e,27d} metallacycles such as **5.7**, which result from C–N bond formation, have been reported (II in Figure 5.8).^{27e,32}

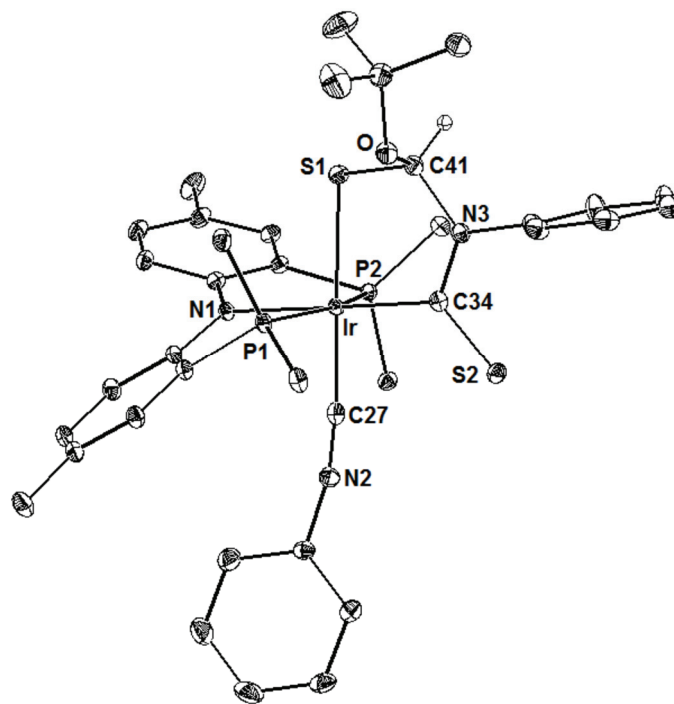
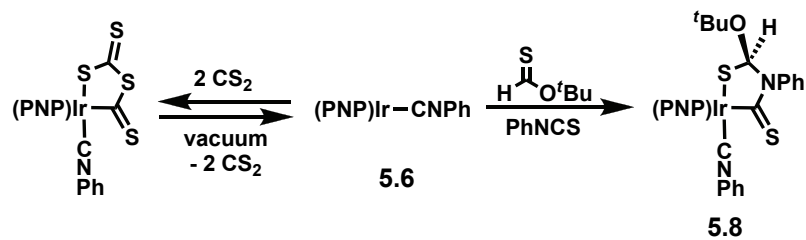


Figure 5.7. Displacement ellipsoid (35%) representation of complex **5.8** with most hydrogen atoms and phosphine substituents (except for *ipso* carbons) omitted for clarity. Selected bond lengths (Å) and angles (°): Ir–C27, 1.937(2); Ir–S1, 2.3648(5); Ir–N1, 2.155(2); Ir–C34, 2.049(2); Ir–P1, 2.3392(6); Ir–P2, 2.3533(6); C27–Ir–S1, 177.47(6); N1–Ir–C34, 177.42(6); P1–Ir–P2, 160.36(2).



Scheme 5.6. Nucleophilic reactivity of (PNP)Ir–CNPh (**5.6**).

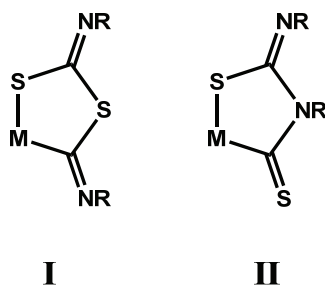


Figure 5.8. Common bonding motifs for isothiocyanate dimers.

Isocyanide complex **5.6** was also shown to react with large excesses of CS_2 , forming varying amounts of a species formulated as the $\text{C}_2\text{S}_4^{2-}$ adduct of the isocyanide complex analogous to CS_2 dimer **5.4** (observed by ^1H and ^{31}P NMR, Scheme 5.6). Unlike **5.4**, which is stable in solution and the solid state at ambient temperature, this adduct is in equilibrium with isocyanide complex **5.6**, and application of vacuum causes quantitative regeneration of **5.6** (Scheme 5.6). Nevertheless, the analogies between the nucleophilic reactivity observed for $(\text{PNP})\text{Ir}-\text{CNPh}$ (**5.6**) and $(\text{PNP})\text{Ir}=\text{C}(\text{H})\text{O}^t\text{Bu}$ (**5.2**) highlight the isoelectronic relationship between these molecules and suggest that computational studies can illuminate the factors controlling reactivity of these types of molecules.

Computational Examination of $(\text{PNP})\text{Ir}-\text{L}$ Complexes

Having obtained experimental support for our proposed mechanism of nucleophilic attack by iridium to initiate atom and group transfer reactions from heterocumulenes, we turned our attention to computational methods to help elucidate the ground-state configuration of the carbene shown to effect these unusual transformations. Using the atomic coordinates determined from the crystal structure of **5.2**, density functional calculations were performed at the B3LYP/LACVP** level of theory. The molecular surfaces of the frontier orbitals produced by these calculations are represented in Figure 5.9 (HOMO-1, HOMO, and LUMO).

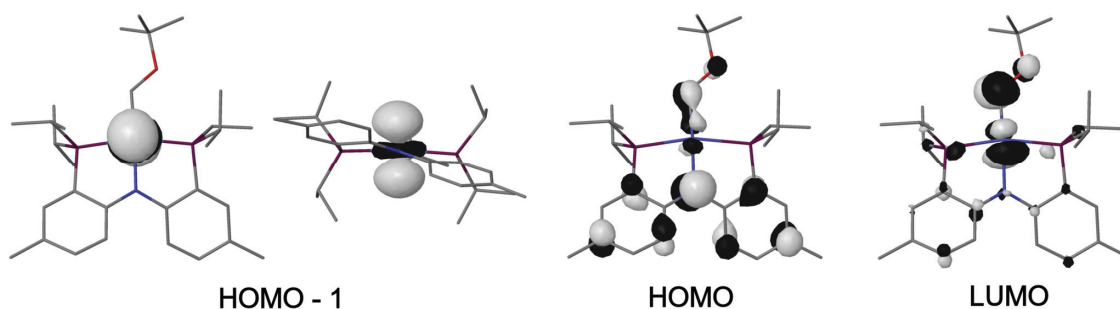


Figure 5.9. Molecular surfaces of frontier orbitals calculated for $(\text{PNP})\text{Ir}=\text{C}(\text{H})\text{O}^t\text{Bu}$ (**5.2**).

As predicted from simple molecular-orbital considerations, the frontier orbitals represent the non-bonding Ir(d_{z^2}), iridium–carbene π , and iridium–carbene π^* orbitals. In contrast to the HOMO and LUMO, which are significantly delocalized over the molecule, the HOMO–1 is localized entirely on iridium, representing a prototypical d_{z^2} orbital. Based on the reactivity patterns observed previously and in this report, we propose that this high-lying, localized orbital is primarily responsible for the nucleophilic activation of heterocumulene substrates, leading to group transfer or reductive condensation.

Since (PNP)Ir=C(H)O^tBu (**5.2**), (PNP)Ir–CO (**5.3**), (PNP)Ir–CS (**5.5**), and (PNP)Ir–CNPh (**5.6**) are isoelectronic, DFT calculations were extended to this entire series of molecules.³³ In fact, the gross ordering and shape of the orbitals remain constant throughout the series. However, the energies of the high-lying orbitals, particularly d_{z^2} (HOMO–1), vary across the series, reflecting to some degree the relative reactivities of the molecules.

As described above, carbene complex **1**, for which the HOMO–1 orbital is highest in energy (Table 5.1), forms the dimeric adduct **4** upon reaction with excess CS₂. Isocyanide complex **6**, which possesses a d_{z^2} orbital close in energy to that calculated for **1**, reacts with CS₂ to generate the analogous dimeric adduct (Scheme 5.6). The carbonyl and thiocarbonyl complexes, which have significantly lower-energy calculated d_{z^2} orbitals (Table 5.1), show no evidence for reactivity with neat CS₂ or PhNCS. Thus, as outlined in Table 5.1, the propensity of a (PNP)Ir–L complex to form a C₂S₄²⁻ adduct with CS₂ is correlated to the relative destabilization of the d_{z^2} molecular orbital (HOMO–1), consistent with our proposed mechanism.

Table 5.1. Energies of Ir(d_{z^2}) orbitals for (PNP)Ir–L molecules

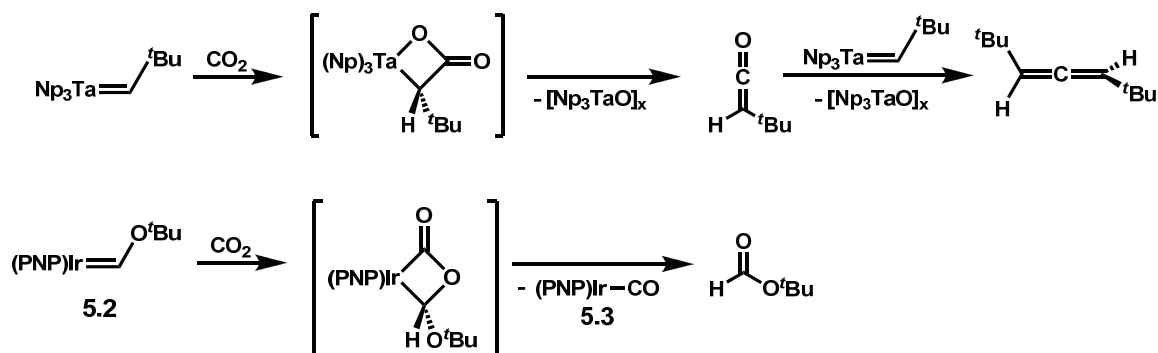
Complex	Energy of HOMO–1 (eV)
(PNP)Ir=C(H)O ^t Bu (5.2)	–4.62
(PNP)Ir–CNPh (5.6)	–4.80
(PNP)Ir–CO (5.3)	–4.99
(PNP)Ir–CS (5.5)	–5.22

Conclusions

In conclusion, we have reported well-defined atom and group transfer reactions from carbon dioxide, carbonyl sulfide, phenyl isocyanate, carbon disulfide, and phenyl isothiocyanate to an iridium-supported Fischer carbene. These reactions represent the first examples of atom and group transfer reactions from heterocumulenes across an M=C bond, and appear to be facilitated by the nucleophilic character of the iridium center of complex **5.2**. Under suitable conditions, exposure of carbene **5.2** to carbonyl sulfide and phenyl isothiocyanate allows observation of trapped kinetic adducts which clearly require a metal-initiated mechanism, in contrast to the standard reactivity patterns observed for metal carbenes.² DFT calculations were performed on a series of (PNP)Ir–L molecules and highlight the importance of a high-lying, nucleophilic Ir(d_{z^2}) orbital in initiating this unusual heterocumulene reactivity.

Drawing from these experimental and theoretical results, we propose that complex **5.2** is best formulated as a nucleophilic-at-metal carbene. It is particularly beneficial to consider these findings in relation to the known reactivity of high-valent alkylidene complexes of the early metals. Schrock has reported that a tris(neopentyl)neopentylidene tantalum(V) complex reacts instantaneously with CO₂ to produce di-*tert*-butylallene and a polymeric tantalum oxide (Scheme 5.7),^{19a} and has proposed that this and related olefination reactions proceed by initial

substrate coordination to the coordinatively unsaturated, highly electrophilic tantalum.³⁴ Subsequent group transfer releases olefin and attaches the strongly π -basic oxo ligand to the high-valent tantalum center. In contrast, we have reported that the square-planar iridium(I) carbene **5.2** attacks the electrophilic central carbon of CO_2 , ultimately oxygenating the carbene ligand and transferring a strongly π -acidic carbonyl to the electron-rich, d^8 iridium center, providing a complementary reactivity pathway to the tantalum case (Scheme 5.7).



Scheme 5.7. Contrasting carbon dioxide reactivity of a high-valent alkylidene and nucleophilic-at-metal carbene **5.2**.

The carbene ligand of **5.2** ultimately acts as an electrophile in the reported reactions, consistent with the classical behavior of Fischer-type carbenes, but this only occurs after substrate activation by the electron-rich iridium center renders the heterocumulene more nucleophilic and the carbene more electrophilic. Thus, the coordinatively unsaturated nature of the carbene complex reveals a distinct pathway for the activation of multiple bonds via a metal- rather than ligand-initiated mechanism. These findings suggest that square-planar carbenes of the late transition metals may generally exhibit a strong propensity to activate electrophilic substrates toward atom and group transfer across metal-carbon multiple bonds, and the application of these types of transformations in catalytic processes is the subject of ongoing investigation.

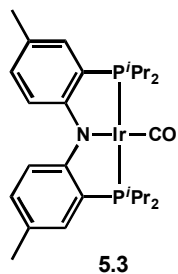
Acknowledgment

The author acknowledges Dr. Patricio Romero for helpful discussions. Larry Henling provided crystallographic assistance, Chris Daeffler aided with low-temperature NMR studies, and Dr. Ian Stewart assisted with DFT calculations.

Experimental Section

General Considerations. All manipulations were carried out using standard Schlenk or glove box techniques under a dinitrogen atmosphere. Unless otherwise noted, solvents were deoxygenated and dried by thorough sparging with argon gas followed by passage through an activated alumina column.³⁵ Hexamethyldisiloxane and *tert*-butyl methyl ether were distilled from CaH₂ and degassed prior to use. Phenyl isocyanate was distilled *in vacuo* from P₂O₅. Phenyl isothiocyanate was purchased from Aldrich and degassed *in vacuo* prior to use. (PNP)IrH₂ (**5.1**)³⁶ and (PNP)Ir=C(H)O^tBu (**5.2**)²⁶ were prepared according to literature procedure. Other reagents were purchased from commercial vendors and used without further purification. Elemental analyses were carried out at Desert Analytics, Tucson, Arizona. NMR spectra were recorded at ambient temperature on a Varian Mercury 300 MHz spectrometer. ¹H NMR chemical shifts were referenced to residual solvent. ³¹P NMR chemical shifts are reported relative to an external standard of 85% H₃PO₄. Infrared spectra were recorded using a Perkin Elmer Spectrum BXII spectrometer. X-ray diffraction studies were carried out in the Beckman Institute Crystallographic Facility on a Bruker KAPPA APEX II diffractometer.

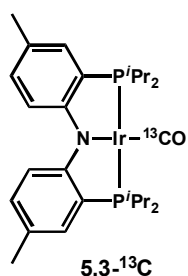
Independent preparation of (PNP)Ir–CO (5.3). In a sealed NMR tube, a red solution of **5.2** (40



mg, 0.064 mmol) in C_6D_6 was frozen and the headspace evacuated and backfilled with carbon monoxide. As the solution melted, an immediate color change to pale yellow was observed. The reaction was allowed to proceed 24 h and complete formation of **5.3** confirmed by NMR. Lyophilization of the

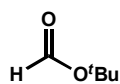
solution yielded **5.3** as an analytically pure yellow powder (41 mg, 98%). X-ray quality crystals were grown at room temperature from a concentrated solution of **5.3** in benzene/hexamethyldisiloxane (1:1). 1H NMR (C_6D_6): δ 7.72 (d, $^3J_{HH} = 8.4$ Hz, 2H, Ar–H), 6.92 (s, 2H, Ar–H), 6.83 (d, $^3J_{HH} = 8.4$ Hz, 2H, Ar–H), 2.27 (m, 4H, $-CH(CH_3)_2$), 2.18 (s, 6H, Ar– CH_3), 1.29 (m, 12H, $-CH(CH_3)_2$), 1.05 (m, 12H, $-CH(CH_3)_2$). $^{31}P\{^1H\}$ NMR (C_6D_6): δ 57.3 (s). IR (THF, KBr, cm^{-1}) $\nu(CO)$: 1930. Anal. calcd. for $C_{27}H_{40}IrNOP_2$: C, 49.98; H, 6.21; N, 2.16. Found: C, 49.97; H, 5.73; N, 2.05.

Synthesis of (PNP)Ir– ^{13}C CO (5.3- ^{13}C). (PNP)Ir– ^{13}C CO was prepared by the same method as **5.3** using



^{13}C CO (99%). 1H NMR characterization data matched those for **5.3**. $^{13}C\{^1H\}$ NMR (C_6D_6): δ 187.6 (t, $^2J_{PC} = 7.5$ Hz, Ir– ^{13}C). $^{31}P\{^1H\}$ NMR (C_6D_6): δ 57.4 (d, $^2J_{PC} = 7.6$ Hz). IR (THF, KBr, cm^{-1}) $\nu(^{13}CO)$: 1883.

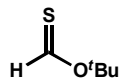
Preparation of *tert*-Butyl Formate from Complex (5.2) and Carbon Dioxide. In a sealed NMR



tube, a purple solution of **5.2** (20 mg) in C_6D_6 was frozen and the headspace evacuated and backfilled with carbon dioxide (1 atm). As the solution thawed, a gradual change in color from purple to pale yellow was observed. After 30 min, the consumption

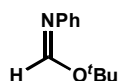
of **5.2** and formation of **5.3** and *tert*-butyl formate (identified by comparison to an authentic sample obtained from Aldrich) were confirmed by NMR, and the presence of **5.3** was confirmed by IR. ^1H NMR (*tert*-butyl formate, C_6D_6): δ 7.64 (s, 1H, $-\text{C}(\text{O})\text{H}$), 1.24 (s, 9H, $-\text{C}(\text{CH}_3)_3$).

Preparation of *tert*-Butyl Thioformate from Complex (5.2) and Carbonyl Sulfide. In a sealed



NMR tube, a purple solution of **5.2** (25 mg) in C_6D_6 was frozen and the headspace evacuated and backfilled with carbonyl sulfide (1 atm). As the solution thawed, a gradual change in color from purple to pale yellow was observed. After 30 min, the consumption of **5.2** and formation of **5.3** and *tert*-butyl thioformate were confirmed by NMR. ^1H NMR (*tert*-butyl thioformate, C_6D_6): δ 9.50 (s, 1H, $-\text{C}(\text{S})\text{H}$), 0.85 (s, 9H, $-\text{C}(\text{CH}_3)_3$).

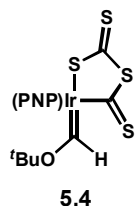
Preparation of *tert*-Butyl *N*-Phenylformimidate from Complex (5.2) and Phenyl Isocyanate. An



NMR tube was charged with a purple solution of **5.2** (40.6 mg, 0.0574 mmol) in C_6D_6 , and phenyl isocyanate (7.0 μL , 0.064 mmol) was added by microsyringe. Over a period of 3 min, the solution lightened and adopted a golden hue. After 15 min, the consumption of **5.2** and formation of **5.3** and *N*-phenyl *tert*-butylformimidate were confirmed by NMR. ^1H NMR (*N*-phenyl *tert*-butylformimidate, C_6D_6): δ 7.51 (s, 1H, $-\text{C}(\text{NPh})\text{H}$), 7.15–7.05 (m, 2H, Ar-*H*), 7.00–6.90 (m, 3H, Ar-*H*), 1.38 (s, 9H, $-\text{C}(\text{CH}_3)_3$).

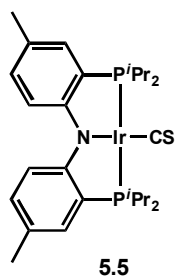
Thermolysis of (PNP)Ir=C(H)O^tBu (5.2) in *tert*-Butyl Methyl Ether in the Presence of CO₂. In a sealed NMR tube, a purple solution of **5.2** (30 mg) in *tert*-butyl methyl ether was frozen and the headspace evacuated and backfilled with carbon dioxide (1 atm). The sealed tube was heated at 70 °C for 4 days, and NMR (^{31}P) analysis revealed **5.3** as the predominant product (>70%). **5.3** is not formed by thermolysis of **5.2** in MTBE in the absence of CO₂.²⁶

Preparation of (PNP)Ir(=C(H)O^tBu)(C₂S₄) (5.4). To a stirring solution of (PNP)Ir=C(H)O^tBu (**5.2**)



(50.0 mg, 0.0707 mmol) in pentane (5 mL) was added excess carbon disulfide (ca. 200 μ L), causing the immediate precipitation of a brown-orange solid. The solution was stirred for 15 min and the orange powder isolated by filtration. The powder was dissolved in a minimal amount of THF and analytically pure red crystals of **5.4** were isolated by vapor diffusion of pentane into the concentrated THF solution (28.0 mg, 46%). ¹H NMR (C₆D₆): δ 15.55 (s, 1H, -C(H)O^tBu), 7.53 (dt, $J_1 = 8.4$ Hz, $J_2 = 2.4$ Hz, 2H, Ar-H), 6.73 (dd, $J_1 = 8.7$ Hz, $J_2 = 1.8$ Hz, 2H, Ar-H), 6.58 (m, 2H, Ar-H), 2.74 (m, 2H, -CH(CH₃)₂), 2.11 (s, 6H, Ar-CH₃), 2.09 (m, 2H, -CH(CH₃)₂), 1.11 (m, 12H, -CH(CH₃)₂), 0.91 (dvt, 6H, -CH(CH₃)₂), 0.77 (s, 9H, -C(CH₃)₃), 0.74 (dvt, 6H, -CH(CH₃)₂). ¹³C{¹H} NMR (CD₂Cl₂): δ 269.7 (Ir-CS₂), 266.7 (Ir-C(H)O^tBu), 236.8 (Ir-SCS₂). ³¹P{¹H} NMR (C₆D₆): δ 20.5 (s). Anal. calcd. for C₃₃H₅₀IrNOP₂S₄: C, 46.13; H, 5.87; N, 1.63. Found: C, 45.98; H, 5.81; N, 1.57.

Preparation of (PNP)Ir-CS (5.5).

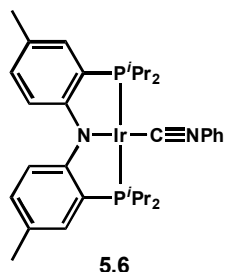


Method A. A resealable NMR tube was charged with compound **5.4** (24.0 mg, 0.0279 mmol) in THF (ca. 1 mL) and heated at 70 °C for 16 h, causing a slight lightening of the solution from brown-red to pale red. NMR spectroscopy confirmed the presence of **5.5** as the sole component.

Method B. Compound **5.2** (31.1 mg, 0.0440 mmol) was dissolved in benzene (3 mL) and carbon disulfide (2.7 μ L, 0.045 mmol) added dropwise as a dilute solution in benzene (1 mL), causing a color change from purple to pale red. After 30 min, volatile components were removed *in vacuo* and the residues were crystallized by slow evaporation of pentane from a concentrated solution to afford brown-red crystals of analytically pure **5.5** (25.4 mg, 87%). ¹H NMR (C₆D₆): δ 7.58 (d, $J = 8.4$ Hz, 2H, Ar-H), 6.96 (br s, 2H, Ar-H), 6.78 (d, $J = 8.7$ Hz, 2H, Ar-H),

2.55 (m, 4H, $-\text{CH}(\text{CH}_3)_2$), 2.17 (s, 6H, Ar- CH_3), 1.42 (dvt, 12H, $-\text{CH}(\text{CH}_3)_2$), 1.15 (dvt, 12H, $-\text{CH}(\text{CH}_3)_2$). $^{13}\text{C}\{^1\text{H}\}$ NMR (C_6D_6): δ 262.0 (Ir-CS). $^{31}\text{P}\{^1\text{H}\}$ NMR (C_6D_6): δ 53.2 (s). Anal. calcd. for $\text{C}_{27}\text{H}_{40}\text{IrNP}_2\text{S}$: C, 48.78; H, 6.06; N, 2.11. Found: C, 48.52; H, 6.06; N, 2.03.

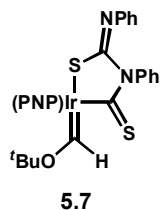
Preparation of (PNP)Ir-CNPh (5.6). Phenyl isothiocyanate (9.15 μL , 0.0765 mmol) was added



dropwise as a solution in benzene (1 mL) over 1 min to a stirring purple solution of compound **5.2** in benzene (5 mL), causing a gradual color change to red-orange over a period of 30 min. Volatiles were removed *in vacuo* to afford an orange powder which was crystallized by slow evaporation of

pentane from a concentrated solution to afford analytically pure **5.6** as orange crystals (40.0 mg, 72%). ^1H NMR (C_6D_6): δ 7.79 (d, $J = 8.7$ Hz, 2H, Ar- H), 7.33 (d, $J = 7.5$ Hz, 2H, Ar- H), 7.10–6.90 (m, 5H, Ar- H), 6.85 (d, $J = 8.1$ Hz, 2H, Ar- H), 2.38 (septet, $^3J_{\text{HH}} = 3.0$ Hz, $-\text{CH}(\text{CH}_3)_2$), 2.22 (s, 6H, Ar- CH_3), 1.35 (dvt, 12H, $-\text{CH}(\text{CH}_3)_2$), 1.14 (dvt, 12H, $-\text{CH}(\text{CH}_3)_2$). $^{13}\text{C}\{^1\text{H}\}$ NMR (C_6D_6): δ 176.8 (t, $^3J_{\text{PC}} = 9.3$ Hz, Ir-CNPh). $^{31}\text{P}\{^1\text{H}\}$ NMR (C_6D_6): δ 53.6 (s). Anal. calcd. for $\text{C}_{33}\text{H}_{45}\text{IrN}_2\text{P}_2$: C, 54.75; H, 6.27; N, 3.87. Found: C, 54.87; H, 6.20; N, 3.86.

Observation of Phenyl Isothiocyanate Dimer Complex (5.7). Phenyl isothiocyanate (9.1 μL ,

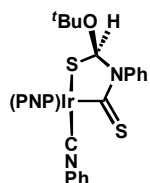


0.076 mmol) was added in one portion to an NMR tube containing a solution of complex **5.2** (24.4 mg, 0.0345 mmol) in C_6D_6 (600 μL), causing an immediate color change from dark purple to bright red. After 15 min, analysis of the solution by

NMR revealed a mixture of complexes **5.7** and **5.6** (70:30). Spectral data for complex **5.7**: ^1H NMR (C_6D_6): δ 15.5 (s, 1H, Ir=C(H)O ^tBu), 7.59 (d, $J = 8.4$ Hz, 2H, Ar- H), 7.53–7.35 (m, 4H, Ar- H), 7.29–7.19 (m, 4H, Ar- H), 6.81–6.63 (m, 6H, Ar- H), 3.01 (m, 2H, $-\text{CH}(\text{CH}_3)_2$), 2.19 (m, 2H,

$-\text{CH}(\text{CH}_3)_2$, 2.13 (s, 6H, Ar- CH_3), 1.47–1.29 (m, 12H, $-\text{CH}(\text{CH}_3)_2$), 1.19 (dvt, 6H, $-\text{CH}(\text{CH}_3)_2$), 1.00 (dvt, 6H, $-\text{CH}(\text{CH}_3)_2$). $^{31}\text{P}\{^1\text{H}\}$ NMR (C_6D_6): δ 18.8 (br s).

Preparation of Complex (5.8). Phenyl isothiocyanate (8.2 μL , 0.069 mmol) was added dropwise



5.8

as a solution in benzene (1 mL) over 1 min to a stirring purple solution of complex **5.2** (48.0 mg, 0.0679 mmol) in benzene (5 mL), causing a gradual color change to red-orange over a period of 30 min. After 2 h, additional phenyl isothiocyanate (ca. 100 μL) was added as a solution in benzene (1 mL) to the stirring reaction,

causing further lightening to bright orange. After 24 h, volatiles were removed *in vacuo* and the residues crystallized by slow evaporation of pentane from a concentrated solution to afford complex **5.8** as bright-orange crystals (25.4 mg, 39 %). ^1H NMR (C_6D_6): 7.68 (d, $J = 6.9$ Hz, 1H, Ar- H), 7.60 (m, 1H, Ar- H), 7.52 (m, 1H, Ar- H), 7.40 (m, 1H, Ar- H), 7.31–7.16 (m, 4H, Ar- H), 7.15–6.94 (m, 3H, Ar- H), 6.92–6.69 (m, 3H, Ar- H), 6.63 (m, 2H, Ar- H), 6.24 (s, 1H, $-\text{CH}(\text{O}^t\text{Bu})$), 3.96 (m, 1H, $-\text{CH}(\text{CH}_3)_2$), 3.45 (m, 1H, $-\text{CH}(\text{CH}_3)_2$), 2.67 (m, 1H, $-\text{CH}(\text{CH}_3)_2$), 2.48 (m, 1H, $-\text{CH}(\text{CH}_3)_2$), 2.18 (s, 3H, Ar- CH_3), 2.16 (s, 3H, Ar- CH_3), 1.97 (m, 3H, $-\text{CH}(\text{CH}_3)_2$), 1.80–1.45 (m, 9H, $-\text{CH}(\text{CH}_3)_2$), 1.38–0.98 (m, 12H, $-\text{CH}(\text{CH}_3)_2$), 0.90 (s, 9H, $-\text{C}(\text{CH}_3)_3$). ^{31}P NMR (C_6D_6): δ 16.1 (d, $^2J_{\text{PP}} = 361$ Hz), 7.5 (d, $^2J_{\text{PP}} = 361$ Hz). Anal. calcd. for $\text{C}_{45}\text{H}_{60}\text{IrN}_3\text{OP}_2\text{S}_2$: C, 55.31; H, 6.19; N, 4.30. Found: C, 55.12; H, 6.15; N, 4.06.

Computational Methods. Hybrid density functional theory calculations were performed for (PNP)Ir-C(H)O t Bu (**5.2**), (PNP)Ir-CO (**5.3**), (PNP)Ir-CS (**5.5**), and (PNP)Ir-CNPh (**5.6**) using the Jaguar package (version 7.5, release 110), employing the B3LYP functional and 6-31G** basis set.³⁷ Iridium was represented with the LACVP** basis set.^{38,39} Atomic coordinates were imported from relevant single-crystal X-ray structures and subjected to geometry optimization.

The molecular surfaces for the frontier orbitals of each of these complexes are rendered and their energies indicated in Figures 5.10–5.13.

X-ray Crystallography Procedures. X-ray quality crystals were grown as indicated in the experimental procedures for each complex. The crystals were mounted on a glass fiber with Paratone-N oil. Structures were determined using direct methods with standard Fourier techniques using the Bruker AXS software package. In some cases, Patterson maps were used in place of the direct methods procedure. Table 5.2 contains the X-ray diffraction experimental details.

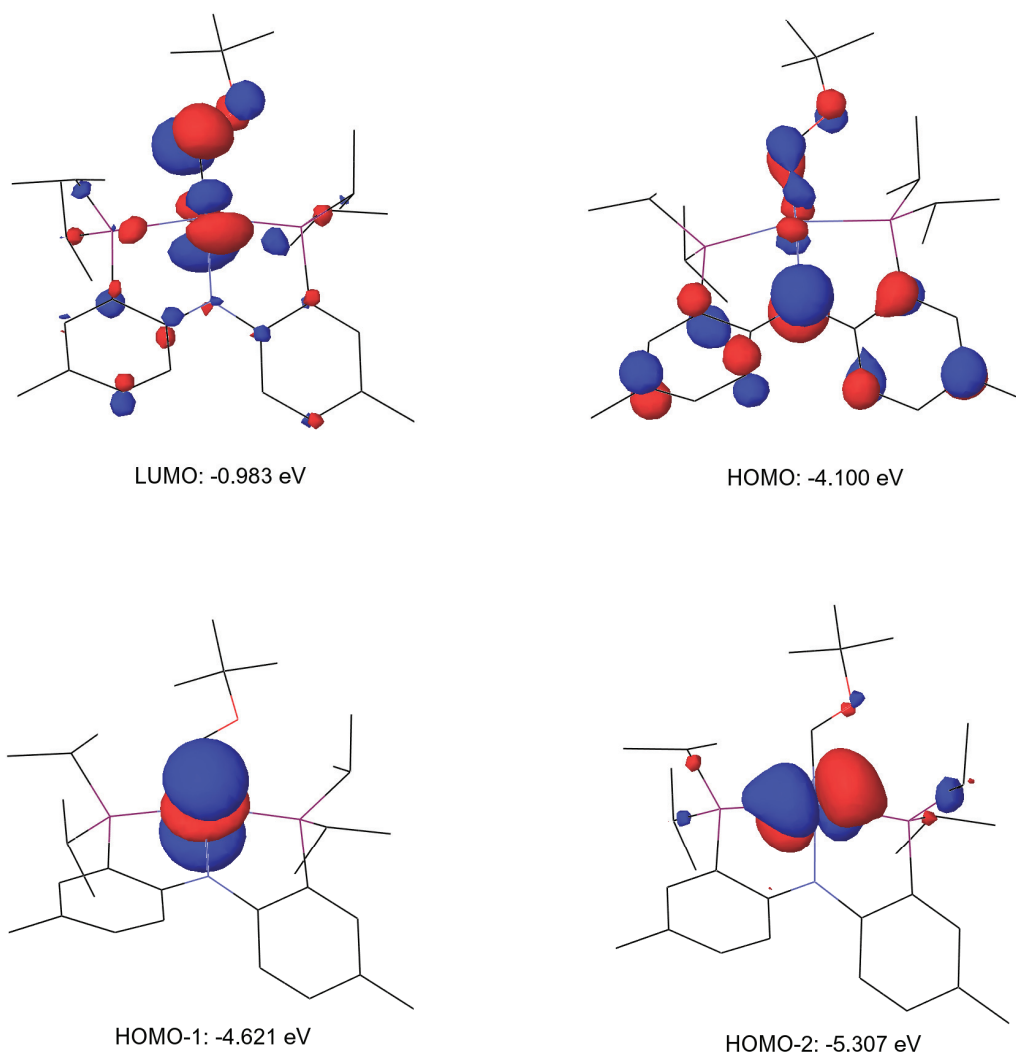


Figure 5.10. Frontier molecular orbitals for (PNP)Ir=C(H)O^tBu (**5.2**).

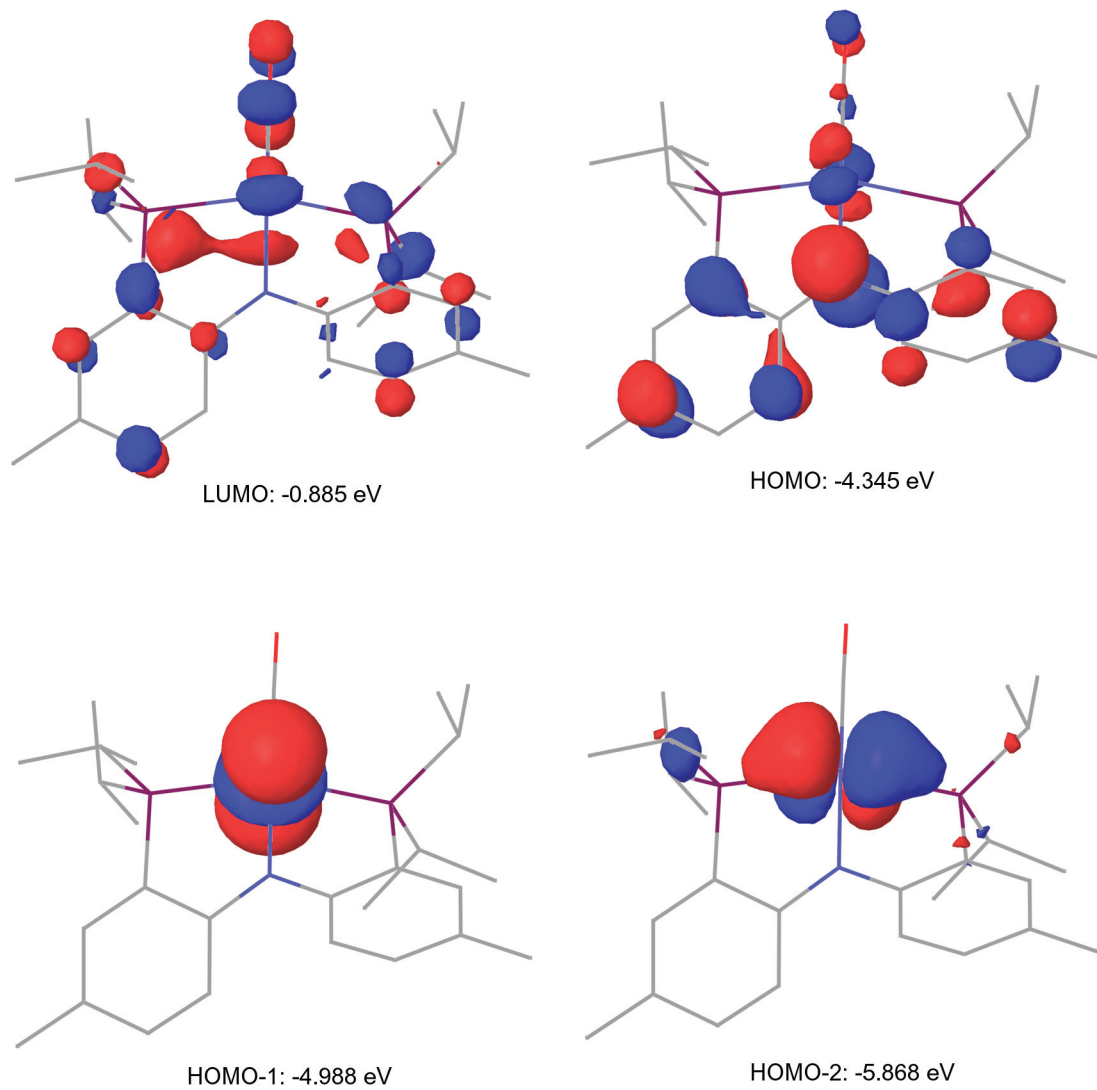


Figure 5.11. Frontier molecular orbitals for (PNP)Ir-CO (**5.3**).

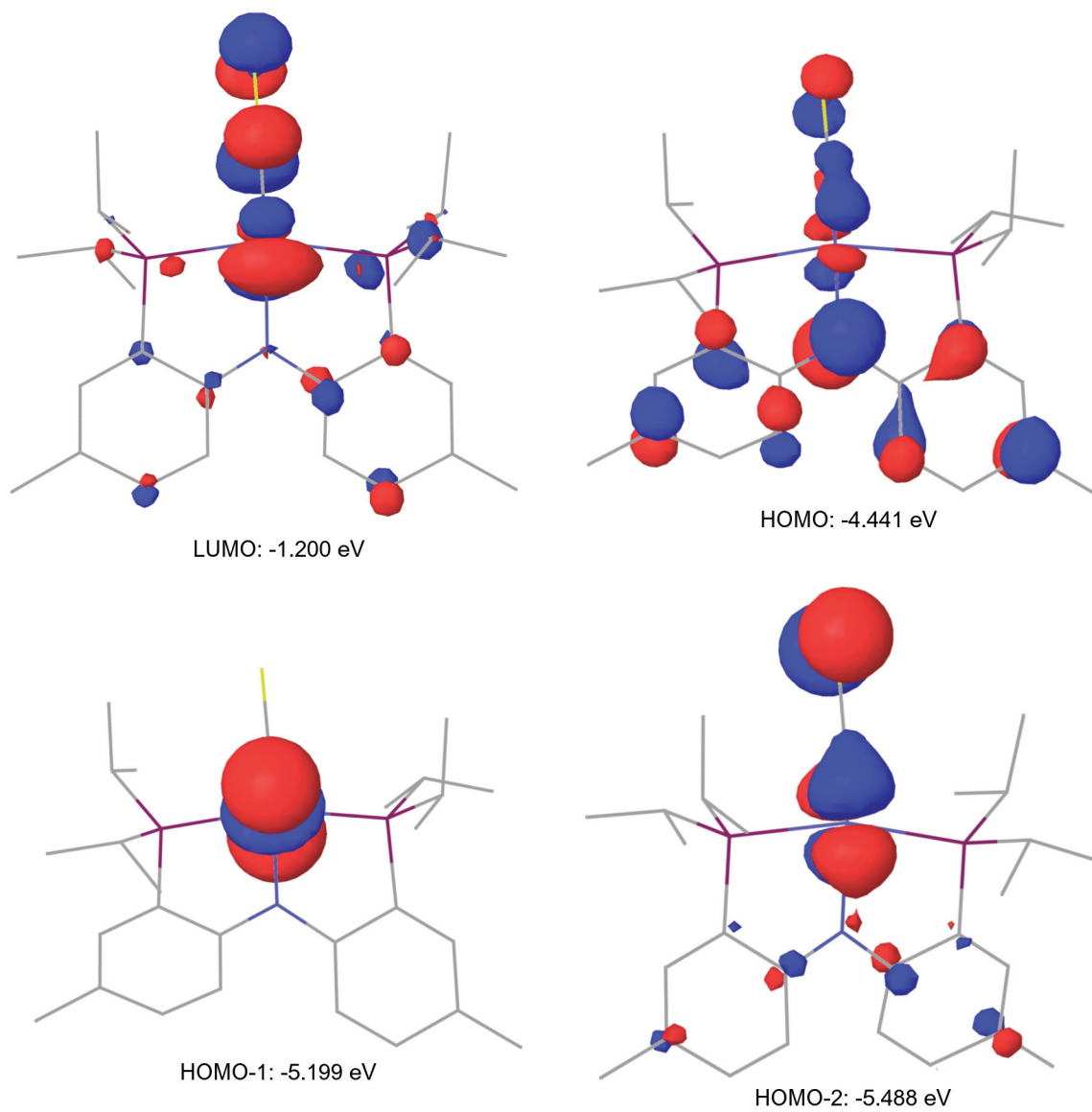


Figure 5.12. Frontier molecular orbitals for (PNP)Ir-CS (5.5).

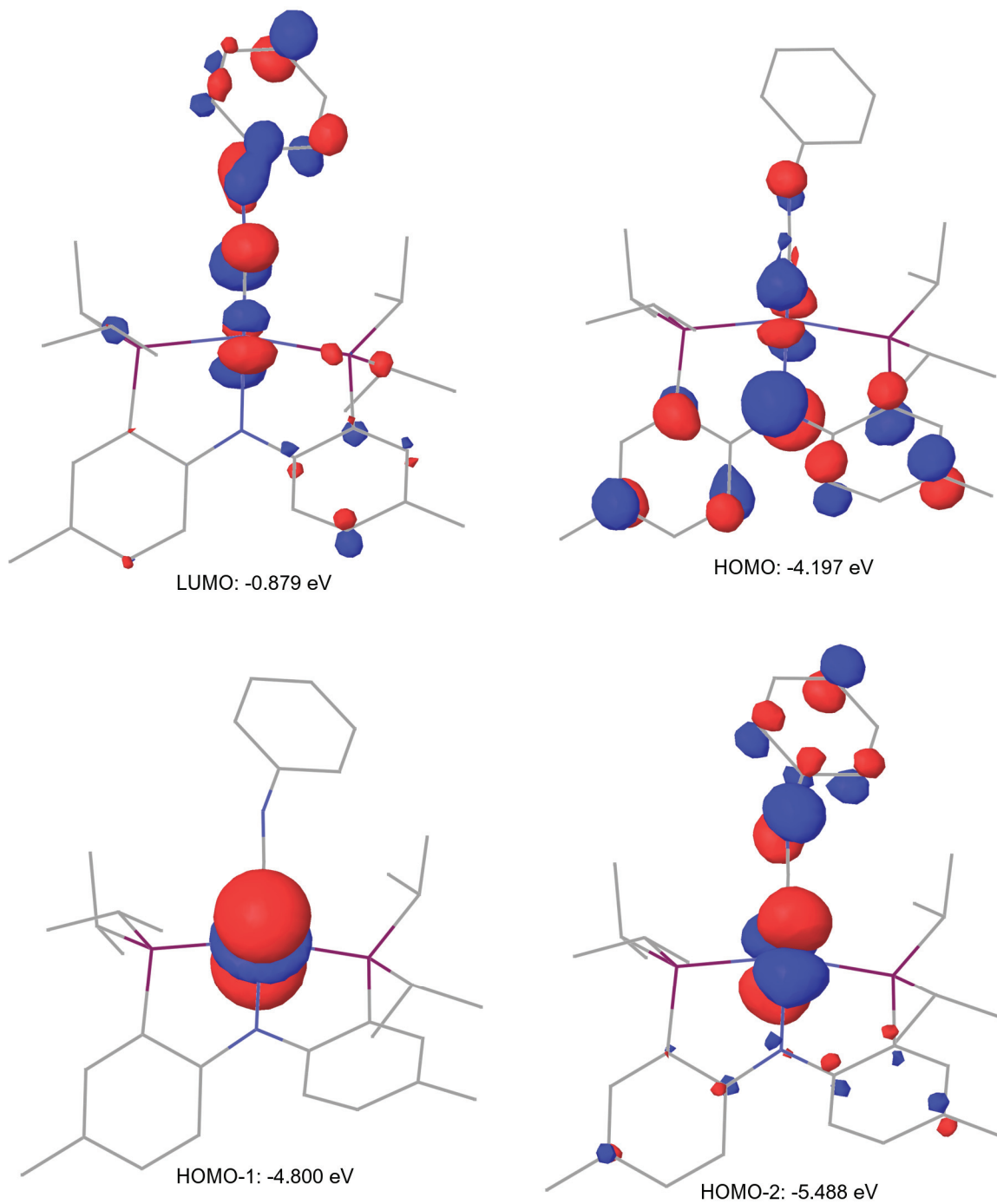


Figure 5.13. Frontier molecular orbitals for (PNP)Ir-CNPh (5.6).

Table 5.2. X-ray crystallographic data

complex	5.3	5.4	5.5
Empirical Formula	$C_{27}H_{40}IrNOP_2 \cdot C_6H_6$	$C_{33}H_{50}IrNOP_2S_4$	$C_{27}H_{40}IrNP_2S$
Formula Weight	726.85	859.12	664.80
λ (Å)	0.71073	0.71073	0.71073
T (K)	100(2)	100(2)	100(2)
a (Å)	12.1315(15)	16.5763(8)	13.8273(10)
b (Å)	9.6222(12)	10.4629(4)	13.4512(9)
c (Å)	27.912(3)	23.7379(10)	16.6229(12)
α (deg)	90	90	90
β (deg)	95.130(3)	101.326(3)	113.660(5)
γ (deg)	90	90	90
V (Å ³)	3245.1(7)	4036.8(3)	2831.9(4)
Z	4	4	4
Crystal System	Monoclinic	Monoclinic	Monoclinic
Space Group	P2(1)/c	P2(1)/n	Pn
d_{calc} (g/cm ³)	1.488	1.414	1.559
GOF on F ²	1.685	1.131	1.055
R1, wR2 ^a ($I > 2\sigma(I)$)	0.0304, 0.0487	0.0463, 0.1080	0.1060, 0.2813

complex	5.6	5.7
Empirical Formula	C ₃₃ H ₄₅ IrN ₂ P ₂	C ₄₅ H ₆₀ IrN ₃ OP ₂ S ₂
Formula Weight	723.85	977.22
λ (Å)	0.71073	0.71073
T (K)	100(2)	100(2)
a (Å)	12.9701(12)	11.9942(12)
b (Å)	10.4300(16)	19.6212(19)
c (Å)	23.824(3)	18.9319(19)
α (deg)	90	90
β (deg)	95.658(4)	98.997(3)
γ (deg)	90	90
V (Å ³)	3207.1(7)	4400.6(8)
Z	4	4
Crystal System	Monoclinic	Monoclinic
Space Group	P2(1)/c	P2(1)/n
d_{calc} (g/cm ³)	1.499	1.475
GOF on F ²	1.375	1.023
R1, wR2 ^a (I > 2 σ (I))	0.0277, 0.0369	0.0307, 0.0594

References and Notes

- (1) For leading references, see: (a) Fischer, E. O. *Pure Appl. Chem.* **1970**, *24*, 407. (b) Fischer, E. O. *Pure Appl. Chem.* **1978**, *50*, 857. (c) Cardin, D. J.; Cetinkaya, B.; Lappert, M. F. *Chem. Rev.* **1972**, *72*, 545. (d) Cotton, F. A.; Lukehart, C. M. *Prog. Inorg. Chem.* **1972**, *16*, 487. (e) Schrock, R. R. *Acc. Chem. Res.* **1979**, *12*, 99. (f) Schrock, R. R. *J. Chem. Soc. Dalton* **2001**, *18*, 2541. (g) Schrock, R. R. *Chem. Rev.* **2002**, *102*, 145. (h) Doyle, M. P. *Chem. Rev.* **1986**, *86*, 919. (i) Brookhart, M.; Studabaker, W. B. *Chem. Rev.* **1987**, *87*, 411. (j) Doetz, K. H.; Minatti, A. Fischer Type Carbene Complexes. In *Transition Metals for Organic Synthesis*; Beller, M., Bolm, C., Eds.; Wiley: Weinheim, 2004; Vol. 2, pp 397-425. (k) *Handbook of Metathesis*; Grubbs, R. H., Ed.; Wiley: Weinheim, 2003.
- (2) (a) Nugent, W. A.; Mayer, J. M. *Metal-Ligand Multiple Bonds*; Wiley: New York, 1988. (b) Schrock, R. R. *J. Am. Chem. Soc.* **1975**, *97*, 6577. (c) Nugent, W. A.; McKinney, R. J.; Kasowski, R. V.; Van-Catledge, F. A. *Inorg. Chim. Acta* **1982**, *65*, L91. (d) Nakatsuji, H.; Ushio, J.; Han, S.; Yonezawa, T. *J. Am. Chem. Soc.* **1983**, *105*, 426. (e) Ushio, J.; Nakatsuji, H.; Yonezawa, T. *J. Am. Chem. Soc.* **1984**, *106*, 5892. (f) Block, T. F.; Fenske, R. F.; Casey, C. P. *J. Am. Chem. Soc.* **1976**, *98*, 441. (g) Gallop, M. A.; Roper, W. R. *Adv. Organomet. Chem.* **1986**, *25*, 121. (h) Taylor, T. E.; Hall, M. B. *J. Am. Chem. Soc.* **1984**, *106*, 1576. (i) Cundari, T. R.; Gordon, M. S. *J. Am. Chem. Soc.* **1991**, *113*, 5231.
- (3) (a) Fan, L.; Foxman, B. M.; Ozerov, O. V. *Organometallics* **2004**, *23*, 326. (b) Ozerov, O. V.; Guo, C.; Papkov, V. A.; Foxman, B. M. *J. Am. Chem. Soc.* **2004**, *126*, 4792.
- (4) Lee, S. K.; Cooper, N. J. *J. Am. Chem. Soc.* **1990**, *112*, 9419.
- (5) Sakakura, T.; Choi, J. C.; Yasuda, H. *Chem. Rev.* **2007**, *107*, 2365.
- (6) (a) Arakawa, H.; et al. *Chem. Rev.* **2001**, *101*, 953. (b) Lewis, N. S.; Nocera, D. G. *Proc. Natl. Acad. Sci. U.S.A.* **2006**, *103*, 15729.
- (7) *CRC Handbook of Chemistry and Physics*, 77th ed.; Lide, D. R., Ed.; CRC Press: Boca Raton, 1996.
- (8) (a) Fachinetti, G.; Floriani, C.; Chiesivilla, A.; Guastini, C. *J. Am. Chem. Soc.* **1979**, *101*, 1767. (b) Bryan, J. C.; Geib, S. J.; Rheingold, A. L.; Mayer, J. M. *J. Am. Chem. Soc.* **1987**, *109*, 2826. (c) Procopio, L. J.; Carroll, P. J.; Berry, D. H. *Organometallics* **1993**, *12*, 3087. (d) Castro-Rodriguez, I.; Meyer, K. *J. Am. Chem. Soc.* **2005**, *127*, 11242.
- (9) (a) Lu, C. C.; Saouma, C. T.; Day, M. W.; Peters, J. C. *J. Am. Chem. Soc.* **2007**, *129*, 4. (b) Sadique, A. R.; Brennessel, W. W.; Holland, P. L. *Inorg. Chem.* **2008**, *47*, 784. (c) Laitar, D. S.; Müller, P.; Sadighi, J. P. *J. Am. Chem. Soc.* **2005**, *127*, 17196. (d) Lee, C. H.; Laitar, D. S.; Müller, P.; Sadighi, J. P. *J. Am. Chem. Soc.* **2007**, *129*, 13802. (e) Anderson, J. S.; Iluc, V. M.; Hillhouse, G. L. *Abstracts of Papers*, 233rd ACS National Meeting, Chicago, IL; American Chemical Society: Washington, DC, 2007; INOR 806.

- (10) Efficient electrocatalytic reduction of CO₂ to CO by late transition metals has been demonstrated: (a) Fisher, B.; Eisenberg, R. *J. Am. Chem. Soc.* **1980**, *102*, 7361. (b) Beley, M.; Collin, J.-P.; Ruppert, R.; Sauvage, J.-P. *J. Am. Chem. Soc.* **1986**, *108*, 7461. (c) Simón-Manso, E.; Kubiak, C. P. *Organometallics* **2005**, *24*, 96.
- (11) (a) Schrock, R. R. *J. Am. Chem. Soc.* **1976**, *98*, 5399. (b) Klein, D. P.; Bergman, R. G. *J. Am. Chem. Soc.* **1989**, *111*, 3079. (c) Lee, S. K.; Cooper, N. J. *J. Am. Chem. Soc.* **1990**, *112*, 9419. (d) Mindiola, D. J.; Hillhouse, G. L. *J. Am. Chem. Soc.* **2002**, *124*, 9976.
- (12) Romero, P. E.; Whited, M. T.; Grubbs, R. H. *Organometallics* **2008**, *27*, 3422.
- (13) (a) Casey, C. P.; Burkhardt, T. J. *J. Am. Chem. Soc.* **1972**, *94*, 6543. (b) Casey, C. P.; Burkhardt, T. J.; Bunnell, C. A.; Calabrese, J. C. *J. Am. Chem. Soc.* **1977**, *99*, 2127. (c) Klabunde, U.; Fischer, E. O. *J. Am. Chem. Soc.* **1967**, *89*, 7141. (d) Gallop, M. A.; Roper, W. R. *Adv. Organomet. Chem.* **1986**, *25*, 121.
- (14) (a) Kistiakowsky, G. B.; Sauer, K. *J. Am. Chem. Soc.* **1958**, *80*, 1066. (b) Kovacs, D.; Jackson, J. E. *J. Phys. Chem. A* **2001**, *105*, 7579.
- (15) (a) Hérisson, J.-L.; Chauvin, Y. *Makromol. Chem.* **1971**, *141*, 161. (b) Romero, P. E.; Piers, W. E. *J. Am. Chem. Soc.* **2005**, *127*, 5032. (c) Wenzel, A. G.; Grubbs, R. H. *J. Am. Chem. Soc.* **2006**, *128*, 16048.
- (16) A similar four-centered transition state has been proposed for oxygen-atom transfer to a Ta methylidene from a Re carbonyl: Proulx, G.; Bergman, R. G. *J. Am. Chem. Soc.* **1993**, *115*, 9802.
- (17) Gaffney, T. R.; Ibers, J. A. *Inorg. Chem.* **1982**, *21*, 2851.
- (18) (a) Collman, J. P.; Kubota, M.; Vastine, F. D.; Sun, J. Y.; Kang, J. W. *J. Am. Chem. Soc.* **1968**, *90*, 5430. (b) Lamonica, G.; Cenini, S.; Freni, M. *J. Organomet. Chem.* **1974**, *76*, 355. (c) Cenini, S.; Lamonica, G. *Inorg. Chim. Acta* **1976**, *18*, 279. (d) Mindiola, D. J.; Hillhouse, G. L. *Chem. Commun.* **2002**, 1840.
- (19) Examples of more commonly observed nucleophilic reactivity between metal carbenes and heterocumulenes: (a) Schrock, R. R. *J. Am. Chem. Soc.* **1976**, *98*, 5399. (b) Klein, D. P.; Bergman, R. G. *J. Am. Chem. Soc.* **1989**, *111*, 3079. (c) Lee, S. K.; Cooper, N. J. *J. Am. Chem. Soc.* **1990**, *112*, 9419. (d) Mindiola, D. J.; Hillhouse, G. L. *J. Am. Chem. Soc.* **2002**, *124*, 9976.
- (20) This behavior is more closely related to what is observed for Sadighi's structurally and electronically similar Cu(I)-boryl complexes: (a) Laitar, D. S.; Müller, P.; Sadighi, J. P. *J. Am. Chem. Soc.* **2005**, *127*, 17196. (b) Laitar, D. S.; Tsui, E. Y.; Sadighi, J. P. *J. Am. Chem. Soc.* **2006**, *128*, 11036.
- (21) Fraser, P. J.; Roper, W. R.; Stone, F. G. A. *J. Chem. Soc. Dalton* **1974**, 760.

- (22) (a) Tebbe, F. N.; Parshall, G. W.; Reddy, G. S. *J. Am. Chem. Soc.* **1978**, *100*, 3611. (b) Pine, S. H.; Zahler, R.; Evans, D. A.; Grubbs, R. H. *J. Am. Chem. Soc.* **1980**, *102*, 3270.
- (23) This binding motif for CS₂ has been observed previously: (a) Werner, H.; Kolb, O.; Feser, R.; Schubert, U. *J. Organomet. Chem.* **1980**, *191*, 283. (b) Cowie, M.; Dwight, S. K. *J. Organomet. Chem.* **1980**, *198*, C20. (c) Cowie, M.; Dwight, S. K. *J. Organomet. Chem.* **1981**, *214*, 233. (d) Mason, G.; Swepston, P. N.; Ibers, J. A. *Inorg. Chem.* **1983**, *22*, 411. (e) Carmona, E.; Galindo, A.; Monge, A.; Muñoz, M. A.; Poveda, M. L.; Ruiz, C. *Inorg. Chem.* **1990**, *29*, 5074. (f) George, D. S. A.; Hilts, R. W.; McDonald, R.; Cowie, M. *Inorg. Chim. Acta* **2000**, *300*, 353.
- (24) Though not observed for our system, an iridium-supported head-to-tail dimer of CO₂ has also been reported: Herskovitz, T.; Guggenberger, L. J. *J. Am. Chem. Soc.* **1976**, *98*, 1615.
- (25) Similar behaviour has been observed for phosphine-supported ruthenium carbenes: (a) Nguyen, S. T.; Johnson, L. K.; Grubbs, R. H.; Ziller, J. W. *J. Am. Chem. Soc.* **1992**, *113*, 3974. (b) Dias, E. L.; Nguyen, S. T.; Grubbs, R. H. *J. Am. Chem. Soc.* **1997**, *119*, 3887. (c) Schwab, P.; Grubbs, R. H.; Ziller, J. W. *J. Am. Chem. Soc.* **1996**, *118*, 100.
- (26) Romero, P. E.; Whited, M. T.; Grubbs, R. H. *Organometallics* **2008**, *27*, 3422.
- (27) (a) Chatt, J. Chatt; Kubota, M.; Leigh, G. J.; March, F. C.; Mason, R.; Yarrow, D. J. *J. Chem. Soc. Chem. Commun.* **1974**, 1033. (b) Fachinetti, G.; Floriani, C.; Chiesi-Villa, A.; Guastini, C. *J. Am. Chem. Soc.* **1979**, *101*, 1767. (c) Pasquali, M.; Floriani, C.; Chiesi-Villa, A.; Guastini, C. *Inorg. Chem.* **1980**, *19*, 3847. (d) Thewissen, D. H. M. W.; Van Gaal, H. L. M. *J. Organomet. Chem.* **1979**, *172*, 69. (e) Gibson, J. A. E.; Cowie, M. *Organometallics* **1984**, *3*, 984.
- (28) It is possible that the CS₂ adduct and dithiolactone shown in Scheme 5.4 are in equilibrium, but we currently have no evidence supporting this view.
- (29) The reactivity of metal-ligand multiple bonds with carbon disulfide is typically initiated by nucleophilic ligands: (a) Mayr, A.; Lee, T.-Y. *Angew. Chem. Int. Ed.* **1993**, *32*, 1726. (b) Zuckerman, R. L.; Bergman, R. G. *Organometallics* **2000**, *19*, 4795.
- (30) The nucleophilicity of d⁸ metal complexes is well known and has been extensively investigated: (a) Shriver, D. F. *Acc. Chem. Res.* **1970**, *3*, 231. (b) Werner, H. *Pure Appl. Chem.* **1982**, *54*, 177. (c) Pearson, R. G.; Figdore, P. E. *J. Am. Chem. Soc.* **1980**, *102*, 1541.
- (31) (a) Manuel, T. A. *Inorg. Chem.* **1964**, *3*, 1703. (b) Werner, H.; Juthani, B. *J. Organomet. Chem.* **1981**, *209*, 211.
- (32) Itoh, K.; Matsuda, I.; Ueda, F.; Ishii, Y.; Ibers, J. A. *J. Am. Chem. Soc.* **1977**, *99*, 2118.
- (33) Further details regarding calculations on **1**, **3**, **5**, and **6** are provided in the Experimental Section.

- (34) The electrophilicity of the metal center in many alkylidene complexes is so pronounced that the M=C–H bond angle is contracted to allow an α -agostic interaction with the electron-deficient metal center: (a) Schultz, A. J.; Williams, J. M.; Schrock, R. R.; Rupprecht, G. A.; Fellmann, J. A. *J. Am. Chem. Soc.* **1979**, *101*, 1593. (b) Schultz, A. J.; Brown, R. K.; Williams, J. M.; Schrock, R. R. *J. Am. Chem. Soc.* **1981**, *103*, 169. (c) Goddard, R. J.; Hoffmann, R.; Jemmis, E. D. *J. Am. Chem. Soc.* **1980**, *102*, 7667.
- (35) Pangborn, A. B.; Giardello, M. A.; Grubbs, R. H.; Rosen, R. K.; Timmers, F. J. *Organometallics* **1996**, *15*, 1518.
- (36) Fan, L.; Parkin, S.; Ozerov, O. V. *J. Am. Chem. Soc.* **2005**, *127*, 16772.
- (37) Jaguar 7.5; Schrodinger, LLC, New York, NY, 2008.
- (38) (a) Becke, A. D. *Phys. Rev. A* **1988**, *38*, 3098. (b) Becke, A. D. *J. Chem. Phys.* **1993**, *98*, 5648. (c) Lee, C. T.; Yang, W. T.; Parr, R. G. *Phys. Rev. B* **1988**, *37*, 785. (d) Vosko, S. H.; Wilk, L.; Nusair, M. *Can. J. Phys.* **1980**, *58*, 1200.
- (39) (a) Hay, P. J.; Wadt, W. R. *J. Chem. Phys.* **1985**, *82*, 270. (b) Wadt, W. R.; Hay, P. J. *J. Chem. Phys.* **1985**, *82*, 284.

Chapter 6

Catalytic Oxidation of Methyl Ethers by a Double C–H Activation-Group Transfer Process

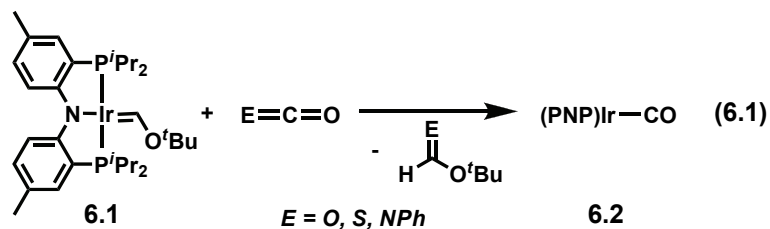
*The text in this chapter is reproduced in part with permission from:
Whited, M. T.; Grubbs, R. H. *J. Am. Chem. Soc.* **2008**, 130, 16476–16477.*

Copyright 2008 American Chemical Society

Introduction

In spite of numerous advances and decades of research, unactivated C–H bonds are still considered almost entirely inert to catalytic cleavage and functionalization. Such unactivated C–H bonds are ubiquitous in organic chemicals and hydrocarbon feedstocks, making their selective transformation an important goal. Myriad transition-metal species have been reported that are capable of selective C–H activation,¹ typically by a *single* oxidative addition or σ -bond metathesis event, though other important mechanisms are known.^{1c,f} In the cases where C_{sp³}–H bonds are activated, these processes generally produce M–C_{sp³} species, imposing limits on the types of products that can be obtained. In contrast, we envisioned an alternate strategy where *multiple* C–H activation events would generate M=C_{sp²} species for further elaboration.² In light of the rich reactivity of metal-bound carbenes,³ generation of such a species could open a new manifold of reactivity for catalytic C–H functionalization.

We have previously reported that pincer-type iridium complexes supported by Ozerov's PNP ligand (PNP = [N(2-PⁱPr₂-4-Me-C₆H₃)₂][−])⁴ effect the double C–H activation of *tert*-butyl methyl ether (MTBE) to generate an unusual square-planar iridium(I) carbene (**6.1**) with loss of H₂.⁵ Unlike most carbenes, which are nucleophilic or electrophilic at carbon, this complex possesses a high-lying Ir(d_{z²}) orbital that renders it nucleophilic at iridium, effecting atom and group transfer to the carbene from electrophilic heterocumulenes (eq 6.1).^{5a,6} In this contribution, we report that (PNP)Ir=C(H)O^tBu (**6.1**) promotes analogous atom and group transfer from nitrous oxide and organic azides, allowing recycling of the resulting iridium complexes and suggesting a new catalytic cycle based on generation of M=C_{sp²} species.⁷ Furthermore, careful tuning of reaction conditions has allowed realization of several catalytic oxidations of methyl ethers to formimidates by this process.

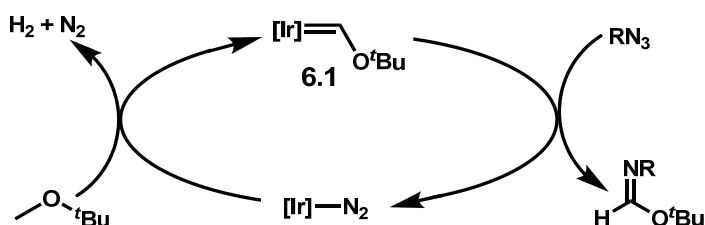


Results and Discussion

Stoichiometric Atom and Group Transfer from Diazo Reagents

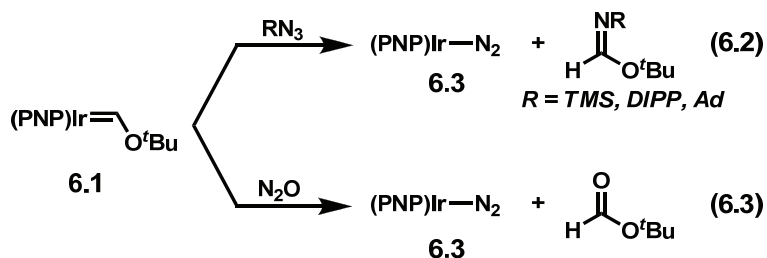
In our previous investigations of atom and group transfer from heterocumulenes, we have noted that the generation of a stable (PNP)Ir-CO species (**6.2**) seems to provide the thermodynamic driving force for the cleavage of strong C=E bonds (E = O, S, NPh).^{5a} Thermolysis and photolysis of complex **6.2** in MTBE produces no observable C-H activation products. Thus, the disadvantage inherent in these reactions is the difficulty in achieving catalytic turnover due to the reluctance of carbonyl complex **6.2** to serve as a precursor for C-H activation.

In light of our previous observation that C-H activation by (PNP)Ir is not hindered by the presence of N₂,⁵ it seemed plausible that a change in oxidant from carbonyl reagents (E=C=O) to the isoelectronic diazo reagents (E=N=N) could offer a related route that circumvents unreactive carbonyl complex **6.2**. By analogy with earlier investigations, organic azides should react with nucleophilic complex **6.1** at the electrophilic central nitrogen.⁶ Subsequent cyclization and elimination of formimidate would generate an iridium-dinitrogen complex, which could serve as a viable precursor for C-H activation to regenerate the iridium carbene, as depicted in Scheme 6.1. This reactivity would find precedent in the work of Hillhouse, wherein organic azides and nitrous oxide were shown to oxidize electron-rich Ni(II) dialkyls by nitrene-group and oxygen-atom insertion, respectively.^{8,9}



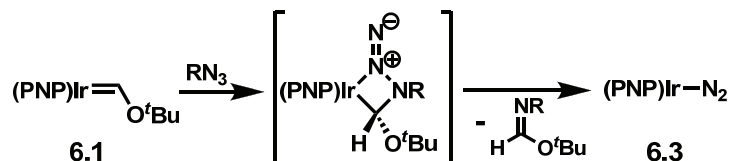
Scheme 6.1. Proposed cycle for MTBE oxidation.

As predicted, exposure of complex **6.1** to organic azides resulted in quantitative nitrene-group transfer to generate the expected formimidate and the previously unknown dinitrogen adduct (PNP)Ir–N₂ (**6.3**, eq 6.2).¹⁰ The transfer reaction proceeded cleanly with trimethylsilyl azide (TMS–N₃), 2,6-diisopropylphenyl azide (DIPP–N₃), and 1-azidoadamantane (AdN₃), with reaction rates reflecting the steric bulk of the azide substituent (DIPP > Ad > TMS). In accord with the isoelectronic analogy between CO₂ and N₂O, carbene **6.1** also reacted with nitrous oxide to effect oxygen-atom transfer, generating *tert*-butyl formate and **6.3** (eq 6.3).



These reactions have few analogues in transition-metal carbene chemistry,^{11,12} presumably because Fischer carbenes are generally electrophilic at carbon and organic azides and N₂O are poor nucleophiles.¹³ The closest precedent comes from elegant studies by Collman and co-workers on the generation of iridium(I)–dinitrogen complexes by nitrene transfer from organic azides to bound carbonyl ligands with release of isocyanate.¹⁴ By analogy with our previous studies, we propose that the transformations proceed through a four-membered

iridacyclic transition state (Scheme 6.2), and tentatively suggest that a similar mechanism is likely operative in the *trans*-Ir(Cl)(CO)(PR₃)₂ systems examined by Collman.^{14,15}



Scheme 6.2. Proposed mechanism of nitrene-group transfer from RN₃ to carbene **6.1**.

Dinitrogen complex **6.3** was characterized by NMR, IR, and single-crystal X-ray diffraction (XRD). XRD analysis (Figure 6.1) revealed a square-planar complex with metric parameters quite similar to the previously reported (PNP)Ir-CO (**6.2**). The dinitrogen ligand exhibits an N-N bond length of 1.13 Å, indicating modest activation of the N₂ unit.¹⁶ The diagnostic IR stretch (2067 cm⁻¹) is lower in energy than those previously reported for N₂ complexes of iridium(I),^{5b,14,17} probably due to the *trans* disposition of the dinitrogen ligand to a strongly π-basic arylamido donor.

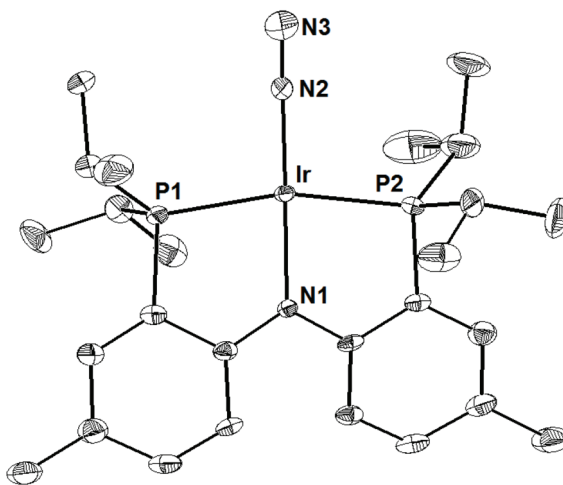


Figure 6.1. Displacement ellipsoid (35%) representation of (PNP)Ir-N₂ (**6.3**) with hydrogen atoms omitted for clarity. Selected bond lengths (Å) and angles (°): Ir-N1, 2.041(3); Ir-N2, 1.859(4); Ir-P1, 2.282(1); Ir-P2, 2.283(1); N2-N3, 1.128(7); N1-Ir-P1, 81.49(9); N1-Ir-N2, 177.6(2); P1-Ir-P2, 162.45(4); P1-Ir-N2, 98.58(12).

Dinitrogen complex **6.3** was found to be a suitable precursor for the double C–H activation of MTBE. Thermolysis of **6.3** in neat MTBE resulted in the slow formation of Fischer carbene **6.1** with loss of H₂ and N₂, though prolonged heating caused the gradual degradation of this complex to the previously reported *trans*-(PNP)Ir(H)₂(CO) (**6.4**, eq 6.4).^{5b} The reaction profile for the thermal conversion of **6.3** → **6.1** → **6.4** is presented in Chart 6.1.

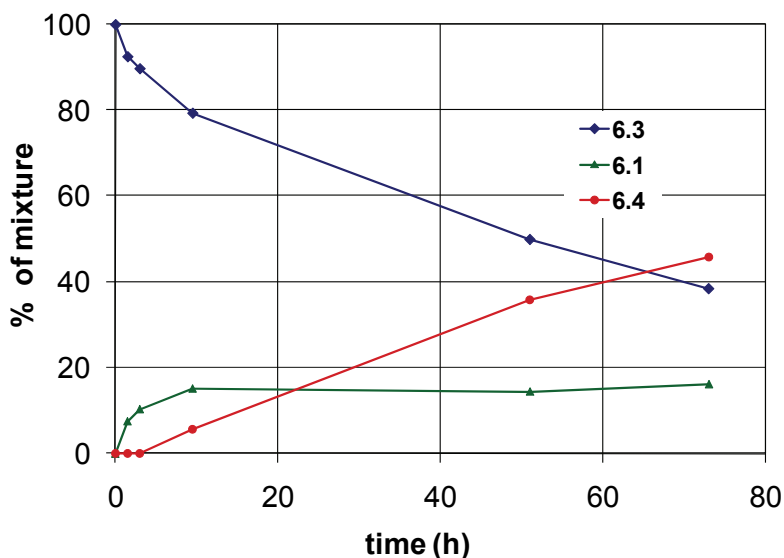
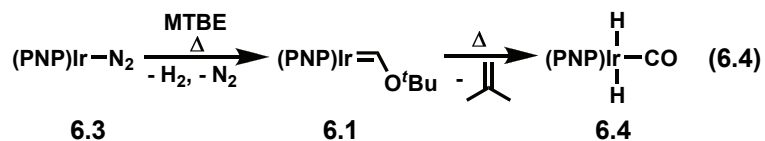
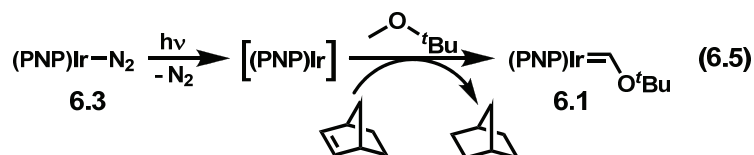


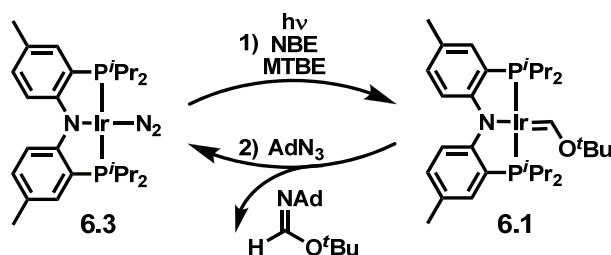
Chart 6.1. Thermolysis of (PNP)Ir–N₂ (**6.3**) in MTBE.

A photolysis route allowed the thermal decomposition of carbene **6.1** to be avoided. Irradiation of dinitrogen adduct **6.3** in MTBE at ambient temperature in the presence of norbornene as a sacrificial hydrogen acceptor facilitated the quantitative conversion of **6.3** to **6.1** (eq 6.5). This process proceeded smoothly in the presence of *tert*-butyl formates and formimidates, indicating that a catalytic cycle based on double C–H activation of MTBE and

subsequent group transfer from organic azides or N_2O would not be hampered by product inhibition.



The development of a continuous process for catalytic oxidation of MTBE to formimidate was hindered by the decomposition of **6.3** upon photolysis in the presence of organic azides, presumably due to preferential reaction with RN_3 over MTBE. However, the feasibility of a photocatalytic scheme was validated by a sequential method. A solution of **6.3** and excess NBE in MTBE was subjected to sequential AdN_3 addition (1 equiv) and photolysis, allowing 4 turnovers to be realized and affording *tert*-butyl *N*-adamantylformimidate in 93% yield (Scheme 6.3).



Scheme 6.3. Stepwise oxidation of MTBE via double C–H activation to generate carbene **6.1**.

Catalytic Oxidation of Methyl Ethers by a Double C–H Activation-Group Transfer Process

The sequential reactions described above and depicted in Scheme 6.3 were translated into a continuous process through the implementation of several important modifications. First, since the reactions was observed to shut down in the presence of excess oxidant (i.e., organic azide or nitrous oxide), the concentration of oxidant was kept low by use of a syringe pump for additions. Second, since carbene generation at $(\text{PNP})\text{Ir}$ is slow at ambient temperature,

moderate heating of the reaction (ca. 60 °C) allowed the catalytic scheme to proceed much more quickly. Finally, substitution of a bright halogen bulb for the mercury arc lamp previously employed for photolysis allowed reactions to be performed on the benchtop rather than in a UV box and also avoided the use of large quantities of water previously required to cool the arc lamp.

Thus, using the modifications described above, catalytic oxidation of MTBE, *sec*-butyl methyl ether, and *n*-butyl methyl ether was investigated (eq 6.6), and the results are presented in Table 6.1.

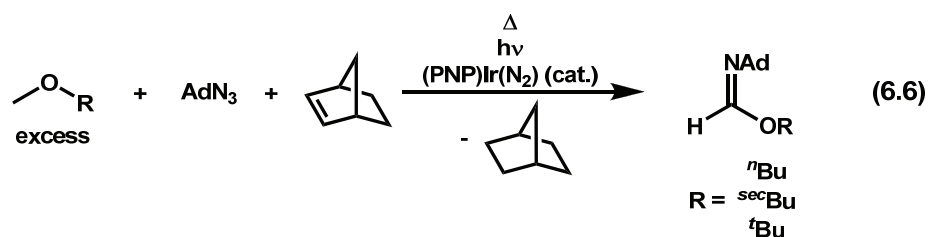


Table 6.1. Iridium-catalyzed oxidation of methyl ethers to formimidates

Substrate	Oxidant	Yield	Turnovers
<i>tert</i> -butyl methyl ether (MTBE)	AdN ₃	96%	10
<i>sec</i> -butyl methyl ether (SBME)	AdN ₃	26%	2.6
<i>n</i> -butyl methyl ether (NBME)	AdN ₃	27%	2.7

All of these reactions suffer from the requirement that the methyl ether substrate must be used as solvent to ensure efficient carbene generation. Additionally, yields are currently much higher for MTBE than for either SBME or NBME, presumably due to a competitive transfer α,β -dehydrogenation process, as described in Chapter 4, which generates vinyl ethers that may serve to poison the system. Nevertheless, these findings are encouraging in that they demonstrate conclusively that carbene formation by multiple C–H activations may be utilized in order to generate reactive intermediates in a catalytic cycle. Further studies to improve the efficiency and scope of these reactions are underway and will be reported in due course.

Conclusions

In conclusion, we have presented a process for the oxidation of methyl ethers to formates and formimidates based on double C–H activation to generate alkoxy-carbene complexes of iridium(I). The active iridium species can be recycled via a one-pot protocol and reasonable yields of formimidate may be obtained by a sequential process. Alternatively, careful control of reaction conditions, including temperature, light source, and rate of oxidant addition, allow the realization of a catalytic cycle for the oxidation of methyl ethers to *N*-adamantyl formimidates through a new double C–H activation-group transfer process. This scheme offers a conceptual alternative to traditional hydrocarbon functionalization pathways and reveals new possibilities for carbon–element multiple bond formation via nucleophilic-at-metal carbene complexes.

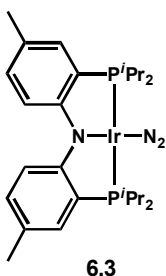
Acknowledgment

The author acknowledges Larry Henling for crystallographic assistance and Professor Oleg Ozerov (Brandeis University) for helpful discussions.

Experimental Section

General Considerations. All manipulations were carried out using standard Schlenk or glove-box techniques under a dinitrogen atmosphere. Unless otherwise noted, solvents were deoxygenated and dried by thorough sparging with Ar gas followed by passage through an activated alumina column.¹⁸ Hexamethyldisiloxane and *tert*-butyl methyl ether were distilled from CaH₂ and degassed prior to use. (PNP)Ir=C(H)O^tBu (**6.1**)^{5a} and 2,6-diisopropylphenylazide¹⁹ were prepared according to literature procedures. Azidotrimethylsilane was purchased from Aldrich and degassed prior to use. Other reagents were purchased from commercial vendors and used without further purification. Elemental analyses were carried out at Desert Analytics, Tucson, Arizona. NMR spectra were recorded at ambient temperature on a Varian Mercury 300 MHz spectrometer. ¹H and ¹³C NMR chemical shifts were referenced to residual solvent. ³¹P NMR chemical shifts are reported relative to an external standard of 85% H₃PO₄. Infrared spectra were recorded using a Perkin Elmer Spectrum BXII spectrometer. X-ray diffraction studies were carried out in the Beckman Institute Crystallographic Facility on a Bruker KAPPA APEX II diffractometer. Photolysis reactions were performed in pyrex vessels with 450 W medium-pressure mercury arc lamp (Ace Glass) or a 120 V/23 W halogen bulb, which produced essentially identical results.

(PNP)Ir-N₂ (6.3). A 50 mL pressure tube was charged with (PNP)Ir=C(H)O^tBu (**6.1**) (42.0 mg,

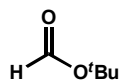


0.0594 mmol) dissolved in toluene (15 mL). The solution was frozen and the headspace evacuated and backfilled with nitrous oxide (1 atm). Upon melting, the color of the solution changed from purple to orange over a period of 5 min. The solution was allowed to warm to ambient temperature, stirred for 15 min,

and volatiles were removed *in vacuo* to afford an orange film. Lyophilization of the residues

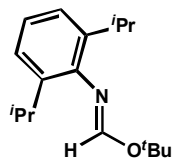
from benzene (5 mL) afforded **6.3** as a flocculent, pale-orange powder (37.9 mg, 98%). Orange crystals of **6.3** suitable for X-ray diffraction were obtained by slow evaporation of pentane from a concentrated solution. Due to its moderate light sensitivity, complex **6.3** was stored at $-35\text{ }^{\circ}\text{C}$ in the dark to prevent decomposition. ^1H NMR (C_6D_6): δ 7.69 (dt, $J_1 = 8.7\text{ Hz}$, $J_2 = 2.1\text{ Hz}$, 2H, Ar- H), 6.94 (m, 2H, Ar- H), 6.76 (dd, $J_1 = 8.4\text{ Hz}$, $J_2 = 1.8\text{ Hz}$, 2H, Ar- H), 2.33 (m, 4H, $-\text{CH}(\text{CH}_3)_2$), 2.18 (s, 6H, Ar- CH_3), 1.32 (dvt, 12H, $-\text{CH}(\text{CH}_3)_2$), 1.12 (dvt, 12H, $-\text{CH}(\text{CH}_3)_2$). $^{13}\text{C}\{^1\text{H}\}$ NMR (C_6D_6): 164.1, 132.0, 131.6, 125.5, 121.7, 116.0, 26.4 (m), 20.3, 19.1, 18.4. $^{31}\text{P}\{^1\text{H}\}$ NMR (C_6D_6): δ 46.9 (s). IR (THF, KBr, cm^{-1}) $\nu(\text{N}_2)$: 2067. Anal. calcd. for $\text{C}_{26}\text{H}_{40}\text{IrN}_3\text{P}_2$: C, 48.13; H, 6.21; N, 6.48. Found: C, 48.57; H, 5.69; N, 6.15.

Preparation of *tert*-butyl formate from complex (6.1). In a sealed NMR tube, a purple solution



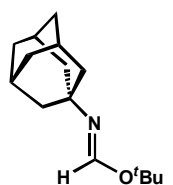
of **6.1** (ca. 15 mg) in C_6D_6 was frozen and the headspace evacuated and backfilled with nitrous oxide (1 atm). As the solution thawed, a gradual change in color from purple to pale yellow was observed. After 15 min, the disappearance of **6.1** was confirmed by NMR spectroscopy, and quantitative conversion to **6.3** and *tert*-butyl formate was inferred as these were the only species observed in the ^1H NMR spectrum. ^1H NMR (*tert*-butyl formate, C_6D_6): δ 7.64 (s, 1H, $-\text{C}(\text{O})\text{H}$), 1.24 (s, 9H, $-\text{C}(\text{CH}_3)_3$). The identity of the *tert*-butylformate organic product was confirmed by comparison to an authentic sample obtained from Aldrich.

Preparation of *tert*-butyl *N*-(2,6-diisopropylphenyl)formimidate from complex (6.1). 2,6-



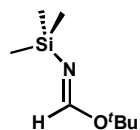
diisopropylphenyl azide (6.1 mg, 0.030 mmol) was added in one portion to a solution of **6.1** (21.5 mg, 0.0304 mmol) in C_6D_6 (800 μ L), causing an immediate change in color from purple to golden. After 15 min, the disappearance of **6.1** was confirmed by NMR spectroscopy, and quantitative conversion to **6.3** and *tert*-butyl *N*-(2,6-diisopropylphenyl)formimidate was inferred as these were the only species observed in the 1H NMR spectrum. 1H NMR (*tert*-butyl *N*-(2,6-diisopropylphenyl)formimidate, C_6D_6): δ 7.32 (s, 1H, $-C(NDIPP)H$), 7.25 – 7.10 (m, 3H, Ar-H), 3.26 (septet, $^3J_{HH} = 6.9$ Hz, 2H, $-CH(CH_3)_2$), 1.45 (s, 9H, $-C(CH_3)_3$), 1.23 (d, $^3J_{HH} = 6.9$ Hz, 12H, $-CH(CH_3)_2$). IR (C_6D_6 , KBr, cm^{-1}) $\nu(C=N)$: 1669. The *tert*-butyl *N*-(2,6-diisopropylphenyl)formimidate organic product was identified by comparison of the distinctive spectral data, namely the 1H chemical shift of the formimidate proton and the energy of the medium-intensity C=N infrared stretch, to those of analogous formimidate complexes.^{5a,20}

Preparation of *tert*-butyl *N*-adamantylformimidate from complex (6.1). 1-Azidoadamantane



(3.8 mg, 0.021 mmol) was added as a solid to a solution of **6.1** (13.1 mg, 0.0185 mmol) in C_6D_6 (800 μ L). Over a period of 15 min, the solution gradually lightened from purple to brown. Conversion to **6.3** and *tert*-butyl *N*-adamantylformimidate was complete in 2 h, and the yield of formimidate was judged to be quantitative by 1H NMR via integration versus an internal standard of hexamethyldisiloxane. 1H NMR (*tert*-butyl *N*-adamantylformimidate, C_6D_6): δ 7.46 (s, 1H, $-C(NAd)H$), 1.96 (m, 3H, $-CH$ (Ad)), 1.67 (d, $^3J_{HH} = 2.7$ Hz, $-NC(CH_2)_3$ (Ad)), 1.58 (m, 6H, $-CH_2$ (Ad)), 1.49 (s, 9H, $-C(CH_3)_3$).

Preparation of *tert*-butyl *N*-trimethylsilylformimidate from complex (6.1). Trimethylsilyl azide



(2.5 μL , 0.019 mmol) was added in one portion to a solution of **6.1** (11.5 mg, 0.0163 mmol). No immediate color change was observed. After 10 h at ambient temperature, nitrene transfer to generate **6.3** and *tert*-butyl *N*-trimethylsilylformimidate was 25% complete, as judged by ^1H and ^{31}P NMR. Extended heating (8 h, 70 $^\circ\text{C}$) brought about the complete consumption of **6.1**, though competitive degradation of **6.1** was noted at elevated temperatures (ca. 18% at 70 $^\circ\text{C}$), as previously described.^{5b} Addition of large excesses (>10 equiv) of trimethylsilyl azide to solutions of **6.1** followed by 12 h of reaction at ambient temperature and 4 h at 70 $^\circ\text{C}$ also facilitated the complete consumption of **6.1** and formation of **6.3** and *tert*-butyl *N*-trimethylsilylformimidate without decomposition. ^1H NMR (*tert*-butyl *N*-trimethylsilylformimidate, C_6D_6): δ 7.64 (s, 1H, $-\text{C}(\text{NTMS})\text{H}$), 1.38 (s, 9H, $-\text{C}(\text{CH}_3)_3$), 0.16 (s, 9H, $-\text{Si}(\text{CH}_3)_3$).

Thermolysis of (PNP)Ir–N₂ (6.3) in MTBE. Complex **6.3** (ca. 10 mg) was dissolved in MTBE (800 μL) and transferred to a resealable NMR tube under a nitrogen atmosphere. The solution was heated at 90 $^\circ\text{C}$ for 76 h, and the distribution of products was periodically monitored by ^{31}P NMR (see Chart 6.1).²¹ After 7 d, the complete disappearance of (PNP)Ir–N₂ and (PNP)Ir=C(H)O^tBu and formation of *trans*-(PNP)Ir(CO)(H)₂ were confirmed by ^1H and ^{31}P NMR spectroscopy.

Stepwise synthesis of *tert*-butyl *N*-adamantylformimidate. A 30 mL resealable flask was charged with complex **6.1** (48.6 mg, 0.0687 mmol) and norbornene (31.9 mg, 0.339 mmol) in *tert*-butyl methyl ether (15 mL). 1-Azidoadamantane (12.2 mg, 0.0688 mmol) was added and the reaction was stirred for 2 h, causing a color change to golden-brown. The solution was irradiated for 30 min, causing a darkening from golden to dark brown, and the reaction allowed to proceed

at ambient temperature for 16 h, causing a color change to red-purple. A second equiv of AdN₃ (12.2 mg, 0.0688 mmol) was added and the solution was stirred for 2 h, causing the color to lighten to golden-brown. The sample was subjected to two additional cycles of photolysis and AdN₃ addition, as described above, and volatiles were removed *in vacuo*, leaving a brownish film. The residues were dissolved in C₆D₆ and the yield of *tert*-butyl *N*-adamantylformimidate (0.256 mmol, 93% based on AdN₃) determined by ¹H NMR spectroscopy via integration relative to an internal standard of hexamethyldisiloxane.

Catalytic oxidation of MTBE to *tert*-butyl *N*-adamantylformimidate. In a typical procedure, (PNP)Ir–N₂ (**6.1**) (21.5 mg, 0.0331 mmol) and norbornene (55.2 mg, 0.586 mmol) were dissolved in MTBE (8 mL) and transferred to a 25 mL pressure flask outfitted with a sidearm. The solution was subjected to photolysis at 60 °C for 2 h, and a solution of 1-azidoadamantane (61.3 mg, 0.346 mmol) in MTBE (10 mL) was added by syringe pump over a period of 30 h as heating and photolysis was allowed to continue. The resulting green-brown solution was dried *in vacuo* and the yield of *tert*-butyl *N*-adamantylformimidate determined by ¹H NMR spectroscopy in C₆D₆ relative to an internal standard of HMDSO by integration of the formimidate proton (δ 7.46 ppm) (0.33 mmol, 96%).

Catalytic oxidation of SBME to *sec*-butyl *N*-adamantyl formimidate. The procedure described above for MTBE oxidation was followed using **6.1** (17.6 mg, 0.0271 mmol), norbornene (68.1 mg, 0.723 mmol), and 1-azidoadamantane (48.8 mg, 0.275 mmol) in SBME. The yield of *sec*-butyl *N*-adamantyl formimidate was determined by ¹H NMR spectroscopy via integration relative to an internal standard of HMDSO, as described above (0.071 mmol, 26%).

Catalytic oxidation of NBME to *n*-butyl *N*-adamantyl formimidate. The procedure described above for MTBE oxidation was followed using **6.1** (16.0 mg, 0.0247 mmol), norbornene (62.2 mg, 0.661 mmol), and 1-azidoadamantane (43.8 mg, 0.247 mmol) in NBME. The yield of *n*-butyl *N*-adamantyl formimidate was determined by ^1H NMR spectroscopy via integration relative to an internal standard of HMDSO, as described above (0.066 mmol, 27%).

X-ray Crystallography Procedures. X-ray quality crystals were grown as indicated in the experimental procedures for each complex. The crystals were mounted on a glass fiber with Paratone-N oil. Structures were determined using direct methods with standard Fourier techniques using the Bruker AXS software package. In some cases, Patterson maps were used in place of the direct methods procedure. Table 6.1 contains the X-ray diffraction experimental details.

Table 6.1. X-ray crystallographic data

complex	6.3	
Empirical Formula	$C_{26}H_{40}IrN_3P_2$	
Formula Weight	648.75	
λ (Å)	0.71073	
T (K)	100(2)	
a (Å)	9.4977(10)	
b (Å)	30.723(4)	
c (Å)	9.5901(11)	
α (deg)	90	
β (deg)	90	
γ (deg)	90	
V (Å ³)	2798.3(6)	
Z	4	
Crystal System	Orthorhombic	
Space Group	Pna2(1)	
d_{calc} (g/cm ³)	1.540	
GOF on F ²	1.065	
R1, wR2 ^a (I > 2 σ (I))	0.0383, 0.0512	

References and Notes

- (1) For leading references, see: (a) Bergman, R. G. *Nature* **2007**, *446*, 391. (b) Arndtsen, B. A.; Bergman, R. G.; Mobley, T. A.; Peterson, T. H. *Acc. Chem. Res.* **1995**, *28*, 154. (c) Crabtree R. H. *Chem. Rev.* **1985**, *85*, 245. (d) Labinger, J. A.; Bercaw, J. E. *Nature*, **2002**, *417*, 507. (e) *Activation and Functionalization of C–H Bonds*; Goldberg, K. I., Goldman, A. S., Eds.; ACS Symposium Series 885; American Chemical Society: Washington, DC, **2004**. (f) Periana, R. A.; Bhalla, G.; Tenn, W. J.; Young, K. J. H.; Liu, X. Y.; Mironov, O.; Jones, C. J.; Ziatdinov, V. R. *J. Mol. Catal. A: Chem.* **2004**, *220*, 7.
- (2) Stoichiometric generation of iridium carbenes by double C–H activation of ethers: (a) Boutry, O.; Gutiérrez, E.; Monge, A.; Nicasio, M. C.; Pérez, P. J.; Carmona, E. *J. Am. Chem. Soc.* **1992**, *114*, 7288. (b) Luecke, H. F.; Arndtsen, B. A.; Burger, P.; Bergman, R. G. *J. Am. Chem. Soc.* **1996**, *118*, 2517. (c) Carmona, E.; Paneque, M.; Santos, L. L.; Salazar, V. *Coord. Chem. Rev.* **2005**, *249*, 1729.
- (3) (a) Gallop, M. A.; Roper, W. R. *Adv. Organomet. Chem.* **1986**, *25*, 121. (b) *Handbook of Metathesis*; Grubbs, R. H., Ed.; Wiley-VCH: Weinheim, 2003. (c) Doyle, M. P. *Chem. Rev.* **1986**, *86*, 919. (d) Doyle, M. P.; Forbes, D. C. *Chem. Rev.* **1998**, *98*, 911.
- (4) (a) Fan, L.; Foxman, B. M.; Ozerov, O. V. *Organometallics* **2004**, *23*, 326. (b) Ozerov, O. V.; Guo, C.; Papkov, V. A.; Foxman, B. M. *J. Am. Chem. Soc.* **2004**, *126*, 4792.
- (5) (a) Whited, M. T.; Grubbs, R. H. *J. Am. Chem. Soc.* **2008**, *130*, 5874. (b) Romero, P. E.; Whited, M. T.; Grubbs, R. H. *Organometallics* **2008**, *27*, 3422.
- (6) Whited, M. T.; Grubbs, R. H. *Organometallics* **2009**, *48*, 161.
- (7) A related but distinct tandem alkane dehydrogenation-olefin metathesis process has recently been reported for catalytic C–H functionalization via metal carbene intermediates: Goldman, A. S.; Roy, A. H.; Huang, Z.; Ahuja, R.; Schinski, W.; Brookhart, M. *Science* **2006**, *312*, 257.
- (8) (a) Matsunaga, P. T.; Hess, C. R.; Hillhouse, G. L. *J. Am. Chem. Soc.* **1994**, *116*, 3665. (b) Matsunaga, P. T.; Hillhouse, G. L.; Rheingold, A. L. *J. Am. Chem. Soc.* **1993**, *115*, 2075.
- (9) Interestingly, Hillhouse reports that pyridine *N*-oxide does not perform this transformation (ref. 8b). We note the same behavior in our system, probably due to the poor electrophilicity of the reagent.
- (10) (PNP)Rh–N₂ has been reported: Gatard, S.; Guo, C.; Foxman, B. M.; Ozerov, O. V. *Organometallics* **2007**, *26*, 6066.
- (11) (a) Fischer, H.; Zeuner, S. *J. Organomet. Chem.* **1985**, *286*, 201. (b) Hu, X.; Meyer, K. J. *Am. Chem. Soc.* **2004**, *126*, 16322. (c) Harrold, N. D.; Waterman, R.; Hillhouse, G. L. *Abstracts of Papers*, 233rd ACS National Meeting, Chicago, IL; American Chemical Society: Washington, DC, 2007; INOR 682.

- (12) Related reactivity of Fischer carbenes with diazoalkanes: (a) Casey, C. P.; Burkhardt, T. J. *J. Am. Chem. Soc.* **1972**, *94*, 6543. (b) Casey, C. P.; Bertz, S. H.; Burkhardt, T. J. *Tetrahedron Lett.* **1973**, 1421.
- (13) For leading references regarding reactivity of organic azides, see Cenini, S.; Gallo, E.; Caselli, A.; Ragaini, F.; Fantauzzi, S.; Piangiolino, C. *Coord. Chem. Rev.* **2006**, *250*, 1234.
- (14) (a) Collman, J. P.; Kang, J. W. *J. Am. Chem. Soc.* **1966**, *88*, 3459. (b) Collman, J. P.; Kubota, M.; Sun, J.-Y.; Vastine, F. D. *J. Am. Chem. Soc.* **1967**, *89*, 169. (c) Collman, J. P.; Kubota, M.; Vastine, F. D.; Sun, J. Y.; Kang, J. W. *J. Am. Chem. Soc.* **1968**, *90*, 5430.
- (15) Recent computations have suggested that a 1,3-dipolar cycloaddition of N₂O is also a likely pathway: Brookes, N. J.; Yates, B. F. University of Tasmania. Personal communication, December 2008.
- (16) MacKay, B. A.; Fryzuk, M. D. *Chem. Rev.* **2004**, *104*, 385.
- (17) (a) Göttker-Schnetman, I.; White, P. S.; Brookhart, M. *Organometallics* **2004**, *23*, 1766. (b) Ghosh, R.; Kanzelberger, M.; Emge, T. J.; Hall, G. S.; Goldman, A. S. *Organometallics* **2006**, *25*, 5668.
- (18) Pangborn, A. B.; Giardello, M. A.; Grubbs, R. H.; Rosen, R. K.; Timmers, F. J. *Organometallics* **1996**, *15*, 1518.
- (19) Spencer, L. P.; Altwer, R.; Wei, P.; Gelmini, L.; Gauld, J.; Stephan, D. W. *Organometallics* **2003**, *22*, 3841.
- (20) (a) Aue, D. H.; Thomas, D. *J. Org. Chem.* **1974**, *39*, 3855. (b) Aue, D. H.; Thomas, D. *J. Org. Chem.* **1975**, *40*, 2360. (c) Guzmán, A.; Muchowski, J. M.; Naal, N. T. *J. Org. Chem.* **1981**, *46*, 1224.
- (21) For a related study on the thermolysis of (PNP)IrH₂ in MTBE, see reference 5b.

Chapter 7

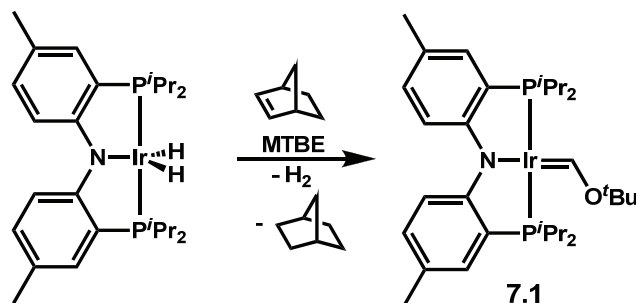
Synthesis and Reactivity of Iridium(III) Dihydrido Aminocarbenes

*The text in this chapter is reproduced in part with permission from:
Whited, M. T.; Grubbs, R. H. *Organometallics* **2008**, 27, 5737–5740.
Copyright 2008 American Chemical Society*

Introduction

The study of metal–carbon multiple bonds has occupied a central role in the field of organometallic chemistry since seminal reports of the first Fischer- and Schrock-type carbenes.¹ A number of transformations of these moieties have been developed, and many have been implemented in catalytic processes.² However, the fact that most synthetically useful transition-metal carbenes are generated from high-energy precursors such as diazoalkanes, ylides, and alkyllithium reagents serves as a fundamental limitation on the types of catalytic reactions that can be developed. Nevertheless, several important reports have indicated that later transition metals can mediate the double C–H activation of ethers and amines to generate heteroatom-substituted carbene complexes.³ Such a process would be highly desirable in the context of a potential catalytic cycle since it directly affords an $M=C_{sp^2}$ fragment for further elaboration but circumvents the use of high-energy carbene precursors.

Recently, we have reported that iridium complexes supported by Ozerov's PNP ligand ($PNP = [N(2-P^iPr_2-4-Me-C_6H_3)_2]^-$)⁴ mediate the double C–H activation of *tert*-butyl methyl ether (MTBE) to afford an unusual square-planar Ir(I) alkoxycarbene (**7.1**) upon loss of H_2 (Scheme 7.1).^{3f} The geometry of the low-valent complex confers nucleophilic character to the metal center, allowing access to unprecedented heterocumulene metatheses across the $M=C$ bond.^{5,6} Thus, we were interested to learn whether the multiple C–H activation processes could be generalized to substrates containing heteroatoms other than oxygen. In this contribution, we report that the (PNP)Ir framework performs the double C–H activation of methyl amines without loss of H_2 , producing octahedral Ir(III) dihydrido aminocarbenes, and the structure and reactivity of these complexes are contrasted with those of the related Ir(I) alkoxycarbenes.

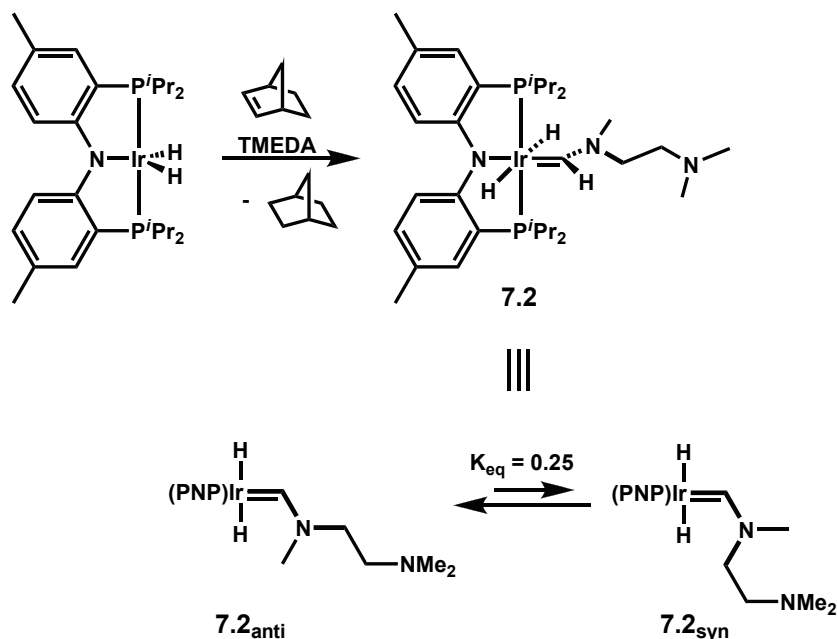


Scheme 7.1. Dehydrogenation of *tert*-butyl methyl ether at (PNP)Ir generates an Ir(I) carbene.

Results and Discussion

Synthesis of Iridium(III) Dihydrido Aminocarbenes

Dehydrogenation of (PNP)IrH₂^{4b} with norbornene (NBE, 1 equiv) in *N,N,N',N'*-tetramethylethylenediamine (TMEDA) affords a mixture of two dihydrido iridium(III) aminocarbene atropisomers (**7.2_{syn}** and **7.2_{anti}**, Scheme 7.2). Although the isomers are initially formed in equal quantities, equilibration over a period of 16 h affords a 4:1 mixture of **7.2_{anti}**:**7.2_{syn}**, indicating that there is not a kinetic preference for formation of either atropisomer but the **7.2_{anti}** conformation is slightly more favorable thermodynamically. This dehydrogenative reactivity is in contrast with the dehydrogenation of methyl ethers by the same system, where H₂ is lost to give square-planar iridium(I) carbene species. Aminocarbene **7.2_{anti}**, which can be isolated cleanly by crystallization,⁷ exhibits a distinctive ¹H NMR chemical shift for the carbene proton (δ 12.4 ppm) as well as a broad hydride signal at -9.3 ppm. Decoalescence of the hydride resonance into two distinct multiplets at -8.4 and -9.8 ppm occurs at -5 °C due to slow rotation about the Ir–C bond, and activation parameters for Ir–C bond rotation were determined by variable-temperature ¹H NMR spectroscopy ($\Delta G^\ddagger = 4.2$ kcal mol⁻¹).⁸ The isomeric complex **7.2_{syn}** exhibits similar properties.



Scheme 7.2. Dehydrogenation of TMEDA at (PNP)Ir yields two isomeric aminocarbenes.

Aminocarbene **7.2_{anti}** has been characterized by single-crystal X-ray diffraction (XRD) analysis (Figure 7.1). Interestingly, the plane of the carbene ligand is perpendicular to the plane defined by the C–N–C bonds of the amidophosphine ligand, preventing the synergistic push–pull effect between the π -donor arylamido and π -acceptor carbene observed for **7.1**.⁵ The less electron-rich metal center is partially responsible for the elongated Ir–C bond (1.97 Å compared with 1.88 Å for **7.1**),^{3f} as is increased π -donation from nitrogen compared with oxygen. A significant π component in the C27–N2 bond is supported by the X-ray crystal structure, which depicts a trigonal-planar nitrogen and a short C27–N2 bond (1.32 Å). As a result of significant N→C π -donation, rotation about the C27–N2 bond is sluggish at room temperature, resulting in the slow (24 h) reappearance of the **7.2_{syn}** atropisomer upon dissolution of crystalline **7.2_{anti}** in benzene. The combination of crystallographic and spectroscopic evidence, therefore, indicates that complex **7.2** is best described by two major resonance structures (eq 7.1), affording

effective Ir–C and C–N bond orders that are between one and two. Similar behavior has been previously noted for aminocarbenes, particularly those of the late transition metals.⁹

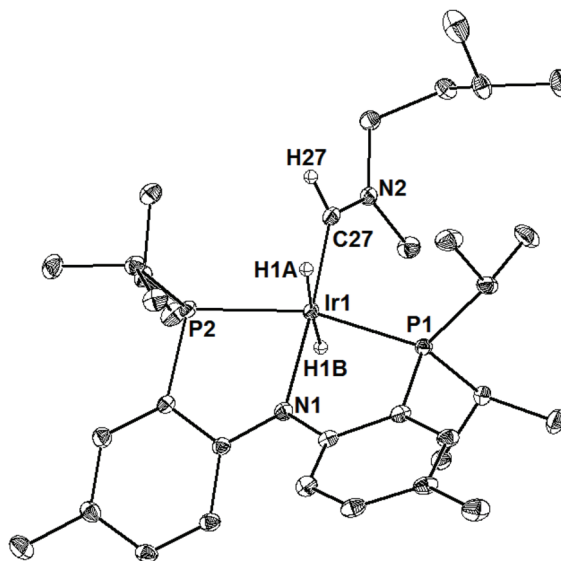
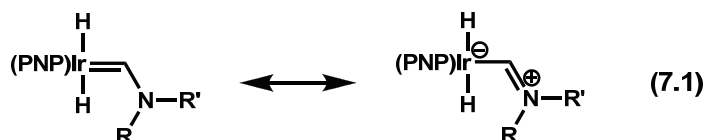
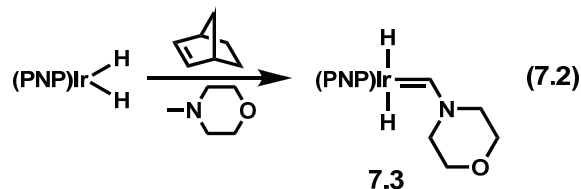


Figure 7.1. Displacement ellipsoid (35%) representation of aminocarbene **7.2_{anti}** with most hydrogen atoms omitted for clarity. Selected bond lengths (Å) and angles (°): Ir1–C27, 1.970(2); Ir1–N1, 2.138(2); Ir1–P1, 2.2947(5); Ir1–P2, 2.2903(5); N1–Ir1–C27, 177.20(7); P1–Ir1–P2, 160.20(2); Ir1–C27–N2, 133.3(2).



A related dihydrido aminocarbene (**7.3**) may be prepared from *N*-methylmorpholine (eq 7.2).⁷ The properties of this complex generally mirror those observed for **7.2**, though *syn* and *anti* isomers are not obtained due to the symmetrical nature of the amine.¹⁰ The activation parameters for Ir–C bond rotation were determined by NMR spectroscopy ($\Delta G^\ddagger = 3.6 \text{ kcal mol}^{-1}$), indicating that the “tied-back” nature of the nitrogen substituent slightly lowers the barrier to rotation. The dihydrido aminocarbene was the only complex observed to form, indicating a preference for N–CH₃ activation over O–CH₂ activation.



Reactivity of Iridium(III) Dihydrido Aminocarbenes

We have previously reported detailed studies on the reactivity of carbene **7.1**, and these generally support reactivity that is dominated by a nucleophilic, low-valent iridium(I) center.^{5,6} The octahedral iridium(III) complexes obtained by dehydrogenation of methyl amines would not be expected to interact with electrophiles due to the lower electron density at iridium and the lack of a vacant coordination site. As predicted, **7.2** did not react with carbon dioxide, even under forcing thermal conditions. However, thermolysis of **7.2** in the presence of trimethylphosphine (20 equiv) resulted in a phosphine-induced 1,2-hydride migration to the carbene, affording complex **7.4** (Scheme 7.3). The phosphine adduct **7.4** was characterized by XRD analysis, revealing elongated Ir1–C27 (2.12 Å compared with 1.97 Å for aminocarbene **7.2**) and C27–N2 (1.48 Å compared with 1.32 Å for **7.2**) bonds, as well as a pyramidalized N2 atom, consistent with a loss of π interaction between C27 and N2 (Figure 7.2). An analogous carbonyl complex (**7.5**) was obtained by thermolysis of **7.2** in the presence of CO (1 atm) (Scheme 7.3). This behavior is not surprising in light of Crabtree's observation that a similar octahedral iridium(III) aminocarbene can undergo reversible α -hydrogen elimination mediated by the presence or absence of an additional acetone ligand.^{3e} Given the coordinatively saturated nature of the starting material and the isomerization of **7.2** that has been observed upon thermolysis (*vide infra*), we tentatively propose that hydride migration precedes phosphine or carbonyl ligand association.

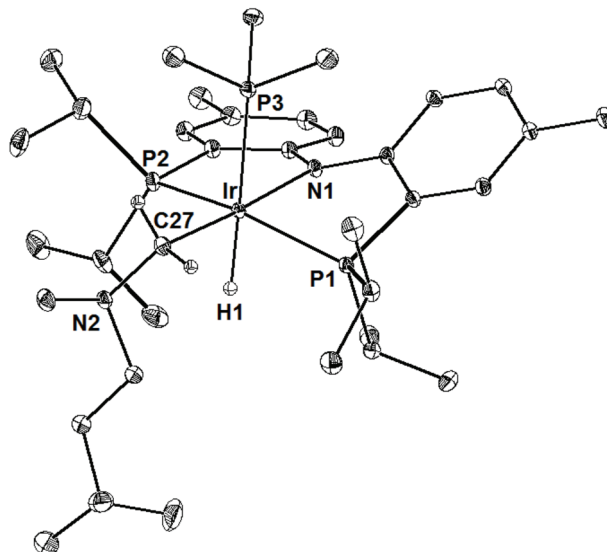
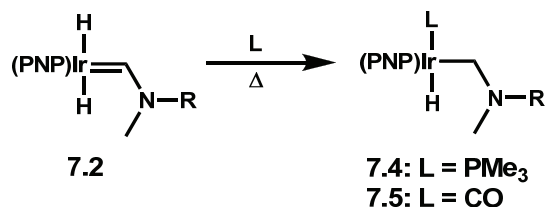


Figure 7.2. Displacement ellipsoid (35%) representation of complex **7.4** with hydrogen atoms omitted for clarity. Selected bond lengths (Å) and angles (°): Ir–C27, 2.125(1); Ir–N1, 2.156(1); Ir–P1, 2.2969(3); Ir–P2, 2.2867(4); Ir–P3, 2.3813(4); Ir–H1, 1.578(9); C27–N2, 1.479(2); N1–Ir–C27, 177.27(5); P1–Ir–P2, 151.67(1); P3–Ir–H1, 177.9(9); Ir–C27–N2, 119.01(9).



Scheme 7.3. Reaction of aminocarbene **7.2** with PMe_3 and CO ($\text{R} = (\text{CH}_2)_2\text{NMe}_2$).

Alkoxy carbene **7.1**, which contains no hydride co-ligands, is clearly incapable of exhibiting the same reactivity patterns. Thus, we examined the reaction of **7.1** with strong L-type ligands with the hope of elucidating potentially divergent pathways. Exposure of **7.1** to an excess (>20 equiv) of PMe_3 resulted in no reaction at ambient temperature, and only decarbonylative decomposition was observed upon prolonged thermolysis.^{3f} However, reaction of **7.1** with CO (1 atm) at ambient temperature resulted in an immediate color change from purple to golden, affording a product of ligand migration quite different from **7.4** or **7.5** (eq 7.3). Spectroscopic evidence (NMR and IR) indicated the presence of two bound carbonyl ligands

($\nu_{\text{sym}} = 1981 \text{ cm}^{-1}$, $\nu_{\text{asym}} = 1924 \text{ cm}^{-1}$), and XRD analysis confirmed the migratory insertion of the carbene into the Ir–N bond, affording a five-coordinate, trigonal-bipyramidal iridium(I) dicarbonyl (**7.6**, Figure 7.3).

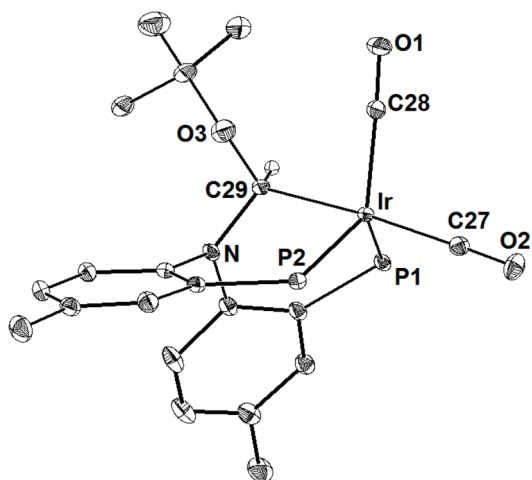
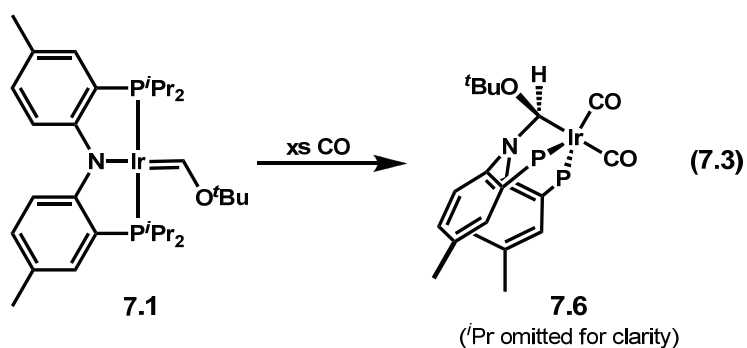
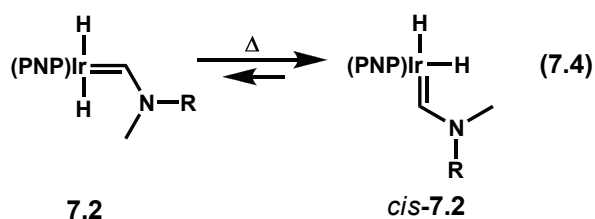


Figure 7.3. Displacement ellipsoid representation of complex **7.6** with *i*Pr phosphine substituents omitted for clarity. Selected bond lengths (Å) and angles (°): Ir–C29, 2.142(4); Ir–C27, 1.907(4); Ir–C28, 1.903(4); Ir–P1, 2.320(1); Ir–P2, 2.327(1); C29–Ir–C27, 175.2(2); P1–Ir–P2, 119.82(3); C29–Ir–C28, 86.4(2); P1–Ir–C28, 120.9(1).

Perhaps most interesting is that thermolysis of this complex results in the formation of (PNP)Ir–CO,⁵ presumably by loss of *tert*-butoxyketene, though organic products have not been definitively identified. Although insertion reactions of metal-bound carbenes are relatively common,¹¹ this reaction represents, to the best of our knowledge, the first example of such an insertion into a metal–amide bond.¹² Moreover, reversible migratory insertions of carbenes such as this are quite rare,^{13,14} and we believe the “masked carbene” observed for complex **7.6** may

presage a new strategy for the formation of C=C bonds via migratory deinsertion from a heteroatom-substituted metal alkyl.

In light of the previously reported decarbonylative degradation of alkoxycarbene **7.1**,^{3f} we were interested in the thermal reactivity of iridium(III) aminocarbenes. Thermolysis of **7.2** results in the partial isomerization from the *trans*-dihydrido aminocarbene to the *cis*-dihydrido aminocarbene (*cis*-**7.2**, eq 7.4), and both *cis*-**7.2**_{syn} and *cis*-**7.2**_{anti} isomers are observed to form. Since prolonged thermolysis of *cis*-**7.2** does not result in loss of H₂, even in the presence of norbornene, it is clear that the retention of hydride ligands in **7.2** is not simply a kinetic preference. Instead, we find it most probable that the increased N→C π-donation associated with the aminocarbenes confers increased basicity to the iridium center, making it reluctant to reductively eliminate H₂. This picture is consistent with the resonance structure depicted for these aminocarbenes (eq 7.1), where a partial negative charge is imparted to iridium by virtue of strong N→C π-donation.



Conclusions

In summary, we have reported the synthesis of iridium-supported dihydrido aminocarbenes by a double C–H activation protocol as well as preliminary reactivity studies on the resulting complexes. This dehydrogenative reactivity is fundamentally different from what has been previously observed at pincer-supported iridium. Goldman and colleagues have reported that a (PCP)Ir complex is competent to generate enamines by the catalytic transfer

dehydrogenation of tertiary amines.¹⁵ However, the (PCP)Ir system does not target methyl substituents and in all cases either α,β -dehydrogenation or no reaction was observed. Thus, it is clear that the PNP ligand examined in this report confers a selectivity pattern that is distinct from the related PCP pincer ligands. This unusual reactivity suggests that a wealth of double C–H activation chemistry may be accessed at low-valent iridium centers by judicious ligand design and substrate selection, affording new routes to $M=C_{sp^2}$ species for further elaboration and catalytic functionalization.

Acknowledgment

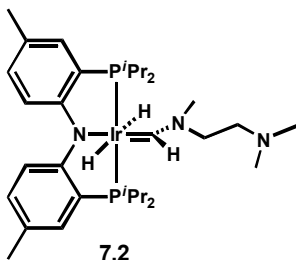
The author acknowledges Larry Henling for crystallographic assistance.

Experimental Section

General Considerations. All manipulations were carried out using standard Schlenk or glove box techniques under a dinitrogen atmosphere. Unless otherwise noted, solvents were deoxygenated and dried by thorough sparging with argon gas followed by passage through an activated alumina column.¹⁶ Hexamethyldisiloxane and *tert*-butyl methyl ether were distilled from CaH_2 and degassed prior to use. $(PNP)IrH_2^{4b}$ and $(PNP)Ir=C(H)O^tBu$ (**7.1**)⁵ were prepared according to literature procedure. Other reagents were purchased from commercial vendors and used without further purification. Elemental analyses were carried out at Desert Analytics, Tucson, Arizona. NMR spectra were recorded at ambient temperature on Varian Mercury 300 MHz and 500 MHz spectrometers. 1H and ^{13}C NMR chemical shifts were referenced to residual solvent. ^{31}P NMR chemical shifts are reported relative to an external standard of 85% H_3PO_4 . Infrared spectra were recorded using a Perkin Elmer Spectrum BXII spectrometer. X-ray

diffraction studies were carried out in the Beckman Institute Crystallographic Facility on a Bruker KAPPA APEX II diffractometer.

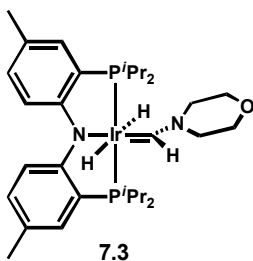
Synthesis of Aminocarbene (7.2). To a solution of (PNP)IrH₂ (139.7 mg, 0.2243 mmol) in



N,N,N',N'-tetramethylethylenediamine (TMEDA, 10 mL) was added a solution of norbornene (24.3 mg, 0.258 mmol) in TMEDA (3 mL), causing a gradual lightening of the solution from red to yellow. The mixture was stirred at ambient temperature for 16 h and volatiles

were removed *in vacuo* to afford an orange film (4:1 mixture of **7.2_{anti}**/**7.2_{syn}** by ³¹P NMR). The residues were dissolved as much as possible in pentane (ca. 3.5 mL), filtered, and large orange blocks of **7.2_{anti}** were recovered by slow evaporation of pentane at ambient temperature (58.1 mg, 35%). Characterization data for **7.2_{anti}**: ¹H NMR (C₆D₆): δ 12.80 (s, 1H, Ir=C(H)N), 7.88 (dt, *J*₁ = 8.7 Hz, *J*₂ = 2.1 Hz, 2H, Ar-H), 7.03 (m, 2H, Ar-H), 6.78 (dd, *J*₁ = 8.7 Hz, *J*₂ = 1.8 Hz, 2H, Ar-H), 3.12 (s, 3H, -NCH₃), 2.76 (t, ³*J*_{HH} = 6.3 Hz, 2H, -NCH₂), 2.30 (s, 6H, Ar-CH₃), 2.20 (m, 4H, -CH(CH₃)₂), 1.90 (t, ³*J*_{HH} = 6.3 Hz, 2H, -NCH₂), 1.80 (s, 6H, -N(CH₃)₂), 1.30–1.09 (m, 24H, -CH(CH₃)₂), -8.90 (br s, 2H, Ir-H). ¹³C{¹H} NMR (C₆D₆): δ 209.1 (Ir=C(H)N), 162.6 (t, *J* = 9 Hz), 131.0, 125.8, 125.6, 122.7, 115.8, 61.3, 57.4, 45.4, 42.8, 26.9 (t, *J* = 16 Hz), 21.1, 19.1, 18.9. ³¹P{¹H} NMR (C₆D₆): δ 49.1 (s). Anal. calcd. for C₃₂H₅₆IrN₃P₂: C, 52.15; H, 7.66; N, 5.70. Found: C, 52.43; H, 7.43; N, 5.60. Although **7.2_{syn}** could not be isolated, it was observed by NMR spectroscopy upon equilibration of **7.2_{anti}** in solution: ¹H NMR (C₆D₆): δ 12.76 (s, 1H, Ir=C(H)N). ³¹P{¹H} NMR (C₆D₆): δ 47.2 (s).

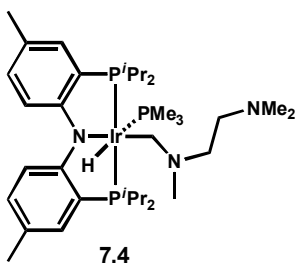
Synthesis of Aminocarbene (7.3). (PNP)IrH₂ (67.2 mg, 0.108 mmol) was dissolved in *N*-



methylmorpholine (7 mL) and norbornene (14.6 mg, 0.155 mmol) was added as a solution in *N*-methylmorpholine (3 mL), causing a change in color from red to red-brown. The reaction was allowed to proceed 12 h, volatiles were removed *in vacuo*, and the residues were extracted into

pentane, filtered, and dried to a reddish film. Analytically pure **7.3** was obtained as red-orange crystals by slow evaporation of pentane from a concentrated solution (10.0 mg, 13%). ¹H NMR (C₆D₆): 12.70 (s, 1H, Ir=C(H)N), 7.85 (dt, *J*₁ = 8.4 Hz, *J*₂ = 2.4 Hz, 2H, Ar-H), 6.99 (m, 2H, Ar-H), 6.77 (dd, *J*₁ = 8.4 Hz, *J*₂ = 1.8 Hz, 2H, Ar-H), 4.08 (m, 2H, morpholine CH₂), 3.30 (t, ³*J*_{HH} = 4.8 Hz, morpholine CH₂), 3.02 (t, ³*J*_{HH} = 4.8 Hz, morpholine CH₂), 2.57 (t, ³*J*_{HH} = 4.8 Hz, morpholine CH₂), 2.28 (s, 6H, Ar-CH₃), 2.15 (m, 4H, -CH(CH₃)₂), 1.18 (dvt, 12H, -CH(CH₃)₂), 1.09 (dvt, 12H, -CH(CH₃)₂), -8.92 (br s, 2H, Ir-H). ¹³C{¹H} NMR (C₆D₆): δ 207.9 (Ir=C(H)N), 162.5 (t, *J* = 9.3 Hz), 131.2, 131.0, 125.3, 123.0, 115.8, 66.6, 66.2, 61.5, 53.4, 34.8, 26.7 (t, *J* = 16 Hz), 23.1, 21.0, 19.0, 18.9, 14.6, 2.4. ³¹P{¹H} NMR (C₆D₆): δ 49.5 (s). Anal. calcd. for C₃₁H₅₁IrN₂OP₂: C, 51.58; H, 7.12; N, 3.88. Found: C, 52.30; H, 7.12; N, 3.89.

Synthesis of Trimethylphosphine Adduct (7.4). Aminocarbene **7.2** (28.1 mg, 0.0381 mmol) was

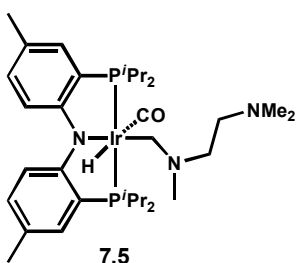


dissolved in benzene (5 mL) and an excess of trimethylphosphine (500 μL, 1.0 M in toluene) was added. The solution was heated at 70 °C for 12 h in a sealed vial, causing lightening to a fluorescent yellow hue. Volatiles were removed *in vacuo*, leaving a pale-yellow film.

Analytically pure crystals of **7.4** suitable for X-ray diffraction were obtained by slow evaporation of pentane from a concentrated solution (28.0 mg, 90%). ¹H NMR (C₆D₆): δ 7.75 (d, *J* = 8.7 Hz, 2H, Ar-H), 7.12 (m, 2H, Ar-H), 6.78 (d, *J* = 8.7 Hz, 2H, Ar-H), 3.21 (m, 2H, Ir-CH₂), 2.78 (m, 2H,

–NCH₂), 2.67 (m, 4H, –CH(CH₃)₂), 2.53 (m, 2H, –NCH₂), 2.44 (s, 3H, –NCH₃), 2.26 (s, 6H, –N(CH₃)₂), 2.25 (s, 6H, Ar–CH₃), 1.42 (dvt, 6H, –CH(CH₃)₂), 1.32 (m, 12H, –CH(CH₃)₂), 1.19 (dvt, 6H, –CH(CH₃)₂), 0.95 (d, ²J_{PH} = 6.6 Hz, 9H, –P(CH₃)₃), –11.61 (dt, ²J_{PH(trans)} = 140 Hz, ²J_{PH(cis)} = 19.8 Hz, 1H, Ir–H). ¹³C{¹H} NMR (C₆D₆): 162.5 (m), 131.7, 131.1, 129.7, 128.9, 126.0, 123.5, 115.9, 60.5, 60.1, 46.8, 45.6, 30.4, 27.9, 21.2, 21.0, 19.9, 19.6, 19.4, 18.0, 17.8, 16.5. ³¹P{¹H} NMR (C₆D₆): 14.9 (d, ²J_{PP} = 17 Hz, 2P, Ir–(PNP)), –53.8 (br, 1P, Ir–P(CH₃)₃). Anal. calcd. for C₃₅H₆₅IrN₃P₃: C, 51.70; H, 8.06; N, 5.17. Found: C, 51.59; H, 8.20; N, 5.11.

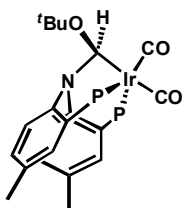
Synthesis of Carbonyl Adduct (7.5). Aminocarbene **7.2** (ca. 10 mg) was dissolved in C₆D₆ (700



μL) and transferred to a resealable NMR tube. The solution was frozen and the headspace evacuated and backfilled with carbon monoxide (1 atm). The solution was warmed to room temperature and allowed to react for 12 h, then heated at 70 °C for 2 h to ensure

complete conversion to **7.5**. Complex **7.5** was not isolated, but its identity was confirmed by NMR, IR, and comparison to the analogous complex **7.4**. ¹H NMR (C₆D₆): δ 7.71 (dt, *J*₁ = 8.1 Hz, *J*₂ = 2.1 Hz, 2H, Ar–H), 6.94 (m, 2H, Ar–H), 6.75 (dd, *J*₁ = 8.7 Hz, *J*₂ = 1.8 Hz, 2H, Ar–H), 3.25 (t, ³J_{PH} = 4.2 Hz, 2H, Ir–CH₂), 2.74 – 2.66 (m, 2H, –NCH₂), 2.58 – 2.40 (m, 6H, –CH(CH₃)₂ and –NCH₂), 2.36 (s, 3H, –NCH₃), 2.21 (s, 6H, –N(CH₃)₂), 2.20 (s, 6H, Ar–H), 1.36 – 1.03 (m, 24H, –CH(CH₃)₂), –7.71 (t, ²J_{PH} = 18 Hz, 1H, Ir–H). ¹³C{¹H} NMR (C₆D₆): δ 181.3 (t, ²J_{PC} = 8.3 Hz, Ir–CO), 161.1, 131.4, 130.8, 123.8, 115.6, 59.2, 59.0, 46.1, 44.8, 25.3 (m), 20.4, 18.6, 18.2, 17.7, 17.2. ³¹P{¹H} NMR (C₆D₆): δ 27.0 (s). IR (C₆D₆, KBr, cm^{–1}) ν(CO): 1976.

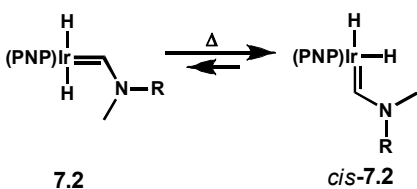
Synthesis of Dicarbonyl Complex (7.6). (PNP)Ir=C(H)O^tBu (**7.1**) (54.4 mg, 0.0770 mmol) was



7.6
(^tPr omitted for clarity)

dissolved in toluene (10 mL) and transferred to a resealable flask. The solution was frozen and the headspace evacuated and backfilled with carbon monoxide (1 atm). As the solution melted a color change from purple to yellow was observed, and the reaction was allowed to continue with stirring for 16 h. Volatiles were removed *in vacuo* to afford a yellow film, and off-white crystals of **7.6** (26.2 mg, 45%) were isolated by slow evaporation of pentane from a concentrated solution at $-35\text{ }^{\circ}\text{C}$. ^1H NMR (C_6D_6): δ 7.42 (d, $J = 6.9$ Hz, 1H, Ar-H), 7.38 – 7.28 (m, 2H, Ar-H), 7.27–7.20 (m, 1H, Ar-H), 6.90 (vt, 2H, Ar-H), 6.37 (dd, $^3J_{\text{PH}} = 16.8$ Hz, $^3J_{\text{PH}} = 2.1$ Hz, 1H, –NC(H)O^tBu), 2.70 (septet, $^3J_{\text{HH}} = 6.3$ Hz, 1H, –CH(CH₃)₂), 2.31 (septet, $^3J_{\text{HH}} = 7.0$ Hz, 1H, –CH(CH₃)₂), 2.19 (m, 2H, –CH(CH₃)₂), 2.13 (s, 3H, Ar-CH₃), 2.12 (s, 3H, Ar-CH₃), 1.49–1.22 (m, 12H, –CH(CH₃)₂), 1.09 (s, 9H, –OC(CH₃)₃), 0.94 – 0.72 (m, 12H, –CH(CH₃)₂). $^{13}\text{C}\{^1\text{H}\}$ NMR (C_6D_6): δ 188.1 (t, $^2J_{\text{PC}} = 37$ Hz, Ir-CO), 184.8 (t, $^2J_{\text{PC}} = 8.7$ Hz, Ir-CO). $^{31}\text{P}\{^1\text{H}\}$ NMR: δ 17.2 (d, $^2J_{\text{PP}} = 95.3$ Hz), 2.9 (d, $^2J_{\text{PP}} = 95.3$ Hz). IR (THF, KBr, cm^{-1}) $\nu(\text{CO}(\text{symmetric}))$: 1981; $\nu(\text{CO}(\text{antisymmetric}))$: 1924. Anal. calcd. for $\text{C}_{33}\text{H}_{50}\text{IrNO}_3\text{P}_2$: C, 51.95; H, 6.61; N, 1.84. Found: C, 53.11, 53.05; H, 6.67, 6.73; N, 1.70, 1.83.

Thermal Isomerization of Aminocarbene (7.2). Aminocarbene **7.2** (ca. 10 mg) was dissolved in



C_6D_6 (ca 600 μL) and transferred to an NMR tube. The sealed sample was heated at $70\text{ }^{\circ}\text{C}$ for 12 h and examined by NMR spectroscopy, revealing a mixture of **7.2**_{anti}, **7.2**_{syn}, and two *cis*-dihydrido isomers of **7.2**. The ^{31}P NMR chemical shifts of the *cis*-**7.2** isomers were observed at δ 48.5 and 46.2 ppm. Each complex also exhibited a distinct carbene proton and two hydrides by ^1H NMR spectroscopy. Characterization data: ^1H NMR (*cis*-**7.2** (major), C_6D_6):

δ 11.92 (s, 1H, Ir=C(H)N), -12.81 (dt, $J_1 = 21$ Hz, $J_2 = 5.4$ Hz, 1H, Ir-H), -19.21 (br s, 1H, Ir-H). ^1H NMR (*cis*-**7.2** (minor), C_6D_6): δ 11.87 (s, 1H, Ir=C(H)N), -12.46 (t, $J_1 = 21$ Hz, $J_2 = 6$ Hz, 1H, Ir-H), -19.38 (br s, 1H, Ir-H).

X-ray Crystallography Procedures. X-ray quality crystals were grown as indicated in the experimental procedures for each complex. The crystals were mounted on a glass fiber with Paratone-N oil. Structures were determined using direct methods with standard Fourier techniques using the Bruker AXS software package. In some cases, Patterson maps were used in place of the direct methods procedure. Table 7.1 contains the X-ray diffraction experimental details.

Table 7.1. X-ray crystallographic data

complex	7.2 _{anti}	7.4	7.6
Empirical Formula	C ₃₂ H ₅₆ IrN ₃ P ₂	C ₃₅ H ₆₅ IrN ₃ P ₃	C ₃₃ H ₅₀ IrO ₃ P ₂
Formula Weight	736.94	813.01	762.88
λ (Å)	0.71073	0.71073	0.71073
T (K)	100(2)	100(2)	100(2)
a (Å)	17.0501(16)	10.5431(9)	10.640(3)
b (Å)	22.666(2)	16.3967(13)	11.968(3)
c (Å)	17.7204(16)	21.8123(18)	14.554(4)
α (deg)	90	90	85.152(5)
β (deg)	96.727(2)	94.963(2)	75.576(4)
γ (deg)	90	90	67.644(4)
V (Å ³)	6801.0(11)	3756.6(5)	1659.9(8)
Z	8	4	2
Crystal System	Monoclinic	Monoclinic	Triclinic
Space Group	P2(1)/c	P2(1)/n	P-1
d_{calc} (g/cm ³)	1.439	1.438	1.526
GOF on F ²	1.023	1.086	1.082
R1, wR2 ^a (I > 2 σ (I))	0.0308, 0.0586	0.0281, 0.0598	0.0393, 0.0813

References and Notes

- (1) (a) Fischer, E. O.; Maasböl, A. *Angew. Chem. Int. Ed.* **1964**, *3*, 580. (b) Schrock, R. R. *J. Am. Chem. Soc.* **1974**, *96*, 6796.
- (2) For leading references, see: (a) Fischer, E. O. *Pure Appl. Chem.* **1970**, *24*, 407. (b) Fischer, E. O. *Pure Appl. Chem.* **1978**, *50*, 857. (c) Cardin, D. J.; Cetinkaya, B.; Lappert, M. F. *Chem. Rev.* **1972**, *72*, 545. (d) Cotton, F. A.; Lukehart, C. M. *Prog. Inorg. Chem.* **1972**, *16*, 487. (e) Schrock, R. R. *Acc. Chem. Res.* **1979**, *12*, 99. (f) *Transition Metal Carbene Complexes*; Seyferth, D., Ed.; Verlag Chemie: Weinheim, 1983. (g) Doyle, M. P. *Chem. Rev.* **1986**, *86*, 919. (h) Brookhart, M.; Studabaker, W. B. *Chem. Rev.* **1987**, *87*, 411. (i) Doyle, M. P.; Forbes, D. C. *Chem. Rev.* **1998**, *98*, 911. (j) Schrock, R. R. *Chem. Rev.* **2002**, *102*, 145. (k) *Handbook of Metathesis*; Grubbs, R. H., Ed.; Wiley: Weinheim, 2003. (l) Doetz, K. H.; Minatti, A. Fischer-Type Carbene Complexes. In *Transition Metals for Organic Synthesis*; Beller, M., Bolm, C., Eds.; Wiley: Weinheim, 2004; vol. 2, pp 397–425.
- (3) (a) Luecke, H. F.; Arndtsen, B. A.; Burger, P.; Bergman, R. G. *J. Am. Chem. Soc.* **1996**, *118*, 2517. (b) Holtcamp, M. W.; Labinger, J. A.; Bercaw, J. E. *J. Am. Chem. Soc.* **1997**, *119*, 848. (c) Slugovc, C.; Mereiter, K.; Trofimenko, S.; Carmona, E. *Angew. Chem. Int. Ed.* **2000**, *39*, 2158. (d) Carmona, E.; Paneque, M.; Santos, L. L.; Salazar, V. *Coord. Chem. Rev.* **2005**, *249*, 1729. (e) Lee, D.-H.; Chen, J.; Faller, J. W.; Crabtree, R. H. *Chem. Commun.* **2001**, 213. (f) Romero, P. E.; Whited, M. T.; Grubbs, R. H. *Organometallics* **2008**, *27*, 3422. (g) Coalter, J. N.; Ferrando, G.; Caulton, K. G. *New J. Chem.* **2000**, *24*, 835. (h) Ferrando-Miguel, G.; Coalter, J. N.; Gerard, H.; Huffman, J. C.; Eisenstein, O.; Caulton, K. G. *New J. Chem.* **2002**, *26*, 687.
- (4) (a) Fan, L.; Foxman, B. M.; Ozerov, O. V. *Organometallics* **2004**, *23*, 326. (b) Ozerov, O. V.; Guo, C.; Papkov, V. A.; Foxman, B. M. *J. Am. Chem. Soc.* **2004**, *126*, 4792.
- (5) Whited, M. T.; Grubbs, R. H. *J. Am. Chem. Soc.* **2008**, *130*, 5874.
- (6) Whited, M. T.; Grubbs, R. H., *Organometallics* **2009**, *28*, 161.
- (7) Although the formation of complexes **2** and **3** was quantitative as judged by ³¹P and ¹H NMR spectroscopy, the difficulty in crystallizing pure **2_{anti}** and **3** to remove norbornane and residual amine resulted in low isolated yields (35% and 13%, respectively).
- (8) Gasparro, F. P.; Kolodny, N. H. *J. Chem. Educ.* **1977**, *54*, 258.
- (9) (a) Busetto, L.; Palazzi, A.; Crociani, B.; Belluco, U.; Badley, E. M.; Kilby, B. J. L.; Richards, R. L. *J. Chem. Soc. Dalton* **1972**, 1800. (b) Albéniz, A. C.; Espinet, P.; Manrique, R.; Pérez-Mateo, A. *Chem.—Eur. J.* **2005**, *11*, 1565. (c) Meana, I.; Albéniz, A. C.; Espinet, P. *Organometallics* **2008**, *27*, 4193.
- (10) Slow N–C bond rotation in complex **3** was confirmed by the presence of four distinct ¹H NMR chemical shifts for the methylene protons on the morpholine ring.

- (11) Representative examples: (a) Threlkel, R. S.; Bercaw, J. E. *J. Am. Chem. Soc.* **1981**, *103*, 2650. (b) Le Bozec, H.; Fillaut, J.-L.; Dixneuf, P. H. *Chem. Commun.* **1986**, 1182. (c) Osborn, V. A.; Parker, C. A.; Winter, M. J. *Chem. Commun.* **1986**, 1185. (d) Hoover, J. F.; Stryker, J. M. *J. Am. Chem. Soc.* **1990**, *112*, 464. (e) Adams, H., Bailey, N. A.; Bentley, G. W.; Tattershall, C. E.; Taylor, B. F.; Winter, M. J. *Chem. Commun.* **1992**, 533. (f) Trace, R. L.; Sanchez, J.; Yang, J.; Yin, J.; Jones, W. M. *Organometallics* **1992**, *11*, 1440. (g) Bergamini, P.; Costa, E.; Cramer, P.; Hogg, J.; Orpen, A. G.; Pringle, P. G. *Organometallics* **1994**, *13*, 1058. (h) Casty, G. L.; Stryker, J. M. *Organometallics* **1997**, *16*, 3083. (i) Werner, H. *Coord. Chem. Rev.* **2004**, *248*, 1693. (j) Jellema, E.; Budzelaar, P. H. M.; Reek, J. N. H.; de Bruin, B. *J. Am. Chem. Soc.* **2007**, *129*, 11631.
- (12) CO insertion into metal–amide bonds: (a) Beers, O. C. P.; Delis, J. G. P.; Mul, W. P.; Vrieze, K.; Elsevier, C. J.; Smeets, W. J. J.; Spek, A. L. *Inorg. Chem.* **1993**, *32*, 3640. (b) Cowan, R. L.; Trogler, W. C. *Organometallics* **1987**, *6*, 2451.
- (13) Latos-Grazynski, L.; Cheng, R.-J.; La Mar, G. N.; Balch, A. L. *J. Am. Chem. Soc.* **1981**, *103*, 4270.
- (14) The related reversible insertion of CO into M–X bonds has been reported: (a) Saruyama, T.; Yamamoto, T.; Yamamoto, A. *Bull. Chem. Soc. Jpn.* **1976**, *49*, 546. (b) Fagan, P. J.; Moloy, K. G.; Marks, T. J. *J. Am. Chem. Soc.* **1981**, *103*, 6959. (c) Ref 12a.
- (15) Zhang, X.; Fried, A.; Knapp, S.; Goldman, A. S. *Chem. Commun.* **2003**, 2060.
- (16) Pangborn, A. B.; Giardello, M. A.; Grubbs, R. H.; Rosen, R. K.; Timmers, F. J. *Organometallics* **1996**, *15*, 1518.